Color superconductivity in cold and dense quark matter

Habilitationsschrift im Fach Theoretische Physik

vorgelegt beim Rektorat
der Technischen Universität Wien

von
Andreas Schmitt
aus Frankfurt am Main (Deutschland)

Wien, März 2010

Abstract

Quantum Chromodynamics (QCD) is the theory of the strong interaction. The precise structure of its phase diagram in the plane of temperature T and quark chemical potential μ, in particular the location and nature of the phase transition lines and the possible existence of critical endpoints, is an unsolved problem. From mapping out the phase diagram and studying the properties of the various phases, one expects to understand and interpret observational data as well as to gain insight into the fundamental nature of strongly-interacting matter. For instance, confinement and chiral symmetry breaking, both intimately related to the strong-coupling nature of QCD, depend on temperature and density, i.e., for sufficiently large temperatures and/or quark chemical potentials, matter is believed to be deconfined and chiral symmetry is restored. This expectation is borne out for instance in relativistic heavy-ion collisions where a Quark-Gluon Plasma (QGP) appears to form in which the degrees of freedom are quarks and gluons rather than baryons and mesons. QCD calculations from first principles on the lattice support this interpretation of the data; more precisely, at zero chemical potential it is widely accepted that there is a crossover from confined hadronic matter to the deconfined QGP, happening around a temperature of about $T_c \simeq 170\,\mathrm{MeV}$. However, detailed properties of the matter in the vicinity of this crossover are extremely difficult to compute although we know the precise form of the underlying theory. The main reason is the large effective value of the strong coupling constant at the relevant energy scale. Only at much larger energies can we apply perturbative methods because, due to asymptotic freedom, the coupling becomes small. In other words, QCD at sufficiently large temperatures and chemical potentials is under good theoretical control. While the more challenging regime of intermediate T (and small μ) is probed by heavy-ion collisions for instance in the Relativistic Heavy-Ion Collider (RHIC) in Brookhaven (and in the near future at the Large Hadron Collider (LHC) at CERN), there is no experiment on earth that can probe the equally, or even more, challenging region of moderately large μ (and small T). (The so-called sign problem prevents lattice QCD from making predictions for finite chemical potentials.) However, this does not mean that matter at these densities does not exist. On the contrary, the cores of compact stars contain such cold and dense matter and thus constitute our "laboratory" to gain experimental insight into strongly-interacting quark or nuclear matter. The first part of this thesis,

- A. Schmitt, "Dense matter in compact stars - A pedagogical introduction," arXiv:1001.3294 [astro-ph.SR], to appear in Lect. Notes Phys. (Springer),

explains the interplay between microscopic calculations, based on perturbative QCD and effective theories, with observational data such as the cooling curve or the rotation frequency of a compact star. The calculations and conclusions are presented in a pedagogical way, which makes this part particularly suited for non-experts and graduate students who are planning to do research in this field.

The second part of this thesis,

- M. G. Alford, A. Schmitt, K. Rajagopal and T. Schäfer,"Color superconductivity in dense quark matter," Rev. Mod. Phys. **80**, 1455 (2008) [arXiv:0709.4635 [hep-ph]] ,

is more specific, although also written in a review style, and is devoted to color superconductivity. At asymptotically large densities, deconfined three-flavor quark matter is in the color-flavor locked (CFL) state. This is a particularly symmetric color superconductor, where the quarks of all colors and flavors participate in pairing. This cold and ultra-dense regime is maybe the best understood region of the QCD phase diagram. One reason is that all gluons acquire Meissner masses such that there are no non-abelian infrared degrees of freedom. Going down in density is theoretically challenging and two scenarios seem conceivable: firstly, CFL may persist down to densities where the hadronic phase takes over, i.e., matter inside a compact star is made of nuclear and/or CFL matter. Or, secondly, there may be other color superconductors between hadronic matter and CFL. The potential breakdown of CFL is suggested by a mismatch between the Fermi surfaces of the quarks that form Cooper pairs. This mismatch increases with decreasing μ, it is not certain, however, if and at which μ the mismatch is large enough (compared to the color-superconducting gap) to disfavor CFL pairing. If CFL is indeed disfavored before the transition to hadronic matter, unconventional color superconductors that break rotational and/or translational invariance are expected to be favored. Properties of CFL and its description within an effective theory as well as a discussion of the unconventional superconductors are discussed in detail in this second part.

Dense matter in compact stars – A pedagogical introduction –

Andreas Schmitt[1,*]

[1]*Institut für Theoretische Physik, Technische Universität Wien, 1040 Vienna, Austria*

(Dated: January 19, 2010)

Cold and dense nuclear and/or quark matter can be found in the interior of compact stars. It is very challenging to determine the ground state and properties of this matter because of the strong-coupling nature of QCD. I give a pedagogical introduction to microscopic calculations based on phenomenological models, effective theories, and perturbative QCD. I discuss how the results of these calculations can be related to astrophysical observations to potentially rule out or confirm candidate phases of dense matter.

Contents

*Electronic address: aschmitt@hep.itp.tuwien.ac.at

I. INTRODUCTION

The purpose and motivation of these lectures can be summarized in the following two questions:

- What is the ground state (and its properties) of dense matter?
- What is the matter composition of a compact star?

The two questions are, of course, strongly coupled to each other. Depending on your point of view, you can either consider the first as the main question and the second as a consequence or application of the first, or vice versa.

If you are interested in fundamental questions in particle physics you may take the former point of view: you ask the question what happens to matter if you squeeze it more and more. This leads to fundamental questions because at some level of sufficient squeezing you expect to reach the point where the fundamental degrees of freedom and their interactions become important. That is, at some point you will reach a form of matter where not molecules or atoms, but the constituents of an atom, namely neutrons, protons, and electrons, are the relevant degrees of freedom. This form of matter, and its variants, constitute one important topic of these lectures and is termed nuclear matter. If you squeeze further, you might reach a level where the constituents of neutrons and protons, namely quarks and gluons, become relevant degrees of freedom. This form of matter, termed quark matter or strange quark matter, is the second important subject we shall discuss. By studying dense matter, we shall thus learn a lot about the fundamental theories and interactions of elementary particles. When trying to understand this kind of dense matter, we would like to perform experiments and check whether our fundamental theories work or whether there are new phenomena, or maybe even new theories, that we have not included into our description. Unfortunately, there are currently no experiments on earth which can produce matter at such ultra-high densities we are talking about. However, this does not mean that this kind of matter does not exist in nature. On the contrary, we are pretty sure that we have observed objects that contain matter at ultra-high density, namely compact stars. We may thus consider compact stars as our "laboratory". Thinking about the first question has therefore led us to the second.

If you are primarily interested in phenomenology, or if you are an astrophysicist, you may start from the second question: you may simply say, I observe a compact star in nature and would like to understand its properties. In this case you start from observations like the rotation frequency, the temperature of the star etc. and ask, why does the star rotate so slow/so fast, why does it cool down so slow/so fast? And these questions will inevitably lead you to the attempt to figure out the microscopic structure of the star, although you have started from macroscopic observables. You need to know whether the star contains nuclear matter or quark matter or both, in which phase the respective matter is present, and which properties these phases have. It is thus very natural, also from the astrophysicist's point of view, to study the first question.

In any case, we see that both questions are closely related and we don't have to decide which of the two points of view we take. If I have to characterize what awaits you in these lectures I would nevertheless say that we shall lean a bit more towards the fundamental aspects. In other words, we shall neglect many complications that arise from considering a realistic compact star. A star is a finite system, it is inhomogeneous, it underlies the laws of general relativity etc. Although our discussions are always motivated by the astrophysical application, we mostly

discuss infinite, homogeneous systems and do not elaborate on general relativistic effects. Only in discussing the consequences of our microscopic calculations we shall, on a qualitative level, discuss the more realistic setting.

So what kind of physics will we discuss and which theoretical tools do we need? Since our focus is on nuclear and quark matter, the dominant interaction that governs the states of matter we are interested in is the strong interaction. The underlying theory for this interaction is Quantum Chromodynamics (QCD). Although this theory is uniquely determined by very simple symmetry principles, it is extremely hard to solve for most applications. Unfortunately (or fortunately, because this makes it interesting and challenging) matter at compact star densities eludes rigorous first-principle calculations. Therefore, we often have to retreat to simple phenomenological models or have to perform rigorous QCD calculations at asymptotically large densities and then extrapolate the results down to the density regime we are interested in.

In the physics of compact stars also the weak interaction plays an important role. We shall see that it is responsible for the chemical equilibration of the system, i.e., it fixes the various chemical potentials. It is also important for the understanding of cooling mechanisms of the star or for transport properties of nuclear and quark matter. Furthermore, our (mostly field-theoretical) treatment always includes nonzero chemical potentials and sometimes nonzero temperature (for many applications the zero-temperature approximation is sufficient). In this sense it goes beyond the standard vacuum field theory formalism. Basic elements of thermal quantum field theory at finite chemical potential are therefore explained in the appendix.

All this may sound exciting on the one hand, because it shows that the physics of compact stars is extremely rich (due to the diversity of involved physics I found it helpful to include a glossary of important terms at the end of these lecture notes). But on the other hand it may also sound like a big challenge for you if you are not familiar with advanced field theory. Nevertheless, these lecture notes are not primarily intended as a review for researchers (although they might find it useful too) but as a pedagogical introduction for graduate students and advanced undergraduate students. For some of our discussions all you need as a prerequisite is some knowledge in thermodynamics and statistical physics, for instance in chapter II, which deals almost exclusively with noninteracting systems. Some other sections, for instance the calculation of the neutrino emissivity in chapter V indeed makes use of advanced field-theoretical methods at finite temperature. It is not the intention of these lectures to develop the theoretical tools in all details before we use them. More importantly, all calculations are physically motivated, thus by understanding the physics behind the results and calculations, these lectures aim at making you familiar with the theories and technicalities via "learning by doing". So at the end of these lectures you will have heard about the basic phenomena and possible microscopic explanations of the physics of compact stars, but also will be prepared to start theoretical research in this exciting field yourself, to possibly contribute to the answer of the two questions we have started with.

A. What is dense matter?

The QCD phase diagram collects the equilibrium phases of QCD in the plane of quark (or baryon) chemical potential μ and temperature T. We show a sketch of this phase diagram in Fig. 1. In this introduction, we are not concerned with the details of this diagram. We observe that compact stars, on the scales of this diagram, live in the region of small temperatures and intermediate densities. They may live in the region where quarks are confined, i.e., in the hadronic phase. This would imply that they are neutron stars. They may also live in the deconfined region which would make them quark stars. A compact star may also contain both deconfined and confined quark matter because the star actually has a density profile rather than a homogeneous density. In the interior, we expect the density to be larger than at the surface. Therefore, the third possibility is a hybrid star with a quark core and a nuclear mantle.

We do currently not know the exact location of most of the phase transition lines in Fig. 1. Therefore, we do not know the ground state of strongly-interacting quark (or nuclear) matter at the relevant density. As a consequence, we can to some extent only speculate about the matter composition of the star. The reason is, simply speaking, that QCD is notoriously hard to solve for temperatures and densities present in a compact star. With the help of the phase diagram we can put this statement in a wider context: QCD is *asymptotically free*, which means that for large momentum exchange the interaction becomes weak. Hence, at sufficiently large temperatures and/or densities, we deal with weakly interacting quarks and gluons. In the case of large densities (or large chemical potentials) this can be understood from the uncertainty principle which relates small distances (the interacting particles are very close to each other) to large momenta. As a result of asymptotic freedom, regions in the phase diagram where μ and/or T are sufficiently large can be understood from rigorous first-principle calculations. These regions, although theoretically under control, are far from being experimentally (even astrophysically) accessible.

If we now go to lower temperatures and densities we have to cross a large unknown territory. Only at small temperatures and densities, when we are deep in the hadronic phase we have reached an area which again is under control, at least to some extent. Theoretically, it is more complicated than the perturbatively treatable asymptotic regions. After all, hadrons are quite complicated objects once we try to describe them in terms of their constituents.

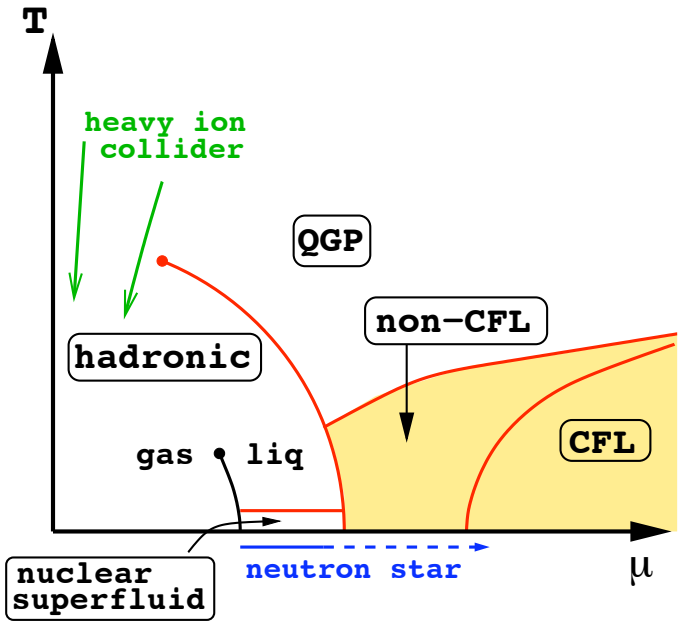

FIG. 1: Conjectured phase diagram of QCD in the plane of quark chemical potential μ and temperature T. While matter at low density and high temperature is probed in heavy-ion collisions, cold and dense matter can only be found in neutron stars (compact stars). We may find (superfluid) nuclear matter and/or deconfined quark matter inside a star. Deconfined quark matter is, at high temperatures, termed quark-gluon plasma (QGP) and is, at low temperatures, expected to be in a color-superconducting state, here labelled by CFL (color-flavor locking), discussed in Sec. IV B, and non-CFL (some color superconductor other than CFL).

However, we can use effective descriptions which can be supported, confirmed, and improved by experiments in the lab. Furthermore, at least for vanishing chemical potentials, we can perform brute-force QCD calculations on the computer which gives us solid theoretical knowledge for certain quantities (at nonvanishing chemical potentials these calculations are problematic due to the so-called *sign problem*).

We thus see that compact stars (as well as the quark-gluon plasma created in heavy-ion collisions) reside in a region of the phase diagram which is hard to access. More positively speaking, this region is interesting and challenging because exciting and unknown physics may be discovered and new theoretical tools may need to be developed. Or, in other words, the cold and dense matter we talk about in these lectures is interesting from the theoretical point of view because, on the characteristic scale of QCD, it is only moderately, not extremely, dense.

The theoretical tools used in current research to describe cold and dense matter are based on the above observations: if we describe quark matter we may use perturbative methods which are valid at asymptotically large densities and extrapolate the results down to intermediate densities. We shall do so for instance in chapter II where we treat quarks as noninteracting or in Sec. IV C where we calculate the color-superconducting gap within perturbative QCD. However, we have to be aware that the extrapolation of the results pushes the calculations out of their range of validity by many orders of magnitude. On the other hand, we may use models for nuclear matter which are established at low densities by experimental data. We do so for instance in chapter III. This time we have to extrapolate to *larger* densities. Again, the extrapolation is in principle uncontrolled.

These theoretical challenges emphasize the significance of astrophysical observations: we do not simply like to *confirm* the results of our calculations by using astrophysical data, we need astrophysical input to *understand* the theory which we believe to be the underlying theory of strongly interacting matter, namely QCD. Therefore, the connection between astrophysical observables and microscopic calculations is one of the main subjects of these lectures.

B. What is a compact star?

Only beaten by black holes, compact stars are the second-densest objects in nature. They have masses of the order of the mass of the sun, $M \sim 1.4\,M_\odot$, but radii of only about ten kilometers, $R \sim 10\,\mathrm{km}$. Thus the mass of the sun $M_\odot = 1.989 \cdot 10^{33}\,\mathrm{g}$ is concentrated in a sphere with a radius 10^5 times smaller than that of the sun, $R_\odot = 6.96 \cdot 10^5\,\mathrm{km}$.

We thus estimate the average mass density in a compact star to be

$$\rho \simeq 7 \cdot 10^{14}\,\mathrm{g\,cm^{-3}}\,. \tag{1}$$

This is a few times larger than the density present in heavy nuclei, the nuclear ground state density

$$\rho_0 = 2.5 \cdot 10^{14}\,\mathrm{g\,cm^{-3}}\,, \tag{2}$$

which corresponds to a baryon number density of $n_0 \simeq 0.15\,\mathrm{fm^{-3}}$. Mass and radius of the star are determined by the equation(s) of state of the matter phase(s) inside the star. This is the subject of chapter II.

In the traditional picture of a compact star, the star is made out of neutron-rich nuclear matter. Hence the traditional name is actually *neutron star*. This is sometimes still the preferred term, even if one talks about a star that contains a quark matter core (which then might be called "exotic neutron star"). Here we shall always use the more general term *compact star* to include the possibilities of more exotic matter; after all, a significant part of these lectures is about this exotic matter. The term compact star will thus be used in these lectures for an object with characteristic mass, radius etc. as given in this subsection. It can either be made of nuclear matter or variants thereof (*neutron star*), of a quark matter core with a surrounding mantle of nuclear matter (*hybrid star*) or exclusively of (strange) quark matter (*quark star* or *strange star*).[1] Here are a few more basic properties of compact stars:

- Compact stars are born in a supernova, a spectacular explosion of a giant or supergiant star due to the gravitational collapse of its core. Supernovae are very complex, nonequilibrium processes which astrophysicists try to understand with hydrodynamic simulations. We shall not be concerned with supernovae in these lectures but should keep in mind that some properties of the star may be a result of these violent explosions. A possible example is the high velocity with which some of the compact stars travel through space.

- Compact stars are not only extreme with respect to their density. Some of them also rotate very fast with rotation periods in the millisecond regime, such that their frequencies are

  $$\nu \lesssim 1\,\mathrm{ms^{-1}}\,. \tag{3}$$

  To see that this is really fast, notice that a point on the equator has a velocity of $2\pi R/1\mathrm{ms} \simeq 0.2\,c$, i.e., it moves with 20% of the speed of light. The current record holder is the star PSR J1748-2446ad,[2] rotating with a period of 1.39 ms. Several observations are related to the rotation frequency. First of all, compact stars have been discovered as *pulsars*, by observing pulsating radio signals, for the first time in 1967. These periodic signals are due to the lighthouse effect, i.e., radio emission is aligned in a beam along the magnetic axis of the pulsar which spins around the rotation axis, crossing the earth's telescopes periodically. More interestingly for our purpose, the pure fact that the rotation of some compact stars can be so fast requires some explanation. From the microscopic point of view, this is related to transport properties such as viscosity of the matter inside the star, see Sec. VI B. Also *pulsar glitches*, sudden jumps in the rotation frequency, must find an explanation in the properties of dense matter.

- Compact stars also have huge magnetic fields,

  $$B \sim 10^{12}\,\mathrm{G}\,. \tag{4}$$

  Even larger surface magnetic fields of the order of $B \sim 10^{15}\,\mathrm{G}$ have been observed (the magnetic field in the core of the star possibly being even higher). Such highly magnetized stars are also termed *magnetars*. Compare these magnetic fields for instance to the earth's magnetic field, $B \sim 0.6\,\mathrm{G}$, a common hand-held magnet, $B \sim 100\,\mathrm{G}$, or the strongest steady magnetic fields in the laboratory, $B \sim 4.5 \cdot 10^5\,\mathrm{G}$.

- Compact stars are cold. This may sound odd, given their temperatures which, right after they are born in a supernova explosion, can be as high as $T \sim 10^{11}\,\mathrm{K}$. This corresponds, in units where the Boltzmann constant is one, $k_B = 1$, to $T \sim 10\,\mathrm{MeV}$. During the evolution of the star, the temperature decreases down to temperatures

---

[1] The term compact star is in general also used to include *white dwarfs*, stars which are less dense than neutron stars, hybrid stars, or quark stars, and sometimes even to include black holes. Since we are not concerned with either of these objects here, we can reserve the term compact star as explained in the text.

[2] The label of the star says that it is a "Pulsating Source of Radio emission" (PSR) located on the celestial sphere at right ascension 17 h 48 min with −24° 46' declination; the 'J' indicates the use of the J2000 coordinate system, the suffix 'ad' is used to distinguish the object from other pulsars in the same globular cluster Terzan 5.

in the keV range. The dominant cooling mechanism is neutrino emission which we discuss in chapter V. There are two reasons why in our context it is appropriate to call compact stars cold, in spite of the apparently large temperatures. First, temperatures in the keV range are small compared to the scale set by QCD, for instance the deconfinement transition at vanishing quark chemical potential of about $T_c \simeq 170\,\mathrm{MeV}$. This means compact stars are located basically on the horizontal axis in the QCD phase diagram in Fig. 1. Second, temperatures in compact stars are small compared to the quark (or baryon) chemical potential, $T \ll \mu$. This is important for our calculations since it implies that $T = 0$ is a good approximation in many cases.

C. Further reading

Before we start with the main part, let's mention some literature. Extensive textbooks about compact stars are Refs. [1–3]. A shorter introduction to compact stars and dense matter can be found in the review article [4]. Similar reviews are Refs. [5, 6], with emphasis on quark matter, and Ref. [7], with emphasis on astrophysical observations. A more theoretical review about quark matter (more precisely, about color-superconducting quark matter), with a section about compact star applications is Ref. [8]. For an introduction to thermal field theory see the textbooks [9] and [10], on which the appendix of these lecture notes is partially based. As became clear above, in this course we shall deal with questions which are under debate in current research. Therefore, some of the material included here has so far only been available in research papers. The respective references will be given in the various chapters. I will not try to be exhaustive in the reference list but rather point out selected references which are useful for a deeper understanding of what we discuss in these lectures. If you are interested in more references you can find plenty in the quoted papers and textbooks.

II. MASS AND RADIUS OF THE STAR

In this chapter, we will discuss the most basic properties of a compact star, its mass and radius. We have already given typical values for these quantities above. Below we shall connect them with microscopic properties of nuclear and quark matter. This connection is made by the equation of state from which, in particular, an estimate for the maximum mass of the star can be obtained. Let us begin with a simple estimate of mass and radius from general relativity. For the stability of the star we need $R > R_s$ where R is the radius of the star, and $R_s = 2MG$ the Schwarzschild radius, with the mass of the star M and the gravitational constant $G = 6.672 \cdot 10^{-11}\,\mathrm{m^3 kg^{-1} s^{-2}} = 6.707 \cdot 10^{-39}\,\mathrm{GeV^{-2}}$. (We shall mostly use units common in nuclear and particle physics, $\hbar = c = k_B = 1$, although astrophysicists often use different units.) For $R < R_s$ the star becomes unstable with respect to the collapse into a black hole. Let us build a simple star made out of a number of nucleons A with mass $m \simeq 939\,\mathrm{MeV}$ and a distance $r_0 \simeq 0.5 \cdot 10^{-13}\,\mathrm{cm}$ (that's where the nucleon interaction becomes repulsive). We thus cover a volume $\sim r_0^3\, A$ and thus have a radius

$$R \sim r_0\, A^{1/3}\,, \tag{5}$$

(for our rough estimate we are not interested in factors of π), and a mass

$$M \sim m\, A\,. \tag{6}$$

Now from the limit $R = 2MG$ we obtain

$$A \sim \left(\frac{r_0}{2mG}\right)^{3/2} \sim 2.6 \cdot 10^{57}\,. \tag{7}$$

This is the number of nucleons up to which we can fill our star before it gets unstable. In other words, the Schwarzschild radius is proportional to the mass of the star and thus increases linearly in the number of nucleons A, while the radius increases with $A^{1/3}$; therefore, for A smaller than the limit $A \sim 2.6 \cdot 10^{57}$ the star is stable, while it collapses into a black hole for nucleon numbers larger than this limit. We can plug the limit value for A back into the radius and mass of the star to obtain

$$R \sim 7\,\mathrm{km}\,, \qquad M \sim 2.3\, M_\odot\,. \tag{8}$$

Adding more nucleons would make the star too heavy in relation to its radius. We see that these values are not too far from the observed ones given in Sec. I B.

Besides giving an estimate for the baryon number in the star, we see from this simple exercise that general relativistic effects will be important because the Schwarzschild radius will be a significant fraction of the radius of the star. We

can also estimate the gravitational energy of the star. To this end, we need the differential mass of the star at a given radius (i.e., the mass of a thin spherical layer)

$$dm = \rho(r)\, dV\,, \tag{9}$$

where $dV = 4\pi r^2 dr$ is the volume of the thin spherical layer at radius r. For a rough estimate let us (unrealistically) assume a constant density $\rho(r) = \rho$ such that the mass $m(r)$ of the star up to a radius $r \leq R$, is given by $m(r) = \frac{4\pi}{3} r^3 \rho$. Then we obtain

$$E_{\rm grav} \simeq \int_0^R \frac{G m(r)\, dm(r)}{r} \simeq \frac{3}{5}\frac{GM^2}{R} \simeq 0.12\, M\,. \tag{10}$$

where we have used the above realistic values $M \simeq 1.4\, M_\odot$ and $R \simeq 10\,$km. We thus see that the gravitational energy $E_{\rm grav}$ is more than 10% of the mass of the star. This suggests that for the mass-radius relation we need an equation that incorporates effects from general relativity. For simplicity, let us first derive the equation that relates mass and radius without general relativistic effects and include them afterwards. We are looking for an equation that describes equilibrium between the gravitational force, seeking to compress the star, and the opposing force coming from the pressure of the matter inside the star. In the case of a compact star, this pressure is the Fermi pressure plus the pressure coming from the strong interactions of the nuclear or quark matter inside. The differential pressure dP at a given radius r is related to the gravitational force dF via

$$dP = \frac{dF}{4\pi r^2}\,, \tag{11}$$

with

$$dF = -\frac{G m(r)\, dm}{r^2}\,. \tag{12}$$

The equation for the differential mass (9), together with Eq. (11) (into which we insert Eqs. (9) and (12)), yields the two coupled differential equations,

$$\frac{dm}{dr} = 4\pi r^2 \epsilon(r)\,, \tag{13a}$$

$$\frac{dP}{dr} = -\frac{G\epsilon(r) m(r)}{r^2}\,. \tag{13b}$$

where we have expressed the mass density through the energy density $\epsilon(r) = \rho(r)$ (in units where $c = 1$). The second equation, which is easy to understand from elementary Newtonian physics, receives corrections from general relativity. It is beyond the scope of these lectures to derive these corrections. We simply quote the resulting equation,

$$\frac{dP}{dr} = -\frac{G\epsilon(r) m(r)}{r^2}\left[1 + \frac{P(r)}{\epsilon(r)}\right]\left[1 + \frac{4\pi r^3 P(r)}{m(r)}\right]\left[1 - \frac{2Gm(r)}{r}\right]^{-1}\,. \tag{14}$$

This equation is called Tolman-Oppenheimer-Volkov (TOV) equation and the derivation can be found for instance in Ref. [11]. In order to solve it, one first needs the energy density for a given pressure. Only then do we have a closed system of equations. This input is given from the microscopic physics which yields an equation of state in the form $P(\epsilon)$. We have thus found a first example how the microscopic physics can potentially be "observed" from astrophysical data, namely from mass and radius of the star. We shall encounter many more of these examples. The equations of state for noninteracting nuclear and quark matter will be discussed in the subsequent sections.

For a given equation of state one needs two boundary conditions for the TOV equation. The first is obviously $m(r = 0) = 0$, the second is a boundary value for the pressure in the center of the star, $P(r = 0) = P_0$. Then, the solution of the equations will produce a mass and pressure profile $m(r)$, $P(r)$ with the pressure going to zero at some point $r = R$, giving the radius of the star. The mass of the star is then read off at this point, $M = m(R)$. Doing this for varying initial pressures P_0 yields a curve $M(R)$ in the mass-radius plane, parametrized by P_0. This curve of course depends on the chosen equation of state.

A. Noninteracting nuclear matter

We start with a very simple system where we neglect all interactions. In this case, all we need is basic statistical physics and thermodynamics. The thermodynamic potential for the grand-canonical ensemble is given by

$$\Omega = E - \mu N - TS\,, \tag{15}$$

with the energy E, chemical potential μ, particle number N, temperature T and entropy S. The pressure is then

$$P = -\frac{\Omega}{V} = -\epsilon + \mu n + Ts\,, \tag{16}$$

where V is the volume of the system. Number density $n \equiv N/V$, energy density $\epsilon = E/V$, and entropy density $s = S/V$ are, for a fermionic system, given by

$$n = 2\int \frac{d^3\mathbf{k}}{(2\pi)^3}\, f_k\,, \tag{17a}$$

$$\epsilon = 2\int \frac{d^3\mathbf{k}}{(2\pi)^3}\, E_k\, f_k\,, \tag{17b}$$

$$s = -2\int \frac{d^3\mathbf{k}}{(2\pi)^3}\, [(1-f_k)\ln(1-f_k) + f_k \ln f_k]\,. \tag{17c}$$

We shall first be interested in a system of neutrons (n), protons (p), and electrons (e) which each give a contribution to the pressure according to Eqs. (16) and (17). Since they are spin-$\frac{1}{2}$ fermions, we have included a factor 2 for the two degenerate spin states. The Fermi distribution function is denoted by f_k,

$$f_k \equiv \frac{1}{e^{(E_k-\mu)/T}+1}\,, \tag{18}$$

and the single-particle energy is

$$E_k = \sqrt{k^2+m^2}\,. \tag{19}$$

Inserting number density, energy density, and entropy density into the pressure (16) yields

$$P = 2T\int \frac{d^3\mathbf{k}}{(2\pi)^3} \ln\left[1+e^{-(E_k-\mu)/T}\right]\,. \tag{20}$$

This corresponds to the result obtained from field-theoretical methods in appendix A 2, see Eq. (A71). There also the antiparticle contribution is included, which can here, due to the large positive chemical potential, safely be neglected. One can easily check that number density and entropy are obtained from the pressure (20) via the usual thermodynamic relations, i.e., by taking the derivatives with respect to μ and T. For the following we now take the limit $T = 0$. This is a good approximation since the temperature of a compact star is typically in the keV range and thus much smaller than the chemical potentials and masses of the nucleons.

For $T = 0$ the Fermi distribution is a step function, $f_k = \Theta(k_F - k)$, and thus the k integrals will be cut off at the Fermi momentum k_F, i.e.,

$$n = \frac{1}{\pi^2}\int_0^{k_F} dk\, k^2 = \frac{k_F^3}{3\pi^2}\,, \tag{21a}$$

$$\epsilon = \frac{1}{\pi^2}\int_0^{k_F} dk\, k^2\sqrt{k^2+m^2} = \frac{1}{8\pi^2}\left[(2k_F^3+m^2k_F)\sqrt{k_F^2+m^2} - m^4\ln\frac{k_F+\sqrt{k_F^2+m^2}}{m}\right]\,. \tag{21b}$$

Then, with $\mu = \sqrt{k_F^2+m^2}$, the pressure is

$$P = \frac{1}{\pi^2}\int_0^{k_F} dk\, k^2(\mu - \sqrt{k^2+m^2}) = \frac{1}{24\pi^2}\left[(2k_F^3-3m^2k_F)\sqrt{k_F^2+m^2} + 3m^4\ln\frac{k_F+\sqrt{k_F^2+m^2}}{m}\right]\,. \tag{22}$$

This can either be obtained by inserting Eqs. (21a) and (21b) into Eq. (16) or, equivalently, by taking the $T = 0$ limit in Eq. (20). For the latter one makes use of $\lim_{T\to 0} T\ln(1+e^{x/T}) = x\,\Theta(x)$.

For n, p, e matter, the total pressure is

$$P = \frac{1}{\pi^2}\sum_{i=n,p,e}\int_0^{k_{F,i}} dk\, k^2(\mu_i - \sqrt{k^2+m_i^2})\,. \tag{23}$$

The Fermi momenta can be thought of as variational parameters which have to be determined from maximizing the pressure, i.e., from the conditions

$$\frac{\partial P}{\partial k_{F,i}} = 0\,, \qquad i = n, p, e\,, \tag{24}$$

which implies

$$\mu_i = \sqrt{k_{F,i}^2 + m_i^2}\,. \tag{25}$$

We have additional constraints on the Fermi momenta from the following two conditions. Firstly, we have to require the star to be electrically neutral,[3], i.e., the densities of protons and electrons has to be equal,

$$n_e = n_p\,. \tag{29}$$

With Eq. (21a) this means

$$k_{F,e} = k_{F,p}\,. \tag{30}$$

Secondly, we require chemical equilibrium with respect to the weak processes

$$n \;\rightarrow\; p + e + \bar{\nu}_e\,, \tag{31a}$$

$$p + e \;\rightarrow\; n + \nu_e\,. \tag{31b}$$

The first of these processes is the usual *β-decay*, the second is sometimes called *inverse β-decay* or *electron capture*. We shall assume that the neutrino chemical potential vanishes, $\mu_{\nu_e} = 0$. This is equivalent to assuming that neutrinos and antineutrinos, once created by the above processes, simply leave the system without further interaction. This assumption is justified for compact stars since the neutrino mean free path is of the order of the size of the star or larger (except for the very early stages in the life of the star). Consequently, β-equilibrium, i.e., equilibrium with respect to the processes (31), translates into the following constraint for the chemical potentials,

$$\mu_n = \mu_p + \mu_e\,. \tag{32}$$

Inserting Eq. (25) into this constraint yields

$$\sqrt{k_{F,n}^2 + m_n^2} = \sqrt{k_{F,p}^2 + m_p^2} + \sqrt{k_{F,e}^2 + m_e^2}\,. \tag{33}$$

We can eliminate the electron Fermi momentum with the help of Eq. (30) and solve this equation to obtain the proton Fermi momentum as a function of the neutron Fermi momentum,

$$k_{F,p}^2 = \frac{(k_{F,n}^2 + m_n^2 - m_e^2)^2 - 2(k_{F,n}^2 + m_n^2 + m_e^2)m_p^2 + m_p^4}{4(k_{F,n}^2 + m_n^2)}\,. \tag{34}$$

---

[3] In fact, a compact star has to be electrically neutral to a very high accuracy, as one can see from the following simple estimate. Suppose the star has an overall charge of Z times the elementary charge, Ze, and we consider the Coulomb repulsion of a test particle, say a proton, with mass m and charge e (e having the same sign as the hypothetical overall charge of the star Ze). The Coulomb force, seeking to expel the test particle, has to be smaller than the gravitational force, seeking to keep the test particle within the star. This gives the condition

$$\frac{(Ze)e}{R^2} \leq \frac{GMm}{R^2}\,, \tag{26}$$

with the mass M and radius R of the star. Even if we are generous with the limit on the right-hand side by assigning the upper limit $M < Am$ to the mass of the star (if the star contains A nucleons, its total mass will be less than Am due to the gravitational binding energy), we will get a very restrictive limit on the overall charge. Namely, we find

$$\frac{(Ze)e}{R^2} < \frac{GAm^2}{R^2} \qquad \Rightarrow \qquad Z < G\frac{m^2}{e^2}\,A\,. \tag{27}$$

With the proton mass $m \sim 10^3$ MeV, the elementary charge $e^2 \sim 10^{-1}$ (remember $\alpha = e^2/(4\pi) \simeq 1/137$), and the gravitational constant $G \sim 7 \cdot 10^{-39}\,\mathrm{GeV}^{-2}$, we estimate

$$Z < 10^{-37}A\,, \tag{28}$$

i.e., the average charge per nucleon has to be extremely small in order to ensure the stability of the star. Since we have found such an extremely small number, it is irrelevant for the argument whether we use a proton or an electron as a test particle. The essence of this argument is the weakness of gravitation compared to the electromagnetic interactions: a tiny electric charge per unit volume, distributed over the star, is sufficient to overcome the stability from gravity.

To illustrate the physical meaning of this relation, let us consider some limit cases. First assume a vanishing proton contribution, $k_{F,p} = 0$. Then the equation gives (which is most easily seen from Eq. (33))

$$k_{F,n}^2 = (m_p + m_e)^2 - m_n^2 < 0\,. \tag{35}$$

This expression is negative because the neutron is slightly heavier than the electron and the proton together, $m_p \simeq 938.3\,\mathrm{MeV}$, $m_n \simeq 939.6\,\mathrm{MeV}$, $m_e \simeq 0.511\,\mathrm{MeV}$. Therefore, $k_{F,p} = 0$ is impossible and there always has to be at least a small fraction of protons. Now let's assume $k_{F,n} = 0$, which leads to

$$k_{F,p}^2 = \left(\frac{m_n^2 + m_e^2 - m_p^2}{2m_n}\right)^2 - m_e^2 \simeq 1.4\,\mathrm{MeV}^2\,. \tag{36}$$

This is the threshold below which there are no neutrons and the charge neutral system in β-equilibrium contains only protons and electrons of equal number density.

In general, we may consider a given baryon density $n_B = n_n + n_p$ to express the neutron Fermi momentum as

$$k_{F,n} = (3\pi^2 n_B - k_{F,p}^3)^{1/3}\,. \tag{37}$$

Inserting this into Eq. (34) yields an equation for $k_{F,p}$ as a function of the baryon density. In the ultrarelativistic limit, i.e., neglecting all masses, Eq. (34) obviously yields $k_{F,p} = k_{F,n}/2$ and thus $n_p = n_n/8$ or

$$n_p = \frac{n_B}{9}\,. \tag{38}$$

One can check that this limit is approached from below, i.e., in a compact star containing nuclear matter we deal with neutron-rich matter, which justifies the term neutron star.

As a crude approximation we may thus consider the simple case of pure neutron matter. We also consider the nonrelativistic limit, $m_n \gg k_{F,n}$. In this case, the energy density (21b) and the pressure (22) become

$$\epsilon \;\simeq\; \frac{m_n^4}{3\pi^2}\left[\frac{k_{F,n}^3}{m_n^3} + \mathcal{O}\left(\frac{k_{F,n}^5}{m_n^5}\right)\right]\,, \tag{39a}$$

$$P \;\simeq\; \frac{m_n^4}{15\pi^2}\left[\frac{k_{F,n}^5}{m_n^5} + \mathcal{O}\left(\frac{k_{F,n}^7}{m_n^7}\right)\right]\,. \tag{39b}$$

(To see this, note that the ln term cancels the term linear in k_F in the case of ϵ, and the linear and cubic terms in k_F in the case of P.) Consequently, keeping the terms to lowest order in $k_{F,n}/m_n$,

$$P(\epsilon) \simeq \left(\frac{3\pi^2}{m_n}\right)^{5/3} \frac{\epsilon^{5/3}}{15 m_n \pi^2}\,. \tag{40}$$

We have thus found a particularly simple equation of state, where the pressure is given by a power of the energy density. The general (numerical) discussion of the equation of state, including protons and electrons, is left to the reader, see problem II.1.

The next step to obtain the mass-radius relation of the star is to insert the equation of state into the TOV equation. The simplest case is a power-law behavior as in Eq. (40). The general form of such a so-called "polytropic" equation of state is

$$P(\epsilon) = K\,\epsilon^\gamma\,. \tag{41}$$

Using the Newtonian form of the mass-radius equations, Eqs. (13), this yields

$$\frac{dm}{dr} \;=\; \frac{4\pi}{K^{1/\gamma}}\, r^2 P^{1/\gamma}(r)\,, \tag{42}$$

$$\frac{dP}{dr} \;=\; -\frac{G}{K^{1/\gamma}}\,\frac{P^{1/\gamma}(r) m(r)}{r^2}\,. \tag{43}$$

Even in this simplest example, we need to solve the equations numerically, see problem II.2. The results of this problem show that the maximum mass reached within this model is about $M < 0.7 M_\odot$ which is well below observed neutron star masses. (See also Refs. [12–14] for a pedagogical introduction into the equation of state and mass-radius relation from solving the TOV equation.) This small maximum mass is a consequence of the assumption of noninteracting nucleons. Taking into account interactions will increase the maximum mass significantly.

B. Noninteracting quark matter

Whenever we talk about quark matter in these lectures we ignore the charm (c), bottom (b), and top (t) quarks. The quark chemical potential inside the star is at most of the order of 500 MeV and thus much too small to create a population of these states. Therefore, we only consider at most three quark flavors, namely up (u), down (d), and strange (s). We shall mostly neglect the masses of the u and d quarks; their *current masses* are $m_u \simeq m_d \simeq 5\,\mathrm{MeV} \ll \mu \simeq (300-500)\,\mathrm{MeV}$. The mass of the strange quark, however, is not negligible. The current strange quark mass is $m_s \simeq 90\,\mathrm{MeV}$, and the density-dependent *constituent mass* can be significantly larger, making it non-negligible compared to the quark chemical potential.

If we consider free quarks, the energy density ϵ, the number density n, and the pressure P, are obtained in the same way as demonstrated for nucleons in the previous subsection. We only have to remember that there are three colors for each quark flavor, $N_c = 3$, i.e., the degeneracy factor for a single quark flavor is $2N_c = 6$, where the factor 2 counts the spin degrees of freedom. Consequently, for each quark flavor $f = u, d, s$ we have at zero temperature (cf. Eqs. (21), (22)),

$$n_f = \frac{k_{F,f}^3}{\pi^2}\,, \tag{44a}$$

$$\epsilon_f = \frac{3}{\pi^2}\int_0^{k_{F,f}} dk\, k^2 \sqrt{k^2+m_f^2}\,, \tag{44b}$$

$$P_f = \frac{3}{\pi^2}\int_0^{k_{F,f}} dk\, k^2 \left(\mu_f - \sqrt{k^2+m_f^2}\right)\,. \tag{44c}$$

Again, we need to impose equilibrium conditions with respect to the weak interactions. In the case of three-flavor quark matter, the relevant processes are the leptonic processes (including a neutrino or an antineutrino)

$$d \to u + e + \bar{\nu}_e\,, \qquad s \to u + e + \bar{\nu}_e\,, \tag{45a}$$

$$u + e \to d + \nu_e\,, \qquad u + e \to s + \nu_e\,, \tag{45b}$$

and the non-leptonic process

$$s + u \leftrightarrow d + u\,. \tag{46}$$

These processes yield the following conditions for the quark and electron chemical potentials,

$$\mu_d = \mu_e + \mu_u\,, \qquad \mu_s = \mu_e + \mu_u\,. \tag{47}$$

(This automatically implies $\mu_d = \mu_s$.) The charge neutrality condition can be written in a general way as

$$\sum_{f=u,d,s} q_f n_f - n_e = 0\,, \tag{48}$$

with the electric quark charges

$$q_u = \frac{2}{3}\,, \qquad q_d = q_s = -\frac{1}{3}\,, \tag{49}$$

and the electron density n_e.

1. Strange quark matter hypothesis

Before computing the equation of state, we discuss the *strange quark matter hypothesis* within the so-called *bag model*. The bag model is a very crude phenomenological way to incorporate confinement into the description of quark matter. The effect of confinement is needed in particular if we compare quark matter with nuclear matter (which is ultimately what we want to do in this section). Put another way, although we speak of noninteracting quarks, we need to account for a specific – in general very complicated – aspect of the interaction, namely confinement.

To understand how the bag constant accounts for confinement, we compare the pressure of a noninteracting gas of massless pions with the pressure of a noninteracting gas of quarks and gluons at finite temperature and zero chemical

potential. The pressure of a single bosonic degree of freedom at $\mu = 0$ and at large temperatures compared to the mass of the boson is

$$P_{\text{boson}} \simeq -T \int \frac{d^3\mathbf{k}}{(2\pi)^3} \ln\left(1 - e^{-k/T}\right) = \frac{\pi^2 T^4}{90} \,. \tag{50}$$

This is derived in appendix A 1 within thermal field theory, see Eq. (A37). Analogously, a single fermionic degree of freedom gives (see Eq. (A72) of appendix A 2)

$$P_{\text{fermion}} \simeq T \int \frac{d^3\mathbf{k}}{(2\pi)^3} \ln\left(1 + e^{-k/T}\right) = \frac{7}{8} \frac{\pi^2 T^4}{90} \,. \tag{51}$$

Therefore, since there are three types of pions, their pressure is

$$P_\pi = 3 \, \frac{\pi^2 T^4}{90} \,. \tag{52}$$

This is a simple approximation for the pressure of the confined phase. In the deconfined phase, the degrees of freedom are gluons (8×2) and quarks ($4 N_c N_f = 24$). Thus with $2 \times 8 + 7/8 \times 24 = 37$ we have

$$P_{q,g} = 37 \, \frac{\pi^2 T^4}{90} - B \,, \tag{53}$$

where the *bag constant* B has been subtracted for the following reason. If B were zero, the deconfined phase would have the larger pressure and thus would be preferred for all temperatures. We know however, that at sufficiently small temperatures, the confined phase (that's the world we live in) must be preferred. This is phenomenologically accounted for by the bag constant B which acts like an energy penalty for the deconfined phase. Without this penalty, at least in this very simply model description, the deconfined phase would be "too favorable" compared to what we observe. As a consequence, by including the bag constant there is certain critical temperature T_c below which the confined phase is preferred, $P_\pi > P_{q,g}$, and above which the deconfined phase is preferred, $P_{q,g} > P_\pi$. This is indeed what one expects from QCD, where the deconfinement transition temperature is expected to be in the range of $T_c \simeq 170\,\text{MeV}$. (As can be seen in the QCD phase diagram in Fig. 1, this deconfinement transition is rather expected to be a crossover than a phase transition in the strict sense.)

In the context of compact stars we are not interested in such large temperatures. In this case, the chemical potential is large and the temperature practically zero. Nevertheless we compare nuclear (confined) with quark (deconfined) matter and thus have to include the bag constant in the pressure and the free energy of quark matter,

$$P + B \;=\; \sum_f P_f \,, \tag{54a}$$

$$\epsilon \;=\; \sum_f \epsilon_f + B \,. \tag{54b}$$

This phenomenological model of confinement is called the *bag model* [15, 16] because the quarks are imagined to be confined in a bag. One can view the microscopic pressure $\sum_f P_f$ of the quarks to be counterbalanced by the pressure of the bag B and an external pressure P.

Equipped with the bag model, we can now explain the strange quark matter hypothesis. For simplicity we consider massless quarks. A nonzero strange quark mass will slightly change the results but is not important for the qualitative argument. We will also ignore electrons. They are not present in three-flavor massless quark matter at zero temperature. They are however required in two-flavor quark matter to achieve electric neutrality. But also in this case their population is small enough to render their effect unimportant for the following argument.

With $m_f = 0$ we simply have

$$n_f = \frac{\mu_f^3}{\pi^2} \,, \qquad \epsilon_f = \frac{3\mu_f^4}{4\pi^2} \,, \qquad P_f = \frac{\mu_f^4}{4\pi^2} \,, \tag{55}$$

which in particular implies

$$P_f = \frac{\epsilon_f}{3} \,. \tag{56}$$

For the strange quark matter hypothesis we consider the energy E per nucleon number A,

$$\frac{E}{A} = \frac{\epsilon}{n_B} \,, \tag{57}$$

where n_B is the baryon number density, given in terms of the quark number densities as

$$n_B = \frac{1}{3}\sum_f n_f \,, \tag{58}$$

because a baryon contains $N_c = 3$ quarks. At zero pressure, $P = 0$, Eqs. (54) and (56) imply $\epsilon = 4B$ and thus

$$\frac{E}{A} = \frac{4B}{n_B} \,. \tag{59}$$

We now apply this formula first to three-flavor quark matter ("strange quark matter"), then to two-flavor quark matter of only up and down quarks. For strange quark matter, the neutrality constraint (48) becomes

$$2n_u - n_d - n_s = 0 \,. \tag{60}$$

Together with the conditions from chemical equilibrium (47) this implies

$$\mu_u = \mu_d = \mu_s \equiv \mu \,. \tag{61}$$

We see that strange quark matter is particularly symmetric. The reason is that the electric charges of an up, down, and strange quark happen to add up to zero. Now with $n_B = \mu^3/\pi^2$ and

$$B = \sum_f P_f = \frac{3\mu^4}{4\pi^2} \tag{62}$$

(still everything at $P = 0$) we have

$$\left.\frac{E}{A}\right|_{N_f=3} = (4\pi^2)^{1/4}\, 3^{3/4}\, B^{1/4} \simeq 5.714\, B^{1/4} \simeq 829\,\mathrm{MeV} B_{145}^{1/4} \,. \tag{63}$$

We have expressed $B^{1/4}$ in units of 145 MeV for reasons that will become clear below, $B_{145}^{1/4} \equiv B^{1/4}/(145\,\mathrm{MeV})$.

For two-flavor quark matter (neglecting the contribution of electrons), the charge neutrality condition is

$$n_d = 2n_u \,. \tag{64}$$

Hence,

$$\mu_d = 2^{1/3}\mu_u \,. \tag{65}$$

Then, with $n_B = \mu_u^3/\pi^2$ and

$$B = \sum_f P_f = \frac{(1+2^{4/3})\mu_u^4}{4\pi^2} \,, \tag{66}$$

we find

$$\left.\frac{E}{A}\right|_{N_f=2} = (4\pi^2)^{1/4}\,(1+2^{4/3})^{3/4}\, B^{1/4} \simeq 6.441\, B^{1/4} \simeq 934\,\mathrm{MeV} B_{145}^{1/4} \,. \tag{67}$$

By comparing this to Eq. (63) we see that two-flavor quark matter has a larger energy per baryon number than three-flavor quark matter. This is a direct consequence of the Pauli principle: adding one particle species (and keeping the total number of particles fixed) means opening a set of new available low-energy states that can be filled, thus lowering the total energy of the system.

We can now compare the results (63) and (67) with the energy per nucleon in nuclear matter. For pure neutron matter, it is simply given by the neutron mass,

$$\left.\frac{E}{A}\right|_{\text{neutrons}} = m_n = 939.6\,\mathrm{MeV} \,. \tag{68}$$

For iron, ^{56}Fe, it is

$$\left.\frac{E}{A}\right|_{^{56}\mathrm{Fe}} = \frac{56\, m_N - 56 \cdot 8.8\,\mathrm{MeV}}{56} = 930\,\mathrm{MeV}\,, \tag{69}$$

with the nucleon mass $m_N = 938.9\,\mathrm{MeV}$ and the binding energy per nucleon in iron of 8.8 MeV. Since we observe iron rather than deconfined quark matter, we know that

$$\left.\frac{E}{A}\right|_{^{56}\mathrm{Fe}} < \left.\frac{E}{A}\right|_{N_f=2} \quad \Rightarrow \qquad B^{1/4} > 144.4\,\mathrm{MeV}\,. \tag{70}$$

We have thus found a lower limit for the bag constant from the stability of iron with respect to two-flavor quark matter. Now what if the bag constant were only slightly larger than this lower limit? What if it were small enough for three-flavor quark matter to have lower energy than iron? The condition for this would be

$$\left.\frac{E}{A}\right|_{N_f=3} < \left.\frac{E}{A}\right|_{^{56}\mathrm{Fe}} \quad \Rightarrow \qquad B^{1/4} < 162.8\,\mathrm{MeV}\,. \tag{71}$$

This would imply that strange quark matter is absolutely stable, while nuclear matter is metastable. This possibility, which would be realized by a bag constant in the window $145\,\mathrm{MeV} < B^{1/4} < 162\,\mathrm{MeV}$, is called *strange quark matter hypothesis*, suggested by Bodmer [17] and Witten [18], see also [19].

Note that the existence of ordinary nuclei does *not* rule out the strange quark matter hypothesis. The conversion of an ordinary nucleus into strange quark matter requires the simultaneous conversion of many (roughly speaking A many) u and d quarks into s quarks. Since this has to happen via the weak interaction, it is practically impossible. In other words, there is a huge energy barrier between the metastable (if the hypothesis is true) state of nuclear matter and absolutely stable strange quark matter. This means that strange quark matter has to be created in another way ("going around" the barrier), by directly forming a quark-gluon plasma. This can for instance happen in a heavy-ion collision. Or, more importantly in our context, it may happen in the universe, giving rise to stars made entirely out of quark matter, so-called *strange stars*.

Small "nuggets" of strange quark matter are called *strangelets* (a strange star would then in some sense simply be a huge strangelet). If a strangelet is injected into an ordinary compact star (a neutron star), it would, assuming the strange quark matter hypothesis to be true, be able to "eat up" the nuclear matter, converting the neutron star into a strange star. Note the difference between this transition and the above described impossible transition from ordinary nuclear matter to strange quark matter: once there is a sufficiently large absolutely stable strangelet, *successive* conversion of up and down quarks into strange quarks increase the size of the strangelet; the energy barrier originating from the *simultaneous* creation of a large number of strange quarks now cannot cause the system to relax back into its original nuclear (metastable) state. This argument has important consequences. If there exist enough sizable strangelets in the universe to hit neutron stars, *every* neutron star would be converted into a strange star. In other words, the observation of a single ordinary neutron star would rule out the strange quark matter hypothesis. Therefore, it is important to understand whether there are enough strangelets around. It has been discussed recently in the literature that there may not be enough strangelets [20], in contrast to what was assumed before.

2. Equation of state

Next we derive the equation of state for strange quark matter. We include the effect of the strange quark mass to lowest order and also include electrons. It is convenient to express the quark chemical potentials in terms of an average quark chemical potential $\mu = (\mu_u + \mu_d + \mu_s)/3$ and the electron chemical potential μ_e,

$$\mu_u = \mu - \frac{2}{3}\mu_e\,, \tag{72a}$$

$$\mu_d = \mu + \frac{1}{3}\mu_e\,, \tag{72b}$$

$$\mu_s = \mu + \frac{1}{3}\mu_e\,. \tag{72c}$$

Written in this form, the conditions from β-equilibrium (47) are automatically fulfilled. Taking into account the strange quark mass, the Fermi momenta for the approximately massless up and down quark and the massive strange

quark are given by

$$k_{F,u} = \mu_u \,, \tag{73a}$$
$$k_{F,d} = \mu_d \,, \tag{73b}$$
$$k_{F,s} = \sqrt{\mu_s^2 - m_s^2} \,. \tag{73c}$$

The energy density and the pressure are

$$\sum_{i=u,d,s,e} \epsilon_i = \frac{3\mu_u^4}{4\pi^2} + \frac{3\mu_d^4}{4\pi^2} + \frac{3}{\pi^2}\int_0^{k_{F,s}} dk\, k^2 \sqrt{k^2+m_s^2} + \frac{\mu_e^4}{4\pi^2} \,, \tag{74a}$$

$$\sum_{i=u,d,s,e} P_i = \frac{\mu_u^4}{4\pi^2} + \frac{\mu_d^4}{4\pi^2} + \frac{3}{\pi^2}\int_0^{k_{F,s}} dk\, k^2 \left(\mu_s - \sqrt{k^2+m_s^2}\right) + \frac{\mu_e^4}{12\pi^2} \,, \tag{74b}$$

where we have neglected the electron mass. The neutrality condition can now be written as

$$0 = \frac{\partial}{\partial \mu_e} \sum_{i=u,d,s,e} P_i = -\frac{2}{3} n_u + \frac{1}{3} n_d + \frac{1}{3} n_s + n_e \,. \tag{75}$$

(Note that μ_e is defined as the chemical potential for *negative* electric charge.) Solving this equation to lowest order in the strange quark mass yields

$$\mu_e \simeq \frac{m_s^2}{4\mu} \,. \tag{76}$$

Consequently, the quark Fermi momenta become

$$k_{F,u} \simeq \mu - \frac{m_s^2}{6\mu} \,, \tag{77a}$$
$$k_{F,d} \simeq \mu + \frac{m_s^2}{12\mu} \,, \tag{77b}$$
$$k_{F,s} \simeq \mu - \frac{5m_s^2}{12\mu} \,. \tag{77c}$$

We see that the Fermi momenta are split by an equal distance of $m_s^2/(4\mu)$, and $k_{F,s} < k_{F,u} < k_{F,d}$, see Fig. 2. The splitting and the order of the Fermi momenta can be understood from the following physical picture: start from the symmetric situation $m_s = \mu_e = 0$. In this case, all quark flavors fill their Fermi spheres to a common Fermi momentum given by μ, and the system is neutral. Now switch on the strange quark mass. This lowers the Fermi momentum of the strange quark according to Eq. (73c). Consequently, there are fewer strange quarks in the system and thus there is a lack of negative charge. To counterbalance this missing negative charge, the system responds by switching on a chemical potential μ_e. Because of β-equilibrium, the Fermi momenta of all quark flavors are rigidly coupled to this change. Electric neutrality is regained by lowering the up quark Fermi momentum and raising the down and strange quark Fermi momenta. Since the strange quark Fermi momentum was already lowered by the finite mass, it is clear that the resulting order is $k_{F,s} < k_{F,u} < k_{F,d}$. The electron contribution to the negative charge density is negligibly low, $n_e \propto \mu_e^3 \propto m_s^6/\mu^3$, while the contribution of the quarks due to the strange quark mass is proportional to μm_s^2. The splitting of the Fermi momenta due to the effects of the strange quark mass, β-equilibrium, and electric neutrality is very important in the context of *color superconductivity*. Since color superconductivity is usually based on Cooper pairing of quarks of different flavor, a mismatch in Fermi surfaces tends to disfavor this pairing. We shall discuss superconductivity in quark and nuclear matter in chapter IV and give a brief qualitative discussion of the consequences of Fermi surface splitting for color superconductivity at the end of that chapter.

Here we continue with unpaired quark matter and insert the result for μ_e (76) back into the energy density and the pressure. Again keeping only terms to lowest order in the strange quark mass yields

$$\sum_i \epsilon_i \simeq \frac{9\mu^4}{4\pi^2} - \frac{3\mu^2 m_s^2}{2\pi^2} \,, \tag{78a}$$

$$\sum_i P_i \simeq \frac{3\mu^4}{4\pi^2} - \frac{3\mu^2 m_s^2}{4\pi^2} \,. \tag{78b}$$

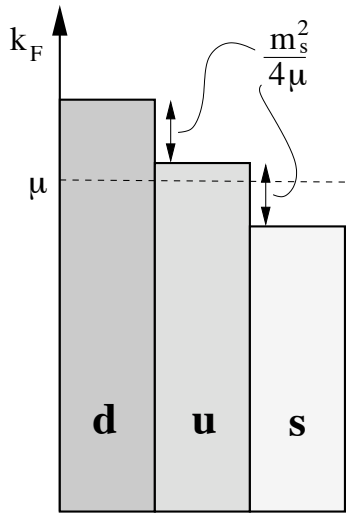

FIG. 2: Illustration of the Fermi momenta for neutral, unpaired quark matter in β-equilibrium with quark chemical potential μ. The splitting of the Fermi momenta is due to the strange quark mass m_s which is assumed to be small compared to μ.

Consequently,

$$\sum_i \epsilon_i \simeq 3\sum_i P_i + \frac{3\mu^2 m_s^2}{2\pi^2}\,. \tag{79}$$

With Eq. (54a) the pressure, including the bag constant, becomes

$$P \simeq \frac{3\mu^4}{4\pi^2} - \frac{3\mu^2 m_s^2}{4\pi^2} - B\,, \tag{80}$$

and, expressing P in terms of the energy density, we obtain with the help of Eq. (54b)

$$P \simeq \frac{\epsilon - 4B}{3} - \frac{\mu^2 m_s^2}{2\pi^2}\,. \tag{81}$$

This is the equation of state of noninteracting, unpaired strange quark matter within the bag model with strange quark mass corrections to lowest order.

C. Mass-radius relation including interactions

Let us briefly discuss the results for the mass-radius relation of a compact star for given equations of state for nuclear and quark matter. Since the underlying calculations in general are complicated and have to be done on a computer, we only quote some results to illustrate the physical conclusions. So far we have only discussed the simplest cases of noninteracting matter. Interactions have a significant effect on both the equation of state and the mass-radius relation. We now discuss these effects briefly, only in the subsequent chapters shall we study the nature and details of these interactions (and discuss their relevance to other observables than the mass and the radius of the star).

The maximum mass of a star for noninteracting nuclear matter is $\sim 0.7 M_\odot$ (see for instance Ref. [14] or solve problem II.2); including interactions increases the mass to values well above $2M_\odot$. The significance of the equation of state and interactions for the maximum mass is easy to understand: if the pressure $P(\epsilon)$ for a given energy density ϵ is large, the system is able to sustain a large gravitational force that seeks to compress it. Comparing two equations of state over a given energy density range, the one with the larger pressure (for all energy densities in the given range) is thus termed stiff, the one with the smaller pressure is termed soft. Soft equations of state can sustain less gravitational force and thus lead to stars with lower maximum masses. In the case of noninteracting nuclear matter, it is only the Fermi pressure from the Pauli exclusion principle that prevents the star from the collapse. Interactions increase this pressure because the dominant effect in the case of nuclear matter at the relevant densities is the short-range repulsion between the nucleons. Therefore, the maximum mass is significantly larger in this case.

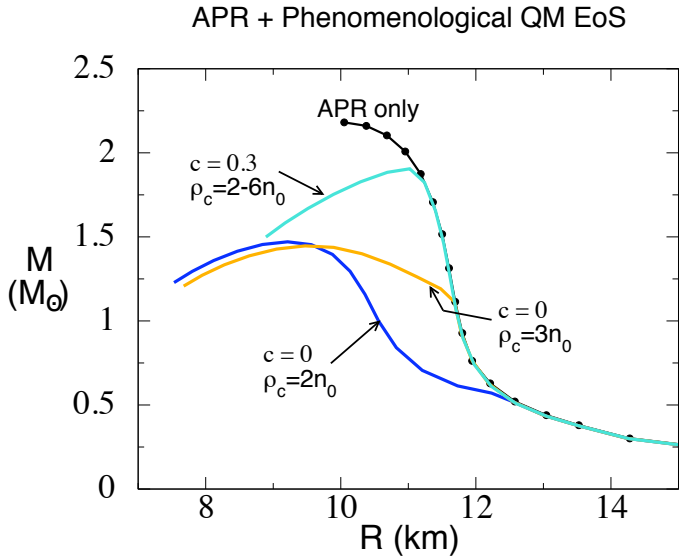

FIG. 3: Mass-radius plot from Ref. [22] which shows the dependence of the mass-radius curve on the (uncertain) parameters of the quark matter equation of state in a hybrid star. We see that reasonable choices of the parameters lead to similar curves as for nuclear matter (here with the APR equation of state). In this plot, the transition density ρ_c (in units of the nuclear ground state density n_0) between quark matter and nuclear matter has been used as a parameter, rather than the bag constant. From our discussion it is clear that one can be translated into the other. The coefficient c describes QCD corrections to the quark Fermi momentum and thus to the μ^4 term in the pressure, see Eq. (82).

In Figs. 3 and 4 several models for the nuclear equation of state are applied to obtain maximum masses up to $2.4\,M_\odot$. For the case of quark matter, we can understand some of the corrections through interactions in the following simple way. A generalization of the pressure (80) is

$$P = \frac{3\mu^4}{4\pi^2}(1-c) - \frac{3\mu^2}{4\pi^2}(m_s^2 - 4\Delta^2) - B\,. \tag{82}$$

This equation contains two corrections compared to Eq. (80). One is included in the coefficient c and originates from the (leading order) correction of the Fermi momentum due to the QCD coupling α_s,

$$p_F = \mu\left(1 - \frac{2\alpha_s}{3\pi}\right)\,, \tag{83}$$

resulting in a correction of the μ^4 term in the pressure with $c = 2\alpha_s/\pi$. (This modification of the Fermi momentum will also become important in the context of neutrino emissivity in chapter V.) Higher order calculations suggest $c \gtrsim 0.3$ at densities relevant for compact stars. However, the exact value of c is unknown because perturbative calculations are not valid in the relevant density regime, cf. discussion in Sec. I A. Therefore, c can only be treated as a parameter with values around 0.3, as done for example in Fig. 3. To get an idea about perturbative calculations beyond leading order in α_s, you may consult the recent Ref. [21].

The second correction in Eq. (82) is the quantity Δ. This is the energy gap arising from color superconductivity whose microscopic origin we discuss in chapter IV. It gives a correction to the μ^2 term in the pressure. One might think that this correction is negligible compared to the μ^4 term and the bag constant. However, it turns out that for reasonable values of the bag constant these two terms largely cancel each other and the μ^2 term becomes important. However, the effect of superconductivity is still hard to determine. Firstly, it would require a precise knowledge of the strange quark mass. Secondly, it turns out that the maximum mass of a hybrid star is not very sensitive to the value of $m_s^2 - 4\Delta^2$ [22].

As a result of this discussion and the results in Figs. 3 and 4, two points are important for the further contents of these lectures. Firstly, we should now be motivated to learn more about the nature and the consequences of interactions in nuclear and quark matter. Secondly, we have learned that, given our ignorance of the precise quantitative effects of the strong interaction and the uncertainty in astrophysical observations, the mass and the radius of the star are not sufficient to distinguish between a neutron star, a hybrid star, and possibly a quark star. Therefore, we also have to take into account other observables which are linked to the microscopic physics. While the equation of state is a

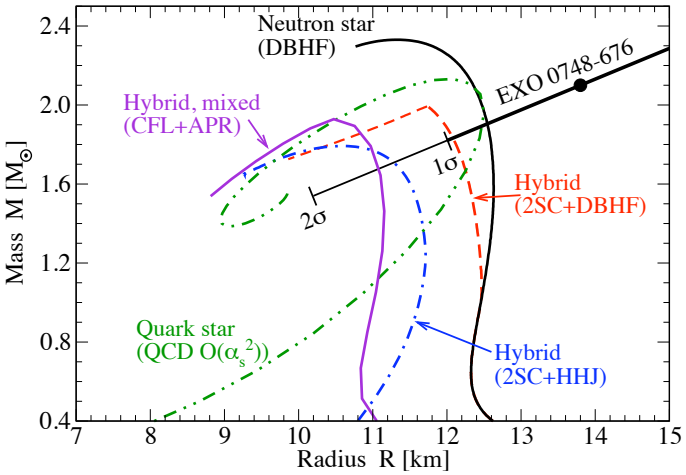

FIG. 4: Mass-radius plot from Ref. [23]. A comparison of a neutron star, different hybrid stars, and a quark star is shown, using several nuclear equations of state (DBHF, APR, HHJ) and several quark phases (CFL, 2SC). For more details and explanations of the various abbreviations, see Ref. [23].

bulk property, i.e., it is determined by the whole Fermi sea, there are other phenomena which are only sensitive to the low-energy excitations at the Fermi surface. One class of such phenomena is given by transport properties. They can possibly be related to observables which are more restrictive than mass and radius for the question of the matter composition of the star. We shall discuss such observables in chapter V where we relate the cooling of the star to neutrino emissivity, and in chapter VI where we qualitatively discuss other such observables.

Problems

II.1 **Equation of state for non-interacting nuclear matter**

Find the full equation of state for noninteracting n, p, e matter at $T = 0$ numerically by plotting P versus ϵ. You should see the onset of neutrons and identify a region where the equation of state is well approximated by the power-law behavior of pure neutron matter in the nonrelativistic limit, Eq. (40).

II.2 **Mass-radius relation**

(a) Solve equations (42) numerically (for nonrelativistic pure neutron matter, i.e., $\gamma = 5/3$) and plot $m(r)$, $P(r)$ for a given value of the pressure $P_0 = P(r = 0)$.
(b) Use P_0 as a parameter to find the mass-radius relation $M(R)$. To this end, you need to do (a) for several values of P_0 and find for each P_0 the radius R at which $P(R) = 0$ and the corresponding mass $M(R)$.
(c) You may incorporate general relativistic effects from the TOV equation (14) and/or the full (numerical) equation of state for noninteracting nuclear matter from Problem II.1.

III. BASIC MODELS AND PROPERTIES OF DENSE NUCLEAR MATTER

There are numerous models to describe cold and dense interacting nuclear matter. Some of them have been used to obtain the curves in Figs. 3 and 4. From these curves we see that the models may differ significantly in their predictions of the properties of neutron stars and hybrid stars. The reason is that they all are extrapolated into a regime where there is little theoretical control. In other words, for densities below the nuclear ground state density there are experimental data for instance from atomic nuclei or neutron scattering which serve to fit the parameters of the nuclear models unambiguously. However, it is very challenging to construct a model which reliably predicts the properties of nuclear matter for larger densities. Put another way, currently the only "experiments" in this density regime are astrophysical observations which themselves are naturally less controlled than experiments in the laboratory. Therefore, the state of the art in describing interacting nuclear matter at high densities is a competition between several models which all are prone to uncertainties. In these lectures we do not attempt to give an overview over these models. We rather focus on two basic models and discuss them in detail. The first is the Walecka model

and its extensions. The second is chiral perturbation theory, which is an effective model based on chiral symmetry of QCD and spontaneous breaking thereof in nuclear matter. We shall use it to discuss kaon condensation in nuclear matter.

To put the following in the perspective of understanding QCD, we should keep in mind that nucleons are ultimately built of quarks and gluons which are the fundamental degrees of freedom of the strong interactions. It is a highly nontrivial task to describe even the mass of a nucleon from quarks and gluons, let alone nuclear interactions. An important tool for such a case is an effective theory which has non-fundamental degrees of freedom, baryons and mesons instead of quarks and gluons. An effective theory can in principle be obtained by taking the low-energy limit of the underlying fundamental theory, in this case QCD. However, this procedure may turn out to be very difficult. Therefore, one tries to "guess" an effective theory, for instance guided by symmetry principles. One obtains a theory with some unknown parameters which have to be fit, for instance to experimental results. Once the parameters are fitted, one may extrapolate the theory beyond the regime where the fit has been done. In our case, this will be the high-density region for which we have no experiments in the laboratory. There is of course no guarantee that this extrapolation works. Models for interacting nuclear matter at high densities have to be understood in this spirit. Of course, an upper density limit for the validity is the deconfinement phase transition to a phase where quarks and gluons are the relevant degrees of freedom. This limit density is not precisely known but may well be reached in compact stars.

A. The Walecka model

The Walecka model contains nucleons which interact via the exchange of the scalar σ meson and the vector ω meson. The Lagrangian is

$$\mathcal{L} = \mathcal{L}_N + \mathcal{L}_{\sigma,\omega} + \mathcal{L}_I \,, \tag{84}$$

Here, the free nucleon Lagrangian is

$$\mathcal{L}_N = \bar{\psi}\left(i\gamma^\mu\partial_\mu - m_N + \mu\gamma^0\right)\psi \,, \tag{85}$$

where $\bar{\psi} \equiv \psi^\dagger\gamma^0$, and $\psi = \begin{pmatrix}\psi_n \\ \psi_p\end{pmatrix}$ with the neutron and proton spinors ψ_n and ψ_p. For a basic discussion of the field-theoretical treatment of noninteracting fermions, in particular the roles of finite temperature and chemical potential, see appendix A 2. The free mesonic Lagrangian is

$$\mathcal{L}_{\sigma,\omega} = \frac{1}{2}\left(\partial_\mu\sigma\partial^\mu\sigma - m_\sigma^2\sigma^2\right) - \frac{1}{4}\omega_{\mu\nu}\omega^{\mu\nu} + \frac{1}{2}m_\omega^2\omega_\mu\omega^\mu \,, \tag{86}$$

where $\omega_{\mu\nu} \equiv \partial_\mu\omega_\nu - \partial_\nu\omega_\mu$, and the interaction Lagrangian with Yukawa interactions between the nucleons and the mesons is

$$\mathcal{L}_I = g_\sigma\bar{\psi}\sigma\psi + g_\omega\bar{\psi}\gamma^\mu\omega_\mu\psi \,. \tag{87}$$

We shall consider isospin-symmetric matter, i.e., the masses and chemical potentials of protons and neutrons are assumed to be identical. In general, μ is a matrix $\mu = \mathrm{diag}(\mu_n, \mu_p) = \mathrm{diag}(\mu_B + \mu_I, \mu_B - \mu_I)$ with the baryon and isospin chemical potentials μ_B and μ_I. Thus, in other words, we assume the isospin chemical potential to vanish. We can then simply denote $\mu \equiv \mu_B = \mu_n = \mu_p$. Also the interactions between the nucleons are assumed to be symmetric, i.e., the nn, pp, and np interactions are identical. An isospin-asymmetry in the interactions can be included by adding ρ-meson exchange. We will briefly discuss this in Sec. III B. Also kaon condensation induces an asymmetry, discussed in Sec. III C.

The parameters of the model are the masses and the coupling constants. The masses are

$$m_N = 939\,\mathrm{MeV} \,, \qquad m_\omega = 783\,\mathrm{MeV} \,, \qquad m_\sigma = (500-600)\,\mathrm{MeV} \,. \tag{88}$$

The σ meson is in fact a broad resonance and thus we can only approximately assign a mass to this meson. Below we shall use $m_\sigma = 550\,\mathrm{MeV}$. The additional parameters are the coupling constants g_σ, g_ω. We shall discuss below how they are fixed.

In order to compute the equation of state, we need to consider the partition function

$$Z = \int \mathcal{D}\bar{\psi}\mathcal{D}\psi\mathcal{D}\sigma\mathcal{D}\omega \, \exp\int_X \mathcal{L} \,, \tag{89}$$

where we abbreviated

$$\int_X \equiv \int_0^\beta d\tau \int d^3x\,, \tag{90}$$

with the inverse temperature $\beta = 1/T$. We shall allow for vacuum expectation values of the mesons. To this end, we write the meson fields as a sum of the condensate and fluctuations,

$$\sigma \;\to\; \bar\sigma + \sigma\,, \tag{91a}$$
$$\omega_\mu \;\to\; \bar\omega_0\delta_{0\mu} + \omega_\mu\,, \tag{91b}$$

as explained in appendix A 1 for a general bosonic field. Now the simplest approximation is to neglect the fluctuations. This corresponds to the mean-field approximation. In this case the interaction between the nucleons and the mesons is simplified to a mesonic background, or mesonic mean field, which is seen by the nucleons. We can then simply drop all derivative terms of the mesons. As a consequence, the meson mean fields merely act as corrections to the nucleon mass and chemical potential, and we obtain the Lagrangian

$$\mathcal{L} = \bar\psi\left(i\gamma^\mu\partial_\mu - m_N^* + \mu^*\gamma_0\right)\psi - \frac{1}{2}m_\sigma^2\bar\sigma^2 + \frac{1}{2}m_\omega^2\bar\omega_0^2\,, \tag{92}$$

with

$$m_N^* \;\equiv\; m_N - g_\sigma\bar\sigma\,, \tag{93a}$$
$$\mu^* \;\equiv\; \mu - g_\omega\bar\omega_0\,. \tag{93b}$$

It is important to keep in mind that the actual chemical potential, associated with nucleon number is μ, not μ^*. This becomes important for the correct thermodynamic relations, see footnote before Eqs. (107). The new effective "chemical potential" μ^* nevertheless has physical meaning since it determines the Fermi energy as we shall see below.

The partition function now becomes

$$Z = e^{\frac{V}{T}\left(-\frac{1}{2}m_\sigma^2\bar\sigma^2+\frac{1}{2}m_\omega^2\bar\omega_0^2\right)}\int\mathcal{D}\bar\psi\mathcal{D}\psi\exp\int_X\bar\psi\left(i\gamma^\mu\partial_\mu - m_N^* + \mu^*\gamma_0\right)\psi\,. \tag{94}$$

The evaluation of the free fermionic part (with modified mass and chemical potential) is now straightforward and is done in detail in appendix A 2. Here we only repeat the most important steps. One first introduces the Fourier transforms

$$\psi(X) = \frac{1}{\sqrt{V}}\sum_K e^{-iK\cdot X}\psi(K)\,,\qquad \bar\psi(X) = \frac{1}{\sqrt{V}}\sum_K e^{iK\cdot X}\bar\psi(K)\,. \tag{95}$$

Our conventions are $K = (-i\omega_n, \mathbf{k})$, $X = (-i\tau, \mathbf{x})$, and $K\cdot X = k_0x_0 - \mathbf{k}\cdot\mathbf{x} = -(\omega_n\tau + \mathbf{k}\cdot\mathbf{x})$, with the fermionic Matsubara frequencies $\omega_n = (2n+1)\pi T$. Thus, after performing the X integral in the exponent one obtains

$$Z = e^{\frac{V}{T}\left(-\frac{1}{2}m_\sigma^2\bar\sigma^2+\frac{1}{2}m_\omega^2\bar\omega_0^2\right)}\int\mathcal{D}\psi^\dagger\mathcal{D}\psi\exp\left[-\sum_K\psi^\dagger(K)\frac{G^{-1}(K)}{T}\psi(K)\right]\,, \tag{96}$$

with the inverse nucleon propagator

$$G^{-1}(K) = -\gamma^\mu K_\mu - \gamma_0\mu^* + m_N^*\,. \tag{97}$$

Now using the standard formula for the functional integral over Grassmann variables one obtains

$$Z = e^{\frac{V}{T}\left(-\frac{1}{2}m_\sigma^2\bar\sigma^2+\frac{1}{2}m_\omega^2\bar\omega_0^2\right)}\det\frac{G^{-1}(K)}{T}\,, \tag{98}$$

where the determinant is taken over momentum space, Dirac space, and the (here trivial) neutron-proton space. Consequently,

$$\ln Z \;=\; \frac{V}{T}\left(-\frac{1}{2}m_\sigma^2\bar\sigma^2 + \frac{1}{2}m_\omega^2\bar\omega_0^2\right) + 4V\int\frac{d^3\mathbf{k}}{(2\pi)^3}\left[\frac{E_k}{T} + \ln\left(1+e^{-(E_k-\mu^*)/T}\right) + \ln\left(1+e^{-(E_k+\mu^*)/T}\right)\right]\,, \tag{99}$$

where we have performed the Matsubara sum and taken the thermodynamic limit, and where we have defined the single-nucleon energy

$$E_k = \sqrt{k^2 + (m_N^*)^2}\,. \tag{100}$$

The pressure then becomes

$$P = \frac{T}{V}\ln Z = -\frac{1}{2}m_\sigma^2\bar{\sigma}^2 + \frac{1}{2}m_\omega^2\bar{\omega}_0^2 + P_N\,, \tag{101}$$

with the nucleon pressure (after subtracting the vacuum part)

$$P_N \equiv 4T\int\frac{d^3\mathbf{k}}{(2\pi)^3}\left[\ln\left(1+e^{-(E_k-\mu^*)/T}\right)+\ln\left(1+e^{-(E_k+\mu^*)/T}\right)\right]. \tag{102}$$

We have thus derived the fermionic pressure already used in chapter II, see Eq. (20), from thermal field theory. The factor 4 counts the two spin degrees of freedom and the two baryon degrees of freedom (proton and neutron). We also have obtained the contribution of antiparticles, for which $\mu^* \to -\mu^*$.

The meson condensates have to be determined by maximizing the pressure. We obtain

$$0 = \frac{\partial P}{\partial\bar{\sigma}} = -m_\sigma^2\bar{\sigma} - g_\sigma\frac{\partial P_N}{\partial m_N^*}\,, \tag{103a}$$

$$0 = \frac{\partial P}{\partial\bar{\omega}_0} = m_\omega^2\bar{\omega}_0 - g_\omega\frac{\partial P_N}{\partial\mu^*}\,. \tag{103b}$$

In terms of the baryon and scalar densities

$$n_B = \langle\psi^\dagger\psi\rangle = \frac{\partial P_N}{\partial\mu} = \frac{\partial P_N}{\partial\mu^*} = 4\sum_{e=\pm}e\int\frac{d^3\mathbf{k}}{(2\pi)^3}\frac{1}{e^{(E_k-e\mu^*)/T}+1}\,, \tag{104a}$$

$$n_s = \langle\bar{\psi}\psi\rangle = -\frac{\partial P_N}{\partial m_N^*} = 4\sum_{e=\pm}\int\frac{d^3\mathbf{k}}{(2\pi)^3}\frac{m_N^*}{E_k}\frac{1}{e^{(E_k-e\mu^*)/T}+1}\,, \tag{104b}$$

we can write the equations for the condensates (103) as

$$\bar{\sigma} = \frac{g_\sigma}{m_\sigma^2}\,n_s\,, \tag{105a}$$

$$\bar{\omega}_0 = \frac{g_\omega}{m_\omega^2}\,n_B\,. \tag{105b}$$

It is useful to rewrite the first of these equations as an equation for the corrected mass m_N^* rather than for the condensate $\bar{\sigma}$,

$$m_N^* = m_N - \frac{g_\sigma^2}{m_\sigma^2}\,n_s\,, \tag{106}$$

where we have used Eq. (93a). We now take the zero temperature limit, $T \ll m_N, \mu$, which is justified since the temperatures of interest are at most of the order of 10 MeV, while the baryon chemical potentials are above 1 GeV. The Fermi distribution function then becomes a step function. In particular, all antiparticle contributions vanish. We obtain

$$P = \frac{1}{2}\frac{g_\omega^2}{m_\omega^2}\,n_B^2 - \frac{1}{2}\frac{g_\sigma^2}{m_\sigma^2}\,n_s^2 + \frac{1}{4\pi^2}\left[\left(\frac{2}{3}k_F^3 - (m_N^*)^2k_F\right)E_F^* + (m_N^*)^4\ln\frac{k_F+E_F^*}{m_N^*}\right], \tag{107a}$$

$$\epsilon = \frac{1}{2}\frac{g_\omega^2}{m_\omega^2}\,n_B^2 + \frac{1}{2}\frac{g_\sigma^2}{m_\sigma^2}\,n_s^2 + \frac{1}{4\pi^2}\left[\left(2k_F^3 + (m_N^*)^2k_F\right)E_F^* - (m_N^*)^4\ln\frac{k_F+E_F^*}{m_N^*}\right], \tag{107b}$$

where we have defined the Fermi energy

$$E_F^* = \mu^* = \sqrt{k_F^2 + (m_N^*)^2}\,, \tag{108}$$

and where the zero-temperature densities are

$$n_B = \frac{2k_F^3}{3\pi^2}\,, \tag{109a}$$

$$n_s = \frac{m_N^*}{\pi^2}\left[k_F E_F^* - (m_N^*)^2 \ln\frac{k_F + E_F^*}{m_N^*}\right]. \tag{109b}$$

Pressure and energy density in Eqs. (107)[4] define the equation of state which has to be determined numerically. We may discuss the limits of small ($k_F \to 0$) and large ($k_F \to \infty$) density analytically. For small density we find

$$n_s \simeq \frac{2k_F^3}{3\pi^2} = n_B\,, \tag{112}$$

neglecting terms of the order of $k_F^5/(m_N^*)^2 \ll k_F^3$ and higher. Therefore, from Eq. (106) we conclude

$$m_N^* \simeq m_N\,, \tag{113}$$

where we have suppressed terms of the order of $k_F^3/m_\sigma^2 \ll m_N$. The pressure and the energy density are, within this small-density approximation, dominated by the nucleonic pressure P_N,

$$P \simeq \frac{2k_F^5}{15\pi^2 m_N}\,, \qquad \epsilon \simeq \frac{2m_N k_F^3}{3\pi^2}\,. \tag{114}$$

Comparing with Eqs. (39) we see that we have exactly reproduced the noninteracting limit. This is no surprise because the only effect of the interactions in the present approach is the modification of μ and m_N. In the small-density limit these effects are negligible and we are back to the noninteracting result, where the equation of state has the form $P \propto \epsilon^{5/3}$.

For large k_F, on the other hand, we have

$$n_s \simeq \frac{m_N^* k_F^2}{\pi^2}\,, \tag{115}$$

and thus

$$m_N^* \simeq \frac{m_N}{1 + \frac{g_\sigma^2 k_F^2}{m_\sigma^2 \pi^2}}\,. \tag{116}$$

We see that the effective nucleon mass goes to zero for large densities. For general values of the Fermi momentum, the effective mass has to be computed numerically from Eqs. (106) and (109b), see Fig. 5.

At large densities, the nucleonic pressure P_N as well as the pressure from the scalar meson (which is proportional to n_s^2/m_σ^2) behave like k_F^4. Therefore, the total pressure is dominated by the vector meson contribution which is proportional to n_B^2/m_ω^2 and thus behaves like k_F^6,

$$P \simeq \epsilon \simeq \frac{1}{2}\frac{g_\omega^2}{m_\omega^2}\, n_B^2\,. \tag{117}$$

Consequently, the speed of sound approaches the speed of light at large densities,

$$c_s^2 \equiv \frac{\partial P}{\partial \epsilon} \simeq 1\,. \tag{118}$$

---

[4] One has to be careful with the thermodynamic relations in deriving the energy density (107b): remember that the actual chemical potential associated with baryon number n_B is μ, not μ^*. This means that the pressure at zero temperature can be written as $P = -\epsilon + \mu n_B$. The last term of the pressure (term in square brackets on the right-hand side of Eq. (107a)) comes from a term of the structure $-\epsilon_0 + \mu^* n_B$, cf. for instance Eq. (22). With $\mu^* = \mu - g_\omega \bar\omega_0$ and the expression for $\bar\omega_0$ in Eq. (105b) we can write this as

$$P = -\epsilon_0 + \mu^* n_B + \frac{1}{2}\frac{g_\omega^2}{m_\omega^2}\, n_B^2 - \frac{1}{2}\frac{g_\sigma^2}{m_\sigma^2}\, n_s^2 = -\left(\epsilon_0 + \frac{1}{2}\frac{g_\omega^2}{m_\omega^2}\, n_B^2 + \frac{1}{2}\frac{g_\sigma^2}{m_\sigma^2}\, n_s^2\right) + \mu n_B\,. \tag{110}$$

From this we can read off the energy density

$$\epsilon = \epsilon_0 + \frac{1}{2}\frac{g_\omega^2}{m_\omega^2}\, n_B^2 + \frac{1}{2}\frac{g_\sigma^2}{m_\sigma^2}\, n_s^2\,, \tag{111}$$

which yields Eq. (107b).

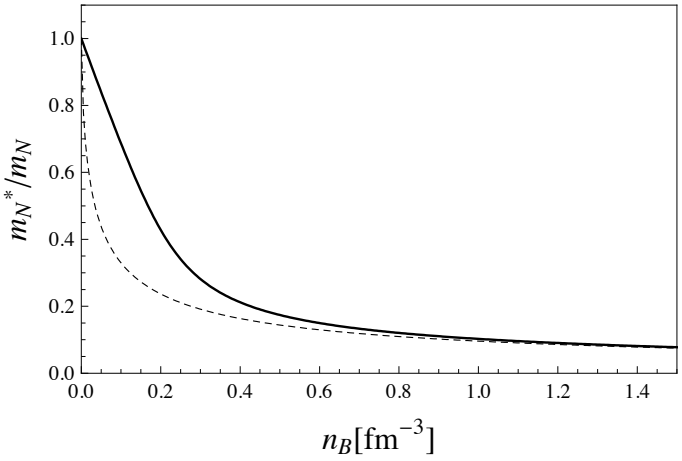

FIG. 5: Density-dependent effective nucleon mass m_N^* at $T = 0$ in the Walecka model in units of the zero-density mass m_N and as a function of the baryon density n_B. Solid line: full numerical result. Dashed line: high-density approximation from Eq. (116).

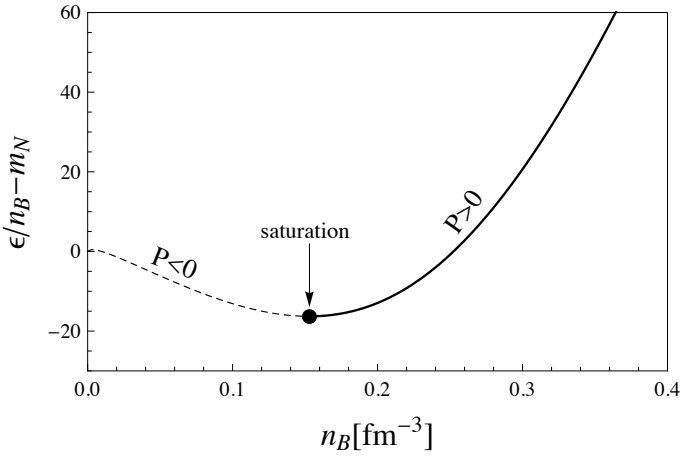

FIG. 6: Binding energy per nucleon at zero temperature in the Walecka model as a function of baryon density, obtained from computing the energy density with the density-modified nucleon mass. The binding energy has a minimum at which the pressure P is zero, i.e., at this point nuclear matter is self-bound, and the corresponding density is called *saturation density*. The two parameters of the model, namely the coupling constants g_σ and g_ω, are fixed such that the binding energy per nucleon is $E_0 = -16.3\,\mathrm{MeV}$ at the saturation density $n_0 = 0.153\,\mathrm{fm}^{-3}$.

So far, our model cannot be used quantitatively since we have not yet fixed the numerical values of the coupling constants. To do so one requires the model to reproduce the saturation density n_0 and the binding energy per nucleon at saturation E_0,

$$n_0 = 0.153\,\mathrm{fm}^{-3}\,, \qquad E_0 \equiv \left(\frac{\epsilon}{n_B} - m_N\right)_{n_B=n_0} = -16.3\,\mathrm{MeV}\,. \tag{119}$$

Note the difference between the binding energy in (infinite) nuclear matter and the binding energy in finite nuclei. The latter is $-8.8\,\mathrm{MeV}$ for iron, see Eq. (69).

We leave it as an exercise to compute the coupling constants from the values (119), see problem III.1. One obtains $g_\omega^2/(4\pi) = 14.717$ and $g_\sigma^2/(4\pi) = 9.537$. The result for the density-dependent binding energy with these values for the coupling constants is shown in Fig. 6. This figure shows that there is a finite density n_0 where the binding energy is minimal. This is a basic feature of nuclear matter which has to be reproduced by any physically meaningful model, reflecting the properties of the nuclear forces. It says in particular that if you add nucleons to a large nucleus the density will stay approximately constant because there is a preferred distance between the nucleons that minimizes

the energy. We have implicitly made use of this fact in our estimate of the nucleon number in a neutron star at the beginning of chapter II. In the limit of infinite symmetric nuclear matter and ignoring the Coulomb forces, this density at which the binding energy is minimal is $n_0 = 0.153\,\mathrm{fm}^{-3}$. It is called *saturation density*. At the saturation density nuclear matter is self-bound, i.e., it is stable at zero pressure. We have indicated in Fig. 6 that the minimum of the binding energy divides the stable density regime with positive pressure from the unstable regime with negative pressure. The behavior of the pressure follows from the thermodynamic relation $P = -\frac{\partial E}{\partial V}$, where E is the energy $E = \epsilon V$ and V the volume, which implies

$$P = n_B^2 \frac{\partial(\epsilon/n_B)}{\partial n_B}\,. \tag{120}$$

Consequently, at the minimum of ϵ/n_B as a function of n_B the system has zero pressure. Moreover, we see that a *decrease* in the binding energy per baryon number upon *increasing* the baryon number leads to a negative pressure. (At very small densities, barely visible in the plot, the energy also increases with density, i.e., $P > 0$. This is the regime where the nucleons are too far apart to feel their attraction; the increasing energy is then a consequence of the increasing kinetic energy.)

In our context of compact stars, the self-boundedness of nuclear matter implies that nuclear matter can exist at the surface of the star where the pressure vanishes. In the interior, the gravitational pressure compresses the matter to densities larger than n_0. As we see from the figure, this compressed matter, in turn, has itself positive pressure to counterbalance the pressure from gravity. This is the reason why the high-density part of the curve in Fig. 6 is relevant for astrophysical applications. We shall see in the next subsection why the Walecka model in the simple form discussed here cannot be trusted for densities much larger than n_0 and how the model can be improved to yield predictions for the high-density regime.

1. Including scalar interactions

The Walecka model accommodates important aspects of nuclear matter such as the existence of a saturation density whose realistic value is reproduced upon fitting the parameters of the model. We have already discussed on general grounds that extrapolations to high densities are uncontrolled, and thus the Walecka model (and all similar models of this kind) have to be improved in an interplay with experimental observations, for example astrophysical data. But there is even a more obvious shortcoming of the simple version of the Walecka model discussed so far. Even at the saturation density it fails in its prediction for the *incompressibility* of nuclear matter which is defined as

$$K \equiv k_F^2 \frac{\partial^2(\epsilon/n_B)}{\partial k_F^2}\,. \tag{121}$$

This quantity is a measure for the stiffness of nuclear matter. In some literature, K is also called *compression modulus* or, somewhat misleadingly, "compressibility". To see that a large value of K corresponds to "stiff" matter, start from the usual thermodynamic definition for the compressibility χ,

$$\frac{1}{\chi} = n_B \frac{\partial P}{\partial n_B} = n_B^2 \frac{\partial^2 \epsilon}{\partial n_B^2}\,. \tag{122}$$

This definition says that easily compressible ("soft") matter has a small change in pressure upon changing the density. For the second equality we have used Eq. (120).

On the other hand, from the definition (121) we obtain

$$K \;=\; k_F^2 \frac{\partial^2(\epsilon/n_B)}{\partial n_B^2}\left(\frac{\partial n_B}{\partial k_F}\right)^2 = 9n_B^2 \frac{\partial^2(\epsilon/n_B)}{\partial n_B^2} = 9n_B \frac{\partial^2 \epsilon}{\partial n_B^2} + 18\left(\frac{\epsilon}{n_B} - \frac{\partial \epsilon}{\partial n_B}\right), \tag{123}$$

where $\partial n_B/\partial k_F = 3n_B/k_F$ (see Eq. (109a)) has been used. Now recall that in equilibrium, i.e., at the saturation density where the pressure vanishes, ϵ/n_B as a function of n_B has a minimum,

$$0 = \left.\frac{\partial(\epsilon/n_B)}{\partial n_B}\right|_{n_B=n_0} = -\frac{1}{n_B}\left(\frac{\epsilon}{n_B} - \frac{\partial \epsilon}{\partial n_B}\right)_{n_B=n_0}. \tag{124}$$

Consequently, the second term on the right-hand side of Eq. (123) vanishes at $n_B = n_0$ and the relation between χ and K becomes

$$\frac{1}{\chi} = \frac{n_B K}{9}\,, \tag{125}$$

i.e., a large compressibility χ corresponds to a small incompressibility K, as it should be.

The calculation of the incompressibility in the given model yields $K \simeq 560\,\mathrm{MeV}$. This is more than twice as much as the experimentally inferred value. Also the nucleon mass itself can be determined experimentally and compared to the prediction of the model. In total, there are thus four values which the model should reproduce. To improve the model, we add cubic and quartic scalar self-interactions of the form

$$\mathcal{L}_{I,\sigma} = -\frac{b}{3} m_N (g_\sigma \sigma)^3 - \frac{c}{4} (g_\sigma \sigma)^4 \tag{126}$$

to the Lagrangian (84). Besides the phenomenological need of these terms, there is also a theoretical reason for their presence: the model becomes renormalizable. With the self-interactions we have introduced two new constants b and c which can be used, together with the two couplings g_σ, g_ω to fit four experimental values. Namely, the two from Eq. (119) plus the incompressibility and the *Landau mass*

$$K \simeq 250\,\mathrm{MeV}\,, \qquad m_L = 0.83\, m_N\,. \tag{127}$$

The Landau mass is defined as

$$m_L = \frac{k_F}{v_F}\,, \tag{128}$$

where

$$v_F = \left.\frac{\partial E_k}{\partial k}\right|_{k=k_F} \tag{129}$$

is the Fermi velocity. It is plausible that the Landau mass is experimentally more accessible than the mass parameter m_N^* since it is an effective mass for fermions at the Fermi surface where all low-energy excitations are located.

In the mean field approximation, it is easy to include the effect of the scalar self-interactions. The pressure becomes

$$P = -\frac{1}{2} m_\sigma^2 \bar{\sigma}^2 - \frac{b}{3} m_N (g_\sigma \bar{\sigma})^3 - \frac{c}{4} (g_\sigma \bar{\sigma})^4 + \frac{1}{2} m_\omega^2 \bar{\omega}_0^2 + P_N\,, \tag{130}$$

with P_N defined in Eq. (102). The implicit equation for the effective nucleon mass (106) now receives contributions from the additional terms and becomes

$$m_N^* = m_N - \frac{g_\sigma^2}{m_\sigma^2} n_s + \frac{g_\sigma^2}{m_\sigma^2} \left[b m_N (m_N - m_N^*)^2 + c (m_N - m_N^*)^3 \right]\,. \tag{131}$$

To fit the four above mentioned values, one has to choose $g_\sigma^2/(4\pi) = 6.003$, $g_\omega^2/(4\pi) = 5.948$, $b = 7.950 \cdot 10^{-3}$, and $c = 6.952 \cdot 10^{-4}$. The numerical evaluation of the binding energy is left as an exercise. The result is plotted in Fig. 7 and shows that the behavior at large densities has changed significantly compared to the case without scalar interactions. In particular, the lower value of the incompressibility goes along with a softer equation of state at large densities. In other words, if you choose a fixed binding energy on the vertical axis you find a larger baryon density after taking into account the scalar interactions. The matter has thus become easier to compress in the high-density regime, in accordance with a lower incompressibility. (See also discussion about stiff and soft equations of state in Sec. II C.)

B. Hyperons

In the interior of a compact star, densities can be as high as several times nuclear saturation density. Therefore, baryons with strangeness, *hyperons*, may occur (as well as muons). The lightest of these states are given by the baryon octet, see Table I. It is rather straightforward to incorporate hyperons in the kind of model discussed above. Of course, the evaluation becomes more laborious, and the model has many more parameters. Let us therefore briefly discuss the model with the hyperon octet without going into too much detail.

The interaction between the baryons is now extended by interactions mediated by the ϕ and ρ vector mesons. (The ϕ meson has quark content $\bar{s}s$; the ρ meson has the same quark content as a pion, i.e., it can be considered as an

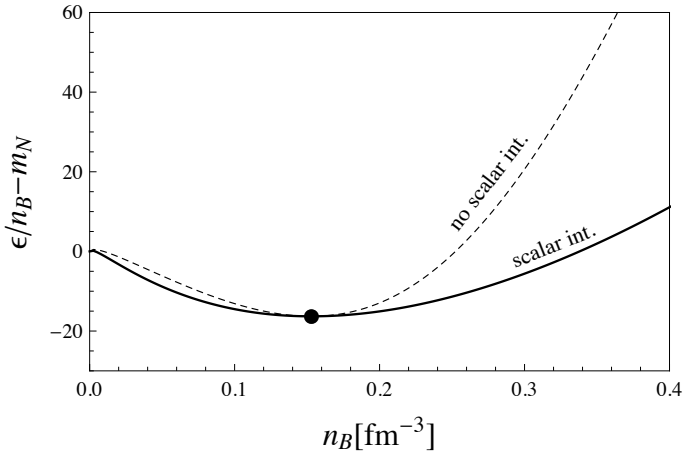

FIG. 7: Binding energy per nucleon as a function of density in the Walecka model, including cubic and quartic scalar self-interactions (solid line). The four parameters of the model are fixed to the saturation density, the binding energy per nucleon at the saturation density, the incompressibility, and the Landau mass. For comparison, the dashed line shows the result from Fig. 6, i.e., without scalar interactions. The scalar interactions account for a much softer equation of state.

	p	n	Λ	Σ^+	Σ^0	Σ^-	Ξ^0	Ξ^-
m (MeV)	939		1115	1190			1315	
I_3	1/2	−1/2	0	1	0	−1	1/2	−1/2
Q	1	0	0	1	0	−1	0	−1
S	0		−1				−2	
J	1/2							
quark content	uud	udd	uds	uus	uds	dds	uss	dss

TABLE I: Mass, isospin, electric charge, strangeness, spin, and quark content for the spin-1/2 baryon octet.

excited state of the pion.) The Lagrangian is

$$\begin{aligned}\mathcal{L} \;=\; & \sum_j \bar\psi_j \left(i\gamma^\mu\partial_\mu - m_j + \mu_j\gamma_0 + g_{\sigma j}\sigma - g_{\omega j}\gamma^\mu\omega_\mu - g_{\phi j}\gamma^\mu\phi_\mu - g_{\rho j}\gamma^\mu\rho^a_\mu\tau_a\right)\psi_j \\ & + \frac{1}{2}\left(\partial^\mu\sigma\partial_\mu\sigma - m_\sigma^2\sigma^2\right) - \frac{b}{3}m_N(g_\sigma\sigma)^3 - \frac{c}{4}(g_\sigma\sigma)^4 \\ & - \frac{1}{4}\omega^{\mu\nu}\omega_{\mu\nu} + \frac{1}{2}m_\omega^2\omega^\mu\omega_\mu \\ & - \frac{1}{4}\phi^{\mu\nu}\phi_{\mu\nu} + \frac{1}{2}m_\phi^2\phi^\mu\phi_\mu \\ & - \frac{1}{4}\rho_a^{\mu\nu}\rho^a_{\mu\nu} + \frac{1}{2}m_\rho^2\rho^\mu_a\rho^a_\mu\,. \end{aligned} \tag{132}$$

Here, j runs over all eight baryons and τ_a are the isospin generators. In a compact star, we have to require chemical equilibrium with respect to the weak interactions. In the case of hyperons, the conditions are

$$\mu_p = \mu_n - \mu_e\,, \qquad \mu_\Lambda = \mu_n \tag{133a}$$
$$\mu_{\Sigma^+} = \mu_n - \mu_e\,, \qquad \mu_{\Sigma^0} = \mu_n \tag{133b}$$
$$\mu_{\Sigma^-} = \mu_n + \mu_e\,, \qquad \mu_{\Xi^0} = \mu_n \tag{133c}$$
$$\mu_{\Xi^-} = \mu_n + \mu_e\,, \tag{133d}$$

and, including muons, $\mu_e = \mu_\mu$. The conditions (133) all come from weak processes which we have already discussed, see Eqs. (45). For example the process $n \to \Sigma^+ + e + \bar\nu_e$, which gives rise to the condition $\mu_{\Sigma^+} = \mu_n - \mu_e$, can be

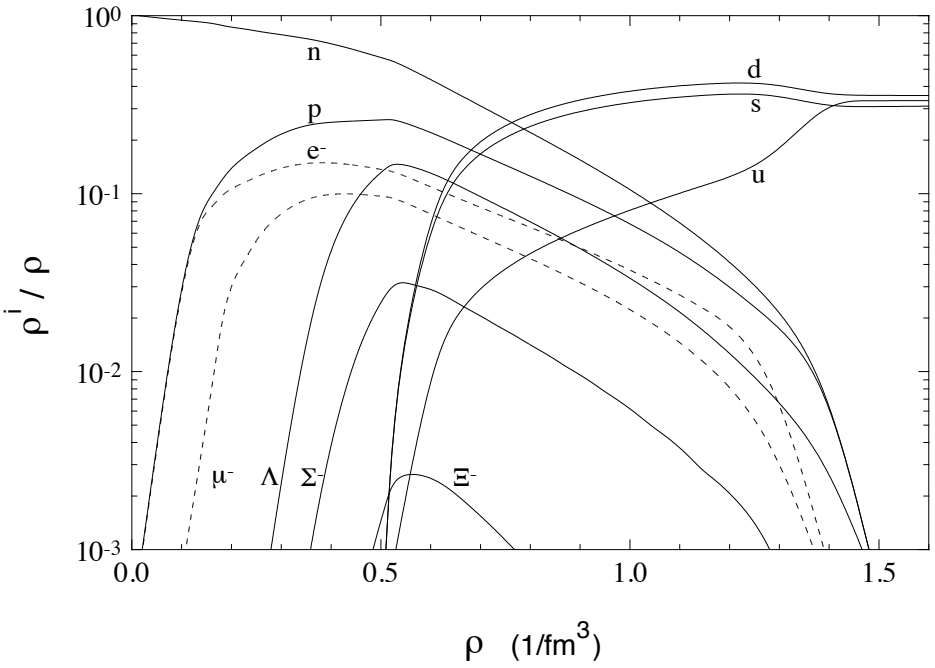

FIG. 8: Density fractions of baryons and leptons (and quarks, for a bag constant $B = 250\,\mathrm{MeV/fm^{-3}}$) as a function of the baryon number density. The figure is taken from Ref. [6] where more details about the underlying calculation can be found. For sufficiently large densities, hyperons and muons appear, and at densities of a few times nuclear ground state densities their density fractions becomes comparable to the fractions of nucleons and electrons. There is a region of coexistence of deconfined quark matter and baryonic matter, see Sec. III D for a discussion of these mixed phases. The curves shown here depend on the chosen models for nuclear and quark matter and the value of the bag constant.

understood from the elementary processes as

$$\left.\begin{array}{l} u + e \to s + \nu_e \\ d \to u + e + \bar{\nu}_e \\ d \to u + e + \bar{\nu}_e \end{array}\right\} \qquad udd \to uus + e + \bar{\nu}_e \,. \tag{134}$$

Electric neutrality is given by the constraint

$$n_p + n_{\Sigma^+} = n_e + n_\mu + n_{\Sigma^-} + n_{\Xi^-} \,. \tag{135}$$

We show the result of baryon and lepton density fractions in a model similar to the one discussed here in Fig. 8.

As a result of this rough discussion and the curves in the figure we learn that hyperons can be included in a rather straightforward extension of the simple Walecka model and that hyperons do appear for sufficiently large densities. The physical reasons are that (*i*) they *can* appear because the baryon chemical potential is large enough to provide energies larger than their mass, (*ii*) they *do* appear because (*a*) the systems seeks to acquire neutrality and does so with electrons at low densities; if hyperons are available, electrons in high-energy states can be replaced by hyperons in low-energy states and (*b*) the system seeks to become isospin symmetric; at low densities it is highly isospin asymmetric, and hyperons with nonzero isospin number provide a means to symmetrize the system.

C. Kaon condensation

Another possible variant of dense nuclear matter, besides the occurrence of hyperons, is the condensation of mesons. Originally, pion condensation was suggested [24]. Only many years later, it was realized that kaon condensation is possible in compact stars [25]. This is somewhat surprising since kaons are much heavier than pions and thus pion condensation seems more likely. However, in the medium, the effective kaon mass becomes sufficiently small to allow for a kaon condensate.

Kaon condensation is of interest for these lectures for several reasons. Besides being a variant of dense matter and thus relevant for the physics of compact stars, its discussion requires the introduction of several important concepts in the theory of the strong interaction. It thus is also interesting from a fundamental point of view. Moreover, we shall encounter kaon condensation again later in these lectures, when we discuss the quark-matter relatives of the kaon, see Sec. IV B 1.

To explain kaon condensation, we will first have to say what a kaon is and will do so with the help of chiral symmetry and spontaneous breaking thereof. Then, we will discuss chiral perturbation theory. This is one possible method to study kaon condensation and has been used in the original work [25]. For another approach, using models similar to the above discussed Walecka model, see for instance Ref. [26] and references therein. The evaluation of the chiral model has to be done numerically, so we will more or less only be concerned with setting up and understanding the basic equations. As a modest goal, we will try to understand the onset of kaon condensation, i.e., we will show how to compute the critical baryon density at which there is a second-order phase transition to the kaon-condensed phase.

1. Chiral symmetry of QCD

Kaon condensation can be discussed in a low-energy effective theory, here chiral perturbation theory. This theory should describe the fundamental theory, QCD, in the low-energy limit. In order to construct the theory, we need to understand the underlying symmetries. The QCD Lagrangian is

$$\mathcal{L}_{\rm QCD} = \bar{\psi}(i\gamma^\mu D_\mu + \mu\gamma_0 - M)\psi + \mathcal{L}_{\rm gluons}\,, \tag{136}$$

with the quark spinor ψ in color, flavor, and Dirac space, the mass matrix in flavor space

$$M = \begin{pmatrix} m_u & 0 & 0 \\ 0 & m_d & 0 \\ 0 & 0 & m_s \end{pmatrix}\,, \tag{137}$$

and the covariant derivative $D_\mu = \partial_\mu - igT_aA^a_\mu$, where $T_a = \lambda_a/2$ ($a = 1, \ldots 8$) are the generators of the color gauge group $SU(3)_c$ with the Gell-Mann matrices λ_a, A^a_μ are the corresponding gauge fields, and g is the strong coupling constant. The chemical potential μ is a diagonal matrix in flavor space. Without taking into account the weak interactions, each flavor is conserved and there are three independent chemical potentials. We have already seen in the previous sections that after taking into account weak interactions there are only two chemical potentials, one for quark (baryon) number, and one for electric charge.

The purely gluonic contribution to the Lagrangian is given by

$$\mathcal{L}_{\rm gluons} = -\frac{1}{4}G^{\mu\nu}_a G^a_{\mu\nu}\,, \tag{138}$$

where $G^a_{\mu\nu} = \partial_\mu A^a_\nu - \partial_\nu A^a_\mu + g f^{abc} A^b_\mu A^c_\nu$ with the $SU(3)_c$ structure constants is the gluon field strength tensor. Here we are not interested in this gluonic part, since we focus on the transformations of the fermion fields and the resulting symmetries of the Lagrangian. Also later, when we shall use QCD for explicit calculations, the gluonic part is negligible because we always work at very small temperatures compared to the quark (or baryon) chemical potential. The interactions of the quarks via gluon exchange, included in the covariant derivative, is of course important; in Sec. IV C this interaction will be used on the microscopic level.

We now introduce the chirality projectors

$$P_R = \frac{1+\gamma_5}{2}\,, \qquad P_L = \frac{1-\gamma_5}{2}\,. \tag{139}$$

They obey the identities

$$P^2_{R/L} = P_{R/L}\,, \qquad P^\dagger_{R/L} = P_{R/L}\,, \qquad P_R P_L = 0\,, \qquad P_R + P_L = 1\,, \tag{140}$$

i.e., they form a complete set of orthogonal projectors. (These identities are obvious with $\gamma_5^2 = 1$ and $\gamma_5^\dagger = \gamma_5$.) For a physical picture, remember that, for massless quarks, chirality eigenstates are also eigenstates of helicity. Therefore, in this case, there is a one-to-one correspondence between chirality and the projection of the fermion momentum onto its spin. We define left- and right-handed quark spinors by

$$\psi_{R/L} \equiv P_{R/L}\psi\,, \tag{141}$$

such that $\psi = P_R\psi + P_L\psi = \psi_R + \psi_L$. Then, using

$$\{\gamma_5, \gamma_\mu\} = 0\,, \tag{142}$$

we can write the Lagrangian as

$$\mathcal{L}_{\rm QCD} \;=\; \bar\psi_R(i\gamma^\mu D_\mu + \mu\gamma_0)\psi_R + \bar\psi_L(i\gamma^\mu D_\mu + \mu\gamma_0)\psi_L - \bar\psi_R M\psi_L - \bar\psi_L M\psi_R + \mathcal{L}_{\rm gluons}\,. \tag{143}$$

Let us first discuss the massless case, $M = 0$. In this case, separate rotations of left- and right-handed spinors leave the Lagrangian invariant,

$$\psi_R \to e^{i\phi_R^a t_a}\psi_R\,, \qquad \psi_L \to e^{i\phi_L^a t_a}\psi_L\,. \tag{144}$$

Since we are interested in three quark flavors, t_a are the nine generators of the flavor group $U(3)$, $t_0 = \mathbf{1}$ and $t_a = T_a$ ($a = 1, \dots 8$). Consequently, the Lagrangian is invariant under $U(3)_L \times U(3)_R$. The corresponding Noether currents are

$$J^\mu_{a,R/L} = \bar\psi_{R/L}\gamma^\mu t_a \psi_{R/L}\,. \tag{145}$$

They can be rewritten in terms of vector and axial-vector currents

$$J^\mu_{a,V} \;\equiv\; J^\mu_{a,R} + J^\mu_{a,L} = \bar\psi\gamma^\mu t_a\psi\,, \tag{146a}$$

$$J^\mu_{a,A} \;\equiv\; J^\mu_{a,R} - J^\mu_{a,L} = \bar\psi\gamma^\mu t_a\gamma_5\psi\,. \tag{146b}$$

To see this, note that $P_R\gamma_5 = P_R$ and $P_L\gamma_5 = -P_L$. In QCD the singlet axial-vector current is in general not conserved,

$$\partial_\mu J^\mu_{0,A} = -\frac{g^2 N_f}{16\pi^2} G^a_{\mu\nu}\tilde G^{\mu\nu}_a\,, \tag{147}$$

where $\tilde G^{\mu\nu} = \frac{1}{2}\epsilon^{\mu\nu\sigma\rho}G_{\sigma\rho}$ is the dual field strength tensor. This is referred to as the *axial anomaly*. We are left with the symmetry group $SU(3)_R \times SU(3)_L \times U(1)_V$. The vector symmetry $U(1)_V$ corresponds to baryon number conservation and is therefore also denoted as $U(1)_B$. The flavor symmetry group $SU(3)_R \times SU(3)_L$ is referred to as *chiral symmetry*. As we can see from Eq. (143), nonzero masses break the chiral symmetry *explicitly*. They do not break the $U(1)_V$ symmetry, and for the special case $m_u = m_d = m_s$ the subgroup $SU(3)_{R+L}$ of simultaneous R and L rotations remains a symmetry of the Lagrangian.

Spontaneous breaking of chiral symmetry is realized by a chiral condensate of the form $\langle\bar\psi_L\psi_R\rangle$. This is analogous to spontaneous symmetry breaking in simple models such as ϕ^4 theory, (see for instance the discussion of Bose-Einstein condensation in appendix A 1), or in a superconductor, or in the Higgs mechanism. The chiral condensate is only invariant under simultaneous right- and left-handed rotations, i.e., the symmetry breaking pattern is

$$G \equiv SU(3)_R \times SU(3)_L \to H \equiv SU(3)_{R+L}\,. \tag{148}$$

As a comparison, in ϕ^4 theory with a complex scalar field ϕ, we have $G = U(1)$, $H = \mathbf{1}$, which gives rise to the familiar "Mexican hat" potential with a negative quadratic and a positive quartic term in $|\phi|$. Spontaneous breaking of a global symmetry goes along with massless Goldstone bosons. In the Mexican hat, there is one massless excitation along the bottom of the Mexican hat, given by the angular component of the order parameter (while the radial component corresponds to a massive mode). Here, the bottom of the Mexican hat is not just a one-dimensional line. It is rather given by the coset space G/H (which is simply $U(1)$ in ϕ^4 theory). This space has $\dim G - \dim H$ generators. Consequently, with $\dim G = 8+8 = 16$ and $\dim H = 8$, there are 8 Goldstone modes. They are described by the $SU(3)$ matrix

$$U = e^{i\theta_a\lambda_a/f_\pi}\,, \tag{149}$$

with the pion decay constant $f_\pi \simeq 93\,\text{MeV}$. The meson fields θ_a of the Goldstone octet are usually reparametrized as

$$\theta_a\lambda_a = \begin{pmatrix} \frac{\pi^0}{\sqrt{2}} + \frac{\eta}{\sqrt{6}} & \pi^+ & K^+ \\ \pi^- & -\frac{\pi^0}{\sqrt{2}} + \frac{\eta}{\sqrt{6}} & K^0 \\ K^- & \bar K^0 & -\sqrt{\frac{2}{3}}\eta \end{pmatrix}. \tag{150}$$

Since the rows (columns) of this matrix carry left-handed flavor (right-handed anti-flavor) labels, it is easy to read off the quark content of the various mesons, e.g., $K^+ \sim \bar{s}u$, $\pi^+ \sim \bar{d}u$ etc. According to its chiral structure, the chiral matrix transforms under a transformation $g = (g_L, g_R) \in G$ as

$$U \to g_L U g_R^\dagger \,. \tag{151}$$

2. Chiral Lagrangian

In the (unrealistic) case of vanishing quark masses, the chiral symmetry is an exact symmetry and the Goldstone bosons are exactly massless. Exploiting the analogy to the Mexican hat potential, this means that the bottom of the Mexican hat is truly flat. Quark masses break the chiral symmetry explicitly. However, if the masses are small compared to the characteristic scale of chiral symmetry breaking $\Lambda \sim 1\,\mathrm{GeV}$ we can still consider the chiral symmetry as approximate. The bottom of the Mexican hat then gets distorted on a scale small compared to the deepness of the potential, and the Goldstone bosons acquire small masses. In this case it is more appropriate to speak of *pseudo*-Goldstone bosons. One might still hope to describe the system at low energies by an effective theory which is built on the underlying chiral symmetry, although this symmetry is strictly speaking broken. The mass matrix M, now nonvanishing, is required to transform just as the chiral field U, i.e.,

$$M \to g_L M g_R^\dagger \,. \tag{152}$$

We require the chiral Lagrangian to be invariant under G. The kinetic term and the mass term of the resulting effective theory are

$$\mathcal{L}_U = \frac{f_\pi^2}{4}\mathrm{Tr}[\partial_\mu U \partial^\mu U^\dagger] + c\mathrm{Tr}[M^\dagger(U + U^\dagger)] \,, \tag{153}$$

where the trace is taken over flavor space. The two constants f_π and c have to be fitted to experimental values, similarly to the constants of the Walecka model. In principle, higher order terms in U are allowed but shall be neglected here. Note that the Goldstone fields themselves appear in the exponent of the field U, i.e., they are already present to all orders.

In the context of compact stars, we do not only want to describe isolated mesons. We also need to include baryons and their interactions. The baryon octet fields are given by the matrix

$$B = \begin{pmatrix} \frac{\Sigma^0}{\sqrt{2}} + \frac{\Lambda}{\sqrt{6}} & \Sigma^+ & p \\ \Sigma^- & -\frac{\Sigma^0}{\sqrt{2}} + \frac{\Lambda}{\sqrt{6}} & n \\ \Xi^- & \Xi^0 & -\sqrt{\frac{2}{3}}\Lambda \end{pmatrix} , \tag{154}$$

which includes the proton p, the neutron n, and the hyperons from Table I. A simple way to understand the structure of this matrix is as follows. Consider the baryons as composed of a diquark and a quark. The diquarks form an antitriplet, i.e., one can think of the columns of the matrix as labelled by $(\bar{u}, \bar{d}, \bar{s})$ which corresponds to the quark content (ds, us, ud). Then the rows are simply labelled by the flavors in the fundamental representation (u, d, s), and one easily checks that this yields the quark content of the baryons as given in Table I.

The free baryon Lagrangian is

$$\mathcal{L}_B = \mathrm{Tr}[\bar{B}(i\gamma^\mu\partial_\mu - m_B)B] \,, \tag{155}$$

where $m_B \simeq 1.2\,\mathrm{GeV}$ is the $SU(3)_L \times SU(3)_R$ symmetric baryon mass. To write down the interaction between baryons and the mesons it is convenient to decompose the chiral field into left- and right-handed fields,

$$U = \xi_L \xi_R^\dagger \,, \tag{156}$$

where, without loss of generality, we may choose

$$\xi \equiv \xi_L = \xi_R^\dagger \,, \tag{157}$$

such that

$$U = \xi^2 \,. \tag{158}$$

We now add the meson-baryon interaction terms

$$\begin{aligned}\mathcal{L}_I &= i\mathrm{Tr}[\bar{B}\gamma_\mu[J_V^\mu, B]] + D\,\mathrm{Tr}[\bar{B}\gamma_\mu\gamma_5\{J_A^\mu, B\}] + F\,\mathrm{Tr}[\bar{B}\gamma_i\gamma_5[J_{A,i}, B]] \\ &+ a_1\mathrm{Tr}[B^\dagger(\xi M\xi + \xi^\dagger M^\dagger\xi^\dagger)B] + a_2\mathrm{Tr}[B^\dagger B(\xi M\xi + \xi^\dagger M^\dagger\xi^\dagger)] \\ &+ a_3\mathrm{Tr}[B^\dagger B]\mathrm{Tr}[M\xi^2 + M^\dagger(\xi^\dagger)^2]\,, \end{aligned} \tag{159}$$

with the additional constants D, F, a_1, a_2, a_3, and the vector and axial-vector currents

$$J_V^\mu = \frac{1}{2}(\xi^\dagger\partial^\mu\xi + \xi\partial^\mu\xi^\dagger)\,, \tag{160a}$$

$$J_A^\mu = \frac{i}{2}(\xi^\dagger\partial^\mu\xi - \xi\partial^\mu\xi^\dagger)\,. \tag{160b}$$

The Lagrangian is an expansion in M/Λ and ∂/Λ with the scale of chiral symmetry breaking Λ. Higher order terms in these parameters are omitted. We shall also drop the terms coming from $\boldsymbol{\gamma}\cdot\mathbf{J}_V$ and $\gamma_0\gamma_5 J_A^0$ which is consistent with this expansion, for more details see for instance Ref. [27]. In summary, we have the Lagrangian

$$\mathcal{L} = \mathcal{L}_U + \mathcal{L}_B + \mathcal{L}_I\,. \tag{161}$$

Later we shall also add electron and muon contributions, but they are simple and we ignore them for now to keep the notation brief.

3. Kaon-nucleon matter

Since we expect (charged) kaon condensation in a compact star rather than any other meson condensation (possibly there is pion condensation) let us for simplicity drop all mesons other than the kaons. We can then write

$$U = e^{iQ} = \cos Q + i\sin Q\,, \tag{162}$$

with

$$Q = \sum_{a=4}^{7}\phi_a\lambda_a = \begin{pmatrix} 0 & 0 & \phi_4 - i\phi_5 \\ 0 & 0 & \phi_6 - i\phi_7 \\ \phi_4 + i\phi_5 & \phi_6 + i\phi_7 & 0 \end{pmatrix}\,, \tag{163}$$

where we have absorbed f_π into the fields $\phi_a \equiv \theta_a/f_\pi$ such that the ϕ_a's are dimensionless. We can now compute a simple expression for the matrix U. To this end we first verify by explicit matrix multiplication

$$Q^3 = \phi^2 Q\,, \tag{164}$$

where

$$\phi^2 \equiv \phi_4^2 + \phi_5^2 + \phi_6^2 + \phi_7^2\,. \tag{165}$$

From Eq. (164) we obtain (for instance via complete induction)

$$Q^{2n} = \phi^{2(n-1)}Q^2\,, \tag{166}$$

for all $n \geq 1$, which can be used to compute

$$\cos Q = 1 - \left(\frac{Q^2}{2!} - \frac{Q^4}{4!} + \ldots\right) = 1 - Q^2\left(\frac{1}{2!} - \frac{\phi^2}{4!} + \ldots\right) = 1 - \frac{Q^2}{\phi^2}(1 - \cos\phi)\,, \tag{167}$$

and

$$\sin Q = Q\left(1 - \frac{Q^2}{3!} + \frac{Q^4}{5!} - \ldots\right) = Q\left(1 - \frac{Q^2}{3!} + \frac{\phi^2 Q^2}{5!} - \ldots\right) = Q - \frac{\phi^2 Q}{3!} + \frac{\phi^4 Q}{5!} - \ldots = \frac{Q}{\phi}\sin\phi\,. \tag{168}$$

As a further simplification let us now drop the neutral kaon fields, $\phi_6 = \phi_7 = 0$, because we expect charged kaon condensation. Then, from Eqs. (167) and (168) we obtain

$$U = \begin{pmatrix} \cos\phi & 0 & i\,\dfrac{\phi_4 - i\phi_5}{\phi}\,\sin\phi \\ 0 & 1 & 0 \\ i\,\dfrac{\phi_4 + i\phi_5}{\phi}\,\sin\phi & 0 & \cos\phi \end{pmatrix} . \tag{169}$$

Now we interpret the fields $\phi_{4,5}$ as vacuum expectation values, $\phi_{4,5} \to \langle\phi_{4,5}\rangle$, and neglect the fluctuations around this background. The general procedure to describe Bose-Einstein condensation, including fluctuations, is explained in appendix A 1 for the ϕ^4 model. The condensates are assumed to be constant in space and to have the time dependence $\phi(t,\mathbf{x}) \to \phi e^{-i\mu_K t}$, i.e., our ansatz is

$$\langle K^-\rangle = \langle\phi_4\rangle + i\langle\phi_5\rangle = \phi e^{-i\mu_K t}\,, \tag{170a}$$
$$\langle K^+\rangle = \langle\phi_4\rangle - i\langle\phi_5\rangle = \phi e^{i\mu_K t}\,. \tag{170b}$$

The real, constant (i.e., space-time independent) value of ϕ has to be determined later from minimizing the free energy; μ_K plays the role of a kaon chemical potential, as we shall see more explicitly below. More precisely, μ_K is the chemical potential for K^- while $-\mu_K$ is the chemical potential for K^+. We thus arrive at

$$U = \begin{pmatrix} \cos\phi & 0 & ie^{i\mu_K t}\sin\phi \\ 0 & 1 & 0 \\ ie^{-i\mu_K t}\sin\phi & 0 & \cos\phi \end{pmatrix} . \tag{171}$$

We are now prepared to evaluate $\mathcal{L}_U$ from Eq. (153). We shall neglect the masses of the up and down quarks such that $M \simeq \mathrm{diag}(0,0,m_s)$. We also define the kaon mass

$$m_K^2 = \frac{2cm_s}{f_\pi^2}\,. \tag{172}$$

Rather than c, we shall later use the kaon mass $m_K \simeq 494\,\mathrm{MeV}$ as a parameter of the model. This yields

$$\mathcal{L}_U = -V(\phi) \tag{173}$$

with the tree-level potential

$$V(\phi) = -\frac{f_\pi^2\mu_K^2}{2}\sin^2\phi + m_K^2 f_\pi^2(1-\cos\phi)\,, \tag{174}$$

where we have subtracted the constant vacuum contribution $V(\phi = 0)$. This potential contains the kaon condensate to all orders. We shall work with this expression below, but it is instructive to expand it up to fourth order in ϕ,

$$V(\phi) \simeq \frac{m_K^2 - \mu_K^2}{2}\,(f_\pi\phi)^2 + \frac{4\mu_K^2 - m_K^2}{24 f_\pi^2}(f_\pi\phi)^4\,. \tag{175}$$

This is the familiar expression from a ϕ^4 model for the free energy of a Bose condensate with chemical potential μ_K, mass m_K, and effective coupling $(4\mu_K^2 - m_K^2)/(6f_\pi^2)$, see for instance Eq. (A18) in the appendix. As expected, condensation occurs for $\mu_K^2 > m_K^2$ because in this case the quadratic term is negative and the quartic term positive, i.e., we have recovered the Mexican hat potential (where we have already picked one direction since ϕ is real).

For the baryonic Lagrangian we only keep the lightest baryons, the proton and the neutron. From Eq. (155) we thus obtain

$$\mathcal{L}_B = \bar{p}(i\gamma^\mu\partial_\mu - m_B + \gamma^0\mu_p)p + \bar{n}(i\gamma^\mu\partial_\mu - m_B + \gamma^0\mu_n)n\,, \tag{176}$$

where we have added the proton and neutron chemical potentials μ_p and μ_n. For the interaction terms we need

$$\xi = \begin{pmatrix} \cos(\phi/2) & 0 & ie^{i\mu_K t}\sin(\phi/2) \\ 0 & 1 & 0 \\ ie^{-i\mu_K t}\sin(\phi/2) & 0 & \cos(\phi/2) \end{pmatrix} , \tag{177}$$

which obviously fulfills $\xi^2 = U$. By inserting this into Eqs. (160) we obtain the spatial axial-vector current $\mathbf{J}_A = 0$ (since there is no spatial dependence in the condensate) and the temporal component of the vector current

$$J_V^0 = i\mu_K \sin^2(\phi/2) \begin{pmatrix} -1 & 0 & 0 \\ 0 & 0 & 0 \\ 0 & 0 & 1 \end{pmatrix} . \tag{178}$$

Hence the various nonzero terms needed for $\mathcal{L}_I$ in Eq. (159) become

$$i\mathrm{Tr}[\bar{B}\gamma_0[J_V^0, B]] = \mu_K \left(2p^\dagger p + n^\dagger n\right) \sin^2(\phi/2) , \tag{179a}$$

$$a_1\mathrm{Tr}[B^\dagger(\xi M\xi + \xi^\dagger M^\dagger \xi^\dagger)B] = -2a_1 m_s\, p^\dagger p \sin^2(\phi/2) , \tag{179b}$$

$$a_2\mathrm{Tr}[B^\dagger B(\xi M\xi + \xi^\dagger M^\dagger \xi^\dagger)] = 2a_2 m_s (p^\dagger p + n^\dagger n) \cos^2(\phi/2) , \tag{179c}$$

$$a_3\mathrm{Tr}[B^\dagger B]\mathrm{Tr}[M\xi^2 + M^\dagger(\xi^\dagger)^2] = 2a_3 m_s (p^\dagger p + n^\dagger n)[1 - 2\sin^2(\phi/2)] . \tag{179d}$$

It is left as an exercise to verify these results. Inserting this into Eq. (159), and putting together the contributions from the chiral field, the baryons, and the interactions between them, the total Lagrangian can be written as

$$\begin{aligned} \mathcal{L} = & -V(\phi) + \bar{p}[i\gamma^\mu\partial_\mu - m_B + \gamma^0(\mu_p + \mu_p^*)]p \\ & + \bar{n}[i\gamma^\mu\partial_\mu - m_B + \gamma^0(\mu_n + \mu_n^*)]n . \end{aligned} \tag{180}$$

Similar to the Walecka model in Sec. III A, the effect of the kaon condensate on the nucleons can be absorbed into an effective chemical potential. In a slightly different notation than in Sec. III A (where μ was absorbed into μ^*), we have kept the real thermodynamic chemical potentials separate, and we have

$$\mu_p^* = 2(a_2 + a_3)m_s + [2\mu_K - 2(a_1 + a_2 + 2a_3)m_s] \sin^2(\phi/2) , \tag{181a}$$

$$\mu_n^* = 2(a_2 + a_3)m_s + [\mu_K - 2(a_2 + 2a_3)m_s] \sin^2(\phi/2) . \tag{181b}$$

We can now, analogously to Sec. III A, evaluate the partition function at $T = 0$ to obtain the thermodynamic potential density $\Omega = -T/V \ln Z$ which can be written as

$$\Omega = V(\phi) + \epsilon_B - (\mu_n^* + \mu_n)n_n - (\mu_p^* + \mu_p)n_p , \tag{182}$$

with the nucleon number densities n_n and n_p, and the nucleon energy density

$$\epsilon_B = 2\sum_{i=p,n} \int \frac{d^3\mathbf{k}}{(2\pi)^3} \sqrt{k^2 + m_B^2}\, \Theta(k_{F,i} - k) , \tag{183}$$

where $k_{F,i}$ are the respective Fermi momenta.

Before adding the lepton contribution we need to find the relations between the various chemical potentials through the conditions of chemical equilibrium. The leptonic processes including nucleons are

$$n \to p + \ell + \bar{\nu}_\ell , \qquad p + \ell \to n + \nu_\ell . \tag{184}$$

Here, $\ell = e, \mu$ can either be an electron or a muon. We also have the purely leptonic processes,

$$e \to \mu + \bar{\nu}_\mu + \nu_e , \qquad \mu \to e + \bar{\nu}_e + \nu_\mu , \tag{185}$$

and the processes involving kaons,

$$n \leftrightarrow p + K^- , \qquad e \leftrightarrow K^- + \nu_e . \tag{186}$$

These processes lead to the independent conditions

$$\mu_e = \mu_K = \mu_\mu , \qquad \mu_n = \mu_p + \mu_e . \tag{187}$$

The system is thus characterized by two independent chemical potentials, say μ_e and μ_n. We implement the constraint $\mu_n = \mu_p + \mu_e$ by rewriting the terms containing the nucleon chemical potentials in the potential (182) as $\mu_n n_n + \mu_p n_p = \mu_n n_B - \mu_e n_p$. Since we want to work at fixed $n_B = n_n + n_p$, we perform a Legendre transformation of Ω with respect

to the variables μ_n and $\frac{\partial\Omega}{\partial\mu_n} = -n_B$. This amounts to adding the term $\mu_n n_B$ to Ω which yields the relevant free energy for the baryons and the kaon condensate,

$$\Omega_{B,K} = V(\phi) + \epsilon_B - \left[(\mu_p^* - \mu_e)x_p + (1-x_p)\mu_n^*\right]\, n_B\,. \tag{188}$$

Here we have introduced the proton fraction

$$x_p \equiv \frac{n_p}{n_B}\,, \tag{189}$$

which has to be determined dynamically from minimizing the free energy. We can now add the lepton contributions to arrive at

$$\Omega_{B,K,\ell} = \Omega_{B,K} + \epsilon_e - \mu_e n_e + \Theta(\mu_e^2 - m_\mu^2)(\epsilon_\mu - \mu_e n_\mu)\,, \tag{190}$$

where we have used $\mu_e = \mu_\mu$, where ϵ_ℓ are the lepton energy densities ($\ell = e, \mu$), and where

$$n_e = \frac{\mu_e^3}{3\pi^2}\,, \qquad n_\mu = \frac{(\mu_e^2 - m_\mu^2)^{3/2}}{3\pi^2} \tag{191}$$

are the corresponding lepton number densities. The step function in the muon contribution accounts for the fact that muons only appear if μ_e is larger than their mass $m_\mu = 106\,\mathrm{MeV}$. On the relevant energy scale, electrons are massless to a very good approximation and thus are present for any nonzero μ_e.

For a given baryon number n_B, the variables of $\Omega_{B,K,\ell}$ are the proton fraction x_p, the kaon condensate ϕ, and the chemical potential for (negative) electric charge μ_e. They are determined by minimizing the free energy with respect to x_p and ϕ and by requiring charge neutrality,

$$\frac{\partial\Omega_{B,K,\ell}}{\partial x_p} = \frac{\partial\Omega_{B,K,\ell}}{\partial\phi} = \frac{\partial\Omega_{B,K,\ell}}{\partial\mu_e} = 0\,. \tag{192}$$

It is straightforward to compute the various derivatives, and after a few lines of algebra the result can be written as

$$\mu_e = -\frac{1}{n_B\cos^2(\phi/2)}\frac{\partial\epsilon_B}{\partial x_p} - 2a_1 m_s\tan^2(\phi/2)\,, \tag{193a}$$

$$0 = \cos\phi - \frac{m_K^2}{\mu_e^2} + \frac{n_B}{\mu_e^2 f_\pi^2}\left[\frac{\mu_e}{2}(1+x_p) - (a_1 x_p + a_2 + 2a_3)m_s\right]\,, \tag{193b}$$

$$0 = f_\pi^2\mu_e\sin^2\phi - n_B\left[x_p\cos^2(\phi/2) - \sin^2(\phi/2)\right] + n_e + n_\mu\Theta(\mu_e^2 - m_\mu^2)\,. \tag{193c}$$

The second equation has been obtained after dividing both sides by $\sin\phi$. This means that $\phi = 0$ is always a solution and Eq. (193b) is only valid for nonvanishing condensates. In the third equation we recover the various contributions to the electric charge density: the first term on the right-hand side is the pure contribution from the kaon condensate. It gives a positive contribution to the negative charge density for $\mu_e > 0$, i.e., in this case there is a K^- condensate. The second term on the right-hand side arises from the nucleons and their interactions with the kaon condensate. Only for $\phi = 0$ does it give the pure proton contribution $-n_p = -x_p n_B$. Finally, the other two terms are the expected contributions from the leptons.

The onset of kaon condensation can be determined by setting $\phi = 0$ in all three equations. This yields three equations which can be solved for x_p^c, μ_e^c, and n_B^c, where n_B^c is the critical density beyond which there is a condensate and x_p^c, μ_e^c the values of the proton fraction and the charge chemical potential at this density. Since Eq. (193b) is only valid for $\phi \neq 0$, this has to be understood as approaching n_B^c from above.

We leave the numerical evaluation of the critical density and the general evaluation for all n_B as an exercise, see problem III.3. An important modification, which we have neglected for simplicity, has to be taken into account for this evaluation. Namely, the energy density ϵ_B has to be modified due to interactions among nucleons. It is beyond the scope of these lectures to derive this modification, see Ref. [27] and references therein for more details. Here we simply quote this modification which is needed in order to get physically sensible results. One needs to use an expansion of ϵ_B around symmetric nuclear matter $x_p = 1/2$ of the form

$$\epsilon_B \to \epsilon_0 + n_B(1-2x_p)^2 S(u)\,, \qquad u \equiv \frac{n_B}{n_0}\,. \tag{194}$$

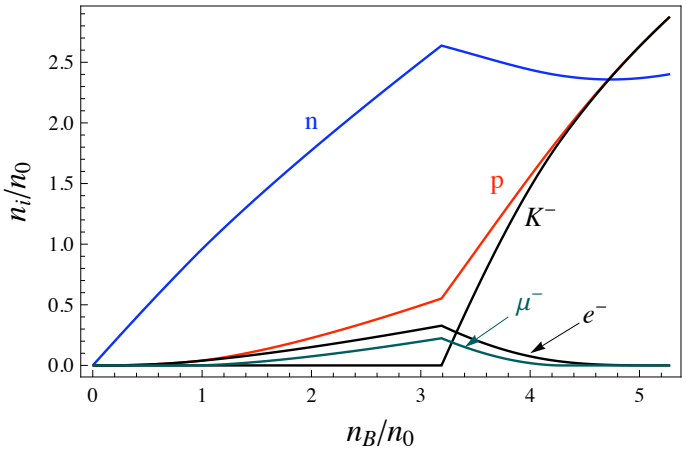

FIG. 9: Density fractions of neutrons (n), protons (p), electrons (e^-), muons (μ^-), and the kaon condensate (K^-) from Eqs. (193) with ϵ_B modified as given in Eqs. (194), (195). The parameters are (see Ref. [27]) $a_1 m_s = -67\,\mathrm{MeV}$, $a_2 m_s = 134\,\mathrm{MeV}$, $a_3 m_s = -222\,\mathrm{MeV}$, $m_\mu = 106\,\mathrm{MeV}$, $f_\pi = 93\,\mathrm{MeV}$, $m_K = 494\,\mathrm{MeV}$, $m_B = 1200\,\mathrm{MeV}$. We see that for this parameter choice the onset of kaon condensation is at about three times nuclear saturation density, $n_B^c \simeq 3.2 n_0$.

Here ϵ_0 is the energy density of symmetric nuclear matter, whose form is not relevant because we only need the derivative of ϵ_B with respect to x_p. The nuclear saturation density is denoted by n_0, and

$$S(u) = (2^{2/3} - 1)\frac{3}{5}\frac{(3\pi^2 n_0/2)^{2/3}}{2m_B}\left[u^{2/3} - F(u)\right] + S_0 F(u) \tag{195}$$

is the nuclear symmetry energy (see Ref. [28] for a discussion of the nuclear symmetry energy in the context of the maximum mass of neutron stars). For the numerical evaluation shown in Fig. 9, the nuclear symmetry energy at the saturation point $S_0 = 30\,\mathrm{MeV}$ has been used, as well as the function $F(u) = u$. See caption of the figure for the choice of the other parameters.

D. From hadronic to quark phases: possibility of a mixed phase

We have already mentioned the possibility of a hybrid star, i.e., a star with a quark matter core surrounded by nuclear matter. How does the interface between these two phases look? Is it a sharp interface or is there a shell in a hybrid star where the hadronic and quark phases coexist in a mixed phase? If the former is true, there will be a jump in the density profile of the star, while the latter allows for a continuous change in density.

Mixed phases are a very general phenomenon. In the context of compact stars, not only the mixed hadronic/quark matter phase is of relevance. Also in the inner crust of a hybrid or neutron star one may find mixed phases. There one expects a neutron superfluid coexisting with a lattice of ions, i.e., a mixed phase of neutron matter and nuclei. In these lectures, we shall not discuss the properties of the crust of a compact star in detail. See Sec. VI B for a brief discussion and Ref. [29] for an extensive review. Other examples of mixed phases in different systems are liquid-gas mixtures or simply a solid, which is a mixture of an electron gas and nuclear matter (sitting in the lattice of ions).

In Fig. 10 the possibility of a mixed phase is illustrated. We see that the condition of charge neutrality plays an important role here. It is important that in a compact star charge neutrality is required globally, not locally. In other words, certain regions in the star may very well have a nonzero electric charge as long as other regions have opposite charge to ensure an overall vanishing charge.

It is plausible that such a mixed phase will have a crystalline structure. For instance, one phase may form spheres sitting at the points of a lattice which is immersed in the other phase. Other possibilities are rods or slabs [30], such that the mixed phase looks like spaghetti or lasagna, wherefore astrophysicists have termed such phases *nuclear pasta*. In any case, if a mixed phase is possible because of a general argument such as given in Fig. 10, this does not mean that it is indeed realized. One has to take into account Coulomb forces (which seek to break charged regions into smaller regions) and surface forces (which seek to minimize the surface and thus work in the opposite direction). We shall not discuss these forces quantitatively but rather give some general arguments about mixed phases.

We start from the simple picture that at small quark density (or quark chemical potential μ) the hadronic phase is preferred and that there is a first-order phase transition to the quark matter phase at some critical chemical potential.

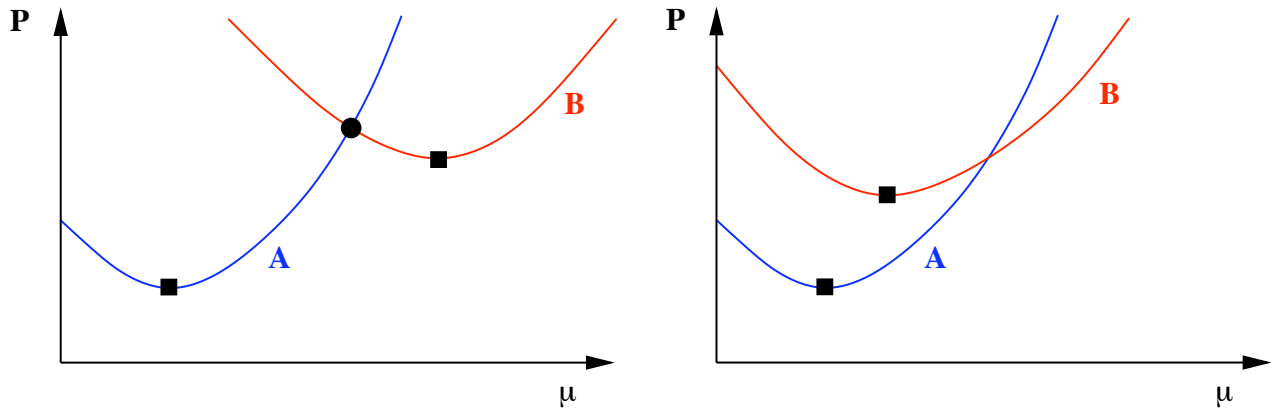

FIG. 10: Illustration of the possibility of a mixed phase. The pressure P of two phases A and B is given by the respective curves as a function of a chemical potential μ. Note that $\partial P/\partial\mu$ has to increase with increasing μ (increasing μ cannot lead to a decrease of the corresponding charge; this would lead to an instability). Suppose μ is the electric charge chemical potential and we require charge neutrality. Then the squares mark the points at which a given phase is charge neutral. The circle in the left panel marks a point where the two phases have equal pressure and opposite charge. Since this point has higher pressure than either of the squares, this is the ground state (neglecting surface tension and Coulomb energy). In this state, phase A and B coexist and occupy different volume fractions, determined by the different slopes of the curves. In the right panel, there is no point where both phases have equal pressure and opposite charges. Therefore, the square on the curve B is the ground state.

The question is whether there is a mixed phase between these two pure phases. The pressures of the two phases $P_h(\mu,\mu_e)$ and $P_q(\mu,\mu_e)$ depend on the quark chemical potential and the charge chemical potential μ_e (we work at zero temperature). Phase coexistence is possible when the pressures of the two phases are equal,

$$P_h(\mu,\mu_e) = P_q(\mu,\mu_e)\,. \tag{196}$$

Now suppose the neutrality condition were *local* (which it isn't in our context). Then the charge must vanish in each phase separately,

$$Q_h(\mu,\mu_e) = Q_q(\mu,\mu_e) = 0\,. \tag{197}$$

These two conditions yield μ_e for each phase separately as a function of μ, $\mu_e^h(\mu)$ and $\mu_e^q(\mu)$. Consequently, the condition of equal pressure,

$$P_h(\mu,\mu_e^h(\mu)) = P_q(\mu,\mu_e^q(\mu))\,, \tag{198}$$

yields a unique μ. Only at this μ do the phases coexist. This amounts to a sharp interface at a given value for the pressure, where on both sides of the interface the pure hadronic and the pure quark phases exist with different densities, i.e., there is a density jump in the profile of the star.

Now we impose the weaker (and realistic) condition of *global* charge neutrality. This means that in any mixed phase only the total charge has to vanish. We denote the quark volume fraction by

$$\chi_q \equiv \frac{V_q}{V_h+V_q} \quad \in [0,1]\,, \tag{199}$$

where V_q and V_h are the volumes occupied by the quark and hadron phases, respectively. Then, neutrality reads

$$(1-\chi_q)Q_h(\mu,\mu_e) + \chi_q Q_q(\mu,\mu_e) = 0\,. \tag{200}$$

This yields a function $\mu_e(\chi_q,\mu)$ which is then inserted into the condition of equal pressure,

$$P_h(\mu,\mu_e(\chi_q,\mu)) = P_q(\mu,\mu_e(\chi_q,\mu))\,. \tag{201}$$

The result is a chemical potential as a function of χ_q, $\mu(\chi_q)$. Thus there is a finite interval on the μ-axis where a mixed phase is possible. We see that the looser condition of global charge neutrality allows for a shell with a mixed phase in a hybrid star. These formal arguments become more transparent in a geometric picture, see Fig. 11.

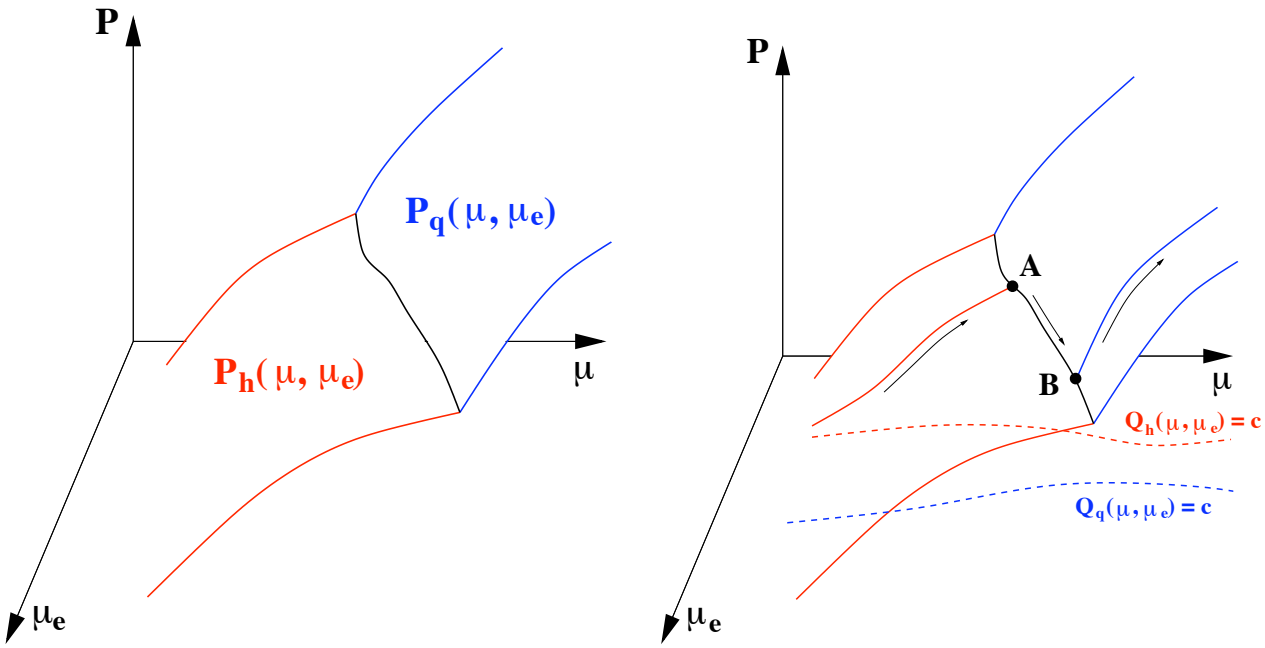

FIG. 11: Schematic picture of a hadron-quark mixed phase in a finite interval of μ. Left panel: the pressures of the two phases define two surfaces parametrized by μ and μ_e. The intersection of the two surfaces forms a line where coexistence of the two phases is possible. Right panel: the neutrality condition for each of the phases defines a curve in the μ-μ_e plane, and thus a curve on the respective surfaces (for illustrative purposes let the charge be nonzero – denoted by c – since for zero charge there would have to be a valley of the pressure). A mixed phase may exist from A (where $\chi_q = 0$) to B (where $\chi_q = 1$), provided that, for a given μ, the pressure on this line is larger than the respective pressure on the neutrality curves of each phase. In this segment none of the phases is neutral separately, but they may combine to a globally neutral phase. Note that the extra direction μ_e is crucial to have a finite segment along the μ axis where a mixed phase is possible. If the mixed phase is realized, the arrows indicate the ground state for increasing values of μ (the pressure also has to increase along this line).

We shall not go into the details of an explicit calculation of the quark/hadron mixed phase because, even neglecting surface tension and Coulomb energy, this calculation eventually has to be performed numerically. Instead we show the result of such a calculation [31] in Fig. 12 (cf. also Fig. 8 where we have already seen a mixed phase). One recovers the (projection of the) topology of Fig. 11 in Fig. 12. The figure shows the mixed phase being the preferred phase in a certain μ interval without taking into account Coulomb energy and surface energy. In the complete calculation one finds that a relatively small surface energy is needed to destroy the mixed phase. It thus appears unlikely that a mixed phase of quarks and hadrons exists in a hybrid star.

Problems

III.1 Binding energy and saturation density in the Walecka model

Solve Eq. (106) at zero temperature numerically for different values of the baryon density. Use the solution to compute the binding energy per nucleon and check that the values (119) are obtained upon using the values of the coupling constants $g_\omega^2/(4\pi) = 14.717$, $g_\sigma^2/(4\pi) = 9.537$. In other words, reproduce the results from Fig. 6. If you are a bit more ambitious you can also do it the other way around: set up and solve the two equations that are needed to determine the coupling constants from the conditions (119).

III.2 Walecka model with scalar interactions

Reproduce the result of Fig. 7 numerically.

III.3 Onset of kaon condensation

Solve equations (193) – with the modifications given in Eqs. (194) and (195) – numerically to determine the density fractions of nucleons, kaons, and leptons at $T = 0$ as a function of baryon density. In particular,

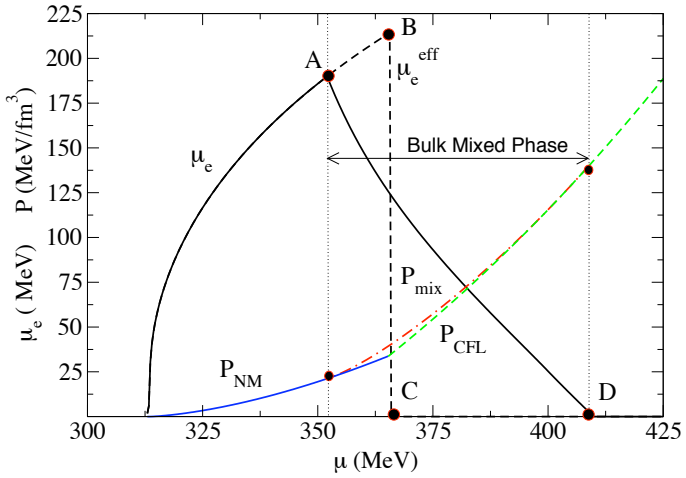

FIG. 12: Figure from Ref. [31] showing the transition from nuclear matter (NM) to a mixed phase (mix) to a quark matter phase (CFL) (color-flavor locking (CFL) is explained in Sec. IV B). In the mixed phase, μ_e is lowered in order to make the nuclear phase positively charged and the CFL phase negatively charged. Taking into account Coulomb energy and surface energy shows that the μ interval for the mixed phase shrinks with increasing surface tension σ until it completely disappears for $\sigma \gtrsim 40\,\mathrm{MeV/fm^2}$. The exact value of σ is not known but it is likely to be larger than that limit value such that a mixed phase appears unlikely. The limit value does not depend much on whether the mixed phase has spheres, rods, or slabs.

compute the critical baryon density for the onset of kaon condensation. See caption of Fig. 9 for the values of the parameters and compare your result to the plot in this figure.

IV. SUPERCONDUCTIVITY AND SUPERFLUIDITY IN A COMPACT STAR

In our discussion of interacting nuclear matter we have so far ignored a very important physical effect. We have not included the possibility of superfluidity and/or superconductivity, although we have briefly mentioned the effect of superconductivity on the equation of state of quark matter, see Sec. II C. In the following, we shall discuss these effects in more detail. But first let us recapitulate what superconductivity is. Once we have introduced the basic concept we shall see that it may appear in several variants in a compact star. And we will see that it is crucial for the understanding of transport properties of dense matter. And the transport properties of dense matter, in turn, are related to the phenomenology of the star.

Consider a system of fermions at zero temperature with chemical potential μ and free energy

$$\Omega = E - \mu N\,. \tag{202}$$

Now first suppose the fermions are non-interacting. Then, adding a fermion with energy μ, i.e., at the Fermi surface, leaves the free energy Ω obviously unchanged: the energy E is increased by μ, but the second term subtracts the same amount since we add $N = 1$ fermion. Now let us switch on an arbitrarily small attractive interaction between the fermions. Then, by adding two fermions at the Fermi surface, we can actually lower the free energy because the attractive interaction will lead to an energy gain from the binding energy. Therefore, the Fermi surface we have started with is unstable. A new ground state is formed in which pairs of fermions are created at the Fermi surface. Since two fermions formally can be viewed as a boson, these fermion pairs will form a Bose condensate.[5] This formation of a

[5] In fact, the fermions are correlated in momentum space, not in real space. Consequently, in the weak-coupling limit, the fermion pairs are not spatially separated bosons. The typical size of a pair is rather larger than the mean distance between fermions. Therefore, one apparently has to be careful to describe the pairs as bosons. However, recent experiments with cold fermionic atoms show that there is no phase transition between the weak-coupling limit (where the pairs are wide spread) and the strong-coupling limit (where the pairs are actual difermions, i.e., bosons). This is the so called BCS-BEC crossover. This observation suggests in particular that it is not too bad to think of the fermion pairs as bosons even in the weak-coupling limit.

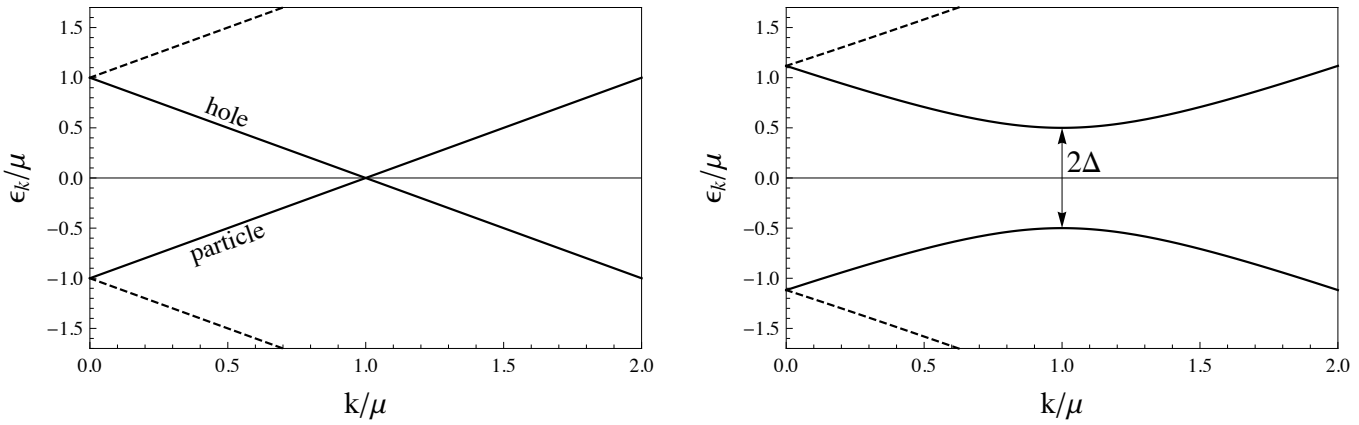

FIG. 13: Left panel: particle and hole excitations (solid lines) in a system of noninteracting ultrarelativistic fermions with chemical potential μ. The dashed lines are the antiparticle and antiparticle hole excitations. Right panel: quasiparticle excitations after switching on small interactions which, via Cooper's Theorem, give rise to an energy gap Δ according to Eq. (203), here chosen to be $\Delta = 0.5\mu$. What were pure particle and pure hole excitations in the left panel have now become momentum-dependent mixtures of particles and holes.

condensate of fermion pairs due to an arbitrarily small interaction is called *Cooper's Theorem* and the fermion pairs are called *Cooper pairs*.

This mechanism is completely general, i.e., it holds for arbitrary fermions with a Fermi surface as long as their interaction is attractive. It holds for electrons in a usual superconductor, i.e., a metal or alloy, for ^{3}He atoms in superfluid helium, for fermionic atoms in an optical trap etc. In our context, it can be applied to protons, neutrons, and quarks. Anticipating that the Cooper mechanism leads to *superfluidity* for neutral fermions and to *superconductivity* for charged fermions, we thus expect (i) neutron superfluidity, (ii) proton superconductivity, and (iii) quark superconductivity to be in principle possible in a compact star. Quarks are of course a bit more complicated since they not only carry electric charge but also color charge. Therefore, we need to make more precise what we mean by quark superconductivity, see Sec. IV B.

Let us first stay on a very general level and discuss the basic consequences of Cooper pairing. A Cooper pair is held together by sort of a "binding energy" (although it is not a bound state), i.e., one needs a finite amount of energy to break a pair. Consequently, the single-particle dispersion relation acquires an energy gap Δ,

$$\epsilon_k = \sqrt{(E_k - \mu)^2 + \Delta^2}\,, \tag{203}$$

with $E_k = \sqrt{k^2 + m^2}$ as in the previous chapters. One might think that ϵ_k does not reproduce the usual dispersion $E_k - \mu$ for a vanishing gap, rather $\epsilon_k \to |E_k - \mu|$. This is no contradiction after taking into account the fermion hole excitations, such that in the ungapped system $\epsilon_k = \pm(E_k - \mu)$ to which the $\Delta = 0$ limit of $\epsilon_k = \pm\sqrt{(E_k - \mu)^2 + \Delta^2}$ is indeed equivalent. The excitation described by Eq. (203) is also called *quasiparticle* since it contains the interaction of the original particles in an effective way. To excite a quasifermion in a superconductor, a finite amount of energy is needed, while a fermion at the Fermi surface of a noninteracting system can be excited by an infinitesimally small energy, see Fig. 13. The energy gap in the dispersion relation is responsible for most of the phenomenological properties of a superconductor. For instance, it gives rise to the frictionless charge transport in an electronic superconductor, since (sufficiently low energy) scattering of electrons off phonons cannot excite a single-electron state. Or, in the context of superfluidity, the energy gap explains the frictionless flow in the same way. For quantitative predictions it is thus crucial to compute the magnitude of Δ. We shall perform this calculation within perturbative QCD for quarks in Sec. IV C.

The energy gap is in general a temperature-dependent quantity. It typically decreases with temperature and becomes zero at and above a certain critical temperature T_c. This critical temperature indicates the phase transition from the superconducting to the non-superconducting phase, as we shall demonstrate with the discontinuity of the specific heat in the following section. Since the onset of superconductivity or superfluidity is a phase transition, there must be a symmetry which is spontaneously broken below the critical temperature. In particular for quark matter, the symmetry breaking pattern is very useful to characterize the superconductor, see Sec. IV B.

A. Specific heat for isotropic and anisotropic superconductors

As a example of the effect of Δ let us compute the specific heat of a superconductor.[6] The specific heat is easy to compute and shows characteristic features of a superconductor. We start from the free energy of a superconductor made of fermions with two degenerate (spin-) degrees of freedom,

$$\Omega = 2T \int \frac{d^3\mathbf{k}}{(2\pi)^3} \ln\left(1 + e^{-\epsilon_k/T}\right) , \tag{204}$$

where the quasiparticle energy ϵ_k is given by Eq. (203). We shall, for simplicity, consider massless fermions, $E_k = k$. The entropy (density) is given by the derivative with respect to the temperature (with respect to the *explicit* temperature dependence only, there is also an implicit temperature dependence in Δ)

$$s = \frac{\partial\Omega}{\partial T} = -2 \int \frac{d^3\mathbf{k}}{(2\pi)^3} \left[(1-f_k)\ln(1-f_k) + f_k \ln f_k\right] . \tag{205}$$

with the Fermi distribution

$$f_k = \frac{1}{e^{\epsilon_k/T}+1} . \tag{206}$$

To derive Eq. (205) one uses the identities

$$\frac{\epsilon_k}{T} = \ln(1-f_k) - \ln f_k , \qquad \ln\left(1+e^{-\epsilon_k/T}\right) = -\ln(1-f_k) . \tag{207}$$

From the entropy we then compute the specific heat (at constant volume)

$$c_V \equiv T\frac{\partial s}{\partial T} = 2\int \frac{d^3\mathbf{k}}{(2\pi)^3} \epsilon_k \frac{\partial f_k}{\partial T} . \tag{208}$$

For the temperature dependence of the gap we assume the following simple form,

$$\Delta(T) = \Theta(T_c - T)\Delta_0 \sqrt{1 - \frac{T^2}{T_c^2}} , \tag{209}$$

such that the zero-temperature gap is Δ_0, the gap approaches zero at $T = T_c$ and vanishes for all temperatures larger than T_c. Then, for $T < T_c$ we have

$$\frac{\partial\Delta}{\partial T} = -\frac{\Delta_0^2}{T_c^2}\frac{T}{\Delta} \quad \Rightarrow \quad \frac{\partial\epsilon_k}{\partial T} = -\frac{T}{\epsilon_k}\frac{\Delta_0^2}{T_c^2} \quad \Rightarrow \quad \frac{\partial f_k}{\partial T} = \frac{1}{\epsilon_k}\frac{e^{\epsilon_k/T}}{\left(e^{\epsilon_k/T}+1\right)^2}\left(\frac{\epsilon_k^2}{T^2} + \frac{\Delta_0^2}{T_c^2}\right) , \tag{210}$$

and consequently

$$c_V = 2\int \frac{d^3\mathbf{k}}{(2\pi)^3} \frac{e^{\epsilon_k/T}}{\left(e^{\epsilon_k/T}+1\right)^2}\left(\frac{\epsilon_k^2}{T^2} + \frac{\Delta_0^2}{T_c^2}\right) . \tag{211}$$

We are only interested in temperatures much smaller than the chemical potential, $T \ll \mu$. Then, the main contribution comes from the Fermi surface, and we can approximate $dk\, k^2 \to \mu^2 dk$. We introduce the new variable $x = (k-\mu)/T$, and define

$$\varphi \equiv \frac{\Delta}{T} . \tag{212}$$

---

[6] More precisely, here we compute the fermionic contribution to the specific heat. There may be light Goldstone modes which dominates the specific heat at small temperatures. In this section we ignore such modes for the purpose of illustrating the effect of the fermionic energy gap.

This yields

$$c_V \simeq \frac{\mu^2 T}{\pi^2}\int_0^\infty dx \int_0^\pi d\theta\, \sin\theta \left(x^2+\varphi^2+\frac{\Delta_0^2}{T_c^2}\right)\frac{e^{\sqrt{x^2+\varphi^2}}}{\left(e^{\sqrt{x^2+\varphi^2}}+1\right)^2}\,, \tag{213}$$

where we have approximated the lower boundary by $-\mu/T \simeq -\infty$ and have used that the integrand is even in x (which gives rise to the new integration boundaries $[0,\infty]$ and a factor 2). We have not yet performed the θ integral since we shall allow for anisotropic gaps. From this general expression we easily get the limit of a vanishing gap, $\varphi = \Delta_0 = 0$, i.e., the result for the non-superconducting state,

$$c_V^0 \simeq \frac{\mu^2 T}{\pi^2}\int_0^\infty dx\, \frac{x^2}{1+\cosh x} = \frac{\mu^2 T}{3}\,. \tag{214}$$

Before evaluating the specific heat in the superconducting phase at small temperatures, let us discuss the behavior of c_V at the critical temperature. This is best done by looking at Eq. (211). Approaching T_c from above, c_V is given by setting Δ_0 and $\Delta(T)$ (appearing in ϵ_k) to zero in that equation. In the superconducting phase, approaching T_c from below, we only set Δ in ϵ_k to zero. Consequently, at T_c there is a jump in the specific heat which is given by

$$\Delta c_V \;=\; 2\frac{\Delta_0^2}{T_c^2}\int \frac{d^3\mathbf{k}}{(2\pi)^3}\frac{e^{\epsilon_k/T}}{\left(e^{\epsilon_k/T}+1\right)^2} \simeq \frac{\Delta_0^2\mu^2}{\pi^2 T_c}\int_0^\infty dx\,\frac{1}{1+\cosh x} = \frac{\Delta_0^2\mu^2}{\pi^2 T_c}\,, \tag{215}$$

where we have assumed the gap to be isotropic. This jump is a typical signature for a second-order phase transition, since the specific heat is the second derivative of the thermodynamic potential.

Next we evaluate Eq. (213) for temperatures much smaller than the gap, i.e., in the limit $\varphi \to \infty$. First we consider an isotropic gap. We can approximate

$$\frac{e^{\sqrt{x^2+\varphi^2}}}{\left(e^{\sqrt{x^2+\varphi^2}}+1\right)^2} \simeq e^{-\sqrt{x^2+\varphi^2}} \simeq e^{-\varphi-\frac{x^2}{2\varphi}}\,. \tag{216}$$

Consequently,

$$c_V \;\simeq\; \frac{2\mu^2 T}{\pi^2}e^{-\varphi}\left[\int_0^\infty dx\, x^2 e^{-\frac{x^2}{2\varphi}} + \left(\varphi^2+\frac{\Delta_0^2}{T_c^2}\right)\int_0^\infty dx\, e^{-\frac{x^2}{2\varphi}}\right] \simeq \frac{\sqrt{2}\mu^2 T}{\pi^{3/2}}\varphi^{5/2}e^{-\varphi}\,, \tag{217}$$

where we used

$$\int_0^\infty dx\, x^2 e^{-\frac{x^2}{2\varphi}} = \varphi^{3/2}\sqrt{\frac{\pi}{2}}\,, \qquad \int_0^\infty dx\, e^{-\frac{x^2}{2\varphi}} = \varphi^{1/2}\sqrt{\frac{\pi}{2}}\,. \tag{218}$$

The main result is that the specific heat is exponentially suppressed by the factor $e^{-\varphi} = e^{-\Delta/T}$ for temperatures much smaller than the gap. The suppression of the specific heat in a superconductor provides a good example to get some intuition for the properties of superconductors. To this end, note that the specific heat is a measure of how many degrees of freedom are available to store heat. A large number of degrees of freedom means a lot of "storage room" and thus a large specific heat. A small specific heat, such as for a superconductor at sufficiently small temperature, thus means there are very few states available. This is a direct consequence of the energy gap which obviously leads to a region in the energy spectrum with no allowed states. Only by increasing the temperature does the exponential suppression disappear because temperature provides the energy to populate states above the gap which in turn are then available to store thermal energy.

Next let us assume an anisotropic gap of the form

$$\Delta \to \Delta \sin\theta\,. \tag{219}$$

In a compact star, anisotropic gaps may be realized in neutron superfluidity and possibly for quark superconductivity. The reason is very different in the two kinds of matter: at large density, the s-wave interactions between neutrons become repulsive and thus only interactions in the p-wave channel can lead to superfluidity (this is in contrast to protons which do form s-wave superconductors). In the case of quark matter, anisotropic gaps may occur due to a mismatch in Fermi momenta of the quarks that form Cooper pairs; anisotropies then arise either because the mismatch allows only for pairing in certain directions in momentum space or because pairing occurs in the spin-one channel

which does not suffer from the mismatch. In either case, there are several possibilities for the specific form of the angular dependence of the gap and it is not entirely clear which one is realized in the relevant density regime. For more details see for instance Refs. [32, 33] for nuclear matter and Ref. [34] for quark matter.

With θ being the angle between the momentum and the z-axis, the form (219) implies point-like nodes of the gap function at the north and south pole of the Fermi sphere. In other words, although there is a nonzero order parameter for superfluidity, there are directions in momentum space where quasiparticles can be excited with infinitesimally small energy. For sufficiently small temperatures, these directions give the dominant contribution to the specific heat. Therefore, in the low-temperature approximation, we only integrate over angles in the vicinity of the nodes. We restrict the angular integration by requiring the quasiparticle energy (with respect to the Fermi surface) to be at most of the order of the scale set by the temperature,

$$\Delta_0 \sin\theta \lesssim \pi T \,, \tag{220}$$

which, for small angles θ and small temperatures implies $\theta \lesssim \pi/\varphi$. Therefore, the specific heat becomes (note the factor 2 since we obtain the same result for north and south pole)

$$c_V \;\simeq\; \frac{\mu^2 T}{\pi^2} \int_0^\infty dx \, \frac{1}{1+\cosh x} \int_0^{\pi/\varphi} d\theta \, \theta(x^2+\varphi^2\theta^2) \simeq \frac{5\pi^2}{4} \frac{\mu^2 T}{3} \frac{1}{\varphi^2} \tag{221}$$

We see that instead of an exponential suppression we now get a power-law suppression $\propto (T/\Delta)^2$ of the specific heat compared to the non-superconducting result. In this sense, the specific heat measures how effectively the quasiparticle excitations are suppressed by the gap. Our result shows that the dimensionality of the zero-energy excitations in momentum space translates into the temperature dependence of the specific heat: in the normal phase, there is a two-dimensional Fermi surface that contributes at $T = 0$, while for an isotropic gap, this Fermi surface is, simply speaking, gone. The anisotropic gap (219) is an intermediate case, its suppression lies between the normal and the completely gapped phase. One may thus expect that between the zero-dimensional point nodes and the fully gapped spectrum there is another intermediate case, namely one-dimensional line nodes, see problem IV.1.

The low-temperature results for the specific heat are relevant for the physics of compact stars because the superconducting gap of either nucleonic superconductivity/superfluidity or quark superconductivity may well be much larger than the temperature of the star. In particular, the specific heat is important in the context of the cooling of the star, for example through neutrino emissivity ϵ_ν. With ϵ_ν being the energy loss per unit time and volume through neutrino emission (for example through the processes (31) in nuclear matter or the processes (45) in quark matter), the relation between ϵ_ν, c_V, and the change in temperature is

$$\epsilon_\nu(T) = -c_V(T) \frac{dT}{dt} \,. \tag{222}$$

(The minus sign is needed since a positive ϵ_ν is an energy loss, i.e., the temperature will decrease, $dT/dt < 0$.) Integrating this relation from a time t_0 (with temperature $T(t_0) = T_0$) yields

$$t - t_0 = -\int_{T_0}^{T} dT' \, \frac{c_V(T')}{\epsilon_\nu(T')} \,. \tag{223}$$

This shows that the ratio of the specific heat and the neutrino emissivity enters the cooling behavior of the star. Typically, for a given phase, the neutrino emissivity will exhibit a similar behavior as the specific heat. For instance, in a superconductor, the emissivity as well as the specific heat are exponentially suppressed in which case the subleading behavior becomes important. In a real compact star, however, there is most likely not just a single phase and the phase that dominates the behavior of the emissivity is not necessarily the one that dominates the specific heat.

The neutrino emissivity is much more difficult to compute than the specific heat, and we devote a whole chapter to its discussion and to a detailed calculation for the case of quark matter, see chapter V.

B. Color-flavor locked (CFL) quark matter

In our discussion of superconductivity and superfluidity in compact stars we first focus on a density regime where we can perform rigorous calculations from first principles. This is the regime of asymptotically large densities, where we deal with weakly coupled, deconfined quark matter.[7] The quarks are weakly coupled due to *asymptotic freedom*,

[7] We shall not go into details of neutron superfluidity and proton superconductivity. For a detailed review of these matters, see Ref. [35]. A shorter discussion can be found for instance in Sec. 3.2 of Ref. [4].

which says that the coupling of QCD becomes weak for large exchanged momenta. For our purpose, the QCD coupling can be considered as a function of the quark chemical potential and becomes arbitrarily small for large chemical potentials. In other words, quarks at infinite chemical potential are free. Because of this important property of QCD we may use perturbative methods at high densities. The high-density region of the QCD phase diagram shown in Fig. 1 is therefore maybe the best understood regime of QCD. The other regimes in that phase diagram are more complicated: we have seen that for nuclear matter one usually relies on phenomenological models; the high-temperature, small-density region, where the QCD coupling also becomes small, has subtle nonperturbative effects because of infrared degrees of freedom; first-principle QCD calculations via computer simulations (*lattice QCD*) are much more complicated than perturbative physics at high densities and are so far restricted to vanishing chemical potential.

This possibility of understanding a region of the phase diagram rigorously from first principles is a good theoretical motivation to study ultra-dense quark matter. However, for our astrophysical purposes we need to point out that these studies are valid at densities much larger than expected in compact stars. In a compact star, the quark chemical potential is at most of the order of $\mu \lesssim 500\,\mathrm{MeV}$. The perturbative calculation of the energy gap Δ, to be discussed in Sec. IV C, can be estimated to be reasonable at chemical potentials of the order of $\mu \gtrsim 10^8\,\mathrm{MeV}$ (!) Given this difference of many orders of magnitude, extrapolation of perturbative results down to compact star densities may seem bold. However, the (rough) quantitative agreement of these extrapolations with different approaches, using phenomenological models, gives us some confidence that the ultra-high density calculation may be of relevance for astrophysical calculations. Furthermore, we shall also apply general arguments, based on symmetries, which we can expect to hold even at moderate density where the coupling is strong. In summary, the following discussion, strictly speaking only valid for extreme densities, is of theoretical interest and may also give us insight into compact star physics.

At this point we may remember that we have already discussed the approach to compact star densities from the opposite side. In the Walecka model of Sec. III A we have constructed the model such that we have reproduced properties of nuclear matter at densities accessible in the laboratory. These densities are *lower* than the ones in compact stars. We had to extrapolate up to higher densities to obtain predictions of astrophysical relevance. Therefore, we learn that matter inside compact stars is quite hard to tackle; we have to approach it from different sides, and currently we do not have rigorous control over our approaches. This reflects the discussion begun in the introduction: it shows that the question "What is the matter composition inside a compact star?" is, due to our lack of understanding of dense, strongly-interacting matter, not only an application of QCD but also relevant to understand QCD.

From this somewhat philosophical discussion now back to superconductivity in quark matter. Cooper's Theorem tells us that an attractive interaction, however small it may be, leads to the formation of a quark Cooper pair condensate. At asymptotically high densities, this attractive interaction is provided by single-gluon exchange. We can formulate quark pairing in terms of representations of the color gauge group $SU(3)_c$,

$$SU(3)_c: \qquad [\mathbf{3}]_c \otimes [\mathbf{3}]_c = [\bar{\mathbf{3}}]_c^A \oplus [\mathbf{6}]_c^S \,. \tag{224}$$

On the left-hand side we have two quarks in the fundamental representation, i.e., two complex three-vectors since the number of colors is three, $N_c = 3$. They interact in an antisymmetric (A) anti-triplet channel and a symmetric (S) sextet channel which are attractive and repulsive, respectively. The attractive channel thus provides an anti-triplet of diquarks which has (anti-)color charge. The attractiveness of this channel can be understood for instance from the existence of baryons. Namely, in a simple picture a baryon contains a diquark in the $[\bar{\mathbf{3}}]_c^A$ representation. If it is made of, say, a red and a green quark it has color anti-blue. The baryon is then color-neutralized by combining this anti-blue diquark with a blue quark.

An obvious property of a quark Cooper pair is that it is color-charged. Therefore, it breaks the color symmetry $SU(3)_c$ spontaneously. In analogy to electronic superconductors, which break the electromagnetic $U(1)_{\mathrm{em}}$, quark Cooper pairing is thus termed *color superconductivity*. For an extensive review of color superconductivity see Ref. [8]. The order parameter of color superconductivity is the expectation value of the quark-quark two-point function $\langle\psi\psi\rangle$. The color structure of this object has to be antisymmetric because the antisymmetric representation $[\bar{\mathbf{3}}]_c^A$ is the attractive channel. The flavor structure is governed by the chiral symmetry group $SU(3)_R \times SU(3)_L$,[8] discussed in Sec. III C 1. For now, we may consider these symmetries to be exact, since at the high densities we are working we may neglect all three quark masses compared to the chemical potential. Each of these global $SU(3)$'s leads to the

[8] As already mentioned in the introduction, we neglect the heavy quark flavors although in this section we consider asymptotically large densities. Since we are ultimately interested in extrapolating our results down to compact star densities, we only take u, d, and s quarks into account.

same representations as the color group,

$$SU(3)_f: \qquad [\mathbf{3}]_f \otimes [\mathbf{3}]_f = [\bar{\mathbf{3}}]_f^A \oplus [\mathbf{6}]_f^S \,, \tag{225}$$

with $f = L, R$. Since the overall wave function of the Cooper pair has to be antisymmetric and since pairing in the antisymmetric spin-zero channel is preferred, we need to pair in the flavor $[\bar{\mathbf{3}}]_f^A$ channel. In other words, the color-flavor structure of the Cooper pair is

$$\langle \psi\psi \rangle \in [\bar{\mathbf{3}}]_c^A \otimes [\bar{\mathbf{3}}]_f^A \,. \tag{226}$$

More specifically, with $A, \alpha, \beta \leq 3$ being color indices and $B, i, j \leq 3$ being flavor indices,

$$\langle \psi_i^\alpha C\gamma_5 \psi_j^\beta \rangle \propto \epsilon^{\alpha\beta A} \epsilon_{ijB} \phi_A^B \,. \tag{227}$$

Here, we have added the Dirac structure with the charge-conjugation matrix $C \equiv i\gamma^2\gamma^0$, leading to even-parity, spin-singlet pairing. The 3×3 matrix ϕ now determines the specific color-flavor structure within the given antisymmetric representations. This shows that there are in principle many different possible color-superconducting phases. They are distinguished by different pairing patterns, i.e., by which quark pairs with which other quark. (At asymptotically large densities, where the flavor symmetries are exact, many pairing patterns are equivalent by symmetry and only a few physically distinct phases exist.) In particular, one may construct phases in which some of the quarks are paired while some others are not.

At high densities, the favored phase is the *color-flavor locked (CFL)* phase [36]. We can characterize it by the following properties,

(i) The CFL order parameter is given by

$$\phi_A^B = \delta_A^B \quad \Rightarrow \quad \langle \psi_i^\alpha C\gamma_5 \psi_j^\beta \rangle \propto \epsilon^{\alpha\beta A} \epsilon_{ijA} \,. \tag{228}$$

(ii) In the CFL phase, all quarks are paired with pairing pattern $rd - gu$, $bu - rs$, $bd - gs$, $ru - gd - bs$ (where rd is a red down quark, gu a green up quark etc.), and there are 8 quasiparticles with gap Δ and 1 quasiparticle with gap 2Δ.

(iii) The CFL phase has the following symmetry breaking pattern,

$$SU(3)_c \times SU(3)_R \times SU(3)_L \times U(1)_B \to SU(3)_{c+L+R} \times \mathbb{Z}_2 \,. \tag{229}$$

These three properties are in fact equivalent. Before discussing their physical implications, many of which can be read off from properties (ii) and (iii), let us show how the physical statement (ii) follows from the more abstract statement (i). To get a clear picture of the matrix structure of the order parameter, let us denote the bases of the color and flavor antitriplet $[\bar{\mathbf{3}}]_c^A$ and $[\bar{\mathbf{3}}]_f^A$ by $(J^A)^{\alpha\beta} = -i\epsilon^{\alpha\beta A}$, $(I_B)_{ij} = -i\epsilon_{ijB}$. Then, we can write Eq. (228) as

$$\langle \psi C\gamma_5 \psi \rangle_{\mathrm{CFL}} \propto \mathbf{J} \cdot \mathbf{I} = i \begin{pmatrix} 0 & -I_3 & I_2 \\ I_3 & 0 & -I_1 \\ -I_2 & I_1 & 0 \end{pmatrix} = \begin{pmatrix} 0 & 0 & 0 & 0 & -1 & 0 & 0 & 0 & -1 \\ 0 & 0 & 0 & 1 & 0 & 0 & 0 & 0 & 0 \\ 0 & 0 & 0 & 0 & 0 & 0 & 1 & 0 & 0 \\ 0 & 1 & 0 & 0 & 0 & 0 & 0 & 0 & 0 \\ -1 & 0 & 0 & 0 & 0 & 0 & 0 & 0 & -1 \\ 0 & 0 & 0 & 0 & 0 & 0 & 0 & 1 & 0 \\ 0 & 0 & 1 & 0 & 0 & 0 & 0 & 0 & 0 \\ 0 & 0 & 0 & 0 & 0 & 1 & 0 & 0 & 0 \\ -1 & 0 & 0 & 0 & -1 & 0 & 0 & 0 & 0 \end{pmatrix} . \tag{230}$$

This 9×9 matrix is obviously symmetric, as required (the color-flavor structure is symmetric, giving overall antisymmetry through the antisymmetric Dirac structure). Its rows and columns are labelled with the nine quarks, ru, rd, rs, gu, gd, gs, bu, bd, bs. A nonzero entry indicates that the corresponding quarks pair. We see that the matrix has a block structure with three 2×2 blocks and one 3×3 block. This leads to the pairing pattern given in point (ii). Note that this is a basis dependent statement. In particular, since the color symmetry is a gauge symmetry, $\langle \psi C\gamma_5 \psi \rangle$ is a gauge variant object. The physically relevant statement, however, is the second part of point (ii) about

the quasiparticle excitations. This statement is gauge invariant. The gap structure is given by the eigenvalues of the square of the above 9×9 matrix,

$$\epsilon_{k,r} = \sqrt{(k-\mu)^2 + \lambda_r \Delta^2}\,, \tag{231}$$

where λ_r are the eigenvalues of

$$L \equiv (\mathbf{J}\cdot\mathbf{I})^2\,. \tag{232}$$

We shall prove the form of the quasiparticle excitations (231) in Sec. IV C. Here we simply compute the eigenvalues λ_r. They are given by the solutions of

$$\det(\lambda - L) = 0\,. \tag{233}$$

This can be rewritten as

$$0 = \exp\left[\mathrm{Tr}\ln(\lambda - L)\right] = \exp\left[\mathrm{Tr}\left(\ln\lambda - \sum_{n=1}^{\infty}\frac{L^n}{n\lambda^n}\right)\right]\,. \tag{234}$$

We now have to compute L^n. First note that

$$(\mathbf{J}\cdot\mathbf{I})^{\alpha\beta}_{ij} = -\epsilon^{\alpha\beta A}\epsilon_{ijA} = -\delta^\alpha_i\delta^\beta_j + \delta^\alpha_j\delta^\beta_i \quad\Rightarrow\quad L^{\alpha\beta}_{ij} = \delta^{\alpha\beta}\delta_{ij} + \delta^\alpha_i\delta^\beta_j\,. \tag{235}$$

This result can be used to compute

$$L^2 = 5L - 4\,. \tag{236}$$

Consequently, all powers of L only have the matrix structures L and $\mathbf{1}$. Thus we make the ansatz

$$L^n = a_n L + b_n\,. \tag{237}$$

Multiplying both sides of this equation by L and using Eq. (236) yields

$$a_{n+1} = 5a_n + b_n\,, \qquad b_{n+1} = -4a_n\,. \tag{238}$$

These recursion relations can be solved with the ansatz $a_n = p^n$. This yields the equation $p^2 = 5p - 4$ which is solved by $p_1 = 4$ and $p_2 = 1$. Consequently, the general solution is the linear combination

$$a_n = \alpha p_1^n + \beta p_2^n = 4^n\alpha + \beta\,. \tag{239}$$

From above we know $a_1 = 1$ and $a_2 = 5$ which yields $\alpha = -\beta = -1/3$. Hence

$$L^n = \frac{4^n - 1}{3}\,L - \frac{4^n - 4}{3}\,. \tag{240}$$

Inserting this into Eq. (234) yields

$$0 = \exp\left\{\mathrm{Tr}\left[\frac{L-1}{3}\ln(\lambda-4) - \frac{L-4}{3}\ln(\lambda-1)\right]\right\}\,. \tag{241}$$

Now we use $\mathrm{Tr}\,\mathbf{1} = 9$ and, from Eq. (235), $\mathrm{Tr}\,L = 12$. Thus we have

$$0 = \exp\left[\ln(\lambda-4) + 8\ln(\lambda-1)\right] = (\lambda-4)(\lambda-1)^8\,. \tag{242}$$

Consequently, the eigenvalues of L are 1 (8-fold) and 4 (1-fold). Physically speaking, together with Eq. (231) this means that in the CFL phase 8 quasiparticle excitations have a gap Δ and 1 quasiparticle excitation has a gap 2Δ. This is the second part of point (ii). Of course, this discussion says nothing about the magnitude of Δ, which has to be computed from the QCD gap equation, see subsequent section. We leave it as an exercise to show that (iii) follows from (i), see problem IV.2.

Points (ii) and (iii) reveal many important physical properties of the CFL state. Since these points are solely based symmetry considerations, they are independent of the details of the interaction. Therefore, they can be expected to hold also at lower densities where perturbative QCD is not applicable. First, one may ask why CFL is the ground state

and not any other order parameter given by a different matrix ϕ_A^B. The simple answer is that the CFL order parameter is the only one in which all quarks participate in pairing, as we have seen. All other possible order parameters leave several excitations ungapped. Therefore, the CFL phase leads to the largest condensation energy and thus is the ground state at high densities (at lower densities the situation is much more complicated). A more formal argument is that the CFL phase is the color superconductor with the largest residual symmetry group. It is thus a particularly symmetric state which also indicates that it is preferred over other color superconductors, although this is not a rigorous argument.

From (iii) we read off the following properties of CFL,

- CFL breaks chiral symmetry. We see that the CFL symmetry breaking pattern (229) is, regarding chiral symmetry, the same as in Eq. (148). However, the mechanisms are different. The latter is caused by a chiral condensate of the form $\langle\bar{\psi}_R\psi_L\rangle$, while the CFL condensate has the form $\langle\psi_R\psi_R\rangle$ (and the same with $R \to L$). At first sight, the CFL condensate thus preserves the full chiral symmetry, i.e., apparently one can still do separate L and R rotations without changing the ground state. However, the symmetry breaking occurs through the "locking" with color, i.e., in order to leave the order parameter invariant, a color rotation has to be undone by equal rotations in the left- and right-handed sectors. Although caused by different mechanisms, the two scenarios lead to similar physics. As for the usual chiral symmetry breaking, the CFL phase also has an octet of Goldstone modes. Since all fermions acquire an energy gap, these Goldstone modes become very important for the phenomenology of the CFL phase. Moreover, at lower densities, where the strange quark mass cannot be neglected, kaon condensation, is expected in the CFL phase, not unlike its nuclear matter relative discussed in Sec. III C. The kaon-condensed CFL phase is usually called CFL-K^0 and will be discussed in the next subsection, Sec. IV B 1.

- The color gauge group is completely broken. While spontaneous breaking of a global group leads to Goldstone bosons, spontaneous breaking of a gauge group leads to masses for the gauge bosons. Here, all gluons acquire a Meissner mass, just as the photon acquires a Meissner mass in an electronic superconductor. A nonzero Meissner mass for a gauge boson is the field-theoretical way of saying that there is a Meissner effect, i.e., that the magnetic field can penetrate the superconductor only up to a certain penetration depth. The inverse of this penetration depth corresponds to the Meissner mass. In the CFL phase, one linear combination of a gluon and the photon remains massless. In other words, there is an unbroken $U(1)_{\tilde{Q}} \subseteq SU(3)_{c+L+R}$, generated by $\tilde{Q}$ which is a linear combination of the original charge generator Q and the eighth gluon generator T_8 (if you have done problem IV.2 you can easily show this and determine the exact form of the linear combination). This phenomenon is also called *rotated electromagnetism*. Since the admixture of the gluon to the new gauge boson is small, one may say that the CFL phase is a color superconductor but no electromagnetic superconductor. This is of relevance for compact stars since it implies that the CFL phase does not expel magnetic fields.

- The CFL phase is a superfluid since it breaks the baryon number conservation group $U(1)_B$. This is important since this is an exact symmetry, even at lower densities where finite quark masses become important. Therefore, there is always one exactly massless Goldstone mode in the CFL phase.

1. *Kaon condensation in CFL quark matter*

We have pointed out that chiral symmetry is not only broken in the hadronic phase, but also in CFL. This is by itself an interesting fact since it means that in QCD chiral symmetry is spontaneously broken at very low and very high densities. How about the region in between? This is unknown, but the possibility remains that chiral symmetry is, at small temperatures, broken for all densities. Since the symmetry breaking patterns of nuclear matter and CFL are identical (note that in a neutron superfluid also the $U(1)_B$ is broken), this implies that possibly there is no real phase transition at moderate densities and small densities in the QCD phase diagram. In Fig. 1 this corresponds to the possibility that the "non-CFL" region is absent, at least at $T = 0$.

Now let us use the chiral symmetry breaking of CFL for a concrete calculation. Since in the CFL phase all (quasi)fermions acquire energy gaps of at least Δ – whose magnitude we compute from first principles in Sec. IV C – the physics of the CFL phase at temperatures smaller than Δ is determined by the pseudo-Goldstone modes associated to chiral symmetry breaking (and the exact Goldstone mode from breaking of $U(1)_B$ which we do not discuss here). As we discuss below, Δ can be expected to be of the order of 10 MeV at densities present in compact stars. This is large enough to make fermionic excitations in a possible CFL phase in a star essentially irrelevant. Therefore, for astrophysical applications, the discussion of the physical properties of the Goldstone modes is crucial.

In the context of kaon condensation in nuclear matter, Sec. III C, we have used an effective theory for the chiral field U and its interactions with nucleons. Also for the mesons in CFL we can write down such a theory. In this case,

the chiral field is given by

$$\Sigma = \phi_L^\dagger \phi_R \,, \tag{243}$$

where ϕ_L and ϕ_R are the 3×3 matrix order parameters in the left- and right-handed sector. In our above discussion we have not distinguished between ϕ_L and ϕ_R since in "pure" CFL we have $\phi_L = \phi_R = \mathbf{1}$. For unitary 3×3 matrices ϕ_L and ϕ_R, Σ is unitary, $\Sigma \in U(3)$. It thus contains 9 degrees of freedom, one of which one usually ignores since it corresponds to the η' which is heavy due to the explicitly broken $U(1)_A$. Eight degrees of freedom remain, $\Sigma \in SU(3)$, and we can identify them as pions, kaons etc. just like in hadronic matter, see Eq. (150). Despite the similarities, there is an important difference to hadronic matter: as one can see from the definition of the chiral field (243), a meson in CFL is composed of two fermions and two fermion holes (each ϕ in Eq. (243) represents a diquark). For example, a neutral kaon should be viewed as an excitation $K^0 \sim \bar{u}\bar{s}du$. Note that this "CFL kaon" has the same quantum numbers as the "usual kaon", composed of a particle and an antiparticle, $K^0 \sim \bar{s}d$. Hence, if you want to construct a CFL kaon from a usual kaon you need to replace $s \to \bar{d}\bar{u}$ and $d \to \bar{u}\bar{s}$. This identification reflects the *anti*-triplet representation in Eq. (225). As a consequence, the meson masses in CFL are ordered inversely compared to the usual mesons. To see this, first note that the quark flavors (u, d, s), ordered with increasing mass, $m_u < m_d < m_s$, have the anti-triplet counterpart $(\bar{d}\bar{s}, \bar{u}\bar{s}, \bar{u}\bar{d})$. Here the masses (squared) have become ordered in the opposite way, $m_d m_s > m_u m_s > m_u m_d$. Therefore, in nuclear matter (and ignoring finite density effects), $m_{\pi^0} < m_{K^0}$ because $m_{\pi^0} \propto m_u + m_d$ and $m_{K^0} \propto m_s + m_d$, whereas in CFL $m_{K^0} < m_{\pi^0}$ because $m_{K^0}^2 \propto m_u m_d + m_u m_s$ and $m_{\pi^0}^2 \propto m_d m_s + m_u m_s$. We shall verify the form of the kaon mass in CFL below within the effective theory.

The effective Lagrangian for mesons in CFL is given by

$$\mathcal{L} = \frac{f_\pi^2}{4}\mathrm{Tr}[\nabla_0\Sigma\nabla_0\Sigma^\dagger - v_\pi^2\partial_i\Sigma\partial_i\Sigma^\dagger] + \frac{a f_\pi^2}{2}\det M\,\mathrm{Tr}[M^{-1}(\Sigma+\Sigma^\dagger)] \,, \tag{244}$$

with

$$\nabla_0\Sigma \equiv \partial_0\Sigma + i[A,\Sigma] \,, \qquad A \equiv -\frac{M^2}{2\mu} \,, \tag{245}$$

where $M = \mathrm{diag}(m_u, m_d, m_s)$ is the quark mass matrix. The matrix A enters the theory as the temporal component of a gauge field; it plays the role of an effective chemical potential for the field Σ. We shall see below how this translates into effective chemical potentials for the neutral and charged kaons.

The original works where this Lagrangian has been proposed are Refs. [37, 38]. There you can find detailed explanations about the structure of the effective Lagrangian and its differences to the effective meson Lagrangian for hadronic matter (153). Comparing with Eq. (153) we see that in CFL we do not have a term linear in the quark masses, rather only quadratic, $M^{-1}\det M \propto m^2$ (and higher even powers which we have neglected). We also have different coefficients in front of the temporal and spatial part of the kinetic term, originating from the breaking of Lorentz invariance in a medium, $v_\pi = 1/\sqrt{3}$. As for the hadronic phase, there are two constants f_π and a. This reminds us of the nature of effective theories like the ones given by Eqs. (153) and (244): they are expected to give at least a qualitatively correct description even beyond the regime where the theory can be tested experimentally or from first-principle calculations. The reason is that they are almost entirely determined by symmetries. Only the coefficients have to be taken from the experiment or an underlying microscopic theory. The former is done in the effective theory of the hadronic phase. The latter, namely fixing the constants f_π and a from perturbative QCD, is done for the effective theory of CFL. In particular, one can expect that, if CFL is the ground state of dense quark matter at densities relevant for compact stars, the effective theory is a powerful tool to compute the phenomenology of a potential quark core of the star.

Although terms of higher order in the fields and the mass matrix have already been neglected in Eq. (244), the Lagrangian still looks complicate. The meson fields θ_a appear in the exponent of Σ,

$$\Sigma = e^{i\theta_a\lambda_a/f_\pi} \,, \tag{246}$$

with the Gell-Mann matrices λ_a, and thus they appear to all orders even in the given truncated theory. Let us first rewrite the Lagrangian by abbreviating $Q \equiv \theta_a\lambda_a/f_\pi$ such that

$$\Sigma = e^{iQ} = \cos Q + i\sin Q \,. \tag{247}$$

Then, the various terms of the Lagrangian become

$$\mathrm{Tr}[\partial_0\Sigma\partial_0\Sigma^\dagger] = \mathrm{Tr}[(\partial_0\cos Q)^2 + (\partial_0\sin Q)^2] \,, \tag{248a}$$

$$\mathrm{Tr}[\partial_i\Sigma\partial_i\Sigma^\dagger] = \mathrm{Tr}[(\nabla\cos Q)^2 + (\nabla\sin Q)^2] \,, \tag{248b}$$

$$\mathrm{Tr}\left[[A,\Sigma][A,\Sigma]^\dagger\right] = 2\mathrm{Tr}[A^2 - (A\cos Q)^2 - (A\sin Q)^2] \,, \tag{248c}$$

$$i\mathrm{Tr}[-\partial_0\Sigma[A,\Sigma]^\dagger + [A,\Sigma]\partial_0\Sigma^\dagger] = 2i\mathrm{Tr}[(\partial_0\cos Q)[A,\cos Q] + (\partial_0\sin Q)[A,\sin Q]] \,, \tag{248d}$$

and thus

$$\begin{aligned}\mathcal{L} &= \frac{f_\pi^2}{2}\mathrm{Tr}[A^2-(A\cos Q)^2-(A\sin Q)^2+2a(\det M)M^{-1}\cos Q]\\ &+\frac{f_\pi^2}{4}\mathrm{Tr}[(\partial_0\cos Q)^2+(\partial_0\sin Q)^2-v_\pi^2[(\nabla\cos Q)^2+(\nabla\sin Q)^2]]\\ &+i\frac{f_\pi^2}{2}\mathrm{Tr}[(\partial_0\cos Q)[A,\cos Q]+(\partial_0\sin Q)[A,\sin Q]]\,. \end{aligned} \tag{249}$$

Let us first interpret Q as a constant background, i.e., as the meson condensate, and neglect the fluctuations. This will allow us to compute the values of the various condensates at zero temperature. In general, all mesons may condense and the parameters of the theory determine which of the condensates becomes nonzero. We recall from the above discussion that we expect the kaons, not the pions, to be the lightest mesons in CFL. Therefore, let us simplify Q by setting all fields except the kaon fields to zero,

$$Q=\sum_{a=4}^{7}\phi_a\lambda_a=\begin{pmatrix}0 & 0 & \phi_4-i\phi_5\\ 0 & 0 & \phi_6-i\phi_7\\ \phi_4+i\phi_5 & \phi_6+i\phi_7 & 0\end{pmatrix}, \tag{250}$$

with the dimensionless condensates $\phi_a\equiv\theta_a/f_\pi$. With this ansatz we shall be able to construct a zero-temperature phase diagram that contains regions of no condensates, charged kaon condensates, neutral kaon condensates, and possibly coexistence of both. This is exactly the same ansatz as we have made in Sec. III C 3 for kaon condensation in nuclear matter, see Eq. (163). We can thus follow the steps below Eq. (163) to obtain

$$\cos Q = 1-\frac{Q^2}{\phi^2}(1-\cos\phi)\,, \tag{251}$$

and

$$\sin Q = \frac{Q}{\phi}\sin\phi\,, \tag{252}$$

where

$$\phi^2\equiv\phi_4^2+\phi_5^2+\phi_6^2+\phi_7^2\,. \tag{253}$$

Since we assume our condensates to be constant in time and space, only the first line of the Lagrangian (249) survives. The tree-level zero-temperature free energy is the negative of this Lagrangian and becomes

$$U = \frac{f_\pi^2}{2}\mathrm{Tr}\left[2\frac{1-\cos\phi}{\phi^2}\left(a(\det M)M^{-1}Q^2-A^2Q^2\right)+\frac{(1-\cos\phi)^2}{\phi^4}(AQ^2)^2+\frac{\sin^2\phi}{\phi^2}(AQ)^2\right], \tag{254}$$

where we have subtracted the "vacuum" contribution

$$U_{\rm CFL}=U(\Sigma=\mathbf{1})=-f_\pi^2 a\det M\,\mathrm{Tr}[M^{-1}]\,, \tag{255}$$

such that the state without kaon condensates, i.e., the pure CFL state has free energy $U=0$. With the definitions of the matrices A and Q in Eqs. (245) and (250), the notations

$$\phi_{K^+}^2\equiv\phi_4^2+\phi_5^2\,,\qquad \phi_{K^0}^2\equiv\phi_6^2+\phi_7^2\,, \tag{256}$$

and abbreviating $A=\mathrm{diag}(a_1,a_2,a_3)$, the various traces are

$$\mathrm{Tr}[a(\det M)M^{-1}Q^2-A^2Q^2] = (m_{K^+}^2-\mu_{K^+}^2)\phi_{K^+}^2+(m_{K^0}^2-\mu_{K^0}^2)\phi_{K^0}^2-2a_3(a_1\phi_{K^+}^2+a_2\phi_{K^0}^2)\,, \tag{257a}$$

$$\mathrm{Tr}[(AQ^2)^2] = (a_1\phi_{K^+}^2+a_2\phi_{K^0}^2)^2+a_3^2\phi^4\,, \tag{257b}$$

$$\mathrm{Tr}[(AQ)^2] = 2a_3(a_1\phi_{K^+}^2+a_2\phi_{K^0}^2)\,, \tag{257c}$$

where we have defined the kaon chemical potentials and masses

$$\mu_{K^+} \equiv \frac{m_s^2-m_u^2}{2\mu}\,,\qquad \mu_{K^0}\equiv\frac{m_s^2-m_d^2}{2\mu}\,, \tag{258a}$$

$$m_{K^+}^2 \equiv am_d(m_s+m_u)\,,\qquad m_{K^0}^2\equiv am_u(m_s+m_d)\,. \tag{258b}$$

It will become clear below that these quantities really act as masses and chemical potentials for the kaons. For simplicity we have omitted the electric charge chemical potential in the Lagrangian which would have appeared in μ_{K^+} as an additional contribution. Inserting Eqs. (257) into Eq. (254), we can write the free energy as

$$\frac{U(\phi_1,\phi_2)}{f_\pi^2} \;=\; (1-\cos\phi)\left[(m_1^2-\mu_1^2)\frac{\phi_1^2}{\phi^2}+(m_2^2-\mu_2^2)\frac{\phi_2^2}{\phi^2}\right]+\frac{1}{2}(1-\cos\phi)^2\left(\mu_1\frac{\phi_1^2}{\phi^2}+\mu_2\frac{\phi_2^2}{\phi^2}\right)^2 . \tag{259}$$

Here and in the following we use, for notational convenience, the subscript 1 for K^+ and 2 for K^0. To understand the expression for the free energy we consider the limit case of small condensates, $\theta_i \ll f_\pi$, i.e., $\phi_i = \theta_i/f_\pi \ll 1$ for $i = K^+, K^0$. Then we can expand $U(\phi_1,\phi_2)$ up to fourth order in the condensates to obtain

$$U(\theta_1^2,\theta_2^2) \;\simeq\; \frac{m_1^2-\mu_1^2}{2}\theta_1^2+\frac{m_2^2-\mu_2^2}{2}\theta_2^2+\frac{\beta_1}{4}\theta_1^4+\frac{\beta_2}{4}\theta_2^4+\frac{\alpha}{4}\theta_1^2\theta_2^2\,, \tag{260}$$

with

$$\beta_i \equiv \frac{4\mu_i^2-m_i^2}{6f_\pi^2} \quad (i=K^+,K^0)\,, \qquad \alpha \equiv \frac{\beta_1+\beta_2}{2}-\frac{(\mu_1-\mu_2)^2}{4f_\pi^2}\,. \tag{261}$$

We have thus reduced the effective theory to a two-component ϕ^4 theory, cf. Eq. (A18) in appendix A 1, with effective coupling constants β_i for the self-coupling of the kaons and an effective coupling constant α for the interaction between charged and neutral kaons.

We may come back to the full free energy (259) to find the ground state of the system for arbitrary chemical potentials μ_1, μ_2. To this end, one has to minimize the free energy through the equations

$$\frac{\partial U}{\partial\phi_1}=\frac{\partial U}{\partial\phi_2}=0\,. \tag{262}$$

By construction, the free energy of the CFL state without kaon condensation, $\phi_1=\phi_2=0$, is given by $U=0$. If one of the condensates vanishes, say $\phi_2=0$, one of the equations (262) is automatically fulfilled, and the other one becomes

$$0=\frac{1}{f_\pi^2}\left.\frac{\partial U}{\partial\phi_1}\right|_{\phi_2=0}=\sin\phi_1\left(m_1^2-\mu_1^2\cos\phi_1\right)\,. \tag{263}$$

This has a nontrivial solution for $m_1^2<\mu_1^2$,

$$\cos\phi_1=\begin{cases}1 & \text{for}\quad m_1^2>\mu_1^2\\ \dfrac{m_1^2}{\mu_1^2} & \text{for}\quad m_1^2<\mu_1^2\end{cases}\,, \tag{264}$$

and the free energy density becomes

$$U(\phi_2=0)=\begin{cases}0 & \text{for}\quad m_1^2>\mu_1^2\\ -\dfrac{f_\pi^2(m_1^2-\mu_1^2)^2}{2\mu_1^2} & \text{for}\quad m_1^2<\mu_1^2\end{cases}\,. \tag{265}$$

By symmetry, we find the same solution for ϕ_2 if we set $\phi_1=0$. Equating the free energies of the two phases $\phi_1=0$, $\phi_2\neq0$ and $\phi_1\neq0$, $\phi_2=0$ one finds the condition for coexistence of two condensates,

$$\mu_2^2(\mu_1^2-m_1^2)^2=\mu_1^2(\mu_2^2-m_2^2)^2\,. \tag{266}$$

This condition can also be obtained by assuming two nonvanishing condensates in Eqs. (262). As a result we obtain the phase diagram shown in Fig. 14, where we restrict ourselves to $\mu_1,\mu_2>0$ without loss of generality.

What are the values of the kaon chemical potentials in the real world? In other words, where in the phase diagram of Fig. 14 does a compact star sit? Let us first see whether in a star we can expect the kaon chemical potentials to be larger than their mass, i.e., whether kaon condensation is possible. As discussed above, for quantitative predictions

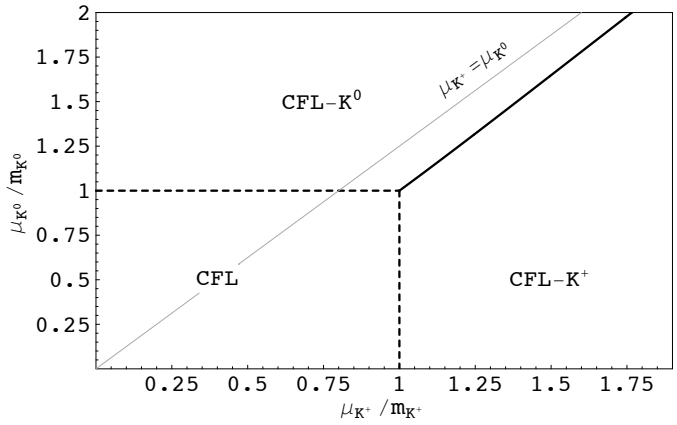

FIG. 14: Zero-temperature phase diagram for kaon condensation in the μ_{K^+}-μ_{K^0}-plane. No condensation occurs if the chemical potential is smaller than the meson mass. Coexistence of the two condensates is only possible along the (solid) line that separates the CFL-K^0 from the CFL-K^+ phase. This line is given by Eq. (266) and marks a first order phase transition. For large chemical potentials, it approaches the line $\mu_{K^+} = \mu_{K^0}$. The (dashed) lines separating either of the two meson-condensed phases from the pure CFL phase are second order phase transition lines. In the condensed phases, the condensate and free energy are given by Eqs. (264) and (265), respectively.

of the effective theory we rely on the results for the constants f_π and a at asymptotically large densities and their extrapolation down to densities in a compact star. This extrapolation yields

$$f_\pi^2 = \frac{21 - 8\ln 2}{18}\frac{\mu^2}{2\pi^2} \simeq (100\,\mathrm{MeV})^2\,, \qquad a = \frac{3\Delta^2}{\pi^2 f_\pi^2} \simeq 0.03\,, \tag{267}$$

where we used a quark chemical potential $\mu \simeq 500\,\mathrm{MeV}$ and a fermionic energy gap $\Delta \simeq 30\,\mathrm{MeV}$. Then, from Eqs. (258) we conclude that both kaon masses are of the order of $m_{K^+} \simeq m_{K^0} \simeq (a\, m_{\mathrm{light}}\, m_s)^{1/2} \simeq 5\,\mathrm{MeV}$, where we used a quark mass for u and d quarks $m_{\mathrm{light}} \simeq 5\,\mathrm{MeV}$ and a strange quark mass $m_s \simeq 150\,\mathrm{MeV}$. The kaon chemical potential then is $\mu_{K^+} \simeq \mu_{K^0} \simeq m_s^2/(2\mu) \simeq 20\,\mathrm{MeV}$. This suggests that the interior of the star sits outside the rectangle given by the dashed lines in Fig. 14, i.e., if there is a color-flavor locked core in a compact star it is likely to be kaon-condensed CFL matter rather than "pure" CFL matter (we shall confirm this conclusion below for nonzero temperatures). Does this matter contain a charged or a neutral kaon condensate? Firstly, the slightly heavier d quark compared to the u quark makes the K^+ slightly heavier than the K^0. This asymmetry is taken into account in Fig. 14. Moreover, the electric charge of a potential K^+ condensate would require the presence of electrons to neutralize the system, which further disfavors the charged kaon condensate. We thus expect the CFL-K^0 phase to be the most likely meson-condensed phase in CFL.

As a second application of the effective theory for mesons in CFL let us compute an estimate of the critical temperature of (neutral) kaon condensation. This is important to answer the question: if there is CFL matter in a compact star and if there is kaon condensation at zero temperature, at which temperature (i.e., at which point in the life of the star) does condensation set in?

The full temperature-dependent theory defined by the effective Lagrangian is very complicated. We therefore expand the Lagrangian (249) up to fourth order in the matrix-valued field Q to obtain

$$\begin{aligned}\mathcal{L} \;=\; & \frac{f_\pi^2}{2}\mathrm{Tr}\left[(A^2 - a(\det M)M^{-1})\left(Q^2 - \frac{A^2Q^4}{12}\right) - (AQ)^2 - \frac{(AQ^2)^2}{4} + \frac{(AQ^2)Q^2}{3}\right] \\ & + \frac{f_\pi^2}{4}\mathrm{Tr}\left[(\partial_0 Q)^2 - v_\pi^2(\nabla Q)^2 + 2i(\partial_0 Q)[A,Q]\right]\,,\end{aligned} \tag{268}$$

where we have neglected terms of fourth order in Q which contain derivatives such as $\mathrm{Tr}[(Q\partial_0 Q)^2]$ etc, and where we have dropped the contribution constant in Q, which serves to normalize the free energy of the pure CFL state to zero, see remark below Eq. (254). Next, one has to separate the condensate from the fluctuations, as demonstrated in appendix A 1. The resulting Lagrangian has the same structure as given in the appendix for the ϕ^4 model, see Eq. (A17): a tree-level potential; terms of second order in the fluctuations which define the tree-level propagator; terms cubic in the fluctuations which correspond to interactions due to the presence of the condensate; and finally terms quartic in the fluctuations. Here we do not discuss the explicit structure of these terms in general, for details you may

consult Ref. [39]. We rather restrict ourselves again to the kaon degrees of freedom. As a further simplification, we set the charged kaon condensate to zero, $\theta_4 = \theta_5 = 0$ (but keep the charged kaon fluctuations). This is motivated by the above discussion about the more favorable neutral kaon condensate. For the neutral kaon condensate we choose, without loss of generality, a direction in the degeneracy space of the condensate by setting $\theta_7 = 0$, and we denote $\theta \equiv \theta_{K^0} = \theta_6$. The tree-level potential from Eq. (260) then simply becomes

$$U(\theta) = \frac{m_2^2 - \mu_2^2}{2}\theta^2 + \frac{\beta_2}{4}\theta^4 \,. \tag{269}$$

The kaon sector of the inverse tree-level propagator is block diagonal,

$$D_0^{-1} = \begin{pmatrix} D_{01}^{-1} & 0 \\ 0 & D_{02}^{-1} \end{pmatrix} , \tag{270}$$

where

$$D_{01}^{-1} = \begin{pmatrix} -K^2 + m_1^2 - \mu_1^2 + \alpha\theta^2 & -2i\mu_1 k_0 \\ 2i\mu_1 k_0 & -K^2 + m_1^2 - \mu_1^2 + \alpha\theta^2 \end{pmatrix} , \tag{271a}$$

$$D_{02}^{-1} = \begin{pmatrix} -K^2 + m_2^2 - \mu_2^2 + 3\beta_2\theta^2 & -2i\mu_2 k_0 \\ 2i\mu_2 k_0 & -K^2 + m_2^2 - \mu_2^2 + \beta_2\theta^2 \end{pmatrix} , \tag{271b}$$

with the abbreviation $K^2 \equiv k_0^2 - v_\pi^2 k^2$. The verification of this form of the kaon tree-level propagator is left as an exercise, see problem IV.3. Analogously to the calculation in the appendix, we obtain the kaon dispersion relations. They are given by the poles of the propagator D_0, which are the zeros of the determinant of the inverse propagator D_0^{-1}. The dispersion for the charged kaon is

$$\epsilon_1^{\pm}(k) = \sqrt{v_\pi^2 k^2 + m_1^2 + \alpha\theta^2} \mp \mu_1 \,. \tag{272}$$

We see that the K^0 condensate gives a contribution to the mass of the K^+. For the neutral kaon we obtain

$$\epsilon_2^{\pm}(k) = \sqrt{E_k^2 + \mu_2^2 \mp \sqrt{4\mu_2^2 E_k^2 + \delta M^4}} \,, \tag{273}$$

where

$$E_k \equiv \sqrt{v_\pi^2 k^2 + m_2^2 + 2\beta_2\theta^2} \,, \qquad \delta M^2 = \beta_2\theta^2 \,. \tag{274}$$

Since kaon condensation breaks a global symmetry of the system, namely the $U(1)$ associated to conservation of strangeness, we expect a Goldstone mode. (Notice the two-fold condensation process: due to the condensation of quark Cooper pairs, chiral symmetry is broken and pseudo-Goldstone bosons appear in the system; on top of that, these pseudo-Goldstone modes – here the neutral kaons – condense themselves, breaking the global symmetry further and giving rise to another Goldstone mode.) This mode is expected to be gapless.[9] To check this expectation, we first compute the condensate from the tree-level potential (269). The nontrivial minimum of this potential is

$$\theta^2 = \frac{\mu_2^2 - m_2^2}{\beta_2} \,. \tag{275}$$

This implies $4\mu_2^2 E_{k=0}^2 + \delta M^4 = (3\mu_2^2 - m_2^2)^2$ and $E_{k=0}^2 + \mu_2^2 = 3\mu_2^2 - m_2^2$ which we can insert into the kaon dispersion (273). The result is

$$\epsilon_2^+(k=0) = 0 \,, \tag{276}$$

confirming the existence of a gapless mode.

---

[9] Due to the weak interactions this mode acquires a small energy gap in the keV range which we neglect here.

Following the calculation in the appendix, we can immediately write down the thermodynamic potential at finite temperature,

$$\Omega = U(\theta) + T \sum_{i=1,2} \sum_{e=\pm} \int \frac{d^3\mathbf{k}}{(2\pi)^3} \ln\left(1 - e^{-\epsilon_i^e/T}\right) . \tag{277}$$

In order to extract an estimate for the critical temperature, we expand the potential for large T,

$$\begin{aligned} \Omega \;&\simeq\; U(\theta) - \frac{2\pi^2}{45 v_\pi^3} T^4 + \left(\frac{\alpha + 2\beta_2}{12 v_\pi^3} \theta^2 + \frac{m_1^2 + m_2^2 - 2(\mu_1^2 + \mu_2^2)}{12 v_\pi^3} \right) T^2 + \dots \\ &=\; \left(\frac{m_2^2 - \mu_2^2}{2} + \frac{\alpha + 2\beta_2}{12 v_\pi^3} T^2 \right) \theta^2 + \frac{\beta_2}{4} \theta^4 - \frac{2\pi^2}{45 v_\pi^3} T^4 + \frac{m_1^2 + m_2^2 - 2(\mu_1^2 + \mu_2^2)}{12 v_\pi^3} T^2 + \dots \end{aligned} \tag{278}$$

The T^4 term is easy to obtain and has also been discussed in appendix A 1. For the T^2 term we have neglected δM in the neutral kaon dispersions (273). Then they assume the same form as the ones for the charged kaons (272) and we can use the expansion for the pressure of a non-interacting Bose gas, see for instance the appendix of Ref. [9].

We have arrived at a potential with terms constant, quadratic, and quartic in θ. Since we assume the existence of a condensate at $T = 0$, we have $\mu_2 > m_2$, which we have argued to be realistic for densities in compact stars. Therefore, the quartic term is always positive, while the quadratic term starts from a negative value at $T = 0$ and becomes positive for sufficiently large temperatures. Consequently, the nontrivial solution for the condensate ceases to exist when the coefficient in front of the quadratic term vanishes. This yields the condition for the critical temperature which we thus estimate to be

$$T_c^2 \simeq 6 v_\pi^3 \frac{\mu_2^2 - m_2^2}{\alpha + 2\beta_2} . \tag{279}$$

With the definitions (261) we can express T_c as a function of kaon chemical potentials and masses.[10] Before we interpret the result we point out a problem of the current approach. We have seen that at zero temperature, with $\theta(T = 0)$ given by Eq. (275), we have $\epsilon_2^+(k = 0) = 0$. At finite temperature we expect the condensate to melt, i.e., $\theta(T) < \theta(T = 0)$ for all T. In this case, however, the excitation of the Goldstone mode (which should remain gapless for all $T < T_c$ due to the Goldstone theorem) becomes imaginary if written in the form (273). This is clearly unphysical and due to the approximation we have made. The solution to this problem is to set up a more elaborate approximation scheme which evaluates the thermal kaon masses self-consistently. This is beyond the scope of these lectures, see Ref. [39] for such a treatment.

It turns out that our estimate of the critical temperature coincides with the self-consistent calculation. We can therefore use Eq. (279) for a physical conclusion. With the definition of the effective coupling constants α and β_2 in Eq. (261) and the approximate numbers for the kaon chemical potentials and masses discussed below Eq. (267) we obtain $T_c \simeq 60\,\mathrm{MeV}$. This is of the order of or even larger than the critical temperature T_c^{CFL} for CFL itself. We do not aim to compute the critical temperature of CFL in these lectures. We simply give the (mean-field) result,

$$T_c^{\mathrm{CFL}} \simeq 2^{1/3} \cdot 0.57 \Delta , \tag{280}$$

where Δ is the zero-temperature gap. This relation differs by a prefactor of order one from the relation obtained from the usual Bardeen-Cooper-Schrieffer (BCS) theory, $T_c \simeq 0.57\Delta$; see remark below Eq. (300) for the origin of this prefactor. For our present purpose it is sufficient to notice that the critical temperature in a superconductor is typically of the same order as the zero-temperature gap. Since Δ is also of the order of tens of MeV, we may apparently conclude that the kaon condensate does not melt before the CFL phase itself melts. However, we need to remember that our effective theory is only valid for temperatures smaller than the gap Δ. Therefore, the estimated critical temperature for kaon condensation is close to or beyond the limit of validity of our effective description. Nevertheless, as a tentative conclusion we can say that as soon as quark matter is cold enough to be in the CFL state, we also expect it to be cold enough for kaon condensation, provided that the parameters are such that kaon condensation is present at zero temperature. In other words, upon decreasing the temperature, one encounters the transition from unpaired quark matter to CFL-K^0, not from unpaired quark matter to CFL and then to CFL-K^0. The critical temperature we have found is larger than all temperatures we are interested in for compact star applications. Therefore, we have learned that the temperature inside a compact star is, for all times in the life of the star, sufficiently low for the CFL-K^0 phase.

---

[10] Notice that for $\alpha + 2\beta_2 < 0$ the critical temperature formally becomes imaginary, i.e., the condensate apparently "refuses" to melt. This situation cannot occur for realistic parameters in our case but is an interesting theoretical possibility. See appendix C in Ref. [39] and references therein for more information.

C. Color-superconducting gap from QCD

Let us now go through a true QCD calculation from first principles. Our goal is to compute the gap Δ with perturbative methods. As explained above, this calculation can be expected to be strictly valid only at densities much larger than present in compact stars.

In the theoretical treatment of superconductivity one introduces charge-conjugate fermions, which can be thought of as hole degrees of freedom. A hole is left in the Fermi sea if you remove a fermion. One might thus say that introducing fermion holes leads to an overcounting of the degrees of freedom because if the theory knows about all fermions it also knows about where a fermion is missing. And indeed, we have formally doubled the degrees of freedom. However, since in a superconductor quasiparticles are mixtures of fermions and fermion holes, this is a necessary extension of the theory. The fermion spinors become spinors in the so-called *Nambu-Gorkov* space and the fermion propagator becomes a 2×2 matrix in this space. The Cooper pair condensate is taken into account in the off-diagonal elements of this propagator, i.e., it couples fermions with holes. The inverse tree-level propagator in Nambu-Gorkov space is

$$S_0^{-1} = \begin{pmatrix} [G_0^+]^{-1} & 0 \\ 0 & [G_0^-]^{-1} \end{pmatrix} , \tag{281}$$

with the inverse tree-level fermion and charge-conjugate fermion propagators

$$[G_0^\pm]^{-1} = \gamma^\mu K_\mu \pm \mu\gamma_0 = \sum_{e=\pm} [k_0 \pm (\mu - ek)]\gamma_0 \Lambda_k^{\pm e} , \tag{282}$$

where

$$\Lambda_k^{\pm e} \equiv \frac{1}{2}\left(1 + e\gamma_0 \boldsymbol{\gamma}\cdot\hat{\mathbf{k}}\right) \tag{283}$$

are projectors onto positive and negative energy states. Since our QCD calculation applies to asymptotically large densities, we can safely neglect all quark masses. See appendix A 2 for a derivation of the tree-level fermion propagator and its representation in terms of energy projectors. From Eq. (282) we immediately get the tree-level propagators

$$G_0^\pm = \sum_{e=\pm} \frac{\Lambda_k^{\pm e}\gamma_0}{k_0 \pm (\mu - ek)} . \tag{284}$$

The full inverse propagator S^{-1} is obtained from a Dyson-Schwinger equation

$$S^{-1} = S_0^{-1} + \Sigma , \tag{285}$$

with the self-energy

$$\Sigma \simeq \begin{pmatrix} 0 & \Phi^- \\ \Phi^+ & 0 \end{pmatrix} . \tag{286}$$

In principle, Σ also has nonvanishing diagonal elements which we neglect here. The off-diagonal elements contain the gap function $\Delta(K)$,

$$\Phi^+(K) = \Delta(K)\mathcal{M}\gamma_5 , \qquad \Phi^-(K) = -\Delta(K)\mathcal{M}^\dagger\gamma_5 , \tag{287}$$

where $\mathcal{M}$ specifies the color-flavor structure of the color-superconducting phase, in the CFL phase $\mathcal{M} = \mathbf{J}\cdot\mathbf{I}$, see Eq. (230). From the Dyson-Schwinger equation (285) we obtain the inverse propagator, which we formally invert to obtain the propagator,

$$S = \begin{pmatrix} G^+ & F^- \\ F^+ & G^- \end{pmatrix} , \tag{288}$$

with

$$G^\pm = \left([G_0^\pm]^{-1} - \Phi^\mp G_0^\mp \Phi^\pm\right)^{-1} , \tag{289a}$$

$$F^\pm = -G_0^\mp \Phi^\pm G^\pm . \tag{289b}$$

The off-diagonal elements $F^\pm$ are termed *anomalous propagators*. They are typical for all superconductors, see for example Ref. [40]. From their structure (289b) we see that they describe the propagation of a charge-conjugate fermion that is converted into a fermion through the condensate (or vice versa). One can thus think of the condensate as a reservoir of fermions and holes, and the quasiparticles are not just single fermions but superpositions of states with fermion number $\ldots, -5, -3, -1, 1, 3, 5, \ldots$.

Inserting Eqs. (282), (284), and (287) into Eq. (289a), we compute the diagonal elements of the propagator (for simplicity we assume $\mathcal{M}^\dagger = \mathcal{M}$ which is true in the CFL phase, but may not be true in other phases),

$$G^\pm = \left\{ \sum_{e=\pm} \left[k_0 \pm (\mu - ek) - \frac{\Delta^2 L}{k_0 \mp (\mu - ek)} \right] \Lambda_k^{\mp e} \gamma_0 \right\}^{-1} , \tag{290}$$

with $L = \mathcal{M}^2$, as defined for the CFL phase in Eq. (232). Now we write L in its spectral representation,

$$L = \sum_{r=1,2} \lambda_r \mathcal{P}_r \, , \tag{291}$$

with λ_r being the eigenvalues of L, $\lambda_1 = 1$, $\lambda_2 = 4$, and $\mathcal{P}_r$ the projectors onto the corresponding eigenstates,

$$\mathcal{P}_1 = -\frac{L-4}{3} \, , \qquad \mathcal{P}_2 = \frac{L-1}{3} \, . \tag{292}$$

Obviously, these projectors are complete, $\mathcal{P}_1 + \mathcal{P}_2 = \mathbf{1}$; they are also orthogonal, $\mathcal{P}_1 \mathcal{P}_2 = 0$, as one can see with the help of Eq. (236). We obtain

$$\begin{aligned} G^\pm &= \left\{ \sum_{e,r} \left[k_0 \pm (\mu - ek) - \frac{\lambda_r \Delta^2}{k_0 \mp (\mu - ek)} \right] \mathcal{P}_r \Lambda_k^{\mp e} \gamma_0 \right\}^{-1} \\ &= \sum_{e,r} \left[k_0 \pm (\mu - ek) - \frac{\lambda_r \Delta^2}{k_0 \mp (\mu - ek)} \right]^{-1} \mathcal{P}_r \gamma_0 \Lambda_k^{\mp e} \\ &= [G_0^\mp]^{-1} \sum_{e,r} \frac{\mathcal{P}_r \Lambda_k^{\mp e}}{k_0^2 - (\epsilon_{k,r}^e)^2} \, , \end{aligned} \tag{293}$$

with

$$\epsilon_{k,r}^e = \sqrt{(ek - \mu)^2 + \lambda_r \Delta^2} \, . \tag{294}$$

The poles of the propagator are $k_0 = \pm \epsilon_{k,r}^e$, i.e., $\epsilon_{k,r}^e$ are the dispersion relations of the quasiparticles ($e = +$) and quasiantiparticles ($e = -$). We have thus confirmed Eq. (231), in particular we now understand why the eigenvalues of L appear in the excitation energies. Note that the structure of the dispersion relations is thus determined entirely by the color-flavor (and Dirac) structure of the order parameter, and thus ultimately by the symmetry breaking pattern. Only the calculation of the magnitude of Δ goes beyond simple symmetry considerations and depends on the form of the interaction between the fermions.

Using the result (293) for $G^\pm$ and Eq. (289b), one easily obtains the anomalous propagators,

$$F^\pm = \pm \Delta \mathcal{M} \gamma_5 \sum_{e,r} \frac{\mathcal{P}_r \Lambda_k^{\mp e}}{k_0^2 - (\epsilon_{k,r}^e)^2} \, . \tag{295}$$

The gap equation is a self-consistent equation for the off-diagonal elements of the self-energy Σ. We shall not discuss the detailed derivation of the gap equation (see Sec. IV.A in Ref. [8] for this derivation). The gap equation reads

$$\Phi^+(K) = g^2 \frac{T}{V} \sum_Q \gamma^\mu T_a^T F^+(Q) \gamma^\nu T_b D_{\mu\nu}^{ab}(K - Q) \, , \tag{296}$$

where g is the QCD coupling constant, which will be our expansion parameter, where $D_{\mu\nu}^{ab}$ is the gluon propagator, and where $T_a = \lambda_a/2$ ($a = 1, \ldots, 8$) with the Gell-Mann matrices λ_a. In Figs. 15 and 16 we show the self-energy and the gap equation diagrammatically.

The first step is to transform the matrix equation (296) into an equation for the scalar gap function $\Delta(K)$. To this end, we multiply both sides of the gap equation with $\gamma_5 \mathcal{M} \Lambda_k^+$ from the right and take the trace on both sides.

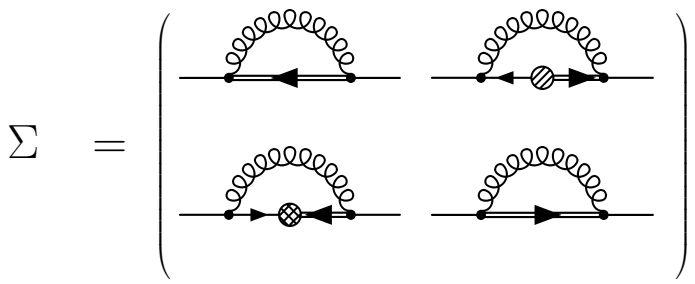

FIG. 15: Diagrammatic representation of the one-loop self-energy in Nambu-Gorkov space. Curly lines are gluon propagators, double lines correspond to G^+ (left-pointing arrow) and G^- (right-pointing arrow), single lines to G_0^+ (left-pointing arrow) and G_0^- (right-pointing arrow), and the circles are the gap matrices Φ^+ (cross-hatched) and Φ^- (hatched). The vertices have the form $g\gamma^\mu T_a$ with the QCD coupling g.

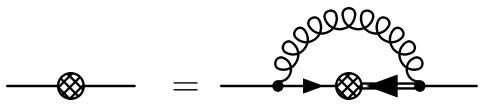

FIG. 16: Diagrammatic representation of the gap equation which arises as follows. On the one hand, the one-loop self-energy is given by cutting a fermion line in the corresponding two-loop diagram of the effective action. In Nambu-Gorkov space, this yields the matrix of four diagrams shown in Fig. 15. On the other hand, the self-energy is given by Eq. (286). Equating these two matrices leads to the gap equation in the off-diagonal elements. The algebraic form of the gap equation is given in Eq. (296). It is a self-consistent equation for Φ^+ (equivalently, one may solve the equation for Φ^-), and thus for the gap function $\Delta(K)$.

Furthermore, we neglect the antiparticle contribution $e = -$ (and denote $\epsilon_{k,r} \equiv \epsilon_{k,r}^+$) and use the fact that the gluon propagator can be taken to be diagonal in color space, $D_{\mu\nu}^{ab} = \delta^{ab} D_{\mu\nu}$. This yields

$$\begin{aligned}\Delta(K) &= \frac{g^2}{24}\frac{T}{V}\sum_Q\sum_r \frac{\Delta(Q)}{q_0^2-\epsilon_{q,r}^2}\mathrm{Tr}[\gamma^\mu\gamma_5\Lambda_q^-\gamma^\nu\gamma_5\Lambda_k^+]\,\mathrm{Tr}[T_a^T\mathcal{M}\mathcal{P}_r T_a\mathcal{M}]D_{\mu\nu}(P)\\ &= -\frac{g^2}{3}\frac{T}{V}\sum_Q\left[\frac{2}{3}\frac{\Delta(Q)}{q_0^2-\epsilon_{q,1}^2}+\frac{1}{3}\frac{\Delta(Q)}{q_0^2-\epsilon_{q,2}^2}\right]\mathrm{Tr}[\gamma^\mu\gamma_5\Lambda_q^-\gamma^\nu\gamma_5\Lambda_k^+]\,D_{\mu\nu}(P)\,, \end{aligned} \tag{297}$$

where we abbreviated $P \equiv K - Q$, and where we have used the results for the color-flavor traces

$$\mathrm{Tr}[T_a^T\mathcal{M}\mathcal{P}_1 T_a\mathcal{M}] = 2\,\mathrm{Tr}[T_a^T\mathcal{M}\mathcal{P}_2 T_a\mathcal{M}] = -\frac{16}{3}\,. \tag{298}$$

It is left as an exercise to verify these traces. With the gluon propagator in Coulomb gauge,

$$D_{00}(P) = D_\ell(P)\,, \qquad D_{0i}(P) = 0\,, \qquad D_{ij} = (\delta_{ij} - \hat{p}_i\hat{p}_j)D_t(P)\,, \tag{299}$$

where D_ℓ and D_t are the longitudinal and transverse components, we have

$$\Delta(K) = \frac{g^2}{3}\frac{T}{V}\sum_Q\left[\frac{2}{3}\frac{\Delta(Q)}{q_0^2-\epsilon_{q,1}^2}+\frac{1}{3}\frac{\Delta(Q)}{q_0^2-\epsilon_{q,2}^2}\right]\Big[(1+\hat{\mathbf{q}}\cdot\hat{\mathbf{k}})D_\ell(P) - 2(1-\hat{\mathbf{p}}\cdot\hat{\mathbf{q}}\,\hat{\mathbf{p}}\cdot\hat{\mathbf{k}})D_t(P)\Big]\,. \tag{300}$$

Again, it is left as an exercise to verify this result by performing the trace in Dirac space. The two terms on the right-hand side arising from $\epsilon_{q,1}$ and $\epsilon_{q,2}$ are due to the two-gap structure of CFL. Let us for simplicity ignore this structure in the following, i.e., we replace $\epsilon_{q,2}$ by $\epsilon_{q,1}$ (for more details about the QCD gap equation for CFL, see Ref. [42]). This simplification does not change the main result which is the dependence of the gap on the QCD coupling g. The two-gap structure has a nontrivial effect for instance on the relation between the critical temperature and the zero-temperature gap, see Eq. (280). In fact the $2^{1/3}$ in that equation is actually $(\lambda_1^{2/3}\lambda_2^{1/3})^{1/2}$ where the exponents $2/3$ and $1/3$ are the prefactors in front of the two fractions in Eq. (300).

For the sake of brevity, let us now skip a few steps in the calculation. One inserts the specific form of the longitudinal and transverse gluon propagators (in the so-called hard-dense loop approximation), performs the Matsubara sum and the angular integral. Details of all these steps can be found for instance in Ref. [41], and one obtains

$$\Delta_k \simeq \frac{g^2}{24\pi^2}\int_{\mu-\delta}^{\mu+\delta} dq\,\frac{\Delta_q}{\epsilon_q}\tanh\frac{\epsilon_q}{2T}\left(\ln\frac{4\mu^2}{3m_g^2}+\ln\frac{4\mu^2}{M^2}+\frac{1}{3}\ln\frac{M^2}{|\epsilon_q^2-\epsilon_k^2|}\right). \tag{301}$$

Here, the three terms in parentheses arise from static electric gluons, non-static magnetic gluons, and (Landau-damped) soft magnetic gluons, respectively. The last of these terms is responsible for the leading behavior of the gap which will turn out to be different from the usual BCS behavior in electronic superconductors. The reason is the existence of a long-range interaction mediated by the magnetic gluons in QCD for which there is no analogue in the interaction of electrons in a metal. We have defined $m_g^2 \equiv N_f g^2\mu^2/(6\pi^2)$ (N_f being the number of flavors), and $M^2 \equiv (3\pi/4)m_g^2$, and we have restricted the momentum integral to a small vicinity around the Fermi surface, $q \in [\mu-\delta,\mu+\delta]$ ($\delta \ll \mu$), where we expect the gap function Δ_q to be peaked. The three logarithms can be combined to obtain

$$\Delta_k = \bar{g}^2\int_0^\delta d(q-\mu)\frac{\Delta_q}{\epsilon_q}\frac{1}{2}\ln\frac{b^2\mu^2}{|\epsilon_q^2-\epsilon_k^2|}, \tag{302}$$

with

$$\bar{g} \equiv \frac{g}{3\sqrt{2}\pi}, \qquad b \equiv 256\pi^4\left(\frac{2}{N_f g^2}\right)^{5/2}, \tag{303}$$

and where we have taken the zero-temperature limit $\tanh\frac{\epsilon_q}{2T}\to 1$. The logarithm can be approximated by

$$\frac{1}{2}\ln\frac{b^2\mu^2}{|\epsilon_q^2-\epsilon_k^2|} \simeq \Theta(k-q)\ln\frac{b\mu}{\epsilon_k}+\Theta(q-k)\ln\frac{b\mu}{\epsilon_q}. \tag{304}$$

Moreover, we define the new integration variable

$$y \equiv \bar{g}\ln\frac{2b\mu}{q-\mu+\epsilon_q}, \tag{305}$$

and abbreviate

$$x \equiv \bar{g}\ln\frac{2b\mu}{k-\mu+\epsilon_k}, \qquad x^* \equiv \bar{g}\ln\frac{2b\mu}{\Delta}, \qquad x_0 \equiv \bar{g}\ln\frac{b\mu}{\delta}, \tag{306}$$

where Δ is the zero-temperature value of the gap at the Fermi surface, $\Delta \equiv \Delta_{q=\mu}$. We have

$$dy = -\frac{\bar{g}}{\epsilon_q}d(q-\mu), \qquad \epsilon_q = b\mu e^{-y/\bar{g}}\left[1+\frac{\Delta_q^2}{(q-\mu+\epsilon_q)^2}\right]. \tag{307}$$

With the latter relation we approximate $\ln(b\mu/\epsilon_q)\simeq y/\bar{g}$, $\ln(b\mu/\epsilon_k)\simeq x/\bar{g}$ to obtain

$$\Delta(x) = x\int_x^{x^*} dy\,\Delta(y)+\int_{x_0}^{x} dy\,y\,\Delta(y). \tag{308}$$

We can rewrite this integral equation as a second-order differential equation,

$$\frac{d\Delta}{dx} = \int_x^{x^*} dy\,\Delta(y) \quad\Rightarrow\quad \frac{d^2\Delta}{dx^2} = -\Delta(x). \tag{309}$$

This equation is solved by

$$\Delta(x) = \Delta\cos(x^*-x), \tag{310}$$

such that the value of the gap at the Fermi surface (which corresponds to $x = x^*$) is Δ, and such that the first derivative of the gap at the Fermi surface vanishes, since the gap peaks at the Fermi surface. To compute the value

of the gap at the Fermi surface, we insert the solution (310) back into the gap equation (308) and consider the point $x = x^*$,

$$\begin{aligned}\Delta &= \Delta \int_{x_0}^{x^*} dy\, y\, \cos(x^* - y) = \Delta \left[\cos(x^* - y) - y \sin(x^* - y)\right]_{y=x_0}^{y=x^*} \\ &= \Delta \left[1 - \cos(x^* - x_0) + x_0 \sin(x^* - x_0)\right] . \end{aligned} \tag{311}$$

Since x_0 is of order $\bar{g}$, we approximate $\cos(x^* - x_0) = \cos x^* \cos x_0 + \sin x^* \sin x_0 \simeq \cos x^* + x_0 \sin x^*$, $\sin(x^* - x_0) = \sin x^* \cos x_0 - \cos x^* \sin x_0 \simeq \sin x^* - x_0 \cos x^*$, and thus

$$\Delta \simeq \Delta(1 - \cos x^*) . \tag{312}$$

Hence, $\cos x^* \simeq 0$ and thus

$$\Delta = 2b\mu \exp\left(-\frac{3\pi^2}{\sqrt{2}g}\right) . \tag{313}$$

This important result, first derived in Ref. [43], shows that the color-superconducting gap is parametrically enhanced compared to the BCS gap in conventional superconductors. In BCS theory there is a contact interaction instead of gluon exchange, and the resulting gap equation has the form

$$\Delta \propto g^2 \int_0^\delta d(q - \mu) \frac{\Delta}{\epsilon_q} . \tag{314}$$

Here the gap does not depend on momentum and one obtains $\Delta \propto \exp(-\text{const}/g^2)$, i.e., the coupling appears quadratic in the denominator of the exponential. This is in contrast to the color-superconducting gap (313) where the coupling appears linear in the denominator of the exponential. As mentioned above, this is due to the long-range interaction from magnetic gluons. For more details and a more general solution of the QCD gap equation see Sec. IV in Ref. [8] and references therein.

The solution of the QCD gap equation is a weak-coupling result and thus only valid at very large chemical potentials where the QCD coupling is sufficiently small. It is nevertheless interesting to extrapolate this result to larger couplings. Of course one should keep in mind that this extrapolation has no theoretical justification. We show the gap as a function of the coupling in Fig. 17. We see the exponentially small gap at small coupling and observe a maximum of the gap at a coupling of about $g \simeq 4.2$. For compact stars we make the following rough estimate. According to the two-loop β-function (which should not be taken too seriously at these low densities), the coupling at $\mu = 400\,\text{MeV}$ is $g \simeq 3.5$. From Fig. 17 we then read off $\Delta \simeq 80\,\text{MeV}$. However in our derivation of the result we have ignored a subleading effect which yields an additional prefactor $\simeq 0.2$. Therefore, we can estimate the color-superconducting gap for compact star densities to be of the order of $\Delta \sim 10\,\text{MeV}$.

This result suggests that the critical temperature of color superconductivity is also of the order of $T_c \sim 10\,\text{MeV}$, cf. Eq. (280). Remember that compact stars have temperatures well below that value (only in the very early stages of the life of the star, temperatures around 10 MeV are reached). This suggests that color superconductors are viable candidates for the matter inside the star. More precisely, if there is deconfined quark matter inside the star, it is very likely that it is in a color-superconducting state.

We conclude this chapter about color superconductivity by noticing that, besides the strong-coupling nature, other interesting questions arise at lower densities. We have seen in Sec. II B 2, that in unpaired quark matter the Fermi momenta of up, down, and strange quarks split apart, see Fig. 2. This is due to the nonzero strange quark mass and the conditions of neutrality and weak equilibrium. In our discussion of superconductivity we have always assumed that the fermions that form Cooper pairs have identical Fermi momenta. This is true in the region of asymptotically large densities where the strange quark mass can be neglected. It is not true, however, at lower densities. The different Fermi momenta rather impose a "stress" on the pairing.[11] It is a quantitative question whether the pairing gap is large enough to overcome this stress. Roughly speaking, if the gap is larger than the mismatch in Fermi momenta, the usual pairing is still possible. It is therefore conceivable that the CFL phase persists down to densities where the transition to hadronic matter takes place. If the gap is too small, however, or the mismatch too large, Cooper pairing in the

[11] Cooper pairing with mismatched Fermi momenta is an interesting general phenomenon and not only relevant for quark matter, but also in condensed matter physics and atomic physics. See for instance Ref. [44] where mismatched pairing of fermionic atoms is investigated experimentally in an optical trap.

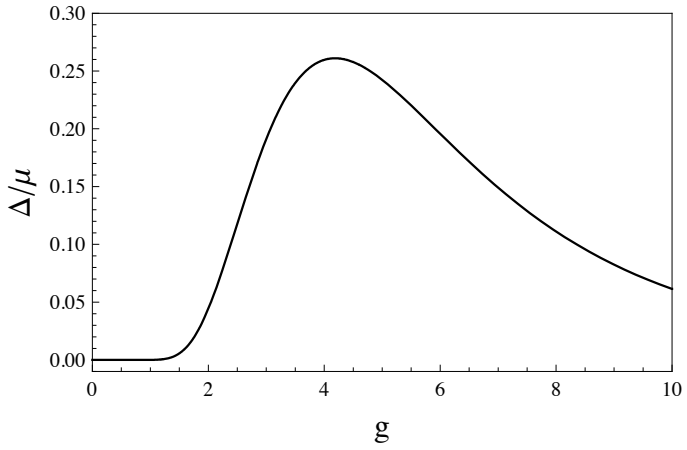

FIG. 17: Color-superconducting gap Δ over quark chemical potential μ as a function of the QCD coupling g. The curve shows the result from Eq. (313) with $N_f = 2$, predicting a weak-coupling behavior $\Delta/\mu \propto \exp(-\text{const}/g)$. The values of Δ/μ for large coupling is a simple (and in principle unreliable) extrapolation of the weak-coupling result.

conventional way is not possible anymore. There are several versions of unconventional pairing which may take over and constitute one or several phases between the CFL phase at high densities and hadronic matter. Some of them break rotational invariance and may lead to nodes of the gap in certain directions in momentum space as discussed in the context of the specific heat in Sec. IV A. Others even break translational invariance and exhibit crystalline structures. All of the unconventional phases have in common that there is less, and less symmetric, pairing than in the CFL phase. There is less pairing because the CFL phase is the only color superconductor where all quarks are gapped in all directions in momentum space. There is less symmetric pairing because the CFL phase is the color superconductor with the largest residual symmetry group. In the phase diagram of Fig. 1 all color superconductors other than CFL are collectively denoted by non-CFL. From what we just said it is clear that this region of the phase diagram may either be completely absent or, if present, may itself contain several phase transition lines separating different color superconductors. More details about stressed pairing in quark matter and unconventional color superconductors can be found in Ref. [8].

In summary, we emphasize that not only the strong-coupling nature but also the less symmetric situation (due to the finite strange quark mass) complicates our understanding of quark matter in compact star. This supports the theme of these lectures that we need to compute properties of candidate phases and check them for their compatibility with astrophysical observations. In the following section we shall turn to one of these properties, namely the neutrino emissivity.

Problems

IV.1 Specific heat for anisotropic superfluid

Compute the low-temperature behavior of the specific heat for a gap function with line nodes, i.e., instead of Eq. (219), take $\Delta \to \Delta|\cos\theta|$ and apply analogous approximations as for the case of point nodes.

IV.2 Symmetries of CFL

Show that from the structure of the CFL order parameter given in Eq. (228) it follows that the CFL symmetry breaking pattern is given by Eq. (229). Hints: it is sufficient to treat the chiral group $SU(3)_L \times SU(3)_R$ as one single flavor group $SU(3)_f$. A color-flavor transformation $(U, V) \in SU(3)_c \times SU(3)_f$ with $U = \exp(i\phi_a^c T_a)$, $V = \exp(i\phi_a^f T_a)$ acts on the order parameter as $(U, V)(\mathbf{J}\cdot\mathbf{I}) = (UJ^AU^T)\,(VI_AV^T)$. One then has to show that only $SU(3)_{c+f}$ transformations leave the order parameter invariant.

IV.3 Kaon propagator

Derive the inverse tree-level propagator for neutral and charged kaons given in Eqs. (270) and (271) from the Lagrangian (268).

V. NEUTRINO EMISSIVITY AND COOLING OF THE STAR

We have seen in Sec. II that measuring mass and radius of a compact star is not sufficient to deduce the matter composition inside the star; it is neither conclusive for a distinction between nuclear matter and quark matter nor between unpaired quark matter and color-superconducting quark matter. We now turn to an observable which is more sensitive to the microscopic properties of dense matter, namely the temperature of the star. More precisely, its cooling curve, i.e., the temperature as a function of the age of the star. Approximately one minute after the star is born, the temperature has cooled below 1 MeV and the star becomes transparent for neutrinos. Consequently, neutrinos (and antineutrinos) which are produced in the star can leave the system and carry away energy. Neutrino emission is thus the dominant cooling mechanism of a compact star in about the first million years of its life. After that, photon emission takes over. We shall not be concerned with this late regime here.

A very detailed review about neutrino emissivity in nuclear matter is Ref. [45]. If you are interested in a shorter review, also discussing quark matter, I recommend Ref. [46]. Before turning to the microscopic calculation of the neutrino emissivity ϵ_ν, let us discuss its importance for the cooling curves. First of all, as already discussed briefly in Sec. IV A it is not only the emissivity which is important for the cooling. Once you know how much energy per time and volume is carried away, you need to know how this affects the temperature of the star. Hence you also need to know the specific heat. The specific heat c_V is a thermodynamic quantity and thus much easier to compute than the neutrino emissivity. We have done so in Sec. IV A and have seen that superconductivity has a huge effect on c_V, namely, due to the energy gap, c_V is exponentially suppressed at sufficiently small temperatures. We shall see that superconductivity has a similar effect on the neutrino emissivity. Besides ϵ_ν and c_V, also the heat conductivity is important for the cooling behavior. Most forms of dense matter are very good heat conductors, such that the star becomes isothermal. As a consequence, in a realistic star which may have layers of different phases of dense matter, cooling tends to be dominated by the phase with the highest emissivity and the phase with the highest specific heat.

A. Urca processes in nuclear matter

In Fig. 18 we show some data and schematic comparison with calculations for the cooling curves. We see that there are different classes of processes which lead to significantly different cooling scenarios. The most efficient process is the so-called *direct Urca process* which leads to a very fast cooling.[12] In nuclear matter, the direct Urca processes are

$$n \to p + e + \bar{\nu}_e \,, \qquad p + e \to n + \nu_e \,. \tag{315}$$

We have discussed these processes in the context of β-equilibrium, where they serve to establish the relation $\mu_p + \mu_e = \mu_n$, assuming that neutrinos and antineutrinos escape from the star, $\mu_\nu = 0$. Here we are interested in the question how both processes contribute to the neutrino emissivity. Since it does not matter for the energy balance whether neutrinos or antineutrinos are emitted, both processes contribute – in chemical equilibrium – equally to the emissivity. For the neutron, proton, and electron, the dominant contribution in momentum space to the processes comes from the momenta close to the Fermi momentum. The neutrino momentum is of the order of the temperature T which can be neglected compared to the Fermi momenta. Therefore, momentum conservation for both processes in Eq. (315) reads

$$\mathbf{k}_{F,n} = \mathbf{k}_{F,p} + \mathbf{k}_{F,e} \,. \tag{316}$$

In other words, the Fermi momenta $\mathbf{k}_{F,n}$, $\mathbf{k}_{F,p}$, and $\mathbf{k}_{F,e}$ must form a triangle. For this triangle to exist, the triangle inequality has to be fulfilled,

$$k_{F,n} < k_{F,p} + k_{F,e} \,. \tag{317}$$

We know that in a neutral system we have $k_{F,p} = k_{F,e}$, and thus the triangle inequality becomes

$$k_{F,n} < 2k_{F,p} \,. \tag{318}$$

Consequently, with $n_i \propto k_{F,i}^3$ $(i = n, p)$,

$$n_n < 8 n_p \quad \Rightarrow \quad \frac{n_p}{n_B} > \frac{1}{9} \,, \tag{319}$$

[12] This process is as efficient in sucking energy out of the star as the *Casino de Urca* in Rio de Janeiro is in sucking money out of the pockets of the gamblers. Hence the name.

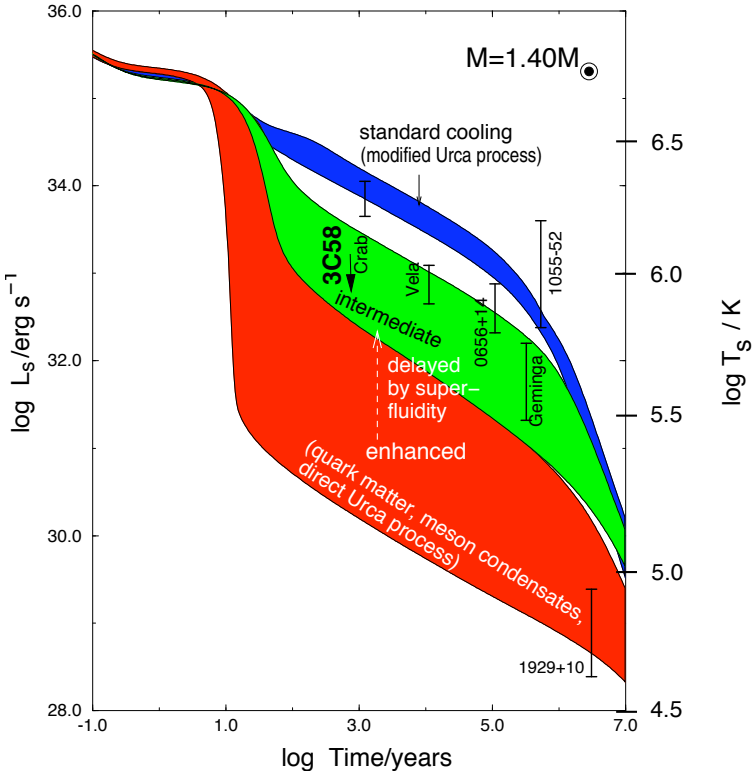

FIG. 18: Effective surface temperature T_s and luminosity L_s vs. age of compact stars, taken from Ref. [6]. Observed values are compared with different cooling scenarios, each represented by a band that reflects the large uncertainties in the microscopic calculations.

i.e., the proton fraction has to be larger than 11%. We have seen in Sec. II A that this is not the case for noninteracting nuclear matter. Interactions can change this, especially for very large densities. At lower densities, this means that the direct Urca process is strongly suppressed in nuclear matter.

This brings us to a second class of processes which are less efficient than the direct Urca process, but may be the most efficient ones to emit neutrinos when the direct Urca process is suppressed. Momentum conservation can be fulfilled by adding a spectator neutron or proton. This is the so-called *modified Urca process*,

$$N + n \to N + p + e + \bar{\nu}_e\,, \qquad N + p + e \to N + n + \nu_e\,, \qquad N = n, p\,. \tag{320}$$

As can be seen from Fig. 18, this process typically results in a much slower cooling. The cooling is thus very sensitive to the proton fraction of nuclear matter, especially around the threshold of 11%. In other words, this sensitivity provides a good check on the equation of state. Phenomenological models with equations of state which predict the proton fraction to be below this threshold can be excluded since the star would cool too fast. There are several other neutrino emissivity processes in nuclear matter which we shall not discuss here. Some of these processes happen only with superconducting protons and superfluid neutrons, and are due to constant formation of Cooper pairs.

B. Direct Urca process in quark matter

The direct Urca processes in quark matter are

$$d \;\to\; u + e + \bar{\nu}_e\,, \qquad u + e \to d + \nu_e\,, \tag{321a}$$
$$s \;\to\; u + e + \bar{\nu}_e\,, \qquad u + e \to s + \nu_e\,. \tag{321b}$$

These processes obviously require the availability of single quarks. If quarks are paired in Cooper pairs one first has to break a pair. This costs energy. Therefore, in a phase where all quarks are paired (gapped), such as the CFL phase, we can expect the direct Urca process to be strongly suppressed. As for the specific heat, we expect an

exponential suppression at temperatures small compared to the gap (at larger temperatures, but still below the color-superconducting phase transition, thermal energy is available to break the pairs). Recall that the gap is of the order of 10 MeV, and the temperature of the star is well below that. Therefore, the exponential suppression $\exp(-\Delta/T)$ forbids any sizable effect of the Urca process. Other processes coming from Goldstone modes dominate the neutrino emissivity in the CFL phase [47]. However, their contribution is much lower than that of the unsuppressed direct Urca process. Therefore, if the core of a hybrid star is made of CFL quark matter, with outer layers of nuclear matter where any kind of Urca process is possible, the cooling properties are utterly dominated by these outer layers.

We have briefly discussed that at lower densities the CFL phase may not be the ground state anymore. Any other color-superconducting phase will have ungapped modes.[13] The simplest example is the so-called *2SC phase* where all blue and strange quarks are ungapped while the others are gapped. There are more complicated candidate phases with ungapped modes only in certain directions in momentum space. In any case, the neutrino emissivity of these phases will be dominated by these ungapped modes, and thus will be comparable to the emissivity of unpaired quark matter. We are thus interested in the neutrino emissivity of unpaired quark matter. To be a bit more ambitious, let us discuss the emissivity in the 2SC phase. From this calculation we will obtain the result for the unpaired phase "for free" because of the unpaired modes in the 2SC phase. Furthermore, we learn something about computing reaction rates in a superconductor which show some interesting features. And also we will see in an actual calculation why the emissivity of the gapped modes is exponentially suppressed. In other words, the goal of this section will be to understand

- the role of the Cooper pair condensate and the energy gap on the Urca process (we shall estimate this qualitatively)
- the result of the emissivity of unpaired (ultrarelativistic) quark matter (we shall compute this quantitatively).

All we shall need from the 2SC phase is the propagator. From Eq. (293) we know that the general form of the propagator can be written as

$$G^{\pm} = \gamma^0 \Lambda_k^{\mp} \sum_r \mathcal{P}_r \frac{k_0 \mp (\mu - k)}{k_0^2 - \epsilon_{k,r}^2}\,, \tag{322}$$

where we used Eq. (284) and where we dropped the antiparticle contribution. Note that this form of the propagator assumes that all flavor chemical potentials are the same. For the neutrino emissivity we need to drop this assumption, see below. The order parameter in the 2SC phase is characterized by $\phi_A^B = \delta_{A3}\delta^{B3}$ where ϕ is the color-flavor matrix from Eq. (227). For simplicity, we drop the strange quarks and consider only a two-flavor system of up and down quarks.[14] Then, the color-flavor structure of the gap matrix is

$$\mathcal{M} = \tau_2 J_3\,, \tag{323}$$

with the second Pauli matrix τ_2 in flavor space and J_3 in color space, as defined above Eq. (230). The color-flavor structure of the 2SC phase is much easier to deal with than the one of the CFL phase because color and flavor matrices factorize. Since $\tau_2^2 = \mathbf{1}$, we have $\mathcal{M}^2 = J_3^2$, whose eigenvalues are $\lambda_1 = 1$ (4-fold) and $\lambda_2 = 0$ (2-fold). This is the formal way of saying that in the 2SC phase quarks of one color, say blue, remain ungapped. The projectors onto the corresponding eigenspaces in color-flavor space are

$$\mathcal{P}_1 = J_3^2\,, \qquad \mathcal{P}_2 = \mathbf{1} - J_3^2\,. \tag{324}$$

They are trivial in flavor space and project onto red and green quarks (which are gapped) and blue quarks (which are ungapped), respectively.

In a neutral two-flavor system, up and down chemical potentials are different, namely $\mu_u + \mu_e = \mu_d$, where μ_e turns out to be nonzero due to the neutrality constraint. The generalization of the propagator (322) to this case can be

---

[13] A possible exception is the *color-spin locked phase* which has Cooper pairs with total angular momentum one and which we do not discuss here.

[14] The weak interaction between u and s quarks is suppressed compared to the one between u and d quarks due to the Cabibbo angle. However, the finite strange quark mass may partially compensate this effect because it leads to a larger phase space for the Urca process. Here in these lectures we do not want to deal with these complications and thus simply consider a system of massless up and down quarks, and thus only the processes (321a).

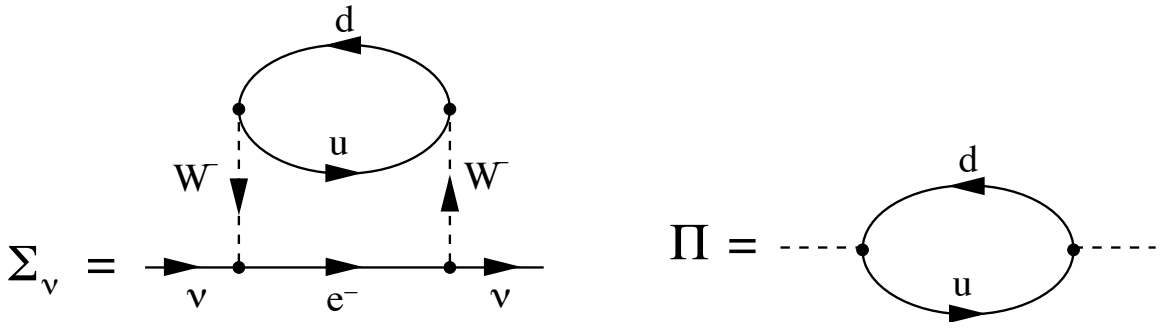

FIG. 19: Neutrino self-energy Σ_ν and W-boson polarization tensor Π needed for the neutrino emissivity from the quark Urca process.

written in terms of the flavor components (see problem V.1)

$$G_u^\pm = \gamma^0\Lambda_k^\mp \sum_r \frac{k_0 \mp (\mu_u - k)}{(k_0 \mp \delta\mu)^2 - \epsilon_{k,r}^2}\mathcal{P}_r\,, \tag{325a}$$

$$G_d^\pm = \gamma^0\Lambda_k^\mp \sum_r \frac{k_0 \mp (\mu_d - k)}{(k_0 \pm \delta\mu)^2 - \epsilon_{k,r}^2}\mathcal{P}_r\,, \tag{325b}$$

with

$$\epsilon_{k,r} \equiv \sqrt{(\bar\mu - k)^2 + \lambda_r\Delta^2}\,, \qquad \delta\mu \equiv \frac{\mu_d - \mu_u}{2}\,, \qquad \bar\mu \equiv \frac{\mu_d + \mu_u}{2}\,, \tag{326}$$

and λ_r, $\mathcal{P}_r$ as above ($\mathcal{P}_r$ now being only matrices in color space since the flavor components are written separately). This structure of the propagator and the resulting quasiparticle dispersion relations are interesting on their own, since they describe Cooper pairing with a mismatch in Fermi momenta, as discussed at the end of Sec. IV C. However, in the present context of neutrino emissivity, we are only interested in the qualitative features of the gapped modes. Thus we shall ignore this complicated structure of the propagator and temporarily set $\mu_u = \mu_d$. Only when we compute the emissivity from the unpaired modes we shall reinstate the difference in up and down chemical potentials.

Next we need to set up the equation that determines the neutrino emissivity. One possible formalism is the finite temperature real-time formalism. We shall not explain this formalism but refer the reader for more details to the textbooks [9] and [10]. For our purpose it is enough to know that the real-time formalism can be used for nonequilibrium calculations. Therefore it is well suited for transport properties and neutrino emissivity. Since these properties are always close-to-equilibrium properties, one often simply uses an equilibrium formalism, such as the imaginary-time formalism, and adds whatever is needed as a small out-of-equilibrium feature by hand. In the real-time formalism we can start from the kinetic equation

$$i\frac{\partial}{\partial t}\mathrm{Tr}[\gamma_0 G_\nu^<(P_\nu)] = -\mathrm{Tr}[G_\nu^>(P_\nu)\Sigma_\nu^<(P_\nu) - \Sigma_\nu^>(P_\nu)G_\nu^<(P_\nu)]\,, \tag{327}$$

where $G_\nu^>$ and $G_\nu^<$ are the so-called "greater" and "lesser" neutrino propagators, and P_ν is the neutrino four-momentum. The greater and lesser propagators are obtained from the retarded propagator in the same way as given in Eqs. (328) for the case of the W-boson polarization tensor. The trace in Eq. (327) is taken over Dirac space. The two terms on the right-hand side correspond to the two directions of both processes (321a), i.e., there is a neutrino gain term from $d \to u + e + \bar\nu_e$, $u + e \to d + \nu_e$, and a neutrino loss term from $u + e + \bar\nu_e \to d$, $d + \nu_e \to u + e$. Since neutrinos, once created, simply leave the system, only the gain terms, namely the directions given in Eq. (321a), contribute. The neutrino self-energies $\Sigma_\nu^{<,>}$ are given by the diagram in Fig. 19. The present formalism amounts to cutting this diagram. The figure shows that a cut through the internal u, d, and e lines produces two diagrams which represent the Urca process. One part of the neutrino self-energies are the W-boson polarization tensors $\Pi^{<,>}$, as shown diagrammatically in Fig. 19. They are defined through the imaginary part of the retarded polarization tensor $\mathrm{Im}\,\Pi_R$,

$$\Pi^>(Q) = -2i[1 + f_B(q_0)]\mathrm{Im}\,\Pi_R(Q)\,, \tag{328a}$$

$$\Pi^<(Q) = -2i f_B(q_0)\mathrm{Im}\,\Pi_R(Q)\,, \tag{328b}$$

with the Bose distribution function f_B. We shall discuss the calculation of $\Pi^{<,>}$ in detail below. The kinetic equation (327) becomes

$$\frac{\partial}{\partial t} f_\nu(t, \mathbf{p}_\nu) \;=\; \frac{G_F^2}{8} \int \frac{d^3\mathbf{p}_e}{(2\pi)^3 p_\nu p_e} L_{\lambda\sigma}(\mathbf{p}_e, \mathbf{p}_\nu) f_F(p_e - \mu_e) f_B(p_\nu + \mu_e - p_e) \mathrm{Im}\, \Pi_R^{\lambda\sigma}(Q)\,, \tag{329}$$

where, due to four-momentum conservation,

$$Q = (p_e - p_\nu - \mu_e, \mathbf{p}_e - \mathbf{p}_\nu)\,, \tag{330}$$

and where

$$L^{\lambda\sigma}(\mathbf{p}_e, \mathbf{p}_\nu) \equiv \mathrm{Tr}\left[(\gamma_0 p_e - \boldsymbol{\gamma}\cdot\mathbf{p}_e)\,\gamma^\sigma(1-\gamma^5)(\gamma_0 p_\nu - \boldsymbol{\gamma}\cdot\mathbf{p}_\nu)\,\gamma^\lambda(1-\gamma^5)\right]. \tag{331}$$

(In this section, Lorentz indices are denoted $\lambda, \sigma, \ldots$ in order to avoid confusion with the subscript ν which indicates neutrino quantities.) If you are interested in the details of the derivation of Eq. (329) or more details about the real-time formalism, see Ref. [48] and references therein. In this reference the neutrino emissivity is computed in the same formalism; however, for anisotropic phases, which leads to more complicated calculations than we shall present here. The following is equally understandable if you simply start with Eq. (329) whose features are physically plausible as we explain now.

The left-hand side of Eq. (329) is the change of the neutrino occupation number in time. It is related to the emissivity by

$$\epsilon_\nu \equiv -2\frac{\partial}{\partial t} \int \frac{d^3\mathbf{p}_\nu}{(2\pi)^3}\, p_\nu\, f_\nu(t, \mathbf{p}_\nu)\,, \tag{332}$$

where the factor 2 accounts for the contribution from antineutrinos. The neutrino emissivity is thus the change in energy per unit time and volume. Our task is to compute the right-hand side of Eq. (329) and integrate over the neutrino momentum according to Eq. (332) to obtain ϵ_ν. To understand the right-hand side of Eq. (329) first note that the vertex Γ^μ for the processes $d \leftrightarrow u + W^-$ and $e \leftrightarrow \nu + W^-$ is given by

$$\Gamma^\mu = -\frac{e}{2\sqrt{2}\sin\theta_W}\gamma^\mu(1-\gamma^5)\,, \tag{333}$$

with the Weinberg angle θ_W. (For the process $d \leftrightarrow u + W^-$ there is an additional factor V_{ud} from the Cabibbo-Kobayashi-Maskawa (CKM) matrix; however, $V_{ud} \simeq 1$.) The W-boson propagators can be approximated by the inverse W-boson mass squared M_W^2 since all momenta we are interested in are much smaller than this mass $M_W \simeq 80\,\mathrm{GeV}$. Thus, pulling out the constant factors of the vertices in the W-boson polarization tensor, we obtain the overall factor G_F^2 with the Fermi coupling

$$G_F = \frac{\sqrt{2}e^2}{8M_W^2\sin^2\theta_W} = 1.16637\cdot 10^{-11}\,\mathrm{MeV}^{-2}\,. \tag{334}$$

The additional factors in the trace of Eq. (331) come from the electron and neutrino propagators. And finally, the distribution functions in Eq. (329) belong to the electron and the W-boson. Eventually, the Bose distribution of the W will drop out since the W-boson polarization tensor will turn out to be $\propto f_B^{-1}$, see below. This makes sense because the W does not appear in the initial or final state of the process we are interested in.

1. *W-boson polarization tensor*

Next we need to compute $\mathrm{Im}\,\Pi_R^{\lambda\sigma}$ for which we first compute

$$\Pi^{\lambda\sigma}(Q) = \frac{T}{V}\sum_K \mathrm{Tr}[\Gamma_-^\lambda S(K)\Gamma_+^\sigma S(P)]\,, \tag{335}$$

where the trace is taken over Dirac, color, flavor, and Nambu-Gorkov space. We have defined $P \equiv K + Q$; K and P will play the role of the u and d quark momentum, respectively. The weak vertices in Nambu-Gorkov space are

$$\Gamma_\pm^\lambda = \begin{pmatrix} \gamma^\lambda(1-\gamma^5)\,\tau_\pm & 0 \\ 0 & -\gamma^\lambda(1+\gamma^5)\,\tau_\mp \end{pmatrix}, \tag{336}$$

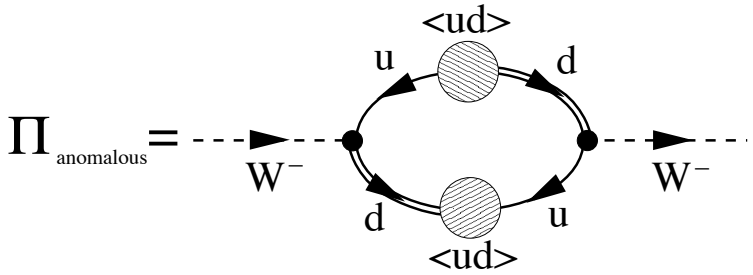

FIG. 20: Anomalous contribution to the W-boson polarization tensor Π. The loop consists of two anomalous fermion propagators, according to Eq. (289b). The lower propagator consists of a full fermion propagator (double line), the condensate (hatched circle), and a charge-conjugate free propagator (single line in opposite direction), and analogously for the upper one. Electric charge conservation at the weak vertices determines the flavor content of each line. As a consequence, one reads off that the condensate acts as a reservoir that can convert a u quark into a d quark hole and vice versa.

where $\tau_\pm \equiv (\tau_1 \pm i\tau_2)/2$ are matrices in flavor space, constructed from the Pauli matrices τ_1, τ_2. They take care of the fact that a u and a d quark interact at the vertices. Recall that, for notational convenience, we have pulled out the constants of the weak vertices already and absorbed them in the overall factor G_F^2. With the quark propagator S from Eq. (288), the trace over Nambu-Gorkov space yields

$$\begin{aligned}\Pi^{\lambda\sigma}(Q) \;=\; \frac{T}{V}\sum_K \Big\{ &\mathrm{Tr}\left[\gamma^\lambda(1-\gamma^5)\tau_- G^+(K)\gamma^\sigma(1-\gamma^5)\tau_+ G^+(P)\right] + \mathrm{Tr}\left[\gamma^\lambda(1+\gamma^5)\tau_+ G^-(K)\gamma^\sigma(1+\gamma^5)\tau_- G^-(P)\right] \\ &- \mathrm{Tr}\left[\gamma^\lambda(1-\gamma^5)\tau_- F^-(K)\gamma^\sigma(1+\gamma^5)\tau_- F^+(P)\right] - \mathrm{Tr}\left[\gamma^\lambda(1+\gamma^5)\tau_+ F^+(K)\gamma^\sigma(1-\gamma^5)\tau_+ F^-(P)\right] \Big\} . \end{aligned} \tag{337}$$

We see that there is a contribution from the anomalous propagators $F^\pm$. The corresponding diagram in Fig. 20 is an instructive example for processes in a superconductor which are only possible due to the Cooper pair condensate, see explanation in the caption of the figure. The anomalous contribution is thus only present for the gapped modes. We shall ignore it here for simplicity (it is smaller than the contribution from the normal propagators, but not negligibly small [49]). This leaves us with the first two traces in Eq. (337) which are the contribution of the normal propagators (they of course also contain the superconducting gap). It turns out that both traces are identical which we use without explicit proof. We thus continue simply with twice the first term,

$$\Pi^{\lambda\sigma}(Q) \;\simeq\; 2\frac{T}{V}\sum_K \sum_{r,s} \mathrm{Tr}\left[\gamma^\lambda(1-\gamma^5)\tau_-\gamma_0\mathcal{P}_r\Lambda_k^-\gamma^\sigma(1-\gamma^5)\tau_+\gamma_0\mathcal{P}_s\Lambda_p^-\right] \frac{k_0-(\mu-k)}{k_0^2-\epsilon_{k,r}^2}\frac{p_0-(\mu-p)}{p_0^2-\epsilon_{p,s}^2} , \tag{338}$$

where we have inserted the propagator (322). (Recall that we have set $\mu_u = \mu_d$ temporarily to avoid complications; this is sufficient to discuss the effects of superconductivity qualitatively, but eventually we shall reinstate the difference in μ_u and μ_d to compute the result for unpaired quark matter. In principle, for the 2SC phase we would have to use the propagators given in Eq. (325)). The color-flavor traces are

$$\mathrm{Tr}[\tau_-\mathcal{P}_1\tau_+\mathcal{P}_1] \;=\; 2\,, \tag{339a}$$
$$\mathrm{Tr}[\tau_-\mathcal{P}_1\tau_+\mathcal{P}_2] \;=\; 0\,, \tag{339b}$$
$$\mathrm{Tr}[\tau_-\mathcal{P}_2\tau_+\mathcal{P}_1] \;=\; 0\,, \tag{339c}$$
$$\mathrm{Tr}[\tau_-\mathcal{P}_2\tau_+\mathcal{P}_2] \;=\; 1\,. \tag{339d}$$

Recalling that $\mathcal{P}_1$ projects onto the gapped red and green quarks and $\mathcal{P}_2$ onto the ungapped blue quarks, this is easy to interpret: the weak interaction cannot change colors. Therefore, the quark loop in the polarization tensor – see right diagram in Fig. 19 – contains an up quark and a down quark of the same color. They are either both gapped (then they are red or green, hence the result 2 in Eq. (339a)), or they are both ungapped (then they are blue). There is no term involving one gapped and one ungapped quark. We thus get two contributions,

$$\Pi^{\lambda\sigma}(Q) \;\simeq\; 2\frac{T}{V}\sum_K \mathcal{T}^{\lambda\sigma}(\hat{\mathbf{k}},\hat{\mathbf{p}}) \left[2\frac{k_0-(\mu-k)}{k_0^2-\epsilon_{k,1}^2}\frac{p_0-(\mu-p)}{p_0^2-\epsilon_{p,1}^2} + \frac{k_0-(\mu-k)}{k_0^2-\epsilon_{k,2}^2}\frac{p_0-(\mu-p)}{p_0^2-\epsilon_{p,2}^2}\right] , \tag{340}$$

where we abbreviated the Dirac trace

$$\mathcal{T}^{\lambda\sigma}(\hat{\mathbf{k}},\hat{\mathbf{p}}) \equiv \mathrm{Tr}\left[\gamma^\lambda(1-\gamma^5)\gamma_0\Lambda_k^-\gamma^\sigma(1-\gamma^5)\gamma_0\Lambda_p^-\right] . \tag{341}$$

We notice that the second contribution in Eq. (340) is obtained from the first upon setting $\Delta = 0$. Thus, for notational convenience, let us simply continue with one color degree of freedom, say the first term without the factor 2, and denote $\epsilon_k \equiv \epsilon_{k,1}$. In the end it is then straightforward to get the full result.

Next one has to perform the sum over the fermionic Matsubara frequencies. This technique is discussed in detail for a simple example in appendix A 2 a. Here we need the more complicated result from problem A.2,

$$T\sum_{k_0} \frac{k_0 - (\mu - k)}{k_0^2 - \epsilon_k^2} \frac{p_0 - (\mu - p)}{p_0^2 - \epsilon_p^2} = -\frac{1}{4\epsilon_k \epsilon_p} \sum_{e_1, e_2} \frac{[\epsilon_k + e_1(\mu - k)][\epsilon_p + e_2(\mu - p)]}{q_0 - e_1\epsilon_k + e_2\epsilon_p} \frac{f_F(-e_1\epsilon_k) f_F(e_2\epsilon_p)}{f_B(-e_1\epsilon_k + e_2\epsilon_p)} \,. \tag{342}$$

(Remember $P = Q + K$.) We comment on the physical meaning of the sum over the signs $e_1, e_2 = \pm$ below. To obtain the retarded polarization tensor, we need to replace $q_0 \to q_0 - i\eta$. Then, the imaginary part is obtained by using the identity

$$\lim_{\eta \to 0^+} \frac{1}{x \pm i\eta} = \mathcal{P}\frac{1}{x} \mp i\pi\delta(x) \,, \tag{343}$$

where $\mathcal{P}$ denotes the principal value. This yields

$$\mathrm{Im}\, \Pi_R^{\lambda\sigma}(Q) \;\simeq\; -2\pi \sum_{e_1 e_2} \int \frac{d^3\mathbf{k}}{(2\pi)^3} \mathcal{T}^{\lambda\sigma}(\hat{\mathbf{k}}, \hat{\mathbf{p}}) B_k^{e_1} B_p^{e_2} \frac{f_F(-e_1\epsilon_k) f_F(e_2\epsilon_p)}{f_B(-e_1\epsilon_k + e_2\epsilon_p)} \, \delta(q_0 - e_1\epsilon_k + e_2\epsilon_p) \,, \tag{344}$$

where we have defined the *Bogoliubov coefficients*

$$B_k^e \equiv \frac{1}{2}\left(1 + e\frac{\mu - k}{\epsilon_k}\right) . \tag{345}$$

These coefficients appear in the theory of any kind of superconductor or superfluid, see for instance Ref. [40]. Inserting the result (344) back into Eq. (329) yields

$$\begin{aligned} \frac{\partial}{\partial t} f_\nu(t, \mathbf{p}_\nu) \;=\; & -\frac{\pi G_F^2}{4} \sum_{e_1 e_2} \int \frac{d^3\mathbf{p}_e d^3\mathbf{k}}{(2\pi)^3 (2\pi)^3 p_\nu p_e} L_{\lambda\sigma}(\mathbf{p}_e, \mathbf{p}_\nu) \mathcal{T}^{\lambda\sigma}(\hat{\mathbf{k}}, \hat{\mathbf{p}}) B_k^{e_1} B_p^{e_2} \\ & \times f_F(p_e - \mu_e) f_F(-e_1\epsilon_k) f_F(e_2\epsilon_p) \delta(q_0 - e_1\epsilon_k + e_2\epsilon_p) \,. \end{aligned} \tag{346}$$

As expected, the Bose distribution from Eq. (329) cancels with the denominator from Eq. (344) since on the one hand $q_0 = p_e - p_\nu - \mu_e$ according to Eq. (330) and on the other hand $q_0 = e_1\epsilon_k - e_2\epsilon_p$ according to the δ-function.

2. Effect of superconductivity on Urca process

Eq. (346) describes the change in the neutrino occupation number due to the process $u + e \to d + \nu_e$. (The other relevant process $d \to u + e + \bar{\nu}_e$ yields the same result and is taken into account by the factor 2 in Eq. (332).) For this process one expects Fermi distributions of the form $f_e f_u (1 - f_d)$, the factors f_e and f_u standing for the incoming fermions, and the factor $1 - f_d$ standing for the outgoing fermion (for the neutrino, $f_\nu \simeq 0$). So what is the meaning of the sum over e_1, e_2? With $f(-x) = 1 - f(x)$ it seems that all combinations $f_e f_u f_d$, $f_e f_u (1 - f_d)$, $f_e (1 - f_u) f_d$, and $f_e (1 - f_u)(1 - f_d)$ appear. In other words, also processes where both the up and down quark are created or annihilated apparently give a contribution. More precisely, the quasiparticles, which are mixtures of up and down particles and holes, are allowed to appear on either side of the reaction. This is an interesting property of a superconductor or superfluid where particle number conservation is spontaneously broken and particles can be created from or deposited into the condensate.

To see explicitly that in the unpaired phase only one of the four subprocesses survives, let us define the new Bogoliubov coefficients and the new dispersion relations

$$\tilde{B}_k^e \equiv \frac{1}{2}\left(1 + e\frac{k - \mu}{\tilde{\epsilon}_k}\right) , \qquad \tilde{\epsilon}_k \equiv \mathrm{sgn}(k - \mu)\epsilon_k \,. \tag{347}$$

Then we use that for any function F we have

$$\sum_e \int_0^\infty dk\, B_k^e F(e\epsilon_k) = \sum_e \int_0^\infty dk\, \tilde{B}_k^e F(-e\tilde{\epsilon}_k) \,. \tag{348}$$

This reformulation is useful to understand the mixing of particles and holes, which is manifest in the Bogoliubov coefficients. Had we taken the limit $\Delta \to 0$ with the original formulation in B_k^e, ϵ_k, we would have obtained the excitation energy $\epsilon_k = |k-\mu|$ which describes a hole for $k < \mu$ and a particle for $k > \mu$. The more conventional excitation $\epsilon_k = k - \mu$ which describes a particle for all k is only obtained as a limit using $\tilde{B}_k^e$, $\tilde{\epsilon}_k$ (both formulations are of course physically equivalent). Now, since in the unpaired phase $\tilde{B}_k^+ = 1$, $\tilde{B}_k^- = 0$, we see that only the subprocess with $e_1 = e_2 = 1$ survives in the unpaired phase. The other three subprocesses are only possible in the superconducting phase.

The general result in the superconducting phase has to be computed numerically. Here we proceed with a discussion of the behavior at temperatures much smaller than the gap, $T \ll \Delta$. The neutrino emissivity is obtained by integrating Eq. (346) over the neutrino momentum according to Eq. (332). For the purpose of a simple estimate we may consider the expression

$$\epsilon_\nu \sim \sum_{e_1,e_2=\pm} \int_{v,x,y} \left(e^{v+e_1\sqrt{y^2+\varphi^2}-e_2\sqrt{x^2+\varphi^2}}+1\right)^{-1} \left(e^{-e_1\sqrt{y^2+\varphi^2}}+1\right)^{-1} \left(e^{e_2\sqrt{x^2+\varphi^2}}+1\right)^{-1}, \tag{349}$$

where we have abbreviated

$$\varphi \equiv \frac{\Delta}{T}, \qquad \int_{v,x,y} \equiv \int_0^\infty dv\, v^3 \int_0^\infty dx \int_0^\infty dy, \tag{350}$$

and introduced the new dimensionless variables

$$x = \frac{p-\mu_d}{T}, \qquad y = \frac{k-\mu_u}{T}, \qquad v = \frac{p_\nu}{T}. \tag{351}$$

The integration over the electron momentum has been rewritten as an integration over the d-quark momentum. We shall discuss the calculation more explicitly for the case of unpaired quark matter below. Especially the angular integral, i.e., the phase space for the process, needs to be considered in detail. For now we are only interested in the suppression due to the gap. In the integrand of Eq. (349) one recovers the distribution functions for the electron, the u-quark, and the d-quark. We may now perform the sum over e_1 and e_2 and approximate $e^{\sqrt{x^2+\varphi^2}} \gg 1$ and $e^{\sqrt{y^2+\varphi^2}} \gg 1$, since $\varphi \to \infty$ for small temperatures. Then the four terms, in the order $(e_1, e_2) = (+,+), (-,-), (-,+), (+,-)$, become

$$\epsilon_\nu \sim \int_{v,x,y} \left(\frac{1}{e^{\sqrt{x^2+\varphi^2}}+e^{v+\sqrt{y^2+\varphi^2}}} + \frac{1}{e^{v+\sqrt{x^2+\varphi^2}}+e^{\sqrt{y^2+\varphi^2}}} + \frac{1}{e^{v}+e^{\sqrt{x^2+\varphi^2}+\sqrt{y^2+\varphi^2}}} + \frac{1}{e^{v+\sqrt{x^2+\varphi^2}+\sqrt{y^2+\varphi^2}}} \right) \tag{352}$$

The terms where e_1, e_2 assume different signs, i.e., the third and fourth term, yield contributions of the order of $e^{-2\varphi}$. They are thus even stronger suppressed than the first two terms which are identical and yield contributions proportional to $e^{-\varphi}$,

$$\int_{v,x,y} \frac{1}{e^{\sqrt{x^2+\varphi^2}}+e^{v+\sqrt{y^2+\varphi^2}}} \simeq \int_{v,x,y} \frac{e^{-\varphi}}{e^{x^2/(2\varphi)}+e^{v+y^2/(2\varphi)}} = 2\varphi e^{-\varphi} \int_{v,x,y} \frac{1}{e^{x^2}+e^{v+y^2}} \simeq 21.27\,\varphi e^{-\varphi}. \tag{353}$$

In the last step we have performed the remaining integral numerically which yields a numerical factor, unimportant for our present purpose. The main result is the expected exponential suppression of the neutrino emissivity for case of gapped u and d quarks, $\epsilon_\nu \propto e^{-\Delta/T}$ for $T \ll \Delta$. The full numerical solution, also taking into account the temperature dependence of the gap Δ, shows that this approximation is valid up to temperatures of about $T \lesssim T_c/3$ where T_c is the critical temperature of superconductivity.

3. Result for unpaired quark matter

With the help of the new Bogoliubov coefficients (347) we can easily take the limit of unpaired quarks. For an explicit calculation of the emissivity for this case we need the following ingredients. First we need to perform the remaining traces in Dirac space and do the contraction over Lorentz indices. This is done in problem V.2 with the result

$$L_{\lambda\sigma}(\mathbf{p}_e, \mathbf{p}_\nu)\mathcal{T}^{\lambda\sigma}(\hat{\mathbf{k}}, \hat{\mathbf{p}}) = 64(p_e - \mathbf{p}_e\cdot\hat{\mathbf{k}})(p_\nu - \mathbf{p}_\nu\cdot\hat{\mathbf{p}}). \tag{354}$$

Next we observe that the result for the right-hand side of Eq. (346) would be zero without further corrections: we have to take into account so-called Fermi liquid corrections which are induced by the strong interaction. We have

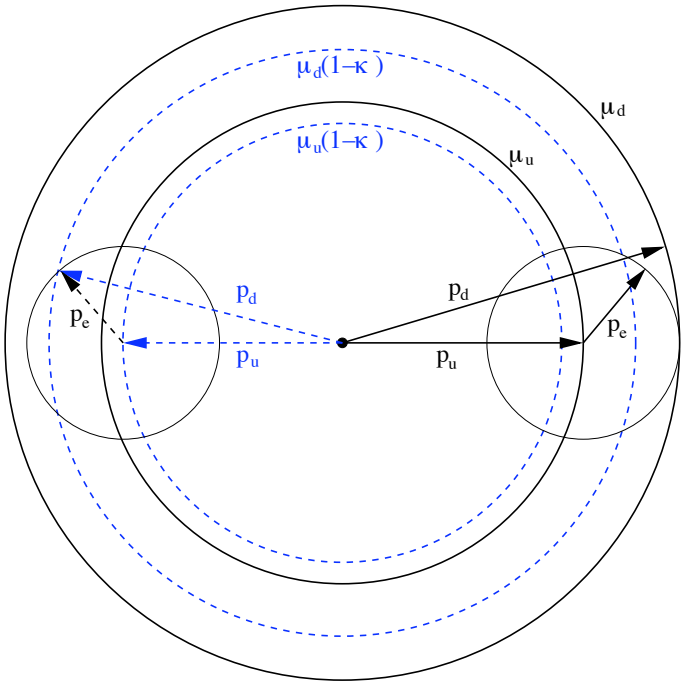

FIG. 21: Illustration of how Fermi liquid effects from the strong interaction open up the phase space for the direct Urca process in unpaired quark matter. Right-hand side (solid Fermi momenta): without Fermi liquid corrections, the Fermi momenta of the ultrarelativistic quarks are given by $p_{F,u} = \mu_u$, $p_{F,d} = \mu_d$. Start with the momentum of the up-quark, $\mathbf{p}_u$. The circle with center at its tip indicates possible endpoints of the electron momentum $\mathbf{p}_e$. Since $p_{F,e} = \mu_e$ and $\mu_u + \mu_e = \mu_d$ (β-equilibrium), one cannot form a triangle with $\mathbf{p}_u$, $\mathbf{p}_e$ and the down-quark momentum $\mathbf{p}_d$, unless one chooses the three vectors to be collinear. In this case, the triangle collapses to a line and the phase space for the Urca process vanishes. Note that the neutrino momentum $p_\nu \sim T$ is negligibly small on the scale of the figure. Left-hand side (dashed Fermi momenta): the strong interaction changes the quark Fermi momenta to $p_{F,u} \simeq \mu_u(1-\kappa)$, $p_{F,d} \simeq \mu_d(1-\kappa)$ with $\kappa = 2\alpha_s/(3\pi)$. In other words, both Fermi momenta are reduced, but the down-quark Fermi momentum is reduced by a larger absolute amount. Since the electron Fermi momentum is not changed, a finite region in phase space opens up. The resulting triangle has a fixed angle between up- and down-quark momenta given by the values of the chemical potentials and κ.

mentioned these corrections briefly in Sec. II C, see Eq. (83). To lowest order in the strong coupling constant α_s – which is related to the coupling g from Sec. IV C by $\alpha_s = g^2/(4\pi)$ – we have

$$p_{F,u/d} = \mu_{u/d}(1-\kappa)\,, \qquad \kappa \equiv \frac{2\alpha_s}{3\pi}\,. \tag{355}$$

We illustrate in Fig. 21 how these corrections open up the phase space for the direct Urca process. As a consequence, there is a fixed angle θ_{ud} between the u and d quarks, and the δ-function in Eq. (346) can be approximated by

$$\delta(p_e - p_\nu + k - p) \simeq \frac{\mu_e}{\mu_u\mu_d}\delta(\cos\theta_{ud} - \cos\theta_0)\,, \qquad \cos\theta_0 \equiv 1 - \kappa\frac{\mu_e^2}{\mu_u\mu_d}\,. \tag{356}$$

(We have reinstated the different chemical potentials μ_u, μ_d.) We denote the angle between the neutrino and the d quark by $\theta_{\nu d}$ and approximate the factor

$$(p_e - \mathbf{p}_e\cdot\hat{\mathbf{k}})(p_\nu - \mathbf{p}_\nu\cdot\hat{\mathbf{p}}) \simeq 2\mu_e p_\nu\kappa(1-\cos\theta_{\nu d})\,. \tag{357}$$

This factor vanishes for the case of collinear scattering. The α_s effect renders it nonzero, hence this factor and in consequence the total neutrino emissivity is proportional to α_s. Putting all this together and changing the integration variable from $\mathbf{p}_e$ to the d quark momentum $\mathbf{p}$ yields

$$\begin{aligned}\frac{\partial}{\partial t}f_\nu(t,\mathbf{p}_\nu) \;&=\; -64G_F^2\alpha_s\mu_e\mu_d\mu_u\int\frac{dp\,d\Omega_p}{(2\pi)^3}\int\frac{dk\,d\Omega_k}{(2\pi)^3}(1-\cos\theta_{\nu d})\\ &\quad\times\delta(\cos\theta_{ud}-\cos\theta_0)\,f_F(p_e-\mu_e)f_F(k-\mu_u)[1-f_F(p-\mu_d)]\,.\end{aligned} \tag{358}$$

Since we have taken only one color degree of freedom from Eq. (340), we have reinstated a factor $N_c = 3$. Next we introduce the dimensionless variables x, y, v from Eq. (351), and with the definition (332) of the total neutrino emissivity we obtain

$$\begin{aligned}\epsilon_\nu &= 128\alpha_s G_F^2 \mu_e \mu_u \mu_d T^6 \int \frac{d\Omega_{p_\nu}}{(2\pi)^3} \int \frac{d\Omega_p}{(2\pi)^3} \int \frac{d\Omega_k}{(2\pi)^3} (1-\cos\theta_{\nu d}) \delta(\cos\theta_{ud} - \cos\theta_0) \\ &\quad \times \int_0^\infty dv\, v^3 \int_{-\infty}^\infty dx \int_{-\infty}^\infty dy\, f_F(v+x-y) f_F(y)[1-f_F(x)] \,. \end{aligned} \tag{359}$$

Here we have approximated the lower boundaries by $-\mu_{u/d}/T \simeq \infty$. With the integral

$$\int_0^\infty dv\, v^3 \int_{-\infty}^\infty dx \int_{-\infty}^\infty dy\, f_F(v+x-y) f_F(y)[1-f_F(x)] = \frac{457}{5040}\pi^6 \,, \tag{360}$$

and the (trivial) angular integral

$$\int \frac{d\Omega_{p_\nu}}{(2\pi)^3} \int \frac{d\Omega_p}{(2\pi)^3} \int \frac{d\Omega_k}{(2\pi)^3} (1-\cos\theta_{\nu d}) \delta(\cos\theta_{ud} - \cos\theta_0) = \frac{1}{16\pi^6} \,, \tag{361}$$

we obtain the final result

$$\epsilon_\nu \simeq \frac{457}{630} \alpha_s G_F^2 \mu_e \mu_u \mu_d T^6 \,. \tag{362}$$

This result has first been computed by Iwamoto in 1980 [50].

C. Cooling with quark direct Urca process

From the result for the neutrino emissivity we can now get a simple cooling curve for unpaired quark matter. Of course we shall ignore a lot of details of realistic stars. The result will simply show how a chunk of unpaired two-flavor quark matter cools via the direct Urca process. Nevertheless, the result is very illustrative and shows that the direct Urca process is indeed an efficient cooling mechanism. We use Eq. (223), which relates the temperature as a function of time to the emissivity and the specific heat. For the emissivity we use the result (362). For the specific heat, recall the result (214) which is valid for two fermionic degrees of freedom, taking into account spin; we thus have to multiply this result by the number of colors and add up the contributions of u and d quarks,

$$c_V = (\mu_u^2 + \mu_d^2) T \,. \tag{363}$$

Then, performing the integration in Eq. (223) yields

$$T(t) = \frac{T_0 \tau^{1/4}}{(t - t_0 + \tau)^{1/4}} \,, \tag{364}$$

where we have defined

$$\tau = \frac{315}{914} \frac{\mu_u^2 + \mu_d^2}{\alpha_s G_F^2 \mu_e \mu_u \mu_d} \frac{1}{T_0^4} \,. \tag{365}$$

To get an estimate for this characteristic time scale, we assume $\mu_d = 500\,\mathrm{MeV}$, $\mu_u = 400\,\mathrm{MeV}$, $\mu_e = 100\,\mathrm{MeV}$, $\alpha_s = 1$, an initial temperature of $T_0 = 100\,\mathrm{keV}$ at an initial time $t_0 = 100\,\mathrm{yr}$, and use the value of the Fermi coupling (334) to obtain

$$\tau \simeq 10^{-5}\,\mathrm{yr} \simeq 5\,\mathrm{min} \,. \tag{366}$$

This is a very short time compared to the astrophysical time scales we are interested in. The function $T(t)$ is plotted in Fig. 22. We see the rapid drop in temperature on a time scale of minutes down to a few keV. We thus recover the shape of the direct Urca cooling from Fig. 18. For late times $t \gg t_0$, we have $T(t) \propto t^{-1/4}$.

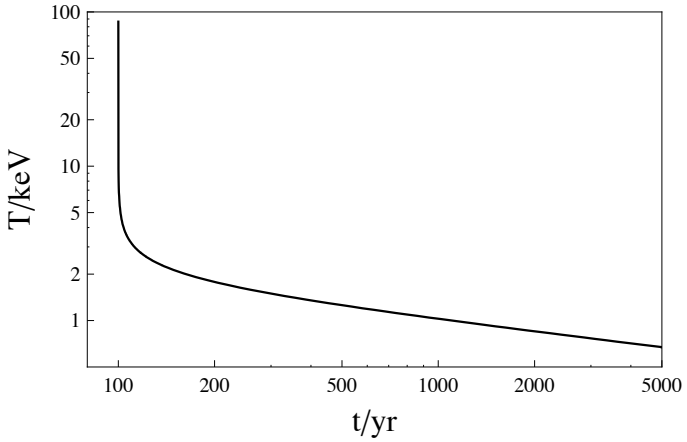

FIG. 22: Cooling curve from the direct Urca process in two-flavor, unpaired, ultrarelativistic quark matter, see Eq. (364).

Problems

V.1 **2SC propagator**

Show that for the case of different flavor chemical potentials the fermion propagator of the 2SC phase is given by Eqs. (325) and (326).

V.2 **Trace over Dirac space**

Show that

$$L_{\lambda\sigma}(\mathbf{p}_e,\mathbf{p}_\nu)\mathcal{T}^{\lambda\sigma}(\hat{\mathbf{k}},\hat{\mathbf{p}}) = 64(p_e-\mathbf{p}_e\cdot\hat{\mathbf{k}})(p_\nu-\mathbf{p}_\nu\cdot\hat{\mathbf{p}})\,, \tag{367}$$

with $L_{\lambda\sigma}(\mathbf{p}_e,\mathbf{p}_\nu)$ and $\mathcal{T}^{\lambda\sigma}(\hat{\mathbf{k}},\hat{\mathbf{p}})$ defined in Eqs. (331) and (341), respectively.

VI. DISCUSSION

Let us summarize what we have learned about compact stars and dense matter, having in mind the two questions we have formulated in the preface. In addition, let us also list a few things which would in principle have fitted into these lectures topic-wise. We haven't discussed them in the main part because either I found them not suitable for a concise, and yet pedagogical, introduction or because they are simply beyond the scope of these lectures, such as some of the theoretical approaches to dense matter listed at the end of Sec. VI B. And, well, some selection has to be made, so for some of the following points there is no good reason why they appear here and not in the main part. The volume of the main part is chosen such that it should conveniently fit into a one-semester course, maybe dropping one or two of the more specialized subsections. In Sec. VI B I will give some selected references where interested readers can find more information about the questions we haven't addressed in the main part.

A. What we have discussed

- *Astrophysical observables and their relation to microscopic physics.* The first thing you should have learned in these lectures is in which sense compact stars are laboratories for the understanding of dense matter. The experiments we can do in this laboratory are less controlled as for example tabletop experiments in condensed matter physics. This means we cannot always measure the quantities we would like to know, or at least not to an accuracy we would need for our purposes. And it means that it is often impossible to switch on or off certain unwanted effects at will, which would be desirable to extract an exact value for a given quantity. For instance we would ideally like to have a precise look into the interior of a compact star, but these kind of observations will always be indirect at best since the information we get from the interior is filtered through the surface and the atmosphere of the star. However, in spite of these restrictions (which, to some extent, have been and will be overcome through improvements in observational technology), we have seen that our observational data of

compact stars can be closely linked to the properties of dense matter. Examples we have discussed in detail are the mass-radius relation which is related to the equation of state and the cooling curve which is related to the neutrino emissivity and the specific heat.

- *Theoretical approaches to dense matter.* We have emphasized at several points in these lectures that the density regime which is of interest for the physics of compact stars is very difficult to tackle. After all, this difficulty led us to consider compact stars not only as an application of QCD but also as an important means to understand QCD. The main reason for the theoretical difficulty is the strong-coupling nature of QCD. We have discussed attempts to approach the relevant density regime from two sides, coming from lower and higher density.

  First, we have discussed nuclear matter, for which we have solid knowledge at low densities. This knowledge is strongly built upon experimental data. In principle, even a single nucleon is theoretically a very complicated object if considered from first principles. First-principle calculations, at least for sufficiently simple properties of nucleons, are possible in computer simulations, but effective theories remain an important tool to describe nuclear matter, and they work well (by construction) at sufficiently low densities. One of the basic examples we have discussed is the Walecka model. However, finding the correct description of nuclear matter at high density is a challenge, and astrophysical data can be used to rule out or confirm certain models.

  Second, we have discussed QCD from first principles in the context of deconfined quark matter. This approach is rigorous at asymptotically high density and therefore is interesting on its own right. We have discussed that it predicts the CFL state. Whether CFL persists down to densities relevant for compact stars is unknown. We have discussed that, to get a rough idea about the low-density region, one may simply extrapolate the rigorous results. But this of course stretches the results beyond their range of validity. We have also introduced a more powerful approach to deduce intermediate-density properties from the high-density calculations. This approach relies on the symmetries of the CFL state. Building on these symmetries, one can construct an effective theory which can give us at least qualitative insight into the properties of CFL at lower densities, although this approach cannot tell us whether CFL is indeed the ground state of matter at densities present in the core of a compact star.

B. What we could have, but haven't, discussed

- *r-modes – bulk/shear viscosity.* We have said little about the rotation of a compact star except for stating that it can rotate very fast, up to almost a thousand times per second. For the purpose of our lecture, however, the rotation frequency is a very interesting observable because it is sensitive to the microscopic physics. One of the reasons is as follows.

  Certain non-radial oscillatory modes of a rotating star, in particular the so-called r-modes,[15] are generically unstable with respect to gravitational radiation. The reason can be understood in a rather simple argument. Consider the situation where the star rotates *counterclockwise*, seen from the polar view, and where an observer in the co-rotating frame sees non-radial oscillations which propagate *clockwise*. These modes lower the total angular momentum of the star, i.e., if the star's angular momentum is positive, the oscillations have negative angular momentum. Now assume that these propagating modes are seen from a distant observer to move counterclockwise, i.e., they are "dragged" by the star's rotation or, in other words, their angular velocity in the co-rotating frame is smaller in magnitude than the angular velocity of the star, seen from a distant observer. The pulsations now couple to gravitational radiation. The emitted radiation has positive angular momentum since a distant observer sees the pulsations move counterclockwise. Consequently, the total angular momentum of the star must be lowered. This, however, means that the angular momentum of the oscillations, which is already negative, is *increased* in magnitude (becomes more negative). Therefore, the emission of gravitational radiation tends to increase the amplitude of the pulsation which in turn leads to a stronger gravitational radiation etc. This is the r-mode instability. Note that the rotation of the star is crucial for this argument. In a non-rotating star, the effect of gravitational radiation is dissipative, i.e., the non-radial oscillations would be damped. For a nice pedagogical introduction into this general relativistic effect see Ref. [51].

  The energy loss from gravitational radiation due to the r-mode instability makes the star spin down drastically and quickly. Consequently, the observation of sufficiently high rotation frequencies implies that some mechanism must be at work to avoid the instability. The above argument for the instability is generic for all rotating perfect

[15] Oscillatory modes of compact stars are classified according to their restoring force. In the case of r-modes, this is the Coriolis force.

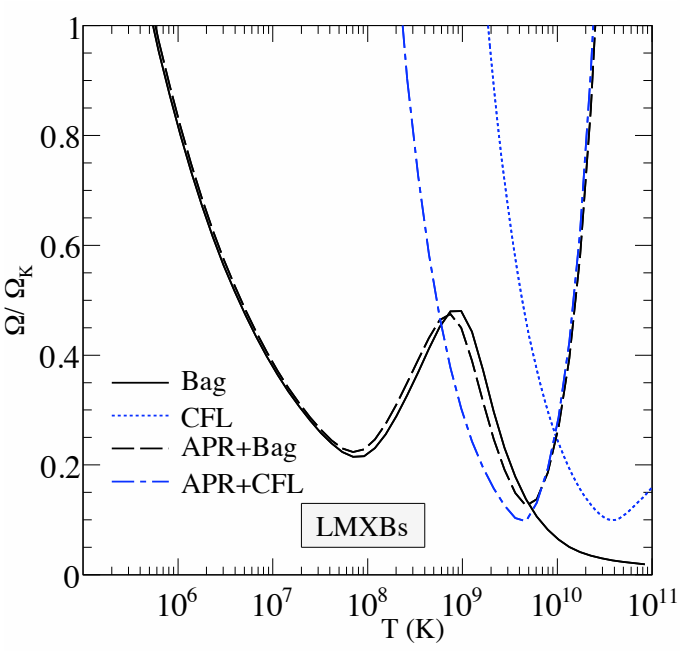

FIG. 23: Critical rotation frequency (normalized to the *Kepler frequency* Ω_K, the upper limit for the rotation frequency beyond which the star would start shedding mass from its equator) as a function of temperature for hybrid and quark stars. If a star is put somewhere above the respective curves, the r-mode instability will set in and the star will spin down quickly. "APR" stands for a certain nuclear equation of state, "Bag" denotes unpaired quark matter in the bag model and the box labelled LMXB indicates the location of observed *low-mass X-ray binaries*. Within the given calculation they are located in a stable region for both hybrid and quark stars. For more explanations and details see Ref. [52] where this figure is taken from.

fluid stars. If there is dissipation, i.e., if the matter inside the star has a nonzero viscosity, the instability can be damped. Put differently, in order to rotate fast the star has to be viscous. This statement seems paradoxical at first sight but makes sense with the above explanation. In Fig. 23 we show an example for critical frequencies of hybrid and quark stars, derived from viscosity calculations.

In hydrodynamics, there are two kinds of viscosity, shear and bulk viscosity.[16] Bulk viscosity describes dissipation for the case of volume expansion or compression while shear viscosity is relevant for shear forces. Both kinds of viscosities are relevant for the damping of the r-mode instability, typically they act in different temperature regimes, bulk viscosity at rather large, shear viscosity at rather small temperatures. What is the microscopic physics behind the viscosity? Let us explain this for the case of the bulk viscosity.

Imagine a chunk of nuclear or quark matter in thermal and chemical equilibrium in a volume V_0. Now we compress and expand this volume periodically, $V(t) = V_0 + \delta V_0 \cos \omega t$. In the astrophysical setting, these will be local volume oscillations where ω is typically of the order of the rotation frequency of the star. Through the volume change the matter gets out of thermal and, possibly, chemical equilibrium. The latter may happen if the matter is composed of different components whose chemical potentials react differently on a density change. An example is unpaired quark matter with massless up and down quarks and massive strange quarks. The system now seeks to reequilibrate. For instance, if the compression has increased the down quark chemical potential compared to the strange quark chemical potential (in chemical equilibrium they are equal), the system reacts by producing strange quarks, for instance via the process $u + d \to u + s$. If it does so on the same time scale as the external oscillation, there can be sizable dissipation (think of compressing a spring which changes its spring constant during the process; you will not get back the work you have put in). Consequently, the calculation of the bulk viscosity requires the calculation of the rate of processes such as $u + d \to u + s$ which indeed turns out to be the dominant process for the bulk viscosity in unpaired quark matter. Other processes which contribute are leptonic processes, such as the direct Urca process we have discussed in the context of neutrino emissivity

[16] In the case of a superfluid, there are in fact several bulk viscosities.

in Sec. V B. It is important to note that again the weak processes are the relevant ones. In principle, also strong processes contribute to the bulk viscosity since they reequilibrate the system thermally. However, they do so on time scales much smaller than the external oscillation. Therefore, the system reequilibrates basically instantaneously during the compression process and no energy is dissipated. These arguments also show that the bulk viscosity is a function of the (external) frequency. Maximum bulk viscosity is obtained when the rate of the respective microscopic process (which is a function of temperature) is closest to this frequency. Hence, it may well be that for a certain temperature regime a superconducting state has *larger* bulk viscosity than a non-superconducting state. This may sound counterintuitive but note that the (partial) suppression of the rate of the microscopic process by $\exp(-\Delta/T)$ may actually help the viscosity if it brings the rate closer to the external frequency. See for instance Sec. VII in Ref. [8] for a brief review about viscosity in quark matter phases, and Refs. [53, 54] for examples of detailed microscopic calculations of bulk viscosity in quark matter.

- *Magnetic fields.* We have mentioned in the introduction that compact stars can have huge magnetic fields, the highest magnetic fields measured for the surface of a star (then called *magnetar*) are about 10^{15} G. The first question one might ask is what the origin of these magnetic fields is. The conventional explanation is that they are inherited from the star's progenitor, a giant star that has exploded in a supernova. While the magnetic flux is conserved in this process, the magnetic field is greatly enhanced because the magnetic field lines are confined in a much smaller region after the explosion.

  Other questions regarding the magnetic field concern their interplay with dense matter. We have learned that nuclear matter can contain superconducting protons. Protons form a type-II superconductor where the magnetic field is confined into flux tubes. Since at the same time the rotating neutron superfluid forms vortices, a complicated picture emerges, where arrays of flux tubes and vortices intertwine each other. Their dynamics is complicated and relevant for instance for the observed precession times of the star, see for instance Ref. [55]. This issue is also related to *pulsar glitches*, see below.

  In the main part we have only touched the interplay of color superconductors with magnetic fields. We have stated without calculation that the CFL phase is not an electromagnetic superconductor, i.e., a magnetic field can penetrate CFL matter. More precisely, Cooper pairs in CFL are neutral with respect to a certain mixture of the photon and one of the gluons. Because of the smallness of the electromagnetic coupling compared to the strong coupling, the gluon admixture is small and the new gauge boson is called "rotated photon". There are color superconductors which do expel magnetic fields, for instance the color-spin-locked (CSL) phase. In this case, Cooper pairs are formed of quarks with the same flavor, and a Cooper pair carries total spin one (instead of zero in the CFL phase). The CSL phase is an electromagnetic superconductor. It is of type I, i.e., expels magnetic fields completely. For a short review about spin-one color superconductors in compact stars and their effect on magnetic fields see Ref. [56].

  Magnetic fields also play a role in the cooling of the star since they have an effect on the heat transport, resulting in an anisotropic surface temperature, see Ref. [46] and references therein. An extensive review about magnetic fields in compact stars is Ref. [57].

- *Crust of the star.* The crust of the star is a very important ingredient for the understanding of observations. In the conventional picture of a neutron star there is an outer crust with an ion lattice, and an inner crust with a neutron (super)fluid immersed in this lattice. This crust typically has a thickness of about 1 km. A lot about the crust can be found in Refs. [3, 29]. In our discussion of neutron stars vs. hybrid stars vs. quark stars it is important that the crust provides a crucial distinction between an ordinary neutron star (or a hybrid star) and a quark star. How does the crust of a quark star look? Several scenarios have been suggested. First suppose that the surface of a quark star exhibits an abrupt transition from strange quark matter to the vacuum. This is possible under the assumption of the strange quark matter hypothesis we discussed in Sec. II B 1, because, if the hypothesis is true, strange quark matter is stable at zero pressure. "Abrupt" means that the density drops to zero on a length scale of about 1 fm, given by the typical length scale of the strong interaction. Now recall that (unpaired) three-flavor quark matter contains electrons. They interact with quark matter through the electromagnetic interaction, therefore their surface will be smeared (several hundred fm) compared to the sharp surface of the quark matter. As a consequence, an outward-pointing electric field develops (i.e., at the surface positively charged test particles are accelerated away from the center of the star). This electric field can support a thin layer of positively charged ions, separated from the quark matter by a layer of electrons. Hence a "normal" crust for a quark star is conceivable, consisting of an ion lattice. In contrast to the crust of a neutron star, such a crust of a quark star would be very thin, at most of the order of 100 m. See Ref. [58] for more details about this picture of the surface of a quark star (and for other properties of quark stars). This picture may be challenged by the possibility of a mixed phase at the surface of the star. Here, mixed phase refers to a crystalline structure of strangelets immersed in a sea of electrons. In this case, there would be no electric field

and thus no possibility for a "normal" crust. The quark matter would rather have its own crystalline crust. Estimates in Ref. [59] show that it is unlikely that such a mixed phase is formed once surface tension is taken into account. In any case, a rigid crust, if at all present, will be much thinner in a quark star than in a neutron star or a hybrid star.

This qualitative difference is relevant in the context of "magnetar seismology". Quasi-periodic oscillations observed in the aftermath of X-ray bursts from magnetars can be related to typical oscillation frequencies of the crust. In other words, "star quakes" have significantly different properties depending on whether one assumes the star to be a neutron star or a quark star. In fact, the ordinary crust explains the data quite well while the crust of a quark star seems to be incompatible with the observed phenomenology [60].

- *Pulsar glitches.* Pulsar glitches are an interesting phenomenon related to the rotation frequency, the crust (more precisely the crystalline structure of the crust), and superfluidity. For spinning-down pulsars one observes sudden spin-ups, i.e., in the overall trend of a decreasing rotation frequency, the frequency increases in irregular intervals significantly on a very short time scale. This is conventionally explained through superfluid vortices in the neutron superfluid that pin at the lattice sites of the inner crust [61].

  To understand this statement and the consequences for glitches, we recall the following property of superfluids. A superfluid, be it superfluid helium, superfluid neutron matter, or any other superfluid, is irrotational in the sense that the superfluid velocity has vanishing curl. Therefore, if the superfluid is rotated it develops regions where the order parameter vanishes, i.e., where it becomes a normal fluid.[17] The angular momentum is then "stored" in these regions which are called vortices. An array of vortices, which are "strings" in the direction of the angular momentum, is formed with the total angular momentum of the superfluid being proportional to the density of vortices (because each vortex carries one quantum of circulation). Consequently, if the rotation frequency decreases, the array of vortices becomes sparser, i.e., the vortices move apart.

  The next ingredient in the glitch mechanism is the pinning of the vortices at the lattice of nuclei in the inner crust. Generally speaking, there is an effective interaction between the vortices and the nuclei, resulting in a certain path of the vortex string through the lattice which minimizes the free energy of the system. You may think of this preferred configuration as follows. Superfluidity, i.e., neutron Cooper pairing, lowers the free energy of the system. Therefore, the system may want to put the vortices, where there is no Cooper pairing, through the lattice sites because they are not superfluid anyway. Otherwise, i.e., by putting them between the lattice sites, one loses pairing energy. The actual details of the pinning mechanism are complicated and, depending on the density, the preferred path of the vortices may in fact be between the sites, in contrast to the above intuitive argument. However, this does not matter for our argument for the mechanism of glitches:

  In a rotating neutron star, the neutron vortices pin at the lattice of the inner crust. Now the star spins down. On the one hand, the vortices "want" to move apart. On the other hand, there is an effective pinning force which keeps them at there sites. Hence, for a while they will not move which implies that the superfluid (the vortex array) is spinning faster than the rest of the star. At some point, when the tension is sufficiently large, the vortices will un-pin, move apart and thus release their angular momentum which spins up in particular the surface of the star whose rotation is observed. Then, they re-pin and the process starts again.

  An alternative scenario, where nuclear matter is replaced by quark matter has been suggested [62]. In our discussion of the CFL phase we have seen that quark matter can be a superfluid. This means that one of the conditions for the mechanism of vortex pinning is fulfilled. The second condition, a sufficiently rigid lattice, may be provided by one of the unconventional color-superconducting phases which are possible in the case of mismatched Fermi momenta, see discussion at the end of in Sec. IV C. Some of these phases indeed exhibit a crystalline structure. Such a quark crystal is of very different nature than the ion lattice because it is the energy gap from superconductivity which varies periodically in space, giving rise to crystals characterized by surfaces where the gap vanishes. It remains to be seen in the future which of these scenarios passes all observational constraints and can explain the pulsar glitches or if there is a yet unknown mechanism for these curious spin-ups.

- *Other theoretical approaches to dense matter.* What are the alternatives to understand QCD at large, but not asymptotically large, densities? *Lattice QCD*, i.e., solving QCD by brute force on a computer, is by now a powerful tool for strong-coupling phenomena at zero chemical potential. However, at nonzero chemical potential,

[17] It is instructive to view this phenomenon in analogy to a type-II superconductor. There, a magnetic field (if sufficiently large but not too large) penetrates the superconductor through flux tubes. It partially destroys superconductivity, i.e., in the center of the flux tubes the order parameter is zero. Hence the analogy is superfluid – superconductor; angular momentum – magnetic field; vortices – flux tubes.

one encounters the so-called *sign problem* which renders lattice calculations unfeasible. Progress has been made to extend lattice calculations to small chemical potentials, more precisely to small values of μ/T. But calculations at large μ and small T, as needed for compact stars, are currently not within reach. See Ref. [63] for a non-technical recent overview article about lattice QCD, in particular its contributions to the QCD phase diagram and about the sign problem; you may also try Ref. [64].

Because of the problems of lattice calculations at finite chemical potential one has to rely on model calculations or on extrapolations similar to the ones discussed in these lectures. One model for quark matter we have not discussed is the Nambu-Jona-Lasinio (NJL) model. This model does not contain gluons and describes the interaction between quarks by an effective pointlike interaction. It has been used to compute the QCD phase diagram at intermediate densities. Since the result depends strongly on the parameters of the model, it should be taken as an indicator for how the phase diagram might look, not as an accurate prediction. Due to its simplicity it is widely used and can indeed give some interesting results which serve as a guideline for the understanding of QCD. For an extensive review about the NJL model in dense quark matter see Ref. [65]; for an application of the NJL model in the context of compact stars, see for instance Ref. [66].

Finally, we point out that arguments for large numbers of colors N_c may be applied to gain some insight to QCD where $N_c = 3$. In particular, it has been argued that at $N_c = \infty$ an interesting novel phase, termed *quarkyonic matter*, populates the T-μ phase diagram [67]. The (yet unsolved) problem is to find out whether this phase, or some modification of it, survives for $N_c = 3$. More generally speaking, the large N_c approach is another approach where calculations can be performed in a regime where everything is under rigorous control. From these rigorous results one then tries to get closer to the regime one is interested in. In this sense, this approach is not unlike the perturbative approach. In view of the possible, but not at all obvious, relevance of large-N_c physics to $N_c = 3$ physics, one can also apply the duality of certain string theories to field theories similar to QCD, based on the so-called *AdS/CFT correspondence*. For pedagogical reviews see Refs. [68, 69]. This somewhat speculative but popular approach to QCD has recently been pursued especially for large-T, small-μ physics, but is, in certain variants, also suited for the physics at finite chemical potential.

Acknowledgments

These lectures are based on a course given in the summer semester 2009 at the Vienna University of Technology. I thank all participants of this course for the lively discussions and the numerous questions and comments that helped improve these lecture notes. I am also grateful to M. Alford, P. Jaikumar, T. Schäfer, I. Shovkovy, P. van Nieuwenhuizen, A. Rebhan, N.-O. Walliser, Q. Wang, and F. Weber for helpful comments and discussions.

Appendix A: Basics of quantum field theory at finite temperature and chemical potential

Many of the discussions in the main part of these lectures rely on field-theoretical methods, in particular on quantum field theory at finite temperature and chemical potential. One purpose of the following basic discussion is therefore to explain how a chemical potential is introduced in quantum field theory. We shall also discuss how finite temperature enters the formalism, although for most quantities we discuss in these lecture notes we consider the zero-temperature limit, which is a good approximation for our purposes. For instance in the discussion of the Walecka model, Sec. III A, we give the finite-temperature expressions, based on appendix A 2, before we set $T = 0$ in the physical discussion. In other parts, we do keep $T \neq 0$ in our results, for instance when we are interested in the cooling behavior of dense matter, see chapter V.

We shall start with the Lagrangian for a complex bosonic field and derive the partition function in the path integral formalism, taking into account Bose-Einstein condensation. This part is particularly useful for our treatment of kaon condensation in CFL quark matter, see Sec. IV B 1. We shall in particular see how bosonic Matsubara frequencies are introduced and how the summation over these is performed with the help of contour integration in the complex frequency plane. In the second part of this appendix we shall then discuss the analogous derivation for fermions.

1. Bosonic field

We start from the Lagrangian

$$\mathcal{L}_0 = \partial_\mu \varphi^* \partial^\mu \varphi - m^2 |\varphi|^2 - \lambda |\varphi|^4 \,, \tag{A1}$$

with a complex scalar field φ with mass m and coupling constant λ. We shall first show how a chemical potential μ is introduced. This will lead to a new Lagrangian $\mathcal{L}$, wherefore we have denoted the Lagrangian without chemical potential by $\mathcal{L}_0$. The chemical potential μ must be associated with a conserved charge. We thus need to identify the conserved current. From Noether's theorem we know that the conserved current is related to the symmetry of the Lagrangian. We see that $\mathcal{L}_0$ is invariant under $U(1)$ rotations of the field,

$$\varphi \to e^{-i\alpha}\varphi\,. \tag{A2}$$

This yields the Noether current

$$j^\mu = \frac{\partial\mathcal{L}_0}{\partial(\partial_\mu\varphi)}\,\frac{\delta\varphi}{\delta\alpha} + \frac{\partial\mathcal{L}_0}{\partial(\partial_\mu\varphi^*)}\,\frac{\delta\varphi^*}{\delta\alpha} = i(\varphi^*\partial^\mu\varphi - \varphi\partial^\mu\varphi^*)\,, \tag{A3}$$

with $\partial_\mu j^\mu = 0$, and the conserved charge (density) is

$$j^0 = i(\varphi^*\partial^0\varphi - \varphi\partial^0\varphi^*)\,. \tag{A4}$$

In the following we want to see how the chemical potential associated to j^0 enters the Lagrangian. The partition function for a scalar field is

$$Z \;=\; \mathrm{Tr}\, e^{-\beta(\hat{H}-\mu\hat{N})} = \int\mathcal{D}\pi\int_{\text{periodic}}\mathcal{D}\varphi\,\exp\left[-\int_X(\mathcal{H}-\mu\mathcal{N}-i\pi\partial_\tau\varphi)\right]\,, \tag{A5}$$

This equation should remind you that the partition function can be written in the operator formalism in terms of the Hamiltonian $\hat{H}$ and the charge operator $\hat{N}$, or, as we shall use here, in terms of a functional integral over φ and the conjugate momentum π, with the Hamiltonian $\mathcal{H}$ and the charge density $\mathcal{N} = j^0$. We have abbreviated the space-time integration by

$$\int_X \equiv \int_0^\beta d\tau\int d^3x\,, \tag{A6}$$

where the integration over "imaginary time" $\tau = it$ goes from 0 to the inverse temperature $\beta = 1/T$. In the following, the four-vector in position space is denoted by

$$X \equiv (t,\mathbf{x}) = (-i\tau,\mathbf{x})\,. \tag{A7}$$

The term "periodic" for the φ integral in Eq. (A5) means that all fields φ over which we integrate have to be periodic in the imaginary time direction, $\varphi(0,\mathbf{x}) = \varphi(\beta,\mathbf{x})$. This is essentially a consequence of the trace operation in the first line of Eq. (A5): the partition function is formally reminiscent of a sum over transition amplitudes which have the same initial and final states at "times" 0 and β.

Let us, for convenience, introduce the two real fields φ_1, φ_2,

$$\varphi = \frac{1}{\sqrt{2}}(\varphi_1 + i\varphi_2)\,. \tag{A8}$$

Then, the Lagrangian becomes

$$\mathcal{L}_0 = \frac{1}{2}\left[\partial_\mu\varphi_1\partial^\mu\varphi_1 + \partial_\mu\varphi_2\partial^\mu\varphi_2 - m^2(\varphi_1^2+\varphi_2^2) - \frac{\lambda}{2}(\varphi_1^2+\varphi_2^2)^2\right]\,. \tag{A9}$$

The conjugate momenta are

$$\pi_i = \frac{\partial\mathcal{L}_0}{\partial(\partial_0\varphi_i)} = \partial^0\varphi_i\,, \qquad i=1,2\,. \tag{A10}$$

Consequently, with $j^0 = \varphi_2\pi_1 - \varphi_1\pi_2$, which follows from Eqs. (A4), (A8), and (A10), we have

$$\begin{aligned}\mathcal{H}-\mu\mathcal{N} \;&=\; \pi_1\partial_0\varphi_1 + \pi_2\partial_0\varphi_2 - \mathcal{L}_0 - \mu\mathcal{N}\\ &=\; \frac{1}{2}\left[\pi_1^2+\pi_2^2+(\nabla\varphi_1)^2+(\nabla\varphi_2)^2+m^2(\varphi_1^2+\varphi_2^2)\right] - \mu(\varphi_2\pi_1-\varphi_1\pi_2)\,.\end{aligned} \tag{A11}$$

The integration over the conjugate momenta π_1, π_2 can be separated from the integration over the fields φ_1, φ_2 after introducing the shifted momenta

$$\tilde{\pi}_1 \equiv \pi_1 - \partial_0\varphi_1 - \mu\varphi_2\,, \qquad \tilde{\pi}_2 \equiv \pi_2 - \partial_0\varphi_2 + \mu\varphi_1\,. \tag{A12}$$

This yields

$$\pi_1\partial_0\varphi_1 + \pi_2\partial_0\varphi_2 - \mathcal{H} + \mu\mathcal{N} = -\frac{1}{2}(\tilde{\pi}_1^2 + \tilde{\pi}_2^2) + \mathcal{L}\,, \tag{A13}$$

where the new Lagrangian $\mathcal{L}$ now includes the chemical potential,

$$\mathcal{L} \;=\; \frac{1}{2}\Big[\partial_\mu\varphi_1\partial^\mu\varphi_1 + \partial_\mu\varphi_2\partial^\mu\varphi_2 + 2\mu(\varphi_2\partial_0\varphi_1 - \varphi_1\partial_0\varphi_2) + (\mu^2 - m^2)(\varphi_1^2+\varphi_2^2) - \frac{\lambda}{2}(\varphi_1^2+\varphi_2^2)^2\Big]\,. \tag{A14}$$

Thus we see that the chemical potential produces, besides the expected term μj^0, the additional term $\mu^2(\varphi_1^2+\varphi_2^2)/2$. This is due to the momentum-dependence of j^0. In terms of the complex field φ, the Lagrangian reads

$$\mathcal{L} = |(\partial_0 - i\mu)\varphi|^2 - |\nabla\varphi|^2 - m^2|\varphi|^2 - \lambda|\varphi|^4\,, \tag{A15}$$

which shows that the chemical potential looks like the temporal component of a gauge field. We can now insert Eq. (A13) into the partition function (A5). The integration over conjugate momenta and over fields factorize, and the momentum integral yields an irrelevant constant N, such that we can write

$$Z = N\int_{\text{periodic}} \mathcal{D}\varphi_1\mathcal{D}\varphi_2\,\exp\int_X \mathcal{L}\,. \tag{A16}$$

In order to take into account Bose-Einstein condensation, we divide the field into a constant background field and fluctuations around this background, $\varphi_i \to \phi_i + \varphi_i$. A nonzero condensate $\phi_1 + i\phi_2$ picks a direction in the $U(1)$ degeneracy space and thus breaks the symmetry spontaneously. We can choose $\phi_2 = 0$ and thus may denote $\phi \equiv \phi_1$. Then, the Lagrangian (A14) becomes

$$\mathcal{L} = -U(\phi^2) + \mathcal{L}^{(2)} + \mathcal{L}^{(3)} + \mathcal{L}^{(4)}, \tag{A17}$$

with the tree-level potential

$$U(\phi^2) = \frac{m^2-\mu^2}{2}\,\phi^2 + \frac{\lambda}{4}\,\phi^4\,, \tag{A18}$$

and terms of second, third, and fourth order in the fluctuations,

$$\mathcal{L}^{(2)} \;=\; -\frac{1}{2}\left[-\partial_\mu\varphi_1\partial^\mu\varphi_1 - \partial_\mu\varphi_2\partial^\mu\varphi_2 - 2\mu(\varphi_2\partial_0\varphi_1 - \varphi_1\partial_0\varphi_2) + (m^2-\mu^2)(\varphi_1^2+\varphi_2^2) + 3\lambda\phi^2\varphi_1^2 + \lambda\phi^2\varphi_2^2\right] \tag{A19a}$$

$$\mathcal{L}^{(3)} \;=\; -\lambda\phi\varphi_1(\varphi_1^2+\varphi_2^2)\,, \tag{A19b}$$

$$\mathcal{L}^{(4)} \;=\; -\frac{\lambda}{4}(\varphi_1^2+\varphi_2^2)^2\,. \tag{A19c}$$

We have omitted the linear terms since they do not contribute to the functional integral. Note that the cubic interactions are induced by the condensate.

In this appendix we are only interested in the tree-level contributions $U(\phi^2)$ and $\mathcal{L}^{(2)}$ in order to explain the basic calculation of the partition function for the simplest case. We therefore shall ignore the cubic and quartic contributions $\mathcal{L}^{(3)}$ and $\mathcal{L}^{(4)}$. We introduce the Fourier transforms of the fluctuation fields via

$$\varphi(X) = \frac{1}{\sqrt{TV}}\sum_K e^{-iK\cdot X}\varphi(K) = \frac{1}{\sqrt{TV}}\sum_K e^{i(\omega_n\tau + \mathbf{k}\cdot\mathbf{x})}\varphi(K)\,, \tag{A20}$$

with the four-momentum

$$K \equiv (k_0, \mathbf{k}) = (-i\omega_n, \mathbf{k})\,, \tag{A21}$$

and with the Minkowski scalar product $K\cdot X = k_0x_0 - \mathbf{k}\cdot\mathbf{x} = -(\tau\omega_n + \mathbf{k}\cdot\mathbf{x})$. (Although for convenience we have defined the time components with a factor i and thus can use Minkowski notation, the scalar product is essentially

Euclidean.) The normalization is chosen such that the Fourier-transformed fields $\varphi(K)$ are dimensionless. The 0-component of the four-momentum is given by the *Matsubara frequency* ω_n. To fulfill the periodicity requirement $\varphi(0,\mathbf{x}) = \varphi(\beta,\mathbf{x})$ we need $e^{i\omega_n\beta} = 1$, i.e., $\omega_n\beta$ has to be an integer multiple of 2π, or

$$\omega_n = 2\pi n T\,, \qquad n \in \mathbb{Z}\,. \tag{A22}$$

With the Fourier transform (A20), and

$$\int_X e^{iK\cdot X} = \frac{V}{T}\delta_{K,0}\,, \tag{A23}$$

we have

$$\int_X \mathcal{L}^{(2)} = -\frac{1}{2}\sum_K (\varphi_1(-K),\varphi_2(-K))\frac{D_0^{-1}(K)}{T^2}\begin{pmatrix}\varphi_1(K)\\ \varphi_2(K)\end{pmatrix}, \tag{A24}$$

with the free inverse propagator in momentum space

$$D_0^{-1}(K) = \begin{pmatrix} -K^2 + m^2 + 3\lambda\phi^2 - \mu^2 & -2i\mu k_0 \\ 2i\mu k_0 & -K^2 + m^2 + \lambda\phi^2 - \mu^2 \end{pmatrix}. \tag{A25}$$

With Eqs. (A16), (A24) and using that $\varphi(K) = \varphi^*(-K)$ (because $\varphi(X)$ is real) we can write the tree-level thermodynamic potential as

$$\begin{aligned}
\frac{\Omega}{V} &= -\frac{T}{V}\ln Z \\
&= U(\phi^2) - \frac{T}{V}\ln\int \mathcal{D}\varphi_1\mathcal{D}\varphi_2 \exp\left[-\frac{1}{2}\sum_K (\varphi_1(-K),\varphi_2(-K))\frac{D_0^{-1}(K)}{T^2}\begin{pmatrix}\varphi_1(K)\\ \varphi_2(K)\end{pmatrix}\right] \\
&= U(\phi^2) + \frac{T}{2V}\ln\det\frac{D_0^{-1}(K)}{T^2}\,,
\end{aligned} \tag{A26}$$

where the determinant is taken over 2×2 space and momentum space. Here we have used the general formula

$$\int d^D x\, e^{-\frac{1}{2}\mathbf{x}\cdot\hat{A}\mathbf{x}} = (2\pi)^{D/2}(\det\hat{A})^{-1/2}\,, \tag{A27}$$

for a Hermitian, positive definite matrix $\hat{A}$, which is a generalization of the one-dimensional Gaussian integral

$$\int_{-\infty}^{\infty} dx\, e^{-\frac{1}{2}\alpha x^2} = \sqrt{\frac{2\pi}{\alpha}}\,. \tag{A28}$$

To further evaluate the thermodynamic potential, we first define the tree-level masses

$$m_1^2 \equiv m^2 + 3\lambda\phi^2\,, \tag{A29a}$$
$$m_2^2 \equiv m^2 + \lambda\phi^2\,. \tag{A29b}$$

Then, we obtain

$$\begin{aligned}
\ln\det\frac{D_0^{-1}(K)}{T^2} &= \ln\prod_K \frac{1}{T^4}[(-K^2 + m_1^2 - \mu^2)(-K^2 + m_2^2 - \mu^2) - 4\mu^2 k_0^2] \\
&= \ln\prod_K \frac{1}{T^4}[(\epsilon_k^+)^2 - k_0^2][(\epsilon_k^-)^2 - k_0^2] \\
&= \sum_K \left[\ln\frac{(\epsilon_k^+)^2 - k_0^2}{T^2} + \ln\frac{(\epsilon_k^-)^2 - k_0^2}{T^2}\right].
\end{aligned} \tag{A30}$$

where we defined the quasiparticle energies

$$\epsilon_k^{\pm} = \sqrt{E_k^2 + \mu^2 \mp \sqrt{4\mu^2 E_k^2 + \delta M^4}}\,, \tag{A31}$$

with

$$E_k \equiv \sqrt{k^2+M^2}\,, \quad M^2 \equiv \frac{m_1^2+m_2^2}{2} = m^2+2\lambda\phi^2\,, \quad \delta M^2 \equiv \frac{m_1^2-m_2^2}{2} = \lambda\phi^2\,. \tag{A32}$$

Even at tree-level, the quasiparticle energies (A31) look complicated, but become simple in the non-interacting limit,

$$\lambda = 0: \qquad \epsilon_k^\pm = \sqrt{k^2+m^2} \mp \mu\,, \tag{A33}$$

and for vanishing chemical potential,

$$\mu = 0: \qquad \epsilon_k^\pm = \sqrt{k^2+m_{2/1}^2}\,. \tag{A34}$$

Further properties of these quasiparticle energies are discussed in the context of kaon condensation in CFL, see Sec. IV B 1. Next, we perform the sum over Matsubara frequencies in Eq. (A30). We use the result

$$\sum_n \ln\frac{\omega_n^2+\epsilon_k^2}{T^2} = \frac{\epsilon_k}{T} + 2\ln\left(1-e^{-\epsilon_k/T}\right) + \text{const}\,, \tag{A35}$$

for a real number ϵ_k, and where "const" is a temperature-independent constant. Before we prove this result via contour integration in the complex plane, we use it to compute the final result for the tree-level thermodynamic potential. We insert Eq. (A35) into Eq. (A30), the result into Eq. (A26), and take the thermodynamic limit to obtain

$$\frac{\Omega}{V} = U(\phi^2) + T\int\frac{d^3\mathbf{k}}{(2\pi)^3}\left[\frac{\epsilon_k^+ + \epsilon_k^-}{2T} + \ln\left(1-e^{-\epsilon_k^+/T}\right) + \ln\left(1-e^{-\epsilon_k^-/T}\right)\right]. \tag{A36}$$

From this expression we can for instance compute the pressure $P = -\Omega/V$. The first term in the integrand yields an infinite contribution which however is temperature-independent. We may thus use a renormalization such that the vacuum pressure vanishes. Then, for sufficiently large temperatures, where in particular $\phi = 0$, particles and antiparticles yield the same contribution and we obtain

$$P \simeq -2\frac{T^4}{2\pi^2}\int_0^\infty dx\, x^2 \ln\left(1-e^{-x}\right) = 2\,\frac{\pi^2 T^4}{90}\,. \tag{A37}$$

a. Summation over bosonic Matsubara frequencies

Here we prove Eq. (A35) via contour integration in the complex frequency plane. Especially for more complicated Matsubara sums this is a very useful technique as can be seen by applying the following method to the Matsubara sums in problems A.1 and A.2.

First, in order to get rid of the logarithm, we write

$$\sum_n \ln\frac{\omega_n^2+\epsilon_k^2}{T^2} = \int_1^{(\epsilon_k/T)^2} dx^2 \sum_n \frac{1}{(2n\pi)^2+x^2} + \sum_n \ln[1+(2n\pi)^2]\,. \tag{A38}$$

We now perform the sum in the integrand which, denoting $\epsilon_k \equiv Tx$, we write as a contour integral,

$$T\sum_n \frac{1}{\omega_n^2+\epsilon_k^2} = -\frac{1}{2\pi i}\oint_C d\omega\,\frac{1}{\omega^2-\epsilon_k^2}\,\frac{1}{2}\coth\frac{\omega}{2T}\,. \tag{A39}$$

The second identity follows from the residue theorem,

$$\frac{1}{2\pi i}\oint_C dz\, f(z) = \sum_n \text{Res}\, f(z)|_{z=z_n}\,, \tag{A40}$$

where z_n are the poles of $f(z)$ in the area enclosed by the contour C. If we can write the function f as $f(z) = \varphi(z)/\psi(z)$, with analytic functions $\varphi(z)$, $\psi(z)$, the residues are

$$\text{Res}\, f(z)|_{z=z_n} = \frac{\varphi(z_n)}{\psi'(z_n)}\,. \tag{A41}$$

The contour C in Eq. (A39) is chosen such that it encloses all poles of $\coth[\omega/(2T)]$ and none of $1/(\omega^2-\epsilon_k^2)$. The poles of $\coth[\omega/(2T)]$ are given by $e^{\omega/2T}-e^{-\omega/2T}=0$, i.e., they are on the imaginary axis, $\omega=i\omega_n$ with the Matsubara frequencies ω_n. In the above notation with the functions φ and ψ,

$$\begin{aligned}\varphi(\omega) &= \frac{1}{2}\frac{e^{\omega/(2T)}+e^{-\omega/(2T)}}{\omega^2-\epsilon_k^2}\,, \qquad \psi(\omega)=e^{\omega/(2T)}-e^{-\omega/(2T)}\,,\\ &\Rightarrow\ \frac{\varphi(i\omega_n)}{\psi'(i\omega_n)}=-T\frac{1}{\omega_n^2+\epsilon_k^2}\,,\end{aligned} \tag{A42}$$

from which Eq. (A39) follows immediately. Next, we may deform the contour C (which consists of infinitely many circles surrounding the poles) and obtain

$$\begin{aligned}T\sum_n\frac{1}{\omega_n^2+\epsilon_k^2} &= -\frac{1}{2\pi i}\int_{-i\infty+\eta}^{i\infty+\eta}d\omega\,\frac{1}{\omega^2-\epsilon_k^2}\frac{1}{2}\coth\frac{\omega}{2T}-\frac{1}{2\pi i}\int_{i\infty-\eta}^{-i\infty-\eta}d\omega\,\frac{1}{\omega^2-\epsilon_k^2}\frac{1}{2}\coth\frac{\omega}{2T}\\ &= -\frac{1}{2\pi i}\int_{-i\infty+\eta}^{i\infty+\eta}d\omega\,\frac{1}{\omega^2-\epsilon_k^2}\coth\frac{\omega}{2T}\,,\end{aligned} \tag{A43}$$

where we have changed the integration variable $\omega\to-\omega$ in the second integral. We now use the residue theorem a second time: we can close the contour in the positive half-plane at infinity and pick up the pole at $\omega=\epsilon_k$,

$$T\sum_n\frac{1}{\omega_n^2+\epsilon_k^2} = \frac{1}{2\epsilon_k}\coth\frac{\epsilon_k}{2T}=\frac{1}{2\epsilon_k}[1+2f_B(\epsilon_k)]\,, \tag{A44}$$

(note minus sign from clockwise contour integration). Here,

$$f_B(\epsilon)\equiv\frac{1}{e^{\epsilon/T}-1} \tag{A45}$$

is the Bose distribution function. We have thus found

$$\frac{1}{T}\sum_n\frac{1}{(2n\pi)^2+x^2}=\frac{1}{Tx}\left(\frac{1}{2}+\frac{1}{e^x-1}\right)\,. \tag{A46}$$

Now we insert the result into the original expression (A38) and integrate over x^2 to obtain (with const denoting T-independent constants)

$$\begin{aligned}\sum_n\ln\frac{\omega_n^2+\epsilon_k^2}{T^2} &= \int_1^{(\epsilon_k/T)^2}dx^2\frac{1}{x}\left(\frac{1}{2}+\frac{1}{e^x-1}\right)+\text{const}\\ &= \frac{\epsilon_k}{T}+2\ln\left(1-e^{-\epsilon_k/T}\right)+\text{const}\,,\end{aligned} \tag{A47}$$

which is the result we wanted to prove.

2. Fermionic field

To describe a system of non-interacting fermions with mass m we start with the Lagrangian

$$\mathcal{L}_0=\overline{\psi}\,(i\gamma^\mu\partial_\mu-m)\,\psi\,, \tag{A48}$$

where $\overline{\psi}=\psi^\dagger\gamma^0$. As for the bosons we are interested in adding a chemical potential to this Lagrangian. To this end, we determine the conserved current as above, i.e., we first identify the global symmetry of the Lagrangian which is given by the transformation $\psi\to e^{-i\alpha}\psi$. The conserved current is

$$j^\mu=\frac{\partial\mathcal{L}_0}{\partial(\partial_\mu\psi)}\frac{\delta\psi}{\delta\alpha}=\overline{\psi}\gamma^\mu\psi\,, \tag{A49}$$

which yields the conserved charge (density)

$$j^0=\psi^\dagger\psi\,. \tag{A50}$$

The conjugate momentum is

$$\pi = \frac{\partial \mathcal{L}_0}{\partial(\partial_0 \psi)} = i\psi^\dagger \,. \tag{A51}$$

This means that in the case of fermions we need to treat ψ and $\psi^\dagger$ as independent variables. The partition function for fermions is

$$Z \;=\; \mathrm{Tr}\, e^{-\beta(\hat{H}-\mu\hat{N})} = \int_{\text{antiperiodic}} \mathcal{D}\psi^\dagger \mathcal{D}\psi \, \exp\left[-\int_X (\mathcal{H} - \mu\mathcal{N} - i\pi\partial_\tau \psi)\right] . \tag{A52}$$

This has to be compared to the analogous expression for bosons, Eq. (A5). Recall that the periodicity of the bosonic fields is a consequence of taking the trace in the operator formalism. In other words, the partition function in the path integral formalism can be derived from a transition amplitude with identical initial and final states. In the case of fermions, the fields in the path integral are Grassmann variables, as a consequence of the anticommutation relations of creation and annihilation operators. In this case, the trace involves a transition amplitude where initial and final states differ by a sign. Therefore, in the fermionic partition function the integration is over antiperiodic fields $\psi(0,\mathbf{x}) = -\psi(\beta,\mathbf{x})$ and $\psi^\dagger(0,\mathbf{x}) = -\psi^\dagger(\beta,\mathbf{x})$.

With the Hamiltonian

$$\mathcal{H} = \pi\partial_0\psi - \mathcal{L}_0 = \overline{\psi}(i\boldsymbol{\gamma}\cdot\nabla + m)\psi \,, \tag{A53}$$

(here and in the following we mean by the scalar product $\boldsymbol{\gamma}\cdot\nabla$ the product where the Dirac matrices appear with a lower index γ_i) we thus obtain

$$Z = \int_{\text{antiperiodic}} \mathcal{D}\psi^\dagger \mathcal{D}\psi \, \exp\left[\int_X \overline{\psi}\left(-\gamma^0\partial_\tau - i\boldsymbol{\gamma}\cdot\nabla + \gamma^0\mu - m\right)\psi\right] . \tag{A54}$$

In this case we cannot separate the $\pi \sim \psi^\dagger$ integration from the ψ integration. Remember that, in the bosonic case, this led to a new Lagrangian which contained the chemical potential not just in the term $j^0\mu$. Here, the Lagrangian with chemical potential simply is

$$\mathcal{L} = \bar{\psi}(i\gamma^\mu\partial_\mu + \gamma^0\mu - m)\psi \,. \tag{A55}$$

Note that again the chemical potential enters just like the temporal component of a gauge field that couples to the fermions. Analogously to the bosonic case, we introduce the (dimensionless) Fourier-transformed fields

$$\psi(X) = \frac{1}{\sqrt{V}}\sum_K e^{-iK\cdot X}\psi(K) \,, \qquad \overline{\psi}(X) = \frac{1}{\sqrt{V}}\sum_K e^{iK\cdot X}\overline{\psi}(K) \,, \tag{A56}$$

(note the different dimensionality of fields compared to bosons; here the field $\psi(X)$ in position space has mass dimension 3/2). Again we denote $k_0 = -i\omega_n$ such that $K\cdot X = -(\omega_n\tau + \mathbf{k}\cdot\mathbf{x})$. Now antiperiodicity, $\psi(0,\mathbf{x}) = -\psi(\beta,\mathbf{x})$, implies $e^{i\omega_n\beta} = -1$ and thus the fermionic Matsubara frequencies are

$$\omega_n = (2n+1)\pi T \,, \qquad n \in \mathbb{Z} \,. \tag{A57}$$

With the Fourier decomposition we find

$$\int_X \overline{\psi}\left(-\gamma^0\partial_\tau - i\boldsymbol{\gamma}\cdot\nabla + \gamma^0\mu - m\right)\psi = -\sum_K \psi^\dagger(K)\frac{G_0^{-1}(K)}{T}\psi(K) \,, \tag{A58}$$

where the free inverse fermion propagator in momentum space is

$$G_0^{-1}(K) = -\gamma^\mu K_\mu - \gamma^0\mu + m \,. \tag{A59}$$

Although not needed for the rest of the calculation in this appendix, let us introduce a useful form of the inverse propagator in terms of energy projectors. This form is convenient for more involved calculations such as done in chapters IV and V. Equivalently to Eq. (A59) we can write

$$G_0^{-1}(K) = -\sum_{e=\pm}(k_0 + \mu - eE_k)\gamma^0\Lambda^e_{\mathbf{k}} \,, \tag{A60}$$

where $E_k = \sqrt{k^2+m^2}$, and where the projectors onto positive and negative energy states are given by

$$\Lambda^e_{\mathbf{k}} \equiv \frac{1}{2}\left(1 + e\gamma^0 \frac{\boldsymbol{\gamma}\cdot\mathbf{k}+m}{E_k}\right). \tag{A61}$$

These (Hermitian) projectors are complete and orthogonal,

$$\Lambda^+_{\mathbf{k}} + \Lambda^-_{\mathbf{k}} = 1\,, \qquad \Lambda^e_{\mathbf{k}}\Lambda^{e'}_{\mathbf{k}} = \delta_{e,e'}\Lambda^e_{\mathbf{k}}\,. \tag{A62}$$

The first property is trivial to see, the second follows with $\{\gamma^0,\gamma^i\}=0$ which follows from the general anticommutation property $\{\gamma^\mu,\gamma^\nu\}=2g^{\mu\nu}$, and with $(\boldsymbol{\gamma}\cdot\mathbf{k})^2 = -k^2$.

From the form of the inverse propagator (A60) we can immediately read off the propagator itself,

$$G_0(K) = -\sum_{e=\pm}\frac{\Lambda^e_{\mathbf{k}}\gamma^0}{k_0+\mu-eE_k}\,. \tag{A63}$$

With the properties (A62) one easily checks that $G_0^{-1}G_0 = 1$. One can also rewrite (A63) as

$$G_0(K) = \frac{-\gamma^\mu K_\mu - \gamma^0\mu - m}{(k_0+\mu)^2 - E_k^2}\,. \tag{A64}$$

Let us now come back to the calculation of the partition function. For the functional integration we use

$$\int\prod_k^N d\eta_k^\dagger d\eta_k \exp\left(-\sum_{i,j}^N \eta_i^\dagger D_{ij}\eta_j\right) = \det D\,. \tag{A65}$$

Note the difference of this integration over Grassmann variables $\eta^\dagger$, η to the corresponding formula for bosons (A27). We obtain for the partition function

$$Z \;=\; \det\frac{G_0^{-1}(K)}{T} = \det\frac{1}{T}\begin{pmatrix} -(k_0+\mu)+m & -\boldsymbol{\sigma}\cdot\mathbf{k} \\ \boldsymbol{\sigma}\cdot\mathbf{k} & (k_0+\mu)+m\end{pmatrix}, \tag{A66}$$

where the determinant is taken over Dirac space and momentum space. We can use the general formula

$$\det\begin{pmatrix} A & B\\ C & D\end{pmatrix} = \det(AD - BD^{-1}CD)\,, \tag{A67}$$

for matrices A, B, C, D with D invertible, to get

$$\ln Z = \sum_K \ln\left(\frac{E_k^2-(k_0+\mu)^2}{T^2}\right)^2, \tag{A68}$$

where we have used $(\boldsymbol{\sigma}\cdot\mathbf{k})^2 = k^2$. With $k_0 = -i\omega_n$ we can write this as

$$\begin{aligned}\ln Z \;&=\; \sum_K \ln\left(\frac{E_k^2+(\omega_n+i\mu)^2}{T^2}\right)^2\\ &=\; \sum_K\left(\ln\frac{E_k^2+(\omega_n+i\mu)^2}{T^2} + \ln\frac{E_k^2+(-\omega_n+i\mu)^2}{T^2}\right)\\ &=\; \sum_K\left(\ln\frac{\omega_n^2+(E_k-\mu)^2}{T^2} + \ln\frac{\omega_n^2+(E_k+\mu)^2}{T^2}\right),\end{aligned} \tag{A69}$$

where, in the second term of the second line, we have replaced ω_n by $-\omega_n$ which does not change the result since we sum over all $n\in\mathbb{Z}$. The third line can be easily checked by multiplying out all terms.

Next we need to perform the sum over fermionic Matsubara frequencies. This is similar to the bosonic case and yields

$$\sum_n \ln\frac{\omega_n^2+\epsilon_k^2}{T^2} = \frac{\epsilon_k}{T} + 2\ln\left(1+e^{-\epsilon_k/T}\right) + \text{const}\,. \tag{A70}$$

Using this result to evaluate Eq. (A69) and taking the thermodynamic limit yields the thermodynamic potential $\Omega = -T \ln Z$,

$$\frac{\Omega}{V} = -2 \int \frac{d^3\mathbf{k}}{(2\pi)^3} \left[E_k + T \ln\left(1 + e^{-(E_k-\mu)/T}\right) + T \ln\left(1 + e^{-(E_k+\mu)/T}\right)\right] . \tag{A71}$$

The overall factor 2 accounts for the two spin states of the spin-1/2 fermion. Together with the particle/antiparticle degrees of freedom (from $\mu = \pm 1$) we recover all four degrees of freedom of the Dirac spinor. Again we conclude this section by computing the pressure for large temperatures,

$$P \simeq 4\frac{T^4}{2\pi^2} \int_0^\infty dx\, x^2 \ln\left(1 + e^{-x}\right) = 4 \cdot \frac{7}{8} \frac{\pi^2 T^2}{90} . \tag{A72}$$

Comparing with the bosonic pressure (A37) we see that for large T a single fermionic degree of freedom contributes 7/8 times as much to the thermal pressure as a single bosonic degree of freedom.

a. Summation over fermionic Matsubara frequencies

It remains to prove Eq. (A70) by summing over fermionic Matsubara frequencies. As for the bosonic case, we write

$$\sum_n \ln \frac{\omega_n^2 + \epsilon_k^2}{T^2} = \int_1^{(\epsilon_k/T)^2} dx^2 \sum_n \frac{1}{(2n+1)^2\pi^2 + x^2} + \sum_n \ln[1 + (2n+1)^2\pi^2] . \tag{A73}$$

This time, we need to use the tanh instead of the coth when we write the sum in terms of a contour integral,

$$T \sum_n \frac{1}{\omega_n^2 + \epsilon_k^2} = -\frac{1}{2\pi i} \oint_C d\omega\, \frac{1}{\omega^2 - \epsilon_k^2} \frac{1}{2} \tanh \frac{\omega}{2T} , \tag{A74}$$

(We have denoted $\epsilon_k \equiv xT$.) The poles of $\tanh[\omega/(2T)]$ are given by the zeros of $e^{\omega/(2T)} + e^{-\omega/(2T)}$, i.e., they are located at i times the fermionic Matsubara frequencies, $\omega = i\omega_n$. The contour C encloses these poles and none of the poles of $1/(\omega^2 - \epsilon_k^2)$. Then, with the residue theorem and with

$$\begin{aligned} \left(e^{\omega/(2T)} - e^{-\omega/(2T)}\right)\Big|_{\omega=i\omega_n} &= 2i(-1)^n , \\ \frac{d}{d\omega}\left(e^{\omega/(2T)} + e^{-\omega/(2T)}\right)\Big|_{\omega=i\omega_n} &= \frac{i(-1)^n}{T} , \end{aligned} \tag{A75a}$$

one confirms Eq. (A74). We can now close the contour in the positive half-plane to obtain

$$\begin{aligned} T \sum_n \frac{1}{\omega_n^2 + \epsilon_k^2} &= -\frac{1}{2\pi i} \int_{-i\infty+\eta}^{i\infty+\eta} d\omega\, \frac{1}{\omega^2 - \epsilon_k^2} \tanh \frac{\omega}{2T} \\ &= \frac{1}{2\epsilon_k} \tanh \frac{\epsilon_k}{2T} = \frac{1}{2\epsilon_k}[1 - 2f_F(\epsilon_k)] , \end{aligned} \tag{A76}$$

where

$$f_F(\epsilon) \equiv \frac{1}{e^{\epsilon/T} + 1} \tag{A77}$$

is the Fermi distribution function. Inserting this result into Eq. (A73) yields

$$\begin{aligned} \sum_n \ln \frac{\omega_n^2 + \epsilon_k^2}{T^2} &= \int_1^{(\epsilon_k/T)^2} dx^2 \frac{1}{x} \left(\frac{1}{2} - \frac{1}{e^x + 1}\right) + \text{const} \\ &= \frac{\epsilon_k}{T} + 2 \ln\left(1 + e^{-\epsilon_k/T}\right) + \text{const} , \end{aligned} \tag{A78}$$

which proves Eq. (A70).

Problems

A.1 **Matsubara sum for boson loop**

Show via contour integration that

$$T\sum_{k_0}\frac{1}{(k_0^2-\epsilon_1^2)[(p_0-k_0)^2-\epsilon_2^2]}=-\sum_{e_1,e_2=\pm}\frac{e_1e_2}{4\epsilon_1\epsilon_2}\frac{1+f_B(e_1\epsilon_1)+f_B(e_2\epsilon_2)}{p_0-e_1\epsilon_1-e_2\epsilon_2}\,, \tag{A79}$$

with $k_0=-i\omega_n$, $p_0=-i\omega_m$ bosonic Matsubara frequencies, and $\epsilon_1,\epsilon_2>0$.

A.2 **Matsubara sum for fermion loop**

Prove via contour integration the following result for the summation over fermionic Matsubara frequencies,

$$T\sum_{k_0}\frac{(k_0+\xi_1)(k_0+q_0+\xi_2)}{(k_0^2-\epsilon_1^2)[(k_0+q_0)^2-\epsilon_2^2]}=-\frac{1}{4\epsilon_1\epsilon_2}\sum_{e_1,e_2=\pm}\frac{(\epsilon_1-e_1\xi_1)(\epsilon_2-e_2\xi_2)}{q_0-e_1\epsilon_1+e_2\epsilon_2}\frac{f_F(-e_1\epsilon_1)f_F(e_2\epsilon_2)}{f_B(-e_1\epsilon_1+e_2\epsilon_2)}\,, \tag{A80}$$

where $k_0=-i\omega_n$ with fermionic Matsubara frequencies ω_n, and $q_0=-i\omega_m$ with bosonic Matsubara frequencies ω_m, and where $\xi_1,\xi_2,\epsilon_1,\epsilon_2>0$ are real numbers. The result of this problem is used in the calculation of the neutrino emissivity in chapter V.

Glossary

2SC phase Color superconductor in which strange quarks and quarks of one color remain unpaired. Because of the asymmetry induced by the strange quark mass, viable candidate for the ground state of quark matter at moderate chemical potential. In these lectures we discuss the 2SC phase in the context of neutrino emissivity, to illustrate the effect of both paired and unpaired quarks.

AdS/CFT correspondence Theoretical tool not discussed in these lectures, but an interesting approach to tackle QCD at strong coupling. The idea is that – relatively simple – calculations in the gravity approximation of a certain string theory provide results for the – otherwise hard to access – strong coupling limit of a corresponding ("dual") field theory. The problem is that currently no gravity dual of QCD is known.

anomalous propagator Technically speaking, off-diagonal components of the propagator in Nambu-Gorkov space; nonzero in the case of a superconductor or a superfluid. More physically speaking, anomalous propagators describe a fermion which is, via the Cooper pair condensate, converted into a fermion hole.

asymptotic freedom Important property of QCD which says that the running coupling constant of QCD becomes small for large exchanged momenta. For our context this means that quarks at large densities, where the distance between them is small and hence the exchanged momentum large, are weakly interacting; quarks at infinite density are free. In compact stars, however, the density is large, but by no means asymptotically large.

axial anomaly Non-conservation of the axial current in QCD. In our context of (moderately) dense matter originating mainly from instantons which are certain semi-classical gauge field configurations. Leads to an explicit breaking of the axial $U(1)_A$, which is a subgroup of the chiral group, and thus gives a large mass to the η'.

bag model (MIT bag model) Simple model to take into account confinement. Via the bag constant, an energy penalty is introduced by hand for the deconfined phase. The model amounts to the picture of a hadron as a bag which confines the quarks; the bag exerts an external pressure on the quarks, given by the bag constant. In our astrophysical context, the bag model is a simple way to compare free energies of dense quark matter and dense nuclear matter.

BCS theory Original theory for electronic superconductors, developed in 1957 by Bardeen, Cooper, and Schrieffer. Many concepts and approximations can be adopted for nuclear and quark matter. In color-superconducting quark matter, an important difference to BCS theory is the parametric dependence of the pairing gap on the coupling constant due to long-range interactions via magnetic gluons.

β-decay Process due to the weak interaction of the form $n \to p + e + \bar{\nu}_e$ in nuclear matter and $d \to u + e + \bar{\nu}_e$ in quark matter. Relevant in these lectures for two reasons: firstly, equilibrium with respect to this process (β-equilibrium) yields important constraints for the chemical potentials and secondly, this process contributes to the neutrino emissivity which in turn is responsible for the cooling of a compact star.

Bogoliubov coefficients Momentum-dependent coefficients in the theory of superconductivity and superfluidity which characterize the mixing of fermions and fermion holes due to Cooper pair condensation. In these lectures, the Bogoliubov coefficients arise naturally in the calculation of the neutrino emissivity in color-superconducting quark matter.

Cabibbo-Kobayashi-Maskawa (CKM) matrix Matrix that characterizes the relative strength of the weak interaction for different quark flavors. In these lectures relevant for the calculation of the neutrino emissivity in quark matter.

chiral symmetry For massless quarks, QCD possesses a global symmetry for right- and left-handed quarks separately, called chiral symmetry. This symmetry can be spontaneously broken, giving rise to Goldstone modes. These Goldstone modes (or pseudo-Goldstone modes in the case of nonzero quark masses) are for instance pions and kaons. In these lectures we discuss kaon condensation in nuclear and quark matter (in quark matter, chiral symmetry is spontaneously broken in the CFL phase).

color superconductivity Cooper pair formation and condensation in cold and dense quark matter, analogous to electronic superconductivity in metals. If quark matter is present in compact stars, it can be expected to be a color superconductor.

color-flavor locking (CFL) Ground state of three-flavor quark matter at asymptotically large densities. Particularly symmetric color superconductor where the order parameter is invariant only under simultaneous color and flavor transformations. May persist down to densities where the hadronic phase takes over or may be replaced before this transition by a different color superconductor because of the effects of the strange quark mass.

compact star Very dense astrophysical object with a mass close to the sun's mass and a radius of about ten kilometers. The term shows our ignorance of the exact composition of these objects. They may be neutron stars, hybrid stars, or quark stars. In a more general terminology, compact star also is used to include white dwarfs and black holes, neither of which are the subject of these lectures.

constituent quark mass Quark mass including the quark's interaction energy in a baryon, such that the sum of the three constituent quark masses adds up to the baryon mass. More generally, in dense matter the density-dependent "constituent" quark mass includes any finite-density effects. Can be hundreds of MeV larger than the *current quark mass*.

Cooper pairs Microscopic explanation for superfluidity and superconductivity within BCS theory. Arise from an instability of the Fermi surface in the presence of an arbitrarily small interaction. In compact stars, there are possibly Cooper pairs of neutrons, protons, hyperons and/or quarks.

crust Outer, km thick, layer of a neutron star or hybrid star. Composed of ordinary nuclei which form a crystalline structure and which, upon increasing the density and thus going further inside the star, become more and more neutron rich. In the inner crust a neutron superfluid is immersed in the lattice of nuclei. Quark stars have, if at all, much thinner crusts.

current quark mass Quark mass without effects from the interactions with other quarks and gluons, see also *constituent quark mass*. Since interactions become weak at asymptotically large densities (much larger than densities in compact stars), current and constituent quark masses become identical in this limit.

dense matter In these lectures, dense matter means matter at densities of a few times nuclear ground state density, as expected in the interior of compact stars. Governed by the strong interaction, and thus very difficult to describe theoretically. We discuss several theoretical concepts and sometimes have to escape to lower or even higher densities, just to make life simpler.

equation of state Relation between the pressure and the energy density for a given form of dense matter. In our context, the equation of state determines, together with the TOV equation, the mass-radius relation of a compact star. In particular, a stiff (soft) equation of state allows for a large (small) maximum mass.

Goldstone boson Massless boson arising from spontaneous symmetry breaking of a global symmetry. The only exact (i.e., truly massless) Goldstone boson in dense matter is the one associated to superfluidity, i.e., to the breaking of baryon number conservation. Such a mode exists in a nuclear superfluid as well as in the color-flavor locked phase.

hybrid star Compact star with a quark matter core and a nuclear mantle. Most likely scenario to find quark matter in a compact star.

hyperon Baryon with nonzero strangeness. Hyperons may occur in hadronic matter at sufficiently large densities. In these lectures only discussed briefly, in the context of Walecka-like models.

incompressibility Thermodynamic property of nuclear matter at the saturation density, sometimes also called compression modulus. Can be (at least indirectly and approximately) determined in the experiment and thus yields a value that can, among other quantities, be used to fit the parameters of theoretical models, in these lectures the coupling constants of the Walecka model with scalar interactions.

kaon condensation Possible example of Bose-Einstein condensation in a compact star. May appear at sufficiently large densities. Is possible not only in nuclear matter, but also in quark matter, where kaons exist in the CFL phase. These kaons carry the same quantum numbers as the usual kaons, however are made of two quarks and two quark holes.

Kepler frequency Absolute upper limit for the rotation frequency of compact stars beyond which mass shedding at the equator sets in. Given by the equality of the centrifugal and gravitational forces (more precisely, the general relativistic version thereof). For typical compact stars in the ms^{-1} regime, i.e., for some pulsars actually observed rotation frequencies are not too far from that limit. Below that limit stars can suffer from other rotational instabilities, for instance the *r-mode* instability.

Landau mass Effective mass of (nonrelativistic) fermions at the Fermi surface, in the framework of Landau's Fermi liquid theory. In these lectures, the Landau mass for nucleons is mentioned in the context of the Walecka model where its experimental value serves to fit the parameters of the model.

lattice QCD QCD on the computer. Powerful, brute-force method to perform calculations from first principles. Not discussed in these lectures, mostly because lattice QCD is currently unable to provide results at large chemical potential and small temperature because of the so-called *sign problem*.

Low-mass X-ray binary (LMXB) System of two stars, where a pulsar is accreting matter from its companion which has a mass typically smaller than one solar mass (as opposed to high-mass X-ray binaries where the companion has a mass larger than about ten solar masses). Measured rotation frequencies of pulsars in LMXBs are mentioned in our brief discussion of the r-mode instability of rotating compact stars.

magnetar Compact star with unusually large magnetic field, up to $10^{15}\,\mathrm{G}$ at the surface and possibly larger in the interior.

Matsubara frequency In thermal field theory, the time direction in Minkowski space becomes imaginary and compact, giving rise to Euclidean space with discrete energies, given by the Matsubara frequencies. In these lectures we mostly consider the zero-temperature limit, but in some instances we have to perform a sum over Matsubara frequencies.

mixed phase Coexistence of two (or more) phases which occupy certain volume fractions – for instance bubbles of one phase immersed in the other phase – in a given total volume. In our context, global charge neutrality, as opposed to local charge neutrality, allows for mixed phases for instance of nuclei and nuclear matter or quark and hadronic matter. These phases may be disfavored by large surface energy costs.

Nambu-Gorkov space Contains Nambu-Gorkov spinors which arise from a doubling of the fermionic degrees of freedom in the theoretical description of superconductors and superfluids. Allows to introduce Cooper pairing in the off-diagonal elements of the Nambu-Gorkov propagators. See also *anomalous propagators*.

Nambu-Jona-Lasinio (NJL) model Phenomenological model, not discussed in these lectures, where the QCD interaction between quarks is replaced by a point-like four-quark interaction. Since it has attraction in the same channels as QCD, this model is frequently used to describe color-superconducting quark matter at moderate densities.

neutron star Compact star made of neutron-rich nuclear matter. In some literature the term neutron star is also used to include the possibility of a quark matter core. Mostly, also in these lectures, these stars are called *hybrid stars*.

nuclear pasta Mixed phase of ordinary nuclei (ions) and nuclear matter, typically found in the inner cores of neutron stars. Because different geometries can be realized – spheres, rods, slabs, the latter two reminiscent of spaghetti or lasagna – these phases have been termed nuclear pasta. In these lectures we discuss the possibility of mixed phases of quark and hadronic matter.

pion condensation Bose-Einstein condensation of pions in nuclear matter. Although pions are lighter than kaons in the vacuum, kaon condensation seems to be more likely in dense nuclear matter. Therefore, in these lectures, kaon condensation, not pion condensation, is discussed.

pseudo-Goldstone boson Less impressive brother of the Goldstone boson, arising from spontaneous breaking of a global symmetry which is broken explicitly by a small amount (small compared to the scale of the spontaneous breaking). Light, but not exactly massless. Dense matter is full of pseudo-Goldstone modes, for instance mesons in nuclear matter or color-flavor-locked quark matter, arising from the spontaneous breaking of chiral symmetry which is explicitly broken by quark masses.

pulsar Star whose radiation is observed in periodic pulses. Pulsars are rotating compact stars with large magnetic fields; their apparent pulsation is due to the alignment of the radiation in a beam along the magnetic axis. When the magnetic axis is different from the rotation axis, the beam may point towards the earth periodically, just as the light of a lighthouse flashes periodically when you observe it from the beach.

pulsar glitch Sudden spin-up of a rotating compact star. Not discussed in detail in these lectures but very interesting phenomenon since closely related to the microscopic physics, presumably to crystalline structures and vortices in the star.

QCD phase diagram Collection of equilibrium states of QCD, typically depicted in the plane of quark (or baryon) chemical potential and temperature. We roughly know where compact stars sit in this diagram, but we do not know the phase(s) that occupy this region of the diagram. These lectures are about exploring this unknown territory.

quantum chromodynamics (QCD) Theory of the strong interaction. Governs the physics that determines the ground state of dense matter present in a compact star. In these lectures we perform one explicit calculation in QCD and discuss several effective approaches to this very elegant, but for most practical purposes very difficult, theory.

quarkyonic matter Form of dense matter covering a large portion of the QCD phase diagram for the case of asymptotically large number of colors. Not discussed in these lectures because there are only three colors in the real world. However, it is a viable option that a small region of quarkyonic matter survives and thus becomes also important for compact stars.

quasiparticle Term originally used in condensed matter physics and carried over to dense QCD matter. Absorbs interactions of the original particles into effective new particles. For instance, quasiparticles in a superconductor are gapped due to the attractive interaction between the original particles.

r-modes Non-radial oscillations of a star with the Coriolis force as the restoring force. Interesting for dense matter physics because they grow unstable in a pulsar unless the matter inside the star is sufficiently viscous.

rotated electromagnetism Effect in some color superconductors which is responsible for them being no electromagnetic superconductors. Therefore important for the physics of compact stars since magnetic fields penetrate these color superconductors. Technically speaking, rotated electromagnetism refers to a gauge boson which is a mixture of a gluon and the photon.

saturation density Density at which the binding energy is minimized, here always used in the context of nuclear matter for which the saturation density is approximately 0.15 baryons per fm^3 and the corresponding binding energy per nucleon is about 16 MeV.

sign problem Problem of QCD lattice calculations at finite values of the baryon chemical potential. For finite chemical potential, the action, more precisely the quark determinant in the functional integral of the partition function, loses its positivity and even becomes complex. This makes the probabilistic sampling method ("Monte Carlo method"), on which lattice QCD is based, unfeasible. In our context this means that currently there is no input from lattice calculations to the properties of dense matter.

strange quark matter hypothesis Hypothesis that strange quark matter, not nuclear matter, is the ground state at zero pressure. The hypothesis does not contradict our existence since, even if the hypothesis is true, the transition from nuclear matter, made of u and d quarks, to strange quark matter is essentially forbidden. We discuss that, within the bag model, the strange quark matter hypothesis is true if the bag constant is between a lower bound (since we know that ordinary nuclear matter is stable with respect to two-flavor quark matter) and an upper limit (beyond which nuclear matter is absolutely stable).

strange star (quark star) Compact star made entirely out of quark matter, thus the most radical scenario for quark matter in compact stars.

strangelet Small nugget of strange quark matter. Stretching the original meaning a bit – well, from femtometers to kilometers – a strange star is a huge strangelet. Relevant for us in the context of the *strange quark matter hypothesis*: since strangelets would convert neutron stars into strange stars, the unambiguous observation of a single neutron star would invalidate the strange quark matter hypothesis, provided that there are enough strangelets in the cosmos to hit neutron stars.

supernova Compact stars are expected to be born in (type II) supernova explosions, where a giant star, after burning its nuclear fuel, undergoes a gravitational collapse. The energy of the explosion is mostly released in the form of neutrinos. The theoretical description of supernovae requires very complicated hydrodynamical simulations.

Tolman-Oppenheimer-Volkov (TOV) equation Differential equation from general relativity for the mass, pressure, and energy density as functions of the distance from the center of the star. In connection with the equation of state, which relates energy density and pressure, used to compute the mass-radius relation for a compact star.

unpaired quark matter Term used for (dense) quark matter which does not form Cooper pairs and thus is no color superconductor. Since dense quark matter is expected to be some kind of color superconductor, completely unpaired dense quark matter is unlikely to exist. Therefore mostly used for reference calculations or when, for the computed quantity, it is a good approximation to paired quark matter.

Urca process Most efficient process for neutrino emission, and thus for the cooling of the star. In quark matter the direct Urca process is given by $u + e \to d + \nu_e$ and variants thereof. We compute the emission rate of this process in detail in these lectures. In the modified Urca process, a spectator particle is added which increases the available phase space.

viscosity (bulk/shear) Transport coefficients of nuclear or quark matter relevant in particular in the context of rotation and oscillation of the star. Requires microscopic calculation of processes typically governed by the weak interaction. Not discussed in detail in these lectures. See also *r-modes*.

Walecka model Phenomenological model for interacting nuclear matter, based on Yukawa couplings of the nucleons with the σ and ω meson. Used for extrapolation to large densities after fitting the parameters of the model at *saturation density*. Discussed in these lectures as a basic example for numerous more complicated nuclear models of similar kind.

white dwarf Dense star with a mass of about the sun's mass and radius of a few thousand kilometers, which makes it less dense than a neutron star. Composed of nuclei immersed in a degenerate electron gas.

---

[1] F. Weber, Pulsars as astrophysical laboratories for nuclear and particle physics, CRC Press, 1999.

[2] N.K. Glendenning, Compact Stars: Nuclear Physics, Particle Physics, and General Relativity, Springer, 2000.
[3] P. Haensel, A.Y. Potekhin, D.G. Yakovlev, Neutron Stars, Springer, 2007.
[4] D. Page and S. Reddy, Dense Matter in Compact Stars: Theoretical Developments and Observational Constraints, Ann. Rev. Nucl. Part. Sci. **56**, 327 (2006) [arXiv:astro-ph/0608360].
[5] J. Madsen, Physics and astrophysics of strange quark matter, Lect. Notes Phys. **516**, 162 (1999) [arXiv:astro-ph/9809032].
[6] F. Weber, Strange quark matter and compact stars, Prog. Part. Nucl. Phys. **54**, 193 (2005) [arXiv:astro-ph/0407155].
[7] J. M. Lattimer and M. Prakash, Neutron Star Observations: Prognosis for Equation of State Constraints, Phys. Rept. **442**, 109 (2007) [arXiv:astro-ph/0612440].
[8] M. G. Alford, A. Schmitt, K. Rajagopal and T. Schäfer, Color superconductivity in dense quark matter, Rev. Mod. Phys. **80**, 1455 (2008) [arXiv:0709.4635 [hep-ph]].
[9] J.I. Kapusta, C. Gale, Finite-temperature field theory: Principles and Applications, Cambridge Univ. Press, New York, 2006.
[10] M. Le Bellac, Thermal Field Theory, Cambridge Univ. Press, Cambridge, 2000.
[11] S.L. Shapiro and S.A. Teukolsky, Black Holes, White Dwarfs and Neutron Stars: The Physics of Compact Objects, Wiley-Interscience, New York, 1983.
[12] R. Balian and J. P. Blaizot, Stars and statistical physics: a teaching experience, arXiv:cond-mat/9909291.
[13] R. R. Silbar and S. Reddy, Neutron Stars for Undergraduates, Am. J. Phys. **72**, 892 (2004) [Erratum-ibid. **73**, 286 (2005)] [arXiv:nucl-th/0309041].
[14] I. Sagert, M. Hempel, C. Greiner and J. Schaffner-Bielich, Compact Stars for Undergraduates, Eur. J. Phys. **27**, 577 (2006) [arXiv:astro-ph/0506417].
[15] A. Chodos, R. L. Jaffe, K. Johnson, C. B. Thorn and V. F. Weisskopf, A New Extended Model Of Hadrons, Phys. Rev. D **9**, 3471 (1974).
[16] A. Chodos, R. L. Jaffe, K. Johnson and C. B. Thorn, Baryon Structure In The Bag Theory, Phys. Rev. D **10**, 2599 (1974).
[17] A. R. Bodmer, Collapsed nuclei, Phys. Rev. D **4**, 1601 (1971).
[18] E. Witten, Cosmic Separation Of Phases, Phys. Rev. D **30**, 272 (1984).
[19] E. Farhi and R. L. Jaffe, Strange Matter, Phys. Rev. D **30**, 2379 (1984).
[20] A. Bauswein *et al.*, Mass Ejection by Strange Star Mergers and Observational Implications, Phys. Rev. Lett. **103**, 011101 (2009) [arXiv:0812.4248 [astro-ph]].
[21] A. Kurkela, P. Romatschke and A. Vuorinen, Cold Quark Matter, arXiv:0912.1856 [hep-ph].
[22] M. Alford, M. Braby, M. W. Paris and S. Reddy, Hybrid stars that masquerade as neutron stars, Astrophys. J. **629**, 969 (2005) [arXiv:nucl-th/0411016].
[23] M. Alford, D. Blaschke, A. Drago, T. Klahn, G. Pagliara and J. Schaffner-Bielich, Quark matter in compact stars?, Nature **445**, E7 (2007) [arXiv:astro-ph/0606524].
[24] A. B. Migdal, π condensation in nuclear matter, Phys. Rev. Lett. **31**, 257 (1973).
[25] D. B. Kaplan and A. E. Nelson, Strange Goings on in Dense Nucleonic Matter, Phys. Lett. B **175**, 57 (1986).
[26] A. Ramos, J. Schaffner-Bielich and J. Wambach, Kaon condensation in neutron stars, Lect. Notes Phys. **578**, 175 (2001) [arXiv:nucl-th/0011003].
[27] V. Thorsson, M. Prakash and J. M. Lattimer, Composition, structure and evolution of neutron stars with kaon condensates, Nucl. Phys. A **572**, 693 (1994) [Erratum-ibid. A **574**, 851 (1994)] [arXiv:nucl-th/9305006].
[28] M. Prakash, T. L. Ainsworth and J. M. Lattimer, Equation of state and the maximum mass of neutron stars, Phys. Rev. Lett. **61**, 2518 (1988).
[29] N. Chamel and P. Haensel, Physics of Neutron Star Crusts, Living Rev. Rel. **11**, 10 (2008) [arXiv:0812.3955 [astro-ph]].
[30] D. G. Ravenhall, C. J. Pethick and J. R. Wilson, Structure Of Matter Below Nuclear Saturation Density, Phys. Rev. Lett. **50**, 2066 (1983).
[31] M. G. Alford, K. Rajagopal, S. Reddy and F. Wilczek, The minimal CFL-nuclear interface, Phys. Rev. D **64**, 074017 (2001) [arXiv:hep-ph/0105009].
[32] K.P. Levenfish, D.G. Yakovlev, Specific heat of neutron star cores with superfluid nucleons, Astron. Rep. **38**, 247 (1994).
[33] K.P. Levenfish, D.G. Yakovlev, Suppression of neutrino energy losses in reactions of direct urca processes by superfluidity in neutron star nuclei, Astron. Lett. **20**, 43 (1994).
[34] A. Schmitt, The ground state in a spin-one color superconductor, Phys. Rev. D **71**, 054016 (2005) [arXiv:nucl-th/0412033].
[35] U. Lombardo and H. J. Schulze, Superfluidity in Neutron Star Matter, Lect. Notes Phys. **578**, 30 (2001) [arXiv:astro-ph/0012209].
[36] M. G. Alford, K. Rajagopal and F. Wilczek, Color-flavor locking and chiral symmetry breaking in high density QCD, Nucl. Phys. B **537**, 443 (1999) [arXiv:hep-ph/9804403].
[37] D. T. Son and M. A. Stephanov, Inverse meson mass ordering in color-flavor-locking phase of high density QCD, Phys. Rev. D **61**, 074012 (2000) [arXiv:hep-ph/9910491].
[38] P. F. Bedaque and T. Schäfer, High Density Quark Matter under Stress, Nucl. Phys. A **697**, 802 (2002) [arXiv:hep-ph/0105150].
[39] M. G. Alford, M. Braby and A. Schmitt, Critical temperature for kaon condensation in color-flavor locked quark matter, J. Phys. G **35**, 025002 (2008) [arXiv:0707.2389 [nucl-th]].
[40] A. Fetter, J.D. Walecka, Quantum Theory of Many-Particle Systems, McGraw Hill, New York, 1971.
[41] R. D. Pisarski and D. H. Rischke, Color superconductivity in weak coupling, Phys. Rev. D **61**, 074017 (2000) [arXiv:nucl-th/9910056].
[42] I. A. Shovkovy and L. C. R. Wijewardhana, On gap equations and color flavor locking in cold dense QCD with three

massless flavors, Phys. Lett. B **470**, 189 (1999) [arXiv:hep-ph/9910225].
[43] D. T. Son, Superconductivity by long-range color magnetic interaction in high-density quark matter, Phys. Rev. D **59**, 094019 (1999) [arXiv:hep-ph/9812287].
[44] M.W. Zwierlein, A. Schirotzek, C.H. Schunck, W. Ketterle, Fermionic Superfluidity with Imbalanced Spin Populations and the Quantum Phase Transition to the Normal State, Science 311 (5760), 492-496 (2006) [arXiv:cond-mat/0511197].
[45] D. G. Yakovlev, A. D. Kaminker, O. Y. Gnedin and P. Haensel, Neutrino emission from neutron stars, Phys. Rept. **354**, 1 (2001) [arXiv:astro-ph/0012122].
[46] D. Page, U. Geppert and F. Weber, The Cooling of Compact Stars, Nucl. Phys. A **777**, 497 (2006) [arXiv:astro-ph/0508056].
[47] P. Jaikumar, M. Prakash and T. Schäfer, Neutrino emission from Goldstone modes in dense quark matter, Phys. Rev. D **66**, 063003 (2002) [arXiv:astro-ph/0203088].
[48] A. Schmitt, I. A. Shovkovy and Q. Wang, Neutrino emission and cooling rates of spin-one color superconductors, Phys. Rev. D **73**, 034012 (2006) [arXiv:hep-ph/0510347].
[49] P. Jaikumar, C. D. Roberts and A. Sedrakian, Direct Urca neutrino rate in colour superconducting quark matter, Phys. Rev. C **73**, 042801 (2006) [arXiv:nucl-th/0509093].
[50] N. Iwamoto, Quark Beta Decay And The Cooling Of Neutron Stars, Phys. Rev. Lett. **44**, 1637 (1980).
[51] L. Lindblom, Neutron star pulsations and instabilities, arXiv:astro-ph/0101136.
[52] P. Jaikumar, G. Rupak and A. W. Steiner, Viscous damping of r-mode oscillations in compact stars with quark matter, Phys. Rev. D **78**, 123007 (2008) [arXiv:0806.1005 [nucl-th]].
[53] J. Madsen, Bulk Viscosity Of Strange Dark Matter, Damping Of Quark Star Vibration, And The Maximum Rotation Rate Of Pulsars, Phys. Rev. D **46**, 3290 (1992).
[54] M. G. Alford and A. Schmitt, Bulk viscosity in 2SC quark matter, J. Phys. G **34**, 67 (2007) [arXiv:nucl-th/0608019].
[55] B. Link, Constraining Hadronic Superfluidity with Neutron Star Precession, Phys. Rev. Lett. **91**, 101101 (2003) [arXiv:astro-ph/0302441].
[56] D. N. Aguilera, Spin-one color superconductivity in compact stars? An analysis within NJL-type models, Astrophys. Space Sci. **308**, 443 (2007) [arXiv:hep-ph/0608041].
[57] A. K. Harding and D. Lai, Physics of Strongly Magnetized Neutron Stars, Rept. Prog. Phys. **69**, 2631 (2006) [arXiv:astro-ph/0606674].
[58] C. Alcock, E. Farhi and A. Olinto, Strange stars, Astrophys. J. **310**, 261 (1986).
[59] M. G. Alford, K. Rajagopal, S. Reddy and A. W. Steiner, The stability of strange star crusts and strangelets, Phys. Rev. D **73**, 114016 (2006) [arXiv:hep-ph/0604134].
[60] A. L. Watts and S. Reddy, Magnetar oscillations pose challenges for strange stars, Mon. Not. Roy. Astron. Soc. **379**, L63 (2007) [arXiv:astro-ph/0609364].
[61] P. W. Anderson and N. Itoh, Pulsar glitches and restlessness as a hard superfluidity phenomenon, Nature **256**, 25 (1975).
[62] M. Mannarelli, K. Rajagopal and R. Sharma, The rigidity of crystalline color superconducting quark matter, Phys. Rev. D **76**, 074026 (2007) [arXiv:hep-ph/0702021].
[63] M. A. Stephanov, QCD phase diagram: An overview, PoS **LAT2006**, 024 (2006) [arXiv:hep-lat/0701002].
[64] C. Schmidt, QCD thermodynamics at zero and non-zero density, PoS C **POD2006**, 002 (2006) [arXiv:hep-lat/0701019].
[65] M. Buballa, NJL model analysis of quark matter at large density, Phys. Rept. **407**, 205 (2005) [arXiv:hep-ph/0402234].
[66] D. Blaschke, S. Fredriksson, H. Grigorian, A. M. Oztas and F. Sandin, The phase diagram of three-flavor quark matter under compact star constraints, Phys. Rev. D **72**, 065020 (2005) [arXiv:hep-ph/0503194].
[67] L. McLerran and R. D. Pisarski, Phases of Cold, Dense Quarks at Large N_c, Nucl. Phys. A **796**, 83 (2007) [arXiv:0706.2191 [hep-ph]].
[68] K. Peeters and M. Zamaklar, The string/gauge theory correspondence in QCD, Eur. Phys. J. ST **152**, 113 (2007) [arXiv:0708.1502 [hep-ph]].
[69] S. S. Gubser and A. Karch, From gauge-string duality to strong interactions: a Pedestrian's Guide, arXiv:0901.0935 [hep-th].

Color superconductivity in dense quark matter

Mark G. Alford,[1,*] Krishna Rajagopal,[2,†] Thomas Schäfer,[3,‡] and Andreas Schmitt[1,§]

[1] *Department of Physics, Washington University, St Louis, MO 63130, USA*
[2] *Center for Theoretical Physics, Massachusetts Institute of Technology, Cambridge, MA 02139, USA*
[3] *Department of Physics, North Carolina State University, Raleigh, NC 27695, USA*

(Dated: 21 Jan 2008)

Matter at high density and low temperature is expected to be a color superconductor, which is a degenerate Fermi gas of quarks with a condensate of Cooper pairs near the Fermi surface that induces color Meissner effects. At the highest densities, where the QCD coupling is weak, rigorous calculations are possible, and the ground state is a particularly symmetric state, the color-flavor locked (CFL) phase. The CFL phase is a superfluid, an electromagnetic insulator, and breaks chiral symmetry. The effective theory of the low-energy excitations in the CFL phase is known and can be used, even at more moderate densities, to describe its physical properties. At lower densities the CFL phase may be disfavored by stresses that seek to separate the Fermi surfaces of the different flavors, and comparison with the competing alternative phases, which may break translation and/or rotation invariance, is done using phenomenological models. We review the calculations that underlie these results, and then discuss transport properties of several color-superconducting phases and their consequences for signatures of color superconductivity in neutron stars.

Contents

*Electronic address: alford@wuphys.wustl.edu
†Electronic address: krishna@lns.mit.edu
‡Electronic address: tmschaef@unity.ncsu.edu
§Electronic address: aschmitt@wuphys.wustl.edu

I. INTRODUCTION

A. General outline

The study of matter at ultra-high density is the "condensed matter physics of quantum chromodynamics". It builds on our understanding of the strong interaction, derived from experimental observation of few-body processes, to predict the behavior of macroscopic quantities in many-body systems where the fundamental particles of the

standard model—quarks and leptons—become the relevant degrees of freedom. As in conventional condensed-matter physics, we seek to map the phase diagram and calculate the properties of the phases. However, we are in the unusual position of having a sector of the phase diagram where we can calculate many properties of quark matter rigorously from first principles. This sector is the region of "asymptotically high" densities, where quantum chromodynamics is weakly coupled. We will review those rigorous results and describe the progress that has been made in building on this solid foundation to extend our understanding to lower and more phenomenologically relevant densities. Quark matter occurs in various forms, depending on the temperature T and quark chemical potential μ (see Fig. 1). At high temperatures ($T \gg \mu$) entropy precludes any pattern of order and there is only quark-gluon plasma (QGP), the phase of strongly interacting matter that has no spontaneous symmetry breaking, and which filled the universe for the first microseconds after the big bang. Quark-gluon plasma is also being created in small, very short-lived, droplets in ultrarelativistic heavy ion collisions at the Relativistic Heavy Ion Collider.

In this review we concentrate on the regime of relatively low temperatures, $T \ll \mu$, where we find a rich variety of spontaneous symmetry breaking phases. To create such material in nature requires a piston that can compress matter to super-nuclear densities and hold it while it cools. The only known context where this might happen is in the interior of neutron stars, where gravity squeezes the star to an ultra-high density state where it remains for millions of years. This gives time for weak interactions to equilibrate, and for the temperature of the star to drop far below the quark chemical potential. We do not currently know whether quark matter exists in the cores of neutron stars. One of the reasons for studying color superconductivity is to improve our understanding of how a quark matter core would affect the observable behavior of a neutron star, and thereby resolve this uncertainty.

When we speak of matter at the highest densities, we shall always take the high density limit with up, down and strange quarks only. We do so because neutron star cores are not dense enough (by more than an order of magnitude) to contain any charm or heavier quarks, and our ultimate goal is to gain insight into quark matter at densities that may be found in nature. For the same reason we focus on temperatures below about ten MeV, which are appropriate for neutron stars that are more than a few seconds old.

As we will explain in some detail, at low temperatures and the highest densities we expect to find a degenerate liquid of quarks, with Cooper pairing near the Fermi surface that spontaneously breaks the color gauge symmetry ("color superconductivity"). Speculations about the existence of a quark matter phase at high density go back to the earliest days of the quark model of hadrons [1–5], and the possibility of quark Cooper pairing was noted even before there was a comprehensive theory of the strong interaction [6, 7]. After the development of quantum chromodynamics (QCD), with its property of asymptotic freedom [8, 9], it became clear that a quark matter phase would exist at sufficiently high density [10–16] and the study of quark Cooper pairing was pioneered by Barrois and Frautschi [17–19], who first used the term "color superconductivity", and by Bailin and Love [20, 21], who classified many of the possible pairing patterns. Iwasaki and Iwado [22, 23] performed mean-field calculations of single-flavor pairing in a Nambu-Jona-Lasinio (NJL) model, but it was not until the prediction of large pairing gaps [24, 25] and the color-flavor locked (CFL) phase [26] that the phenomenology of color-superconducting quark matter became widely studied. At present there are many reviews of the subject from various stages in its development [21, 27–39], and the reader may wish to consult them for alternative presentations with different emphases. As these reviews make clear, the last decade has seen dramatic progress in our understanding of dense matter. We are now able to obtain, directly from QCD, rigorous and quantitative answers to the basic question: "What happens to matter if you squeeze it to arbitrarily high density?". In Sec. IV we will show how QCD becomes analytically tractable at arbitrarily high density: the coupling is weak and the physics of confinement never arises, since long-wavelength magnetic interactions are cut off, both by Landau damping and by the Meissner effect. As a result, matter at the highest densities is known to be in the CFL phase, whose properties (see Sec. II) are understood rigorously from first principles. There is a well-developed effective field theory describing the low energy excitations of CFL matter (see Sec. V), so that at any density at which the CFL phase occurs, even if this density is not high enough for a weak-coupling QCD calculation to be valid, many phenomena can nevertheless be described quantitatively in terms of a few parameters, via the effective field theory.

It should be emphasized that QCD at arbitrarily high density is more fully understood than in any other context. High energy scattering, for example, can be treated by perturbative QCD, but making contact with observables brings in poorly understood nonperturbative physics via structure functions and/or fragmentation functions. Or, in quark-gluon plasma in the high temperature limit much of the physics is weakly-coupled but the lowest energy modes remain strongly coupled with nonperturbative physics arising in the nonabelian color-magnetic sector. We shall see that there are no analogous difficulties in the analysis of CFL matter at asymptotic densities.

If the CFL phase persists all the way down to the transition to nuclear matter then we have an exceptionally good theoretical understanding of the properties of quark matter in nature. However, less symmetrically paired phases of quark matter may well intervene in the intermediate density region between nuclear and CFL matter (Sec. I E). We enumerate some of the possibilities in Sec. III. In principle this region could also be understood from first principles, using brute-force numerical methods (lattice QCD) to evaluate the QCD path integral, but unfortunately current

lattice QCD algorithms are defeated by the fermion sign problem in the high-density low-temperature regime [40].[1] This means we have to use models, or try to derive information from astrophysical observations. In Sec. VI we sketch an example of a (Nambu–Jona-Lasinio) model analysis within which one can compare some of the possible intermediate-density phases suggested in Sec. I E. We finally discuss the observational approach, which involves elucidating the properties of the suggested phases of quark matter (Secs. VI C and VII), and then finding astrophysical signatures by which their presence inside neutron stars might be established or ruled out using astronomical observations (Sec. VIII).

B. Inevitability of color superconductivity

At sufficiently high density and low temperature it is a good starting point to imagine that quarks form a degenerate Fermi liquid. Because QCD is asymptotically free — the interaction becomes weaker as the momentum transferred grows — the quarks near the Fermi surface are almost free, with weak QCD interactions between them. (Small-angle quark-quark scattering via a low-momentum gluon is no problem because it is cut off by Landau damping, which, together with Debye screening, keeps perturbation theory at high density much better controlled than at high temperature [54, 55].) The quark-quark interaction is certainly attractive in some channels, since we know that quarks bind together to form baryons. As we will now argue, these conditions are sufficient to guarantee color superconductivity at sufficiently high density.

At zero temperature, the thermodynamic potential (which we will loosely refer to as the "free energy") is $\Omega = E - \mu N$, where E is the total energy of the system, μ is the chemical potential, and N is the number of fermions. If there were no interactions then the energy required to add a particle to the system would be the Fermi energy $E_F = \mu$, so adding or subtracting particles or holes near the Fermi surface would cost zero free energy. With a weak attractive interaction in any channel, if we add a pair of particles (or holes) with the quantum numbers of the attractive channel, the free energy is lowered by the potential energy of their attraction. Many such pairs will therefore be created in the modes near the Fermi surface, and these pairs, being bosonic, will form a condensate. The ground state will be a superposition of states with different numbers of pairs, breaking the fermion number symmetry. This argument, originally developed by Bardeen, Cooper, and Schrieffer (BCS) [56] is completely general, and can be applied to electrons in a metal, nucleons in nuclear matter, ^{3}He atoms, cold fermionic atoms in a trap, or quarks in quark matter.

The application of the BCS mechanism to pairing in dense quark matter is in a sense more direct than in its original setting. The dominant interaction between electrons in a metal is the repulsive Coulomb interaction, and it is only because this interaction is screened that the attraction mediated by phonons comes into play. This means that the effective interactions that govern superconductivity in a metal depend on band structure and other complications and are very difficult to determine accurately from first principles. In contrast, in QCD the "color Coulomb" interaction is attractive between quarks whose color wave function is antisymmetric, meaning that superconductivity arises as a direct consequence of the primary interaction in the theory. This has two important consequences. First, at asymptotic densities where the QCD interaction is weak we can derive the gap parameter and other properties of color superconducting quark matter rigorously from the underlying microscopic theory. Second, at accessible densities where the QCD interaction is stronger the ratio of the gap parameter to the Fermi energy will be much larger than in conventional BCS superconducting metals. Thus, superconductivity in QCD is more robust, both in the theoretical sense and in the phenomenological sense, than superconductivity in metals.

It has long been known that, in the absence of pairing, an unscreened static magnetic interaction results in a "non-Fermi-liquid" [57–70]. However, in QCD the magnetic interaction is screened at nonzero frequency (Landau damping) and this produces a particularly mild form of non-Fermi-liquid behavior, as we describe in Sec. V A 2. In the absence of pairing but in the presence of interactions, there are still quark quasiparticles and there is still a "Fermi surface", and the BCS argument goes through. This argument is rigorous at high densities, where the QCD coupling g is small. The energy scale below which non-Fermi liquid effects would become strong enough to modify the quasiparticle picture qualitatively is parametrically of order $\exp(-\text{const}/g^2)$ whereas the BCS gap that results from pairing is parametrically larger, of order $\exp(-\text{const}/g)$ as we shall see in Sec. IV. This means that pairing occurs in a regime where the basic logic of the BCS argument remains valid.

Since pairs of quarks cannot be color singlets, the Cooper pair condensate in quark matter will break the local color symmetry $SU(3)_c$, hence the term "color superconductivity". The quark pairs play the same role here as the Higgs particle does in the standard model: the color-superconducting phases can be thought of as Higgs phases of QCD.

[1] Condensation of Cooper pairs of quarks has been studied on the lattice in 2-color QCD [41–49], for high isospin density rather than baryon density [50–52] and in NJL-type models [53].

Here, the gauge bosons that acquire a mass through the process of spontaneous symmetry breaking are the gluons, giving rise to color Meissner effects. It is important to note that quarks, unlike electrons, have color and flavor as well as spin degrees of freedom, so many different patterns of pairing are possible. This leads us to expect a panoply of different possible color superconducting phases.

As we shall discuss in Sec. II, at the highest densities we can achieve an *ab initio* understanding of the properties of dense matter, and we find that its preferred state is the CFL phase of three-flavor quark matter, which is unique in that *all* the quarks pair (all flavors, all colors, all spins, all momenta on the Fermi surfaces) and all the nonabelian gauge bosons are massive. The suppression of all of the infrared degrees of freedom of the types that typically indicate either instability toward further condensation or strongly coupled phenomena ensures that, at sufficiently high density, the CFL ground state, whose only infrared degrees of freedom are Goldstone bosons and an abelian photon, is stable. In this regime, quantitative calculations of observable properties of CFL matter can be done from first principles; there are no remaining nonperturbative gaps in our understanding.

As the density decreases, the effect of the strange quark mass becomes more noticeable, imposing stresses that may modify the Cooper pairing and the CFL phase may be replaced by other forms of color superconducting quark matter. Furthermore, as the attractive interaction between quarks becomes stronger at lower densities, correlations beyond the two-body correlation that yields Cooper pairing may become important, and at some point the ground state will no longer be a Cooper-paired state of quark matter, but something quite different. Indeed, by the time we decrease the density down to that of nuclear matter, the average separation between quarks has increased to the point that the interactions are strong enough to bind quarks into nucleons. It is worth noting that quark matter is in this regard different from Cooper-paired ultracold fermionic atoms (to be discussed in Sec. III I). For fermionic atoms, as the interaction strength increases there is a crossover from BCS-paired fermions to a Bose-Einstein condensate (BEC) of tightly-bound, well-separated, weakly-interacting di-atoms (molecules). In QCD, however, the color charge of a diquark is the same as that of an antiquark, so diquarks will interact with each other as strongly as quarks, and there will not be a literal analogue of the BCS/BEC crossover seen in fermionic atoms. In QCD, the neutral bound states at low density that are (by QCD standards) weakly interacting are nucleons, containing three quarks not two.

We shall work with $N_c = 3$ colors throughout. In the limit $N_c \to \infty$ with fixed $\Lambda_{\rm QCD}$ (i.e fixed $g^2 N_c$), Cooper pairing is not necessarily energetically preferred. A strong competitor for the large-N_c ground state is the chiral density wave (CDW), a condensate of quark-hole pairs, each with total momentum $2p_F$ [71]. Quark-hole scattering is enhanced by a factor of N_c over quark-quark scattering, but, unlike Cooper pairing, it only uses a small fraction of the Fermi surface, and in the case of short range forces the CDW phase is energetically favored in one-dimensional systems, but not in two or more spatial dimensions [72]. However, in QCD in the large N_c limit the equations governing the CDW state become effectively one-dimensional because the gluon propagator is not modified by the medium, so the quark-hole interaction is dominated by almost collinear scattering. Since pairing gaps are exponentially small in the coupling but medium effects only vanish as a power of N_c, the CDW state requires an exponentially large number of colors. It is estimated that for $\mu \sim 1$ GeV, quark-hole pairing becomes favored over Cooper pairing when $N_c \gtrsim 1000$ [73]. Recent work [74] discusses aspects of physics at large N_c at lower densities that may also be quite different from physics at $N_c = 3$.

Before turning to a description of CFL pairing in Sec. II and less-symmetrically paired forms of color superconducting quark matter in Sec. III, we discuss some generic topics that arise in the analysis of color-superconducting phases: the gap equations, neutrality constraints, the resultant stresses on Cooper pairing, and the expected overall form of the phase diagram.

C. Quark Cooper pairing

The quark pair condensate can be characterized in a gauge-variant way by the expectation value of the one-particle-irreducible quark-quark two-point function, also known as the "anomalous self-energy",

$$\langle \psi^{\alpha}_{ia} \psi^{\beta}_{jb} \rangle = P^{\alpha\beta}_{ij\,ab} \Delta \tag{1}$$

Here ψ is the quark field operator, color indices α, β range over red, green, and blue (r, g, b), flavor indices i, j range over up, down and strange (u, d, s), and a, b are the spinor Dirac indices. The angle brackets denote the one-particle-irreducible part of the quantum-mechanical ground-state expectation value. In general, both sides of this equation are functions of momentum. The color-flavor-spin matrix P characterizes a particular pairing channel, and Δ is the gap parameter which gives the strength of the pairing in this channel. A standard BCS condensate is position-independent (so that in momentum space the pairing is between quarks with equal and opposite momentum) and a spin singlet (so that the gap is isotropic in momentum space). However, as we will see later, there is good reason to expect non-BCS condensates as well as BCS condensates in high-density quark matter.

Although (1) defines a gauge-variant quantity, it is still of physical relevance. Just as electroweak symmetry breaking is most straightforwardly understood in the unitary gauge where the Higgs vacuum expectation value is uniform in space, so color superconductivity is typically analyzed in the unitary gauge where the quark pair operator has a uniform color orientation in space. We then relate the gap parameter Δ to the spectrum of the quark-like excitations above the ground state ("quasiquarks"), which is gauge-invariant.

In principle, a full analysis of the phase structure of quark matter in the μ-T plane would be performed by writing down the free energy Ω, which is a function of the temperature, the chemical potentials for all conserved quantities, and the gap parameters for all possible condensates, including the quark pair condensates but also others such as chiral condensates of the form $\langle\bar{q}q\rangle$. We impose neutrality with respect to gauge charges (see Sect. I D below) and then within the neutral subspace we minimize the free energy with respect to the strength of the condensate:

$$\frac{\partial\Omega}{\partial\Delta} = 0, \qquad \frac{\partial^2\Omega}{\partial\Delta^2} > 0 \ . \tag{2}$$

We have written this gap equation and stability condition somewhat schematically since for many patterns of pairing there will be gap parameters with different magnitudes in different channels. The free energy must then be minimized with respect to each of the gap parameters, yielding a coupled set of gap equations. The solution to (2) with the lowest free energy that respects the neutrality constraints discussed below yields the favored phase.

D. Chemical potentials and neutrality constraints

Why do we describe "matter at high density" by introducing a large chemical potential μ for quark number but no chemical potentials for other quantities? The answer is that this reflects the physics of neutron stars, which are the main physical arena that we consider. Firstly, on the long timescales relevant to neutron stars, the only global charges that are conserved in the standard model are quark number and lepton number, so only these can be coupled to chemical potentials (we shall discuss gauged charges below). Secondly, a neutron star is permeable to lepton number because neutrinos are so light and weakly-interacting that they can quickly escape from the star, so the chemical potential for lepton number is zero. Electrons are present because they carry electric charge, for which there is a nonzero potential. In the first few seconds of the life of a neutron star the neutrino mean free path may be short enough to sustain a nonzero lepton number chemical potential, see for instance [75–78], but we will not discuss that scenario.

Stable bulk matter must be neutral under all gauged charges, whether they are spontaneously broken or not. Otherwise, the net charge density would create large electric fields, making the energy non-extensive. In the case of the electromagnetic gauge symmetry, this simply requires zero charge density, $Q = 0$. The correct formal requirement concerning the color charge of a large lump of matter is that it should be a color *singlet*, i.e., its wavefunction should be invariant under a general color gauge transformation. However, it is sufficient for us to impose color *neutrality*, meaning equality in the numbers of red, green, and blue quarks. This is a less stringent constraint (singlet $\Rightarrow$ neutral but neutral $\not\Rightarrow$ singlet) but the projection of a color neutral state onto a color singlet costs no extra free energy in the thermodynamic limit [79]. (See also [80, 81].) In general there are 8 possible color charges, but because the Cartan subalgebra of $SU(3)_c$ is two-dimensional it is always possible to transform to a gauge where all are zero except Q_3 and Q_8, the charges associated with the diagonal generators $T_3 = \frac{1}{2}\,\mathrm{diag}(1,-1,0)$ and $T_8 = \frac{1}{2\sqrt{3}}\,\mathrm{diag}(1,1,-2)$ in (r,g,b) space [82, 83]. In this review, we only discuss such gauges. So to impose color neutrality we just require $Q_3 = Q_8 = 0$.

In nature, electric and color neutrality are enforced by the dynamics of the electromagnetic and QCD gauge fields, whose zeroth components serve as chemical potentials coupled to the charges Q, Q_3, Q_8, and which are naturally driven to values that set these charges to zero [84–88]. In an NJL model with fermions but no gauge fields (see Sec. VI) one has to introduce the chemical potentials μ_e, μ_3 and μ_8 by hand in order to enforce color and electric neutrality. The neutrality conditions are then

$$\begin{aligned} Q &= \frac{\partial\Omega}{\partial\mu_e} &&= 0 \\ Q_3 &= -\frac{\partial\Omega}{\partial\mu_3} &&= 0 \\ Q_8 &= -\frac{\partial\Omega}{\partial\mu_8} &&= 0 \ . \end{aligned} \tag{3}$$

(Note that we define an electrostatic potential μ_e that is coupled to the *negative* electric charge Q, so that in typical neutron star conditions, where there is a finite density of electrons rather than positrons, μ_e is positive.)

Finally we should note that enforcing local neutrality is appropriate for uniform phases, but there are also non-uniform charge-separated phases ("mixed phases"), consisting of positively and negatively charged domains which are neutral on average. These are discussed further in Sec. III H.

E. Stresses on BCS pairing

The free energy argument that we gave in Sec. I B for the inevitability of BCS pairing in the presence of an attractive interaction relies on the assumption that the quarks that pair with equal and opposite momenta can each be arbitrarily close to their common Fermi surface. However, as we will see in Sec. II, the neutrality constraint, combined with the mass of the strange quark and the requirement that matter be in beta equilibrium, tends to pull apart the Fermi momenta of the different flavors of quarks, imposing an extra energy cost ("stress") on the formation of Cooper pairs involving quarks of different flavors. This raises the possibility of non-BCS pairing in some regions of the phase diagram.

To set the stage here, let us discuss a simplified example: consider two massless species of fermions, labeled 1 and 2, with different chemical potentials μ_1 and μ_2, and an attractive interaction between them that favors cross-species BCS pairing with a gap parameter Δ. It will turn out that to a good approximation the color-flavor locked pairing pattern contains three such sectors, so this example captures the essential physics we will encounter in later sections. We define the average chemical potential and the stress parameter

$$\begin{aligned} \bar{\mu} &= \tfrac{1}{2}(\mu_1 + \mu_2) \\ \delta\mu &= \tfrac{1}{2}(\mu_1 - \mu_2) \ . \end{aligned} \tag{4}$$

As long as the stress $\delta\mu$ is small enough relative to Δ, BCS pairing between species 1 and 2 can occur, locking their Fermi surfaces together and ensuring that they occur in equal numbers. At the Chandrasekhar-Clogston point [89, 90], where $\delta\mu = \Delta/\sqrt{2}$, the two-species model undergoes a first-order transition to the unpaired phase. At this point BCS pairing still exists as a locally stable state, with a completely gapped spectrum of quasiparticles. When $\delta\mu$ reaches Δ the spectrum becomes gapless at momentum $p = \bar{\mu}$, indicating that cross-species BCS pairing is no longer favored at all momenta [91]. If the two species are part of a larger pairing pattern, the Chandrasekhar-Clogston transition can be shifted, and we shall see that in the two-species subsectors of the CFL pattern it is shifted to $\delta\mu > \Delta$. The onset of gaplessness is therefore the relevant threshold for our purposes, and it always occurs at $\delta\mu = \Delta$, independent of the larger context in which the two flavors pair. This follows from the fact that BCS pairing only occurs if the energy gained from turning a 1 quark into a 2 quark with the same momentum (namely $\mu_1 - \mu_2$) is less than the cost of breaking the Cooper pair formed by these quarks, which is 2Δ [92]. Thus the 1-2 Cooper pairs are energetically stable (or metastable) as long as $\delta\mu < \Delta$. A more detailed treatment of this illustrative example can be found in [93].

This example uses massless quarks, but it can easily be modified to include the leading effect of a quark mass M. A difference in the masses of the pairing quarks also stresses the pairing, because it gives them different Fermi momenta at the same chemical potential, so the quarks in a 1-2 Cooper pair, which have equal and opposite momenta, will not both be close to their Fermi energies. The leading-order effect is easily calculated, since for a quark near its Fermi surface it acts like a shift in the quark chemical potential by $-M^2/(2\bar{\mu})$ (given that Fermi momentum $p_F \approx \bar{\mu}$ to this order).

Returning from our toy model to realistic quark matter, the quark flavors that are potentially relevant at neutron-star densities are the light up (u) and down (d) quarks, with current masses m_u and m_d that are $\lesssim 5$ MeV, and a medium-weight flavor, the strange (s) quark, with current mass $m_s \sim 90$ MeV. Their effective "constituent" masses in the vacuum are hundreds of MeV larger, but are expected to decrease with increasing quark density. We shall refer to the density-dependent constituent masses as $M_{u,d,s}$ and shall typically neglect M_u and M_d. As our toy model has illustrated, however, the strange quark mass M_s will contribute to stresses on cross-flavor pairing, and those stresses will become more severe as the density (and hence $\bar{\mu}$) decreases. This will be a major theme of later sections.

F. Overview of the quark matter phase diagram

Fig. 1 shows a schematic phase diagram for QCD that is consistent with what is currently known. Along the horizontal axis the temperature is zero, and the density is zero up to the onset transition where it jumps to nuclear density, and then rises with increasing μ. Neutron stars are in this region of the phase diagram, although it is not known whether their cores are dense enough to reach the quark matter phase. Along the vertical axis the temperature rises, taking us through the crossover from a hadronic gas to the quark-gluon plasma. This is the regime explored by high-energy heavy-ion colliders.

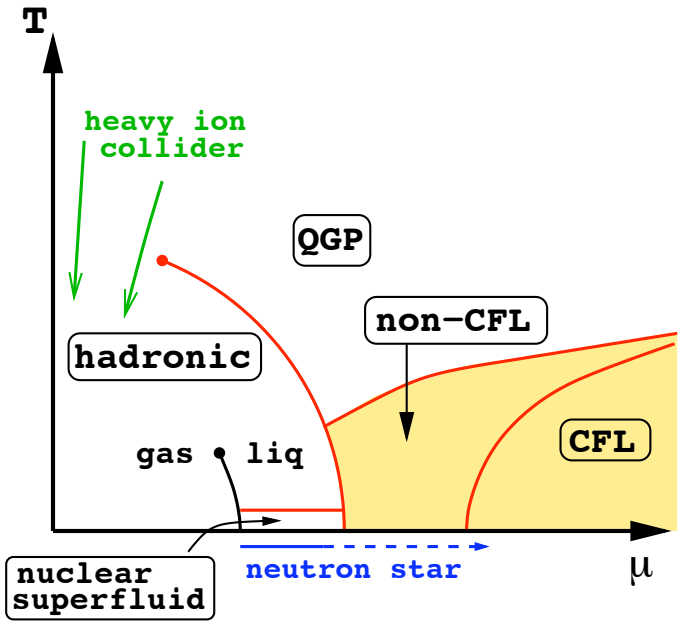

FIG. 1: (Color online) A schematic outline for the phase diagram of matter at ultra-high density and temperature. The CFL phase is a superfluid (like cold nuclear matter) and has broken chiral symmetry (like the hadronic phase).

At the highest densities we find the color-flavor locked color-superconducting phase,[2] in which the strange quark participates symmetrically with the up and down quarks in Cooper pairing. This is described in more detail in Secs. II, IV, and V. It is not yet clear what happens at intermediate density, and in Secs. III and VI we will discuss the factors that disfavor the CFL phase at intermediate densities, and survey the color superconducting phases that have been hypothesized to occur there.

Various aspects of color superconductivity at high temperatures have been studied, including the phase structure (see Sec. VI A), spectral functions, pair-forming and -breaking fluctuations, possible precursors to condensation such as pseudogaps, and various collective phenomena [95–104]. However, this review centers on quark matter at neutron star temperatures, and throughout Secs. II and III we restrict ourselves to the phases of quark matter at zero temperature. This is because most of the phases that we discuss are expected to persist up to critical temperatures that are well above the core temperature of a typical neutron star, which drops below 1 MeV within seconds of its birth before cooling down through the keV range over millions of years.

II. MATTER AT THE HIGHEST DENSITIES

A. Color-flavor locked (CFL) quark matter

Given that quarks form Cooper pairs, the next question is who pairs with whom? In quark matter at sufficiently high densities, where the up, down and strange quarks can be treated on an equal footing and the disruptive effects of the strange quark mass can be neglected, the most symmetric and most attractive option is the color-flavor locked phase, where quarks of all three colors and all three flavors form conventional zero-momentum spinless Cooper pairs. This pattern, anticipated in early studies of alternative condensates for zero-density chiral symmetry breaking [105], is encoded in the quark-quark self-energy [26]

$$\begin{aligned}\langle \psi_i^\alpha C\gamma_5 \psi_j^\beta \rangle &\propto \Delta_{\rm CFL}(\kappa{+}1)\delta_i^\alpha\delta_j^\beta + \Delta_{\rm CFL}(\kappa{-}1)\delta_j^\alpha\delta_i^\beta \\ &= \Delta_{\rm CFL}\epsilon^{\alpha\beta A}\epsilon_{ijA} + \Delta_{\rm CFL}\kappa(\delta_i^\alpha\delta_j^\beta + \delta_j^\alpha\delta_i^\beta)\end{aligned} \tag{5}$$

[2] As explained in Sec. I A, we fix $N_f = 3$ at all densities, to maintain relevance to neutron star interiors. Pairing with arbitrary N_f has been studied [94]. For N_f a multiple of three one finds multiple copies of the CFL pattern; for $N_f = 4, 5$ the pattern is more complicated.

The symmetry breaking pattern is

$$[SU(3)_c] \times U(1)_B \times \underbrace{SU(3)_L \times SU(3)_R}_{\supset [U(1)_Q]} \to \underbrace{SU(3)_{c+L+R}}_{\supset [U(1)_{\tilde{Q}}]} \times \mathbb{Z}_2 \tag{6}$$

Color indices α, β and flavor indices i, j run from 1 to 3, Dirac indices are suppressed, and C is the Dirac charge-conjugation matrix. Gauge symmetries are in square brackets. $\Delta_{\rm CFL}$ is the CFL gap parameter. The Dirac structure $C\gamma_5$ is a Lorentz singlet, and corresponds to parity-even spin-singlet pairing, so it is antisymmetric in the Dirac indices. The two quarks in the Cooper pair are identical fermions, so the remaining color+flavor structure must be symmetric. The dominant color-flavor component in (5) transforms as $(\bar{\mathbf{3}}_A, \bar{\mathbf{3}}_A)$, antisymmetric in both. The subdominant term, multiplied by κ, transforms as $(\mathbf{6}_S, \mathbf{6}_S)$. It is almost certainly not energetically favored on its own (all the arguments in Sec. II A 5 for the color triplet imply repulsion for the sextet), but in the presence of the dominant pairing it breaks no additional symmetries, so κ is in general small but not zero [26, 94, 106, 107].

1. *Color-flavor locking and chiral symmetry breaking*

A particularly striking feature of the CFL pairing pattern is that it breaks chiral symmetry. Because of color-flavor locking, chiral symmetry remains broken up to arbitrarily high densities in three-flavor quark matter. The mechanism is quite different from the formation of the $\langle\bar{\psi}\psi\rangle$ condensate that breaks chiral symmetry in the vacuum by pairing left-handed (L) quarks with right-handed (R) antiquarks. The CFL condensate pairs L quarks with each other and R quarks with each other (quarks in a Cooper pair have opposite momentum, and zero net spin, hence the same chirality) and so it might naively appear chirally symmetric. However, the Kronecker deltas in (5) connect color indices with flavor indices, so that the condensate is not invariant under color rotations, nor under flavor rotations, but only under simultaneous, equal and opposite, color and flavor rotations. Color is a vector symmetry, so the compensating flavor rotation must be the same for L and R quarks, so the axial part of the flavor group, which is the chiral symmetry, is broken by the locking of color and flavor rotations to each other [26]. Such locking is familiar from other contexts, including the QCD vacuum, where a condensate of quark-antiquark pairs locks $SU(3)_L$ to $SU(3)_R$ breaking chiral symmetry "directly", and the B phase of superfluid ^{3}He, where the condensate transforms nontrivially under rotations of spin and orbital angular momentum, but is invariant under simultaneous rotations of both.

The breaking of the chiral symmetry is associated with an expectation value for a gauge-invariant order parameter with the structure $\bar{\psi}\bar{\psi}\psi\psi$ (see Sec. V). There is also a subdominant "conventional" chiral condensate $\langle\bar{\psi}\psi\rangle \ll \langle\psi C\gamma_5\psi\rangle$ [94]. These gauge-invariant observables distinguish the CFL phase from the QGP, and if a lattice QCD algorithm applicable at high density ever becomes available, they could be used to map the presence of color-flavor locking in the phase diagram.

We also expect massless Goldstone modes associated with chiral symmetry breaking (see Secs. II A 4 and V). In the real world there is small explicit breaking of chiral symmetry from the current quark masses, so the order parameters will not go to zero in the QGP, and the Goldstone bosons will be light but not massless.

2. *Superfluidity*

The CFL pairing pattern spontaneously breaks the exact global baryon number symmetry $U(1)_B$, leaving only a discrete $\mathbb{Z}_2$ symmetry under which all quark fields are multiplied by -1. There is an associated gauge-invariant 6-quark order parameter with the flavor and color structure of two Lambda baryons, $\langle\Lambda\Lambda\rangle$ where $\Lambda = \epsilon^{abc}\epsilon_{ijk}\psi_i^a\psi_j^b\psi_k^c$. This order parameter distinguishes the CFL phase from the QGP, and there is an associated massless Goldstone boson that makes the CFL phase a superfluid, see Sec. V C 2. The vortices that result when CFL quark matter is rotated have been studied in [108–111].

3. *Gauge symmetry breaking and electromagnetism*

As explained above, the CFL condensate breaks the $SU(3)_c \times SU(3)_L \times SU(3)_R$ symmetry down to the diagonal group $SU(3)_{c+L+R}$ of simultaneous color and flavor rotations. Color is a gauge symmetry, and one of the generators of $SU(3)_{L+R}$ is the electric charge, which generates the $U(1)_Q$ gauge symmetry. This means that the unbroken $SU(3)_{c+L+R}$ contains one gauged generator, corresponding to an unbroken $U(1)_{\tilde{Q}}$ which consists of a simultaneous electromagnetic and color rotation. The rest of the color group is broken, so by the Higgs mechanism seven gluons and

one gluon-photon linear combination become massive via the Meissner effect. The orthogonal gluon-photon generator $\tilde{Q}$ remains unbroken, because every diquark in the condensate has $\tilde{Q} = 0$. The mixing angle is $\cos\theta \equiv g/\sqrt{g^2 + 4e^2/3}$ where e and g are the QED and QCD couplings. Because $e \ll g$ the angle is close to zero, meaning that the $\tilde{Q}$ photon is mostly the original photon with a small admixture of gluon.

The $\tilde{Q}$ photon is massless. Given small but nonzero quark masses, there are no gapless $\tilde{Q}$-charged excitations; the lightest ones are the pseudoscalar pseudo-Goldstone bosons $\pi^\pm$ and $K^\pm$ (see Secs. II A 4 and V), so for temperatures well below their masses (and well below the electron mass [112]) the CFL phase is a transparent insulator, in which $\tilde{Q}$-electric and magnetic fields satisfy Maxwell's equations with a dielectric constant and index of refraction that can be calculated directly from QCD [113],

$$n = 1 + \frac{e^2 \cos^2\theta}{9\pi^2} \frac{\mu^2}{\Delta^2_{\rm CFL}} \ . \tag{7}$$

(This result is valid as long as $n - 1 \ll 1$.) Apart from the fact that $n \neq 1$, the emergence of the $\tilde{Q}$ photon is an exact QCD-scale analogue of the TeV-scale spontaneous symmetry breaking that gave rise to the photon as a linear combination of the W_3 and hypercharge gauge bosons, with the diquark condensate at the QCD scale playing the role of the Higgs condensate at the TeV scale.

If one could shine a beam of ordinary light on a lump of CFL matter in vacuum, some would be reflected and some would enter, refracted, as a beam of $\tilde{Q}$-light. The reflection and refraction coefficients are known [114] (see also [115]). The static limit of this academic result is relevant: if a volume of CFL matter finds itself in a static magnetic field as within a neutron star, surface currents are induced such that a fraction of this field is expelled via the Meissner effect for the non-$\tilde{Q}$ component of Q, while a fraction is admitted as $\tilde{Q}$-magnetic field [116]. The magnetic field within the CFL volume is not confined to flux tubes, and is not frozen as in a conducting plasma: CFL quark matter is a color superconductor but it is an electromagnetic insulator.

All Cooper pairs have zero net $\tilde{Q}$-charge, but some have neutral constituents (both quarks $\tilde{Q}$-neutral) and some have charged constituents (the two quarks have opposite $\tilde{Q}$-charge). The $\tilde{Q}$-component of an external magnetic field will not affect the first type, but it will affect the pairing of the second type, so external magnetic fields can modify the CFL phase to the so-called magnetic CFL ("MCFL") phase. The MCFL phase has a different gap structure [117, 118] and a different effective theory [119]. The original analyses of the MCFL phase were done for rotated magnetic fields $\tilde{B}$ large enough that all quarks are in the lowest Landau level; solving the gap equations at lower $\tilde{B}$ shows that the gap parameters in the MCFL phase exhibit de Haas-van Alphen oscillations, periodic in $1/\tilde{B}$ [120, 121].

4. Low-energy excitations

The low-energy excitations in the CFL phase are: the 8 light pseudoscalars arising from broken chiral symmetry, the massless Goldstone boson associated with superfluidity, and the $\tilde{Q}$-photon. The pseudoscalars form an octet under the unbroken $SU(3)$ color+flavor symmetry, and can naturally be labeled according to their $\tilde{Q}$-charges as pions, kaons, and an η. The effective Lagrangian that describes their interactions, and the QCD calculation of their masses and decay constants will be discussed in Sec. V. We shall find, in particular, that even though the quark-antiquark condensate is small, the pion decay constant is large, $f_\pi \sim \mu$.

The symmetry breaking pattern (6) does not include the spontaneous breaking of the $U(1)_A$ "symmetry" because it is explicitly broken by instanton effects. However, at large densities these effects become arbitrarily small, and the spontaneous breaking of $U(1)_A$ will have an associated order parameter and a ninth pseudo-Goldstone boson with the quantum numbers of the η'. This introduces the possibility of a second type of vortices [111, 122].

Among the gapped excitations, we find the quark-quasiparticles which fall into an $\mathbf{8} \oplus \mathbf{1}$ of the unbroken global $SU(3)_{c+L+R}$, so there are two gap parameters Δ_1 and Δ_8. The singlet has the larger gap $\Delta_1 = (2 + \mathcal{O}(\kappa))\Delta_8$. We also find an octet of massive vector mesons, which are the gluons that have acquired mass via the Higgs mechanism. The symmetries of the 3-flavor CFL phase are the same as those one would expect for 3-flavor hypernuclear matter, and even the pattern of gapped excitations is remarkably similar, differing only in the absence of a ninth massive vector meson. It is therefore possible that there is no phase transition between hypernuclear matter and CFL quark matter [123]. This hadron-quark continuity can arise in nature only if the strange quark is so light that there is a hypernuclear phase, and this phase is characterized by proton-Ξ^-, neutron-Ξ^0 and Σ^+-Σ^- pairing, which can then continuously evolve into CFL quark matter upon further increasing the density [124].

5. Why CFL is favored

The dominant component of the CFL pairing pattern is the color $\bar{\mathbf{3}}_A$, flavor $\bar{\mathbf{3}}_A$, and Dirac $C\gamma_5$ (Lorentz scalar). There are many reasons to expect the color $\bar{\mathbf{3}}_A$ to be favored. First, this is the most attractive channel for quarks interacting via single-gluon exchange which is the dominant interaction at high densities where the QCD coupling is weak; second, it is also the most attractive channel for quarks interacting via the instanton-induced 't Hooft interaction, which is important at lower densities; third, qualitatively, combining two quarks that are each separately in the color-**3** representation to obtain a diquark that is a color-$\bar{\mathbf{3}}_A$ lowers the color-flux at large distances; and, fourth, phenomenologically, the idea that baryons can be modeled as bound states of a quark and a color-antisymmetric diquark, taking advantage of the attraction in this diquark channel, has a long history and has had a recent renaissance [125–129].

It is also easy to understand why pairing in the Lorentz-scalar channel is favorable: it leaves rotational invariance unbroken, allowing for quarks at all angles on the entire Fermi-sphere to participate coherently in the pairing. Many calculations have shown that pairing is weaker in channels that break rotational symmetry [22, 24, 130–133]. There is also a rotationally invariant pairing channel with negative parity described by the order parameter $\langle\psi C\psi\rangle$. Perturbative gluon exchange interactions do not distinguish between positive and negative parity diquarks, but non-perturbative instanton induced interactions do, favoring the positive parity channel [24, 25, 134].

Once we have antisymmetry in color and in Dirac indices, we are forced to antisymmetrize in flavor indices, and the most general color-flavor structure that the arguments above imply should be energetically favored is

$$\langle\psi_i^\alpha C\gamma_5\psi_j^\beta\rangle \propto \epsilon^{\alpha\beta A}\epsilon_{ijB}\phi_B^A \ . \tag{8}$$

CFL pairing corresponds to $\phi_B^A = \delta_B^A$, and this is the only pattern that pairs all the quarks and leaves an entire $SU(3)$ global symmetry unbroken. The 2SC pattern is $\phi_B^A = \delta_3^A\delta_B^3$, in which only u and d quarks of two colors pair [18, 21, 24, 25], see Sec. III A. As long as the strange quark mass can be neglected (the parametric criterion turns out to be $\Delta_{\rm CFL} \gg M_s^2/\mu$, see Sec. III B) calculations comparing patterns of the structure (8) always find the CFL phase to have the highest condensation energy, making it the favored pattern. This has been confirmed in weak-coupling QCD calculations valid at high density [94, 106, 135], in the Ginzburg-Landau approximation [84], and in many calculations using Nambu–Jona-Lasinio models [26, 123, 124, 134, 136]. In the high-density limit where $\Delta \gg M_s^2/\mu$ and $\Delta \ll \mu$ we can expand in powers of Δ/μ and explicitly compare CFL to 2SC pairing. The CFL condensation energy is $(8\Delta_8^2+\Delta_1^2)\mu^2/(4\pi^2)$ which is $12\Delta_{\rm CFL}^2\mu^2/(4\pi^2)$ when $\kappa \ll 1$ (see Sec. II A 4) whereas the condensation energy in the 2SC phase is only $4\Delta_{\rm 2SC}^2\mu^2/(4\pi^2)$. We shall see later that the 2SC gap parameter turns out to be larger than the CFL gap parameter by a factor of $2^{1/3}$, so up to corrections of order κ the CFL condensation energy is larger than that in the 2SC phase by a factor of $3\times 2^{-2/3}$. At lower densities the condensation energies become smaller, and we cannot neglect negative M_s^4 terms which are energy penalties induced by the neutrality requirement. Their coefficient is larger for CFL than for 2SC, partly (but usually not completely) cancelling the extra condensation energy—see Fig. 3 and Sec. III A.

B. Intermediate density: stresses on the CFL phase

As we noted in section I E, BCS pairing between two species is suppressed if their chemical potentials are sufficiently different. In real-world quark matter such stresses arise from the strange quark mass, which gives the strange quark a lower Fermi momentum than the down quark at the same chemical potentials μ and μ_e, and from the neutrality requirement, which gives the up quark a different chemical potential from the down and strange quarks at the same μ and μ_e. Once flavor equilibrium under the weak interactions is reached, we find that all three flavors prefer to have different Fermi momenta at the same chemical potentials. This is illustrated in Fig. 2, which shows the Fermi momenta of the different species of quarks.

In the unpaired phase (Fig. 2, left panel), the strange quarks have a lower Fermi momentum because they are heavier, and to maintain electrical neutrality the number of down quarks is correspondingly increased. To lowest order in the strange quark mass, the separation between the Fermi momenta is $\delta p_F = M_s^2/(4\mu)$, so the splitting becomes larger as the density is reduced, and smaller as the density is increased. The phase space at the Fermi surface is proportional to μ^2, so the resultant difference in quark number densities is n_d–$n_u = n_u$–$n_s \propto \mu^2\delta p_F \sim \mu M_s^2$. Electrons are also present in weak equilibrium, with $\mu_e = M_s^2/(4\mu)$, so their charge density is parametrically of order $\mu_e^3 \sim M_s^6/\mu^3 \ll \mu M_s^2$, meaning that they are unimportant in maintaining neutrality.

In the CFL phase all the colors and flavors pair with each other, locking all their Fermi momenta together at a common value (Fig. 2, right panel). This is possible as long as the energy cost of forcing all species to have the same Fermi momentum is compensated by the pairing energy that is released by the formation of the Cooper pairs.

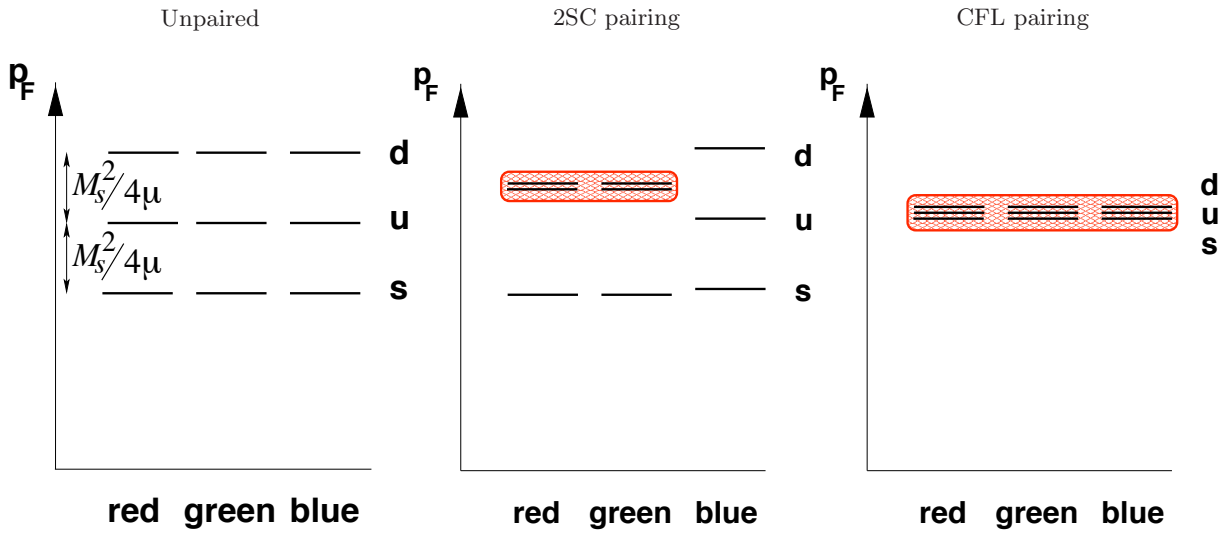

FIG. 2: (Color online) Illustration of the splitting apart of the Fermi momenta of the various colors and flavors of quarks (exaggerated for easy visibility). In the unpaired phase, requirements of neutrality and weak interaction equilibration cause separation of the Fermi momenta of the various flavors. The splittings increase with decreasing density, as μ decreases and $M_s(\mu)$ increases. In the 2SC phase, up and down quarks of two colors pair, locking their Fermi momenta together. In the CFL phase, all colors and flavors pair and have a common Fermi momentum.

Still working to lowest order in M_s^2, we can say that parametrically the cost is $\mu^2\delta p_F^2 \sim M_s^4$, and the pairing energy is $\mu^2\Delta_{\rm CFL}^2$, so we expect CFL pairing to become disfavored when $\Delta_{\rm CFL} \lesssim M_s^2/\mu$. In fact, the CFL phase remains favored over the unpaired phase as long as $\Delta_{\rm CFL} > M_s^2/4\mu$ [85], but already becomes unstable against unpairing when $\Delta_{\rm CFL} \gtrsim M_s^2/2\mu$ (see Sec. III B). NJL model calculations [85, 137–141] find that if the attractive interaction were strong enough to induce a 100 MeV CFL gap when $M_s = 0$ then the CFL phase would survive all the way down to the transition to nuclear matter. Otherwise, there must be a transition to some other quark matter phase: this is the "non-CFL" region shown schematically in Fig. 1. When the stress is small, the CFL pairing can bend rather than break, developing a condensate of K^0 mesons, described in Sec. II C below. When the stress is larger, however, CFL pairing becomes disfavored. A comprehensive survey of possible BCS pairing patterns shows that all of them suffer from the stress of Fermi surface splitting [83], so in the intermediate-density "non-CFL" region we expect more exotic non-BCS pairing patterns. In Sec. III we give a survey of possibilities that have been explored.

C. Kaon condensation: the CFL-K^0 phase

Bedaque and Schäfer [142] showed that when the stress is not too large (high density), it may simply modify the CFL pairing pattern by inducing a flavor rotation of the condensate. This modification can be interpreted as a condensate of "K^0" mesons. The K^0 meson carries negative strangeness (it has the same strangeness as a $\bar{s}$ quark), so forming a K^0 condensate relieves the stress on the CFL phase by reducing its strangeness content. At large density kaon condensation occurs for $M_s \gtrsim m^{1/3}\Delta^{2/3}$, where m is mass of the light (u and d) quarks. At moderate density the critical strange quark mass is increased by instanton contribution to the kaon mass [143]. Kaon condensation was initially demonstrated using an effective theory of the Goldstone bosons, but with some effort can also be seen in an NJL calculation [144, 145]. The CFL-K^0 phase is a superfluid; it is a neutral insulator; all its quark modes are gapped (as long as $M_s^2/(2\mu) < \Delta$); it breaks chiral symmetry. In all these respects it is similar to the CFL phase. Once we turn on small quark masses, different for all flavors, the $SU(3)_{c+L+R}$ symmetry of the CFL phase is reduced by explicit symmetry breaking to just $U(1)_{\tilde{Q}} \times U(1)_{\tilde{Y}}$, with $\tilde{Y}$ a linear combination of a diagonal color generator and hypercharge. In the CFL-K^0 phase, the kaon condensate breaks $U(1)_{\tilde{Y}}$ spontaneously. This modifies the spectrum of both quarks and Goldstone modes, and thus can affect transport properties.

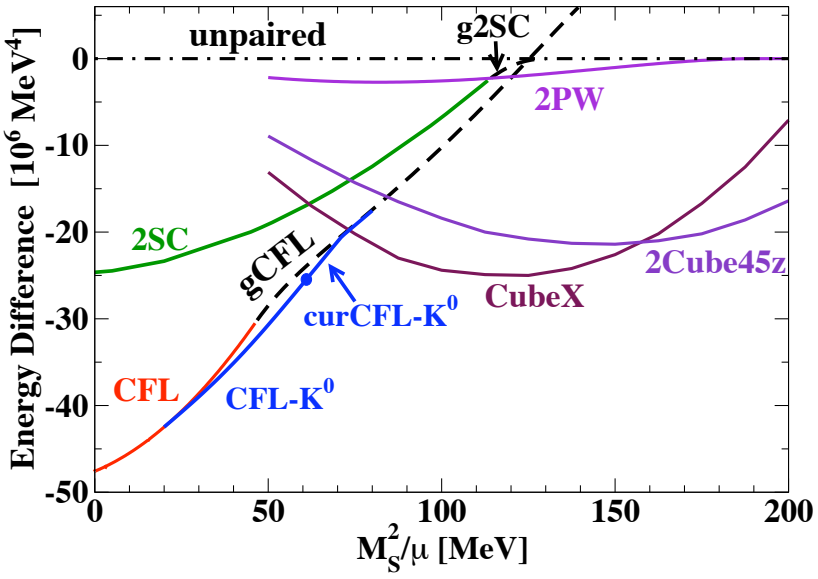

FIG. 3: (Color online) Free energy of various phases of dense 3-flavor quark matter, assuming $\Delta_{\rm CFL} = 25$ MeV. The homogeneous phases are CFL and 2SC, their gapless analogs gCFL and g2SC, and the kaon-condensed phase CFL-K^0. The true ground state must have a free energy below that of the gCFL phase, which is known to be unstable. The inhomogeneous phases are curCFL-K^0, which is CFL-K^0 with meson supercurrents, and 2PW, CubeX, and 2Cube45z, which are crystalline color superconducting phases. The transition from CFL-K^0 to curCFL-K^0 is marked with a dot. In 2PW the condensate is a sum of only two plane waves. CubeX and 2Cube45z involve more plane waves, their condensation energies are larger but less reliably determined, so their curves should be assumed to have error bands comparable in size to the difference between them.

III. BELOW CFL DENSITIES

As we discussed in the introduction (end of Sec. I A) and above (Sec. II B), at intermediate densities the CFL phase suffers from stresses induced by the strange quark mass, combined with beta-equilibration and neutrality requirements. It can only survive down to the transition to nuclear matter (occurring at quark chemical potential $\mu = \mu_{\rm nuc}$) if the pairing is strong enough: roughly $\Delta_{\rm CFL} > M_s(\mu_{\rm nuc})^2/2\mu_{\rm nuc}$, ignoring strong interaction corrections, which are presumably important in this regime. It is therefore quite possible that other pairing patterns occur at intermediate densities, and in this section we survey some of the possibilities that have been suggested.

Fig. 3 shows a comparison of the free energies of some of these phases. We have chosen $\Delta_{\rm CFL} = 25$ MeV, so there is a window of non-CFL pairing between nuclear density and the region where the CFL phase becomes stable. (For stronger pairing, $\Delta_{\rm CFL} \sim 100$ MeV, there would be no such window.) The curves for the CFL, 2SC, gCFL, g2SC, and crystalline phases (2PW, CubeX and 2Cube45z) are obtained from an NJL model as described in Sec. VI. The curves for the CFL-K^0 and meson supercurrent (curCFL-K^0) phases are calculated using the CFL effective theory with parameters chosen by matching to weak-coupling QCD, as described in Sec. V, except that the gap was chosen to match $\Delta_{\rm CFL} = 25$ MeV. The phases displayed in Fig. 3 are discussed in the following sections.

A. Two-flavor pairing: the 2SC phase

After CFL, 2SC is the most straightforward less-symmetrically paired form of quark matter, and was one of the first patterns to be analyzed [18, 20, 21, 24, 25]. In the 2SC phase, quarks with two out of three colors (red and green, say) and two out of three flavors, pair in the standard BCS fashion. The flavors with the most phase space near their Fermi surfaces, namely u and d, are the ones that pair, leaving the strange and blue quarks unpaired (middle panel of Fig. 2). According to NJL models, if the coupling is weak then there is no 2SC region in the phase diagram [146]. This can be understood by an expansion in powers of M_s, which finds that the CFL→2SC transition occurs at the same point as the 2SC→unpaired transition, leaving no 2SC window [85] (this is the situation in Fig. 3). However, NJL models with stronger coupling leave open the possibility of a 2SC window in the "non-CFL" region of the phase diagram [141, 147]. (These calculations have to date not included the possibility of meson current or crystalline color superconducting phases, discussed below, that may prove more favorable.)

The 2SC pairing pattern, corresponding to $\phi_B^A = \delta_3^A \delta_B^3$ in (8), is $\langle \psi_i^\alpha C\gamma_5 \psi_j^\beta \rangle \propto \Delta_{\rm 2SC} \epsilon_{ij3} \epsilon^{\alpha\beta 3}$, where the symmetry breaking pattern, assuming massless up and down quarks, is

$$\begin{aligned} & [SU(3)_c] \times \underbrace{SU(2)_L \times SU(2)_R \times U(1)_B \times U(1)_S}_{\supset [U(1)_Q]} \\ \rightarrow\ & [SU(2)_{rg}] \times \underbrace{SU(2)_L \times SU(2)_R \times U(1)_{\tilde{B}} \times U(1)_S}_{\supset [U(1)_{\tilde{Q}}]} \end{aligned} \tag{9}$$

using the same notation as in Eq. (6). The unpaired massive strange quarks introduce a $U(1)_S$ symmetry. The color $SU(3)_c$ gauge symmetry is broken down to an $SU(2)_{rg}$ red-green gauge symmetry, whose confinement distance rises exponentially with density, as $\Delta^{-1} \exp(\text{const}\,\mu/(g\Delta))$ [148] (see also [149, 150]). An interesting feature of 2SC pairing is that no global symmetries are broken. The condensate is a singlet of the $SU(2)_L \times SU(2)_R$ flavor symmetry, and baryon number survives as $\tilde{B}$, a linear combination of the original baryon number and the broken diagonal T_8 color generator. Electromagnetism, originally a linear combination of B, S, and I_3 (isospin), survives as an unbroken linear combination $\tilde{Q}$ of $\tilde{B}$, S, and I_3. 2SC quark matter is therefore a color superconductor but is neither a superfluid nor an electromagnetic superconductor, and there is no order parameter that distinguishes it from the unpaired phase or the QGP [24]. With respect to the unbroken $U(1)_{\tilde{Q}}$ gauge symmetry, the 2SC phase is a conductor not an insulator because some of the ungapped blue and strange quarks are $\tilde{Q}$-charged.

B. The unstable gapless phases

As was noted in Sec. II B, and can be seen in Fig. 3, the CFL phase becomes unstable when $\mu \approx \frac{1}{2} M_s^2/\Delta_{\rm CFL}$. At this point the pairing in the *gs*-*bd* sector suffers the instability discussed in Sec. I E, and it becomes energetically favorable to convert *gs* quarks into *bd* quarks (both near their common Fermi momentum).[3] If we restrict ourselves to diquark condensates that are spatially homogeneous, the result is a modification of the pairing in which there is still pairing in all the color-flavor channels that characterize CFL, but *gs*-*bd* Cooper pairing ceases to occur in a range of momenta near the Fermi surface [91, 137, 138]. In this range of momenta there are *bd* quarks but no *gs* quarks, and quark modes at the edges of this range are ungapped, hence this is called a gapless phase ("gCFL"). Such a phenomenon was first proposed for two flavor quark matter ("g2SC") [151], see also [152]. It has been confirmed in NJL analyses such as those in [91, 137–139, 141, 147, 153–155], which predict that at densities too low for CFL pairing there will be gapless phases.

In Fig. 3, where $\Delta_{\rm CFL} = 25$ MeV, we see the transition from CFL to gCFL at $M_s^2/\mu \approx 2\Delta_{\rm CFL} = 50$ MeV. (It is interesting to note that, whereas the CFL phase is a $\tilde{Q}$-insulator, the gCFL phase is a $\tilde{Q}$-conductor, because it has a small electron density, balanced by unpaired *bu* quarks from a very thin momentum shell of broken *bu*-*rs* pairing; the CFL→gCFL transition is the analogue of an insulator to metal transition at which a "band" that was unfilled in the insulating phase drops below the Fermi energy, making the material a metal.) The gCFL phase then remains favored beyond the value $M_s^2/\mu \approx 4\Delta_{\rm CFL} = 100$ MeV at which the CFL phase would become unfavored relative to completely unpaired quark matter [85].

However, it turns out that in QCD the gapless phases, both g2SC [156, 157] and gCFL [158, 159], are unstable at zero temperature. (Increasing the temperature above a critical value removes the instability; the critical value varies dramatically between phases, from a fraction of an MeV to of order 10 MeV [159].) The instability manifests itself in an imaginary Meissner mass m_M for some of the gluons. m_M^2 is the low-momentum current-current two-point function, and $m_M^2/(g^2\Delta^2)$ (where the strong interaction coupling is g) is the coefficient of the gradient term in the effective theory of small fluctuations around the ground-state condensate, so a negative value indicates an instability towards spontaneous breaking of translational invariance [160–164]. Calculations in a simple two-species model [93] show that gapless charged fermionic modes generically lead to imaginary m_M.

The instability of the gapless phases indicates that there must be other phases of even lower free energy, that occur in their place in the phase diagram. The nature of those phases is not reliably determined at present; likely candidates are discussed below.

---

[3] The onset of gaplessness occurs at the μ at which $\frac{1}{2}(\mu_{bd} - \mu_{gs}) = \Delta_{\rm CFL}$, as explained in Sec. I E. Note that in the CFL phase $(\mu_{bd} - \mu_{gs}) = M_s^2/\mu$, twice its value in unpaired quark matter because of the nonzero color chemical potential $\mu_8 \propto M_s^2/\mu$ required by color neutrality in the presence of CFL pairing [85, 146].

C. Crystalline color superconductivity

The Meissner instability of the gCFL phase points to a breaking of translational invariance, and crystalline color superconductivity represents a possible resolution of that instability. The basic idea, first proposed in condensed matter physics [165, 166] and more recently analyzed in the context of color superconductivity [167–169], is to allow the different quark flavors to have different Fermi momenta, thus accommodating the stress of the strange quark mass, and to form Cooper pairs with nonzero momentum, each quark lying close to its respective Fermi surface. The price one must pay for this arrangement is that only fermions in certain regions on the Fermi surface can pair. Pairs with nonzero momenta chosen from some set of wave vectors $\mathbf{q}_a$ yield condensates that vary in position space like $\sum_a \exp(i\mathbf{q}_a \cdot \mathbf{x})$, forming a crystalline pattern whose Bravais lattice is the set of $\mathbf{q}_a$.

Analyses to date have focused on u-d and u-s pairing, neglecting pairing of d and s because the separation of their Fermi momenta is twice as large (Fig. 2). If the $\langle ud \rangle$ condensate includes only pairs with a single nonzero momentum $\mathbf{q}$, this means that in position space the condensate is a single plane-wave and means that in momentum space pairing is allowed on a single ring on the u Fermi surface and a single ring on the opposite side of the d Fermi surface. The simplest "crystalline" phase of three-flavor quark matter that has been analyzed [170, 171] includes two such single-plane wave condensates ("2PW"), one $\langle ud \rangle$ and one $\langle us \rangle$. The favored orientation of the two $\mathbf{q}$'s is parallel, keeping the two "pairing rings" on the u Fermi surface (from the $\langle us \rangle$ and $\langle ud \rangle$ condensates) as far apart as possible [171]. This simple pattern of pairing leaves much of the Fermi surfaces unpaired, and it is much more favorable to choose a pattern in which the $\langle us \rangle$ and $\langle ud \rangle$ condensates each include pairs with more than one $\mathbf{q}$-vector, thus more than one ring and more than one plane wave. Among such more realistic pairing patterns, the two that appear most favorable have either four $\mathbf{q}$'s per condensate that together point at the eight corners of a cube in momentum space ("CubeX") or eight $\mathbf{q}$'s per condensate that each point at the corners of separate cubes, rotated relative to each other by 45 degrees ("2Cube45z") [172]. It has been shown that the chromomagnetic instability is no longer present in these phases [173]. The free energies of the 2PW, CubeX and 2Cube45z phases as calculated within an NJL model (see Sec. VI) are shown in Fig. 3. The calculation is an expansion in powers of $(\Delta/\delta p_F)^2$ which in the CubeX and 2Cube45z phases turns out to be of order a tenth to a quarter. According to results obtained in a calculation done to third order in this expansion parameter, the CubeX and 2Cube45z condensation energies are large enough that one or other of them is favored over a wide range of M_s^2/μ as illustrated in Fig. 3. The uncertainty in each is of the same order as the difference between them, so one cannot yet say which is favored, but the overall scale is plausible (one would expect condensation energies an order of magnitude bigger than that of the 2PW state). We discuss crystalline color superconductivity in greater detail in Sec. VI.

D. Meson supercurrent ("curCFL-K^0")

Kaon condensation alone does not remove the gapless modes that occur in the CFL phase when M_s becomes large enough, but it does affect the number of gapless modes and the onset value of M_s. In the CFL-K^0 phase, the electrically charged (bs) mode becomes gapless at $M_s^2/\mu \approx 8\Delta/3$ (compared to 2Δ in the CFL phase), and the electrically neutral (bd) mode becomes gapless for $M_s^2/\mu \approx 4\Delta$ [174, 175]. (In an NJL model analysis [145], the charged mode in the CFL-K^0 phase becomes gapless at $M_s^2/\mu \approx 2.44\Delta$ for $\Delta = 25$ MeV as in Fig. 3). The gapless CFL-K^0 phase has an instability which is similar to the instability of the gCFL phase. This instability can be viewed as a tendency towards spontaneous generation of Goldstone boson (kaon) currents [176, 177]. The currents correspond to a spatial modulation of the kaon condensate. There is no net transfer of any charge because the Goldstone boson current is counterbalanced by a backflow of ungapped fermions. The meson supercurrent ground state is lower in energy than the CFL-K^0 state and the magnetic screening masses are real [178]. Because the ungapped fermion mode is electrically charged, both the magnitude of the Goldstone boson current needed to stabilize the phase and the magnitude of the resulting energy gain relative to the phase without a current are very small. Goldstone boson currents can also be generated in the gCFL phase without K^0 condensation. In this case gauge invariance implies that the supercurrent state is equivalent to a single plane-wave LOFF state, but the analyses can be carried out in the limit that the gap is large compared to the magnitude of the current [179]. This analysis is valid near the onset of the gCFL phase, but not for larger mismatches, where states with multiple currents are favored.

E. Single-flavor pairing

If the stress due to the strange quark mass is large enough then there may be a range of quark matter densities where no pairing between different flavors is possible, whether spatially uniform or inhomogeneous. From Fig. 3 we can estimate that this will occur when $M_s^2/(\mu\Delta_{\rm CFL}) \gtrsim 10$, so it requires a large effective strange quark mass and/or

small CFL pairing gap. The best available option in this case is Cooper pairing of each flavor with itself. Single-flavor pairing may also arise among the strange quarks in a 2SC phase, since they are not involved in two-flavor pairing. We will discuss these cases separately below.

To maintain fermionic antisymmetry of the Cooper pair wavefunction, single-flavor pairing phases have to either be symmetric in color, which greatly weakens or eliminates the attractive interaction, or symmetric in Dirac indices, which compromises the uniform participation of the whole Fermi sphere. As a result, they have much lower critical temperatures than multi-flavor phases such as the CFL or 2SC phases, perhaps as large as a few MeV, more typically in the eV to many keV range [24, 130–133, 180].

Matter in which each flavor only pairs with itself has been studied using NJL models and weakly-coupled QCD. These calculations agree that the energetically favored state is color-spin-locked (CSL) pairing for each flavor [20, 130, 180]. CSL pairing involves all 3 colors, with the color direction of each Cooper pair correlated with its spin direction, breaking $SU(3)_c \times SO(3)_{\rm rot} \to SO(3)_{c+{\rm rot}}$. The phase is isotropic, with rotational symmetry surviving as a group of simultaneous spatial and color rotations. Other possible phases exhibiting spin-one, single-flavor, pairing include the polar, planar, and A phases described in [130, 180] (for an NJL model treatment see [132]). Some of these phases exhibit point or line nodes in the energy gap at the Fermi surface, and hence do break rotational symmetry.

If 2SC pairing occurs with strange quarks present, one might expect the strange quarks of all three colors to undergo CSL self-pairing, yielding an isotropic "2SC+CSL" pattern. However, the 2SC pattern breaks the color symmetry, and in order to maintain color neutrality, a color chemical potential is generated, which splits the Fermi momentum of the blue strange quarks away from that of the red and green strange quarks. This is a small effect, but so is the CSL pairing gap, and NJL model calculations indicate that the color chemical potential typically destroys CSL pairing of the strange quarks [181]. The system falls back on the next best alternative, which is spin-one pairing of the red and green strange quarks.

Because their gaps and critical temperatures can range as low as the eV scale, single-flavor pairing phases in compact stars would appear relatively late in the life of the star, and might cause dramatic changes in its behavior. For example, unlike the CFL and 2SC phases, many single-flavor-paired phases are electrical superconductors [182], so their appearance could significantly affect the magnetic field dynamics of the star.

F. Gluon condensation

In the 2SC phase (unlike in the CFL phase) the magnetic instability arises at a lower value of the stress on the BCS pairing than that at which the onset of gapless pairing occurs. In this 2SC regime, analyses done using a Ginzburg-Landau approach indicate that the instability can be cured by the appearance of a chromoelectric condensate [183–186]. The 2SC condensate breaks the color group down to the $SU(2)_{rg}$ red-green subgroup, and five of the gluons become massive vector bosons via the Higgs mechanism. The new condensate involves some of these massive vector bosons, and because they transform non-trivially under $SU(2)_{rg}$ it now breaks that gauge symmetry. Because they are electrically charged vector particles, rotational symmetry is also broken, and the phase is an electrical superconductor. Alternatively, it has been suggested [187] that the gluon condensate may be inhomogeneous with a large spontaneously-induced $\tilde{Q}$ magnetic field.

G. Secondary pairing

Since the Meissner instability is generically associated with the presence of gapless fermionic modes, and the BCS mechanism implies that any gapless fermionic mode is unstable to Cooper pairing in the most attractive channel, one may ask whether the instability could be resolved without introducing spatial inhomogeneity simply by "secondary pairing" of the gapless quasiparticles, which would then acquire their own gap Δ_s [188, 189]. Furthermore, there is a mode in the gCFL phase whose dispersion relation is well approximated as quadratic, $\epsilon \propto (k - {\rm const})^2$, yielding a greatly increased density of states at low energy (diverging as $\epsilon^{-1/2}$), so its secondary pairing is much stronger than would be predicted by BCS theory: $\Delta_s \propto G^2$ for an effective four-fermion coupling strength G, as compared with the standard BCS result $\Delta \propto \exp(-{\rm const}/G)$ [188]. This result is confirmed by an NJL study in a two-species model [190], but the secondary gap Δ_s was found to be still much smaller than the primary gap Δ_p, so it does not generically resolve the magnetic instability (in the temperature range $\Delta_s \ll T \ll \Delta_p$, for example).

H. Mixed phases

Another way for a system to deal with a stress on its pairing pattern is to form a mixed phase, which is a charge-separated state consisting of positively and negatively charged domains which are neutral on average. The coexisting phases have a common pressure and a common value of the charge chemical potential which is not equal to the neutrality value for either phase [191, 192]. The size of the domains is determined by a balance between surface tension (which favors large domains) and electric field energy (which favors small domains). Separation of color charge is expected to be suppressed by the very high energy cost of color electric fields, but electric charge separation is quite possible, and may occur at the interface between color-superconducting quark matter and nuclear matter [193] and an interface between quark matter and the vacuum [194, 195], just as it occurs at interfaces between nuclear matter and a nucleon gas [191]. Mixed phases are a generic phenomenon, since, in the approximation where Coulomb energy costs are neglected, any phase can always lower its free energy density by becoming charged (this follows from the fact that free energies are concave functions of chemical potentials). In this approximation, if two phases A and B can coexist at the same pressure with opposite charge densities then such a mixture will always be favored over a uniform neutral phase of either A or B. For a pedagogical discussion, see [137]. Surface and Coulomb energy costs can cancel this energy advantage, however, and have to be calculated on a case-by-case basis.

In quark matter it has been found that as long as we require local color neutrality such mixed phases are not the favored response to the stress imposed by the strange quark mass [91, 153]. Phases involving color charge separation have been studied [196] but it seems likely that the energy cost of the color-electric fields will disfavor them.

I. Relation to cold atomic gases

An interesting class of systems in which stressed superconductivity can be studied experimentally is trapped atomic gases in which two different hyperfine states ("species") of the atom pair with each other [197]. This is a useful experimental model because the stress and interaction strength are both under experimental control, unlike quark matter where one physical variable (μ) controls both the coupling strength and the stress. The atomic pairing stress can be adjusted by changing the relative number of atoms of the two species ("polarization"). The scattering length of the atoms can be controlled using Feshbach resonances, making it possible to vary the strength of the inter-atomic attraction from weak (where BCS pairing occurs) through the unitarity limit (where a bound state forms) to strong (Bose-Einstein condensation of diatomic molecules).

The theoretical expectation is that, in the weak coupling limit, there will be BCS pairing as long as $\delta\mu$, the chemical potential difference between the species, is small enough. The BCS phase is unpolarized because the Fermi surfaces are locked together. A first-order transition from BCS to crystalline (LOFF) pairing is expected at $\delta\mu = \Delta_0/\sqrt{2}$, where Δ_0 is the BCS gap at $\delta\mu = 0$; then at $\delta\mu_c$ a continuous transition to the unpaired phase [89, 90, 165, 166]. For the single plane wave LOFF state $\delta\mu_c \simeq 0.754\Delta_0$, but for multiple plane wave states $\delta\mu_c$ may be larger.

Experiments with cold trapped atoms near the unitary limit (strong coupling) have seen phase separation between an unpolarized superfluid and a polarized normal state [198–200]. If one ignores the crystalline phase (perhaps only favored at weak coupling [201–203]) this is consistent with the theoretical expectation for the BCS regime: the net polarization forces the system to phase separate, yielding a mixture of BCS and unpaired phases with $\delta\mu$ fixed at the first order transition between them [204, 205]. It remains an exciting possibility that crystalline superconducting (LOFF) phases of cold atoms may be observed: this may require experiments closer to the BCS regime.

In the strong coupling limit the superfluid consists of tightly bound molecules. Adding an extra atom requires energy Δ. For $|\delta\mu| > \Delta$ the atomic gas is a homogeneous mixture of an unpolarized superfluid and a fully polarized Fermi gas, so the system is a stable gapless superfluid. This means that in strong coupling polarization can be carried by a gapless superfluid, whereas in weak coupling even a small amount of polarization leads to the appearance of a mixed BCS/LOFF phase. It is not known what happens at intermediate coupling, but one possibility is that the gapless superfluid and the LOFF phase are connected by a phase transition [206]. This transition would correspond to a magnetic instability of the gapless superfluid.

IV. WEAK-COUPLING QCD CALCULATIONS

We have asserted in Secs. I and II that at sufficiently high densities it is possible to do controlled calculations of properties of CFL quark matter directly from the QCD Lagrangian. We describe how to do such calculations in this section. We shall focus on the calculation of the gap parameter, but shall also discuss the critical temperature T_c for the transition from the CFL phase to the quark-gluon plasma and the Meissner and Debye masses that control color-magnetic and color-electric effects in the CFL phase. Phenomena that are governed by the massless Goldstone bosons

and/or the light pseudo-Goldstone bosons are most naturally described by first constructing the appropriate effective theory and then, if at sufficiently high densities, calculating its parameters directly from the QCD Lagrangian. We defer these analyses to Sec. V.

Although the weak-coupling calculations that we describe in this section are only directly applicable in the CFL phase, we shall present them in a sufficiently general formalism that they can be applied to other spatially homogeneous phases also, including for example the 2SC and CSL phases. These phases can be analyzed at weak-coupling either just by ansatz, or by introducing such a large strange quark mass that CFL pairing is disfavored even at enormous densities. Such calculations provide insights into the properties of these phases, even though they do not occur in the QCD phase diagram at high enough densities for a weak-coupling approach to be applicable. To keep our notation general, we shall refer to the gap parameter as Δ; in the CFL phase, $\Delta_{\rm CFL} \equiv \Delta$.

We shall see that at weak coupling the expansion parameter that controls the calculation of $\log(\Delta/\mu)$ is at best g, certainly not g^2. (The leading term is of order $1/g$; the $\log g$ and g^0 terms have also been calculated. The $\mathcal{O}(g \log g)$ and $\mathcal{O}(g)$ terms are nonzero, and have not yet been calculated. Beyond $\mathcal{O}(g)$, it is possible that fractional powers of g may arise in the series.) We therefore expect the weak-coupling calculations to be quantitatively reliable only at densities for which $g(\mu) < 1$, which corresponds to densities many orders of magnitude greater than that at the centers of neutron stars. Indeed, it has been shown [207] that some of the $\mathcal{O}(g)$ contributions start to decline in magnitude relative to the g^0 term only for $g(\mu) \lesssim 0.8$ which corresponds, via the two-loop QCD beta function, to $\mu \gtrsim 10^8$ MeV meaning densities 15-16 orders of magnitude greater than those at the centers of compact stars. The reader may therefore be tempted to see this section as academic. From a theoretical point of view, it is exceptional to have an instance where the properties of a superconducting phase can be calculated rigorously from a fundamental short-distance theory, making this exploration a worthy pursuit even if academic. From a practical point of view, the quantitative understanding that we derive from calculations reviewed in this section provides a completely solid foundation from which we can extrapolate downwards in μ. The effective field theory described in Sec. V gives us a well-defined way of doing so as long as we stay within the CFL phase, meaning that we can come down from $\mu > 10^8$ MeV all the way down to $\mu \sim M_s^2/(2\Delta_{\rm CFL})$. Finally, we shall gain qualitative insights into the CFL phase and other color superconducting phases, insights that guide our thinking at lower densities.

The QCD Lagrangian is given by

$$\mathcal{L} = \overline{\psi}(i\gamma^\mu D_\mu + \hat{\mu}\gamma_0 - \hat{m})\psi - \frac{1}{4}G_a^{\mu\nu}G^a_{\mu\nu}\,. \tag{10}$$

Here, ψ is the quark spinor in Dirac, color, and flavor space, i.e., a $4N_cN_f$-component spinor, and $\overline{\psi} \equiv \psi^\dagger\gamma_0$. The covariant derivative acting on the fermion field is $D_\mu = \partial_\mu + igT_aA^a_\mu$, where g is the strong coupling constant, A^a_μ are the gauge fields, $T^a = \lambda^a/2$ $(a = 1, \ldots, 8)$ are the generators of the gauge group $SU(3)_c$, and λ^a are the Gell-Mann matrices. The field strength tensor is $G_a^{\mu\nu} = \partial_\mu A^a_\nu - \partial_\nu A^a_\mu + gf^{abc}A^b_\mu A^c_\nu$ with the $SU(3)_c$ structure constants f^{abc}. The chemical potential $\hat{\mu}$ and the quark mass $\hat{m} = {\rm diag}(m_u, m_d, m_s)$ are diagonal matrices in flavor space. If weak interactions are taken into account flavor is no longer conserved and there are only two chemical potentials, one for quark (baryon) number, μ, and one for electric charge, μ_e. At the very high densities of interest in this section, the constituent quark masses are essentially the same as the current quark masses m_u, m_d and m_s meaning that we need not distinguish between them. Furthermore, at asymptotic densities we can neglect even the strange quark mass, so throughout most of this section we shall set $m_u = m_d = m_s = 0$.

If the coupling is small then the natural starting point is a free Fermi gas of quarks. In a degenerate quark gas all states with momenta $p < p_F = (\mu^2 - m_q^2)^{1/2}$ are occupied, and all states with $p > p_F$ are empty. Because of Pauli-blocking, interactions mainly modify states in the vicinity of the Fermi surface. Since the Fermi momentum is large, typical interactions between quarks near the Fermi surface involve large momentum transfer and are governed by the weak coupling $g(\mu)$. Interactions in which quarks scatter by only a small angle involve only a small momentum transfer and are therefore potentially dangerous. However, small momenta correspond to large distances, and medium modifications of the exchanged gluons are therefore important. In a dense medium, electric gluons are Debye screened at momenta $q \sim g\mu$. The dominant interaction for momenta below the screening scale is due to unscreened, almost static, magnetic gluons. In a hot quark-gluon gas, interactions between magnetic gluons become nonperturbative for momenta less than g^2T. This phenomenon does not take place in a very dense quark liquid, and gluon exchanges with arbitrarily small momenta remain perturbative. On a qualitative level this can be attributed to the absence of Bose enhancement factors in soft gluon propagators. A more detailed explanation will be given in Sec. V A 2. The unscreened magnetic interactions nevertheless make the fluid a "non-Fermi liquid" at temperatures above the critical temperature for color superconductivity. We shall discuss this also in Sec. V A 2, where we shall see that these non-Fermi liquid effects do not spoil the basic logic of the BCS argument that diquark condensation must occur in the presence of an attractive interaction, but are crucial in the calculation of the gap that results.

A. The gap equation

As discussed in Sec. I B, any attractive interaction in a many-fermion system leads to Cooper pairing. QCD at high density provides an attractive interaction via one-gluon exchange. In terms of quark representations of $SU(3)_c$, the attractive channel is the antisymmetric anti-triplet $\overline{\mathbf{3}}_A$, appearing by "pairing" two color triplets: $\mathbf{3} \otimes \mathbf{3} = \overline{\mathbf{3}}_A \oplus \mathbf{6}_S$. Consequently, only quarks of different colors form Cooper pairs. There is an induced pairing in the symmetric sextet channel $\mathbf{6}_S$. However, this pairing is much weaker [26, 94, 106, 107, 124], and we shall largely neglect it in the following. As in an electronic superconductor, Cooper pairing results in an energy gap in the quasiparticle excitation spectrum. Its magnitude at zero temperature Δ is crucial for the phenomenology of a superconductor. In addition, it also sets the scale for the critical temperature T_c of the phase transition which can be expected to be of the same order as Δ (in BCS theory, $T_c = 0.57\Delta$). Over the course of the next five subsections, we shall discuss the QCD gap equation, which is used to determine both Δ and T_c.

Our starting point is the partition function

$$\mathcal{Z} = \int \mathcal{D}A\, \mathcal{D}\overline{\psi}\, \mathcal{D}\psi\; e^{i\mathcal{S}}\,, \tag{11}$$

with the action $\mathcal{S} = \int d^4x\, \mathcal{L}$ and the Lagrangian (10). In the following we shall only sketch the derivation of the gap equation. Details following the same lines can be found in [36, 63, 133, 180, 208–210].

We begin by introducing Nambu-Gorkov spinors. This additional two-dimensional structure proves convenient in the theoretical description of a superconductor or a superfluid, see for instance [211, 212]. It allows for the introduction of a source that couples to quark bilinears (as opposed to quark-anti-quark bilinears). Spontaneous symmetry breaking is realized by taking the limit of a vanishing source. The Nambu-Gorkov basis is given by

$$\Psi = \begin{pmatrix} \psi \\ \psi_C \end{pmatrix}\,, \qquad \overline{\Psi} = (\overline{\psi}, \overline{\psi}_C)\,, \tag{12}$$

where $\psi_C = C\overline{\psi}^T$ is the charge-conjugate spinor, obtained by multiplication with the charge conjugation matrix $C \equiv i\gamma^2\gamma^0$. In a free fermion system, the new basis is a pure doubling of degrees of freedom with the inverse fermion propagator consisting of the original free propagators,

$$S_0^{-1} = \begin{pmatrix} [G_0^+]^{-1} & 0 \\ 0 & [G_0^-]^{-1} \end{pmatrix} \tag{13}$$

where $[G_0^\pm]^{-1}(X,Y) \equiv -i\,(i\gamma^\mu\partial_\mu \pm \mu\gamma_0)\,\delta^{(4)}(X-Y)$. Here and in the following capital letters denote four-vectors, e.g., $X \equiv (x_0, \mathbf{x})$. The effect of a nonzero diquark condensate can now be taken into account through adding a suitable source term to the action and computing the effective action Γ as a functional of the gluon and fermion propagators D and S [36, 210, 213–216]:

$$\Gamma[D,S] \;=\; -\frac{1}{2}\mathrm{Tr}\log D^{-1} - \frac{1}{2}\mathrm{Tr}(D_0^{-1}D - 1) + \frac{1}{2}\mathrm{Tr}\log S^{-1} + \frac{1}{2}\mathrm{Tr}(S_0^{-1}S - 1) + \Gamma_2[D,S]\,. \tag{14}$$

This functional is called the "2PI effective action" since the contribution $\Gamma_2[D,S]$ consists of all two-particle irreducible diagrams [217–219]. This formalism is particularly suitable for studying spontaneous symmetry breaking in a self-consistent way. The ground state of the system is obtained by finding the stationary point of the effective action. The stationarity conditions yield Dyson-Schwinger equations for the gauge boson and fermion propagators,

$$D^{-1} \;=\; D_0^{-1} + \Pi\,, \tag{15a}$$
$$S^{-1} \;=\; S_0^{-1} + \Sigma\,, \tag{15b}$$

where the gluon and fermion self-energies are the functional derivatives of Γ_2 at the stationary point,

$$\Pi \equiv -2\frac{\delta\Gamma_2}{\delta D}\,, \qquad \Sigma \equiv 2\frac{\delta\Gamma_2}{\delta S}\,. \tag{16}$$

Writing the second of these equations as $\Gamma_2[S] = (1/4)\,\mathrm{Tr}(\Sigma\, S)$, we can then use the Dyson-Schwinger equation (15b) to evaluate the fermionic part of the effective action at the stationary point, obtaining the pressure

$$P = \frac{1}{2}\mathrm{Tr}\log S^{-1} - \frac{1}{4}\mathrm{Tr}\left(1 - S_0^{-1}S\right)\,. \tag{17}$$

We shall return to this expression for the pressure in Sec. IV C.

Here, we proceed to analyze the Dyson-Schwinger equation (15b) for the fermion propagator. We denote the entries of the 2×2 matrix Σ in Nambu-Gorkov space as

$$\Sigma \equiv \begin{pmatrix} \Sigma^+ & \Phi^- \\ \Phi^+ & \Sigma^- \end{pmatrix} , \tag{18}$$

where the off-diagonal elements are related via $\Phi^- = \gamma_0(\Phi^+)^\dagger\gamma_0$. One can invert the Dyson-Schwinger equation formally to obtain the full fermion propagator in the form

$$S = \begin{pmatrix} G^+ & F^- \\ F^+ & G^- \end{pmatrix} , \tag{19}$$

where the fermion propagators for quasiparticles and charge-conjugate quasiparticles are

$$G^\pm = \left\{ [G_0^\pm]^{-1} + \Sigma^\pm - \Phi^\mp ([G_0^\mp]^{-1} + \Sigma^\mp)^{-1} \Phi^\pm \right\}^{-1} , \tag{20}$$

and the so-called anomalous propagators, typical for a superconducting system, are given by

$$F^\pm = -([G_0^\mp]^{-1} + \Sigma^\mp)^{-1} \Phi^\pm G^\pm . \tag{21}$$

They can be thought of as describing the propagation of a charge-conjugate particle (i.e., a hole) with propagator $([G_0^-]^{-1} + \Sigma^-)^{-1}$ that is converted into a particle with propagator G^+, via the condensate Φ^+. (Or, a particle that is converted into a hole via the condensate.) The essence of superconductivity or superfluidity is the existence of a difermion condensate that makes the quasiparticle excitations superpositions of elementary states with fermion-number $\ldots, -5, -3, -1, 1, 3, 5, \ldots$; we see the formalism accommodating this phenomenon here.

We shall approximate Γ_2 by only taking into account two-loop diagrams. Upon taking the functional derivative with respect to S, this corresponds to a one-loop self-energy Σ. We show Σ diagrammatically in Fig. 4. We shall argue later that this approximation is sufficient to calculate $\log(\Delta/\mu)$ up to terms of order g^0. Upon making this approximation, the gap equation takes the form shown in the lower panel of Fig. 4, namely

$$\Phi^+(K) = g^2 \int_Q \gamma^\mu \, T_a^T \, F^+(Q) \, \gamma^\nu \, T_b \, D_{\mu\nu}^{ab}(K-Q) , \tag{22}$$

in momentum space, where $D_{\mu\nu}^{ab}(K-Q)$ is the gluon propagator.

Note that in the derivation of the gap equation we have assumed the system to be translationally invariant. This assumption fails for crystalline color superconductors, see Sec. VI. There has been some work on analyzing a particularly simple crystalline phase in QCD at asymptotically high densities and weak coupling [220], but the formalism we are employing does not allow us to incorporate it into our presentation and, anyway, this subject remains to date largely unexplored.

B. Quasiparticle excitations

Before we proceed with solving the gap equation, it is worthwhile to derive the dispersion relations for the fermionic quasiparticle excitations in a color superconductor. That is, we suppose that the gap parameter(s) Δ have been obtained in the manner that we shall describe below and ask what are the consequences for the quasiparticle dispersion relations. Based on experience with ordinary superconductors or superfluids, we expect (and shall find) gaps in the dispersion relations for the fermionic quasiparticles. We may also expect that in some color superconducting phases, quasiparticles with different colors and flavors, or different linear combinations of color and flavor, differ in their gaps and dispersion relations. Indeed, some gaps may vanish or may be nonzero only in certain directions in momentum space.

The quasiparticle dispersion relations are encoded within the anomalous self-energy Φ^+, defined in (18), which satisfies the gap equation (22). We shall assume that Φ^+ can be written in the form

$$\Phi^+(K) = \sum_{e=\pm} \Delta^{(e)}(K) \, \mathcal{M} \, \Lambda_{\mathbf{k}}^{(e)} , \tag{23}$$

where $\mathcal{M}$ is a matrix in color, flavor and Dirac space, and $\Lambda_{\mathbf{k}}^{(e)} \equiv (1 + e\gamma_0 \boldsymbol{\gamma}\cdot\hat{\mathbf{k}})/2$ are projectors onto states of positive ($e = +$) or negative ($e = -$) energy. The corresponding gap functions are denoted as $\Delta^{(e)}(K)$ and will be determined

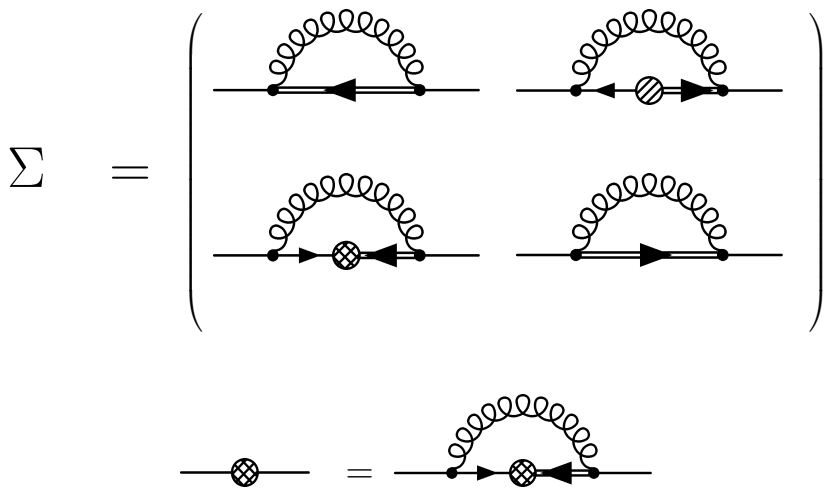

FIG. 4: Upper panel: Diagrammatic representation of the quark self-energy in Nambu-Gorkov space. Curly lines correspond to the gluon propagator D. The quasiparticle propagators G^+ and G^- are denoted by double lines with an arrow pointing to the left and right, respectively. The anomalous propagators $F^\pm$ in the off-diagonal entries are drawn according to their structure given in Eq. (21): thin lines correspond to the term $([G_0^\mp]^{-1} + \Sigma^\mp)^{-1}$, while the cross-hatched and hatched circles denote the gap matrices Φ^+ and Φ^-, respectively. Lower panel: The QCD gap equation (22) is obtained by equating Φ^+ with the lower left entry of the self-energy depicted in the upper panel (the other off-diagonal component yields an equivalent equation for Φ^-).

by the gap equation. Here and in the following the energy superscript is denoted in parentheses to distinguish it from the superscript that denotes components in Nambu-Gorkov space. In our presentation we shall assume that $\mathcal{M}$ is momentum-independent, corresponding to a condensate of Cooper pairs with angular momentum $J = 0$, but the formalism can easily be extended to allow a momentum-dependent $\mathcal{M}_{\mathbf{k}}$ as required for example in the analysis of the CSL phase and we shall quote results for this case also. Note that in Eq. (23) we are assuming that every nonzero entry in $\mathcal{M}$ is associated with the same gap functions $\Delta^{(e)}$; the formalism would have to be generalized to analyze phases in which there is more than one independent gap function, as for example in the gCFL phase.

We shall analyze color superconducting phases whose color, flavor and Dirac structure takes the form

$$\mathcal{M}_{ij}^{\alpha\beta} = \phi_A^B \epsilon^{\alpha\beta A}\, \epsilon_{ijB}\, \gamma_5\,, \tag{24}$$

where the γ_5 Dirac structure selects a positive parity condensate, where, as described in Secs. I and II, the antisymmetric color matrix is favored since QCD is attractive in this channel and the antisymmetric flavor matrix is then required, and where ϕ is a 3×3 matrix. We note that because the full flavor symmetry is the chiral $SU(3)_L \times SU(3)_R$ symmetry, the matrix ϕ is actually a pair (ϕ^L, ϕ^R). In this section we shall assume $\phi^R = \phi^L$. The case $\phi^R \neq \phi^L$, which corresponds to a meson condensate in the CFL phase, is discussed in Sec. V C.

The excitation spectrum is given by the poles of the propagator S in (19). (We shall see that the diagonal and the off-diagonal entries in S have the same poles.) It will turn out that the Hermitian matrix $\mathcal{M}\mathcal{M}^\dagger$ determines which quasiparticles are gapped and determines the ratios among the magnitudes of (possibly) different gaps. It is convenient to write this matrix via its spectral representation

$$\mathcal{M}\mathcal{M}^\dagger = \sum_r \lambda_r\, \mathcal{P}_r\,, \tag{25}$$

where λ_r are the eigenvalues and $\mathcal{P}_r$ the projectors onto the corresponding eigenstates.

The final preparation that we must discuss prior to computing the propagator is that we approximate the diagonal elements of the quark self-energy as [63, 221, 222]

$$\Sigma^\pm \simeq \gamma_0 \Lambda_{\mathbf{k}}^{(\pm)} \frac{g^2}{18\pi^2} k_0 \log\frac{48 e^2 m_g^2}{\pi^2 k_0^2}\,, \tag{26}$$

where $m_g^2 = N_f g^2 \mu^2/(6\pi^2)$ is the square of the effective gluon mass at finite density, and e is the Euler constant. The expression (26) is the low energy approximation to the one-loop self-energy, valid for $k_0 \sim \Delta \ll m_g$, for the positive

energy ($e = +$) states. Taking the low energy approximation to $\Sigma^{\pm}$ and neglecting the self-energy correction to the negative energy states will prove sufficient to determine $\log(\Delta/\mu)$ up to order g^0.

With all the groundwork in place, we now insert G_0, Σ from (26), and Φ from (23) into (20) and (21), and hence (19), and use (25) to simplify the result. We find that the diagonal entries in the fermion propagator S are given by

$$G^{\pm} = \left(\left[G_0^{\mp} \right]^{-1} + \Sigma^{\mp} \right) \sum_{e,r} \frac{\mathcal{P}_r \, \Lambda_{\mathbf{k}}^{(\mp e)}}{\left[k_0 / Z^{(e)}(k_0) \right]^2 - \left[\epsilon_{k,r}^{(e)} \right]^2} \,, \tag{27}$$

while the anomalous propagators are

$$F^{+}(K) \;=\; -\sum_{e,r} \frac{\gamma_0 \, \mathcal{M} \, \gamma_0 \, \mathcal{P}_r \Lambda_{\mathbf{k}}^{(-e)} \, \Delta^{(e)}}{\left[k_0 / Z^{(e)}(k_0) \right]^2 - \left[\epsilon_{k,r}^{(e)} \right]^2} \,, \tag{28a}$$

$$F^{-}(K) \;=\; -\sum_{e,r} \frac{\mathcal{M}^{\dagger} \, \mathcal{P}_r \Lambda_{\mathbf{k}}^{(e)} \, (\Delta^{(e)})^*}{\left[k_0 / Z^{(e)}(k_0) \right]^2 - \left[\epsilon_{k,r}^{(e)} \right]^2} \,. \tag{28b}$$

In writing these expressions, we have defined the wave function renormalization factor

$$Z^{(+)}(k_0) \equiv \left(1 + \frac{g^2}{18\pi^2} \log \frac{48 e^2 m_g^2}{\pi^2 k_0^2} \right)^{-1} \,, \tag{29}$$

for the positive energy $e = +$ components, originating from the self-energy (26). (By neglecting the negative energy contribution to $\Sigma^{\pm}$ in (26), we are setting the negative energy wave function renormalization $Z^{(-)}(k_0) = 1$.) We have furthermore defined

$$\epsilon_{k,r}^{(e)} \equiv \sqrt{(ek - \mu)^2 + \lambda_r \, |\Delta^{(e)}|^2} \,. \tag{30}$$

The r'th quasiparticle and antiquasiparticle energies are then given by solving $k_0 = Z^{(e)}(k_0) \epsilon_{k,r}^{(e)}$ for k_0. To leading order in g, wave function renormalization can be neglected and the quasiparticle and antiquasiparticle energies are given by the $\epsilon_{k,r}^{(e)}$ themselves. We see from (30) that the antiparticles have $\epsilon > \mu$ — in fact, for k near μ they have $\epsilon \sim 2\mu$. They therefore never play an important role at high density. This justifies our neglect of the negative energy $\Sigma^{\pm}$ and hence of $Z^{(-)}$. And, it justifies the further simplification that we shall henceforth employ, setting the antiparticle gap to zero, $\Delta^{(-)} = 0$, and denoting $\Delta \equiv \Delta^{(+)}$. We shall also use the notation $Z(k_0) \equiv Z^{(+)}(k_0)$ and $\epsilon_{k,r} \equiv \epsilon_{k,r}^{(+)}$. We then see that the minimum value of $\epsilon_{k,r}$ occurs at the Fermi surface, where $k = \mu$, and is given by $\sqrt{\lambda_r}\Delta$ which is conventionally referred to as the gap, again neglecting wave function renormalization. We see that although we must solve the gap equation in order to determine the magnitude of the gap parameter Δ, as we will do in Secs. IV D and IV E, the ratios among the actual gaps in the quasiparticle spectra that result are determined entirely by the λ_r's, namely the eigenvalues of $\mathcal{M}\mathcal{M}^{\dagger}$.

We close this subsection by evaluating the pattern of quasiparticle gaps explicitly for the CFL and 2SC phases. We list the order parameters ϕ_A^B, eigenvalues λ_r, and corresponding projectors $\mathcal{P}_r$ for these two phases in Table I. In the CFL phase, one finds the eigenvalues $\lambda_1 = 4$ with degeneracy $\mathrm{Tr}[\mathcal{P}_1] = 1$ and $\lambda_2 = 1$ with degeneracy $\mathrm{Tr}[\mathcal{P}_2] = 8$. This means that all nine quasiparticles are gapped. There is an octet with gap Δ, and a singlet with gap 2Δ. The octet Cooper pairs are *gu-rd*, *bd-gs*, *bu-rs*, as well as two linear combinations of the three quarks *ru-gd-bs*. (Here, *gu* refers to a green up quark, etc.) The singlet Cooper pair with twice the gap is the remaining orthogonal combination of *ru-gd-bs*. In the 2SC phase, on the other hand, we find four quasiparticles with $\lambda_1 = 1$ and hence gap Δ and 5 quasiparticles with $\lambda_2 = 0$ that are unpaired. The gapped quasiparticles involve the first two colors, red and green, and the first two flavors, up and down. The Cooper pairs have color-flavor structure *ru-gd* and *gu-rd*. (Note that all these color-flavor combinations depend on the chosen basis of the color and flavor (anti)triplets. This basis is fixed by Eq. (24); applying color (flavor) rotations to $\epsilon^{\alpha\beta A}$ (ϵ_{ijB}) would change the basis and yield different, physically equivalent, color-flavor combinations for the 2SC and CFL phases.)

The formalism of this section can easily be applied to patterns of pairing in which $\mathcal{M}_{\mathbf{k}}$ depends on the direction of the quark momentum $\mathbf{k}$. Such phases arise if the Cooper pairs carry total angular momentum $J = 1$. This allows for pairing between quarks of the same flavor, as discussed in Sec. III E. Depending on the specific structure of $\mathcal{M}_{\mathbf{k}}$, the eigenvalues λ_r may become momentum dependent and lead to nodes in the gap function along certain directions in momentum space.

phase	ϕ_A^B	λ_1	λ_2	$(\mathcal{P}_1)^{ij}_{\alpha\beta}$	$(\mathcal{P}_2)^{ij}_{\alpha\beta}$
CFL	δ_A^B	4 (1–fold)	1 (8–fold)	$\delta^i_\alpha\delta^j_\beta/3$	$\delta_{\alpha\beta}\delta^{ij} - \delta^i_\alpha\delta^j_\beta/3$
2SC	$\delta_{A3}\delta^{B3}$	1 (4–fold)	0 (5–fold)	$(\delta_{\alpha\beta} - \delta_{\alpha 3}\delta_{\beta 3})(\delta^{ij} - \delta^{i3}\delta^{j3})$	$\delta_{\alpha 3}\delta_{\beta 3}\delta^{i3}\delta^{j3}$

TABLE I: Color-flavor structure of CFL and 2SC phases: Order parameters ϕ_A^B, eigenvalues λ_r of the matrix $\mathcal{M}\mathcal{M}^\dagger$, and corresponding projectors $\mathcal{P}_r$, derived from Eq. (24). Color (flavor) indices are denoted α, β, $(i,\, j)$.

C. Pressure and condensation energy

We can now return to our expression (17) for the pressure P (equivalently, the thermodynamic potential since $\Omega = -P$) for a color superconductor and use the results of Sec. IV B to evaluate it for a superconducting phase of the form (24). We first substitute the expressions (27) and (28) for the fermion propagator (19) in the pressure (17). In order to obtain a result that is valid at both nonzero and zero temperature, it is then convenient to switch to Euclidean space, and perform the sum over Matsubara frequencies. Upon doing the trace over Nambu-Gorkov, color, flavor, and Dirac space we find

$$P \;=\; \sum_{e,r} \int \frac{d^3k}{(2\pi)^3}\, \mathrm{Tr}[\mathcal{P}_r] \left\{ \epsilon^{(e)}_{k,r} + 2\,T\, \log\left(1 + e^{-\epsilon^{(e)}_{k,r}/T}\right) - \frac{\lambda_r\, |\Delta|^2}{2\,\epsilon^{(e)}_{k,r}}\, \tanh\left(\frac{\epsilon^{(e)}_{k,r}}{2\,T}\right) \right\}. \tag{31}$$

Including the effects of wave function renormalization would modify this expression at order g. In most contexts, we shall only consider the pressure (31) at zero temperature. In this case, with $\sum_r \mathrm{Tr}[\mathcal{P}_r] = N_c N_f$,

$$P = N_c N_f \frac{\mu^4}{12\pi^2} + \delta P\ . \tag{32}$$

where we denote the pressure difference of the color-superconducting phase compared to the unpaired phase by δP. If we make the simplifying assumption (corrected in the next subsection) that the gap function is a constant in momentum space in the vicinity of the Fermi surface, we find the easily interpretable result

$$\delta P = \frac{\mu^2}{4\pi^2} \sum_r \mathrm{Tr}[\mathcal{P}_r]\, \lambda_r \Delta^2\,. \tag{33}$$

At $T = 0$ this quantity is the condensation energy density of the color-superconducting state. The fact that $\delta P > 0$ implies that the superconducting state is favored relative to the normal phase. We observe that δP is proportional to the sum of the energy gap squared of the r-th branch, multiplied by the corresponding degeneracy $\mathrm{Tr}[\mathcal{P}_r]$.

We can use the result (33) to understand how to compare the favorability of different patterns of color superconducting pairing: the phase with lowest free energy (highest δP) is favored. As an example, in the CFL phase $\delta P = (\mu^2/(4\pi^2))(8\cdot 1 + 1\cdot 4)\Delta^2_{\mathrm{CFL}}$ while in the 2SC phase $\delta P = (\mu^2/(4\pi^2))(4\cdot 1 + 0\cdot 5)\Delta^2_{\mathrm{2SC}}$ suggesting that the CFL phase is favored. (We shall make this conclusion firm in Sec. IV E, where we shall find that Δ_{CFL} is smaller than Δ_{2SC} but only by a factor of $2^{1/3}$. This factor will also turn out to be determined entirely by the λ_r's and $\mathrm{Tr}[\mathcal{P}_r]$'s.)

In principle, in order to generalize the conclusion that the CFL phase is favored one has to compare the condensation energies of all possible phases described by the order parameter $\mathcal{M}$ in Eq. (24). This is difficult because ϕ is an arbitrary complex 3×3 matrix. At asymptotic densities, however, we can neglect the strange quark mass and treat the quarks as degenerate in mass. The resulting $SU(3)_c \times SU(3)_f$ symmetry simplifies the task. (f is L or R for ϕ_L or ϕ_R.) The matrix ϕ transforms under color-flavor rotations as $\phi \to U^T \phi V$ with $U \in SU(3)_c$, $V \in SU(3)_f$. This means that two order parameters ϕ and $U^T\phi V$ describe the same physics. Now note that for any ϕ there exists a transformation (U, V) such that $U^T\phi V$ is diagonal. Therefore, we need consider only diagonal matrices ϕ. Choosing all diagonal elements to be nonzero corresponds to the maximum number of gapped quasiparticles. Hence, once we show (below) that Δ_{2SC} is not much larger than Δ_{CFL} it is easy to understand that the CFL phase with $\phi = \mathbf{1}$, yielding an order parameter that is invariant under the largest possible subgroup of the original symmetries, is the ground state at asymptotically large densities.

At lower densities, the flavor symmetry is explicitly broken by the mass of the strange quark (the symmetries are further broken by different chemical potentials due to neutrality constraints). In this case, the above argument fails and non-diagonal matrices ϕ become possible candidates for the ground state [83, 136].

D. Weak coupling solution of the gap equation

We are now in a position to solve the QCD gap equation (22) for an order parameter with a given matrix structure $\mathcal{M}$. The matrix structure of the gap equation (22) is handled by multiplying both sides of the equation by $\mathcal{M}^\dagger\Lambda_{\mathbf{k}}^{(+)}$ and taking the trace over color, flavor, and Dirac indices.

The gap equation is sensitive to gluon modes with small momentum ($p \ll m_g$) and even smaller energy ($p_0 \sim p^3/m_g^2 \ll p$), meaning that medium effects in the gluon propagator have to be taken into account. In the low momentum limit, the gluon propagator takes on the standard hard-dense loop approximation form [223], which we shall give below in Eqs. (36) and (37) upon simplifying it as appropriate for $p_0 \ll p$. In order to obtain $\log(\Delta/\mu)$ to order g^0, it suffices to keep only the leading terms in the propagator in the $p_0 \ll p$ limit. We shall work in Coulomb gauge. Gauge independence of the gap in a generalized Coulomb gauge was established in [224], and a more formal proof of gauge invariance was given in [86, 225]. The gap equation reads

$$\Delta_{k,r} \;=\; \frac{g^2}{4}\int\frac{d^3q}{(2\pi)^3}\sum_s Z(\epsilon_{q,s})\frac{\Delta_{q,s}}{\epsilon_{q,s}}\tanh\left(\frac{\epsilon_{q,s}}{2T}\right)\left[D_\ell(p)\,\mathcal{T}^s_{00}(\mathbf{k},\mathbf{q}) + D_t(p,\epsilon_{q,s},\epsilon_{k,r})\,\mathcal{T}^s_t(\mathbf{k},\mathbf{q})\right], \tag{34}$$

where we have abbreviated $P \equiv K - Q$ and have denoted the gap function on the quasiparticle mass shell by $\Delta_{k,r} \equiv \Delta(\epsilon_{k,r},\mathbf{k})$. We have denoted the traces over color, flavor, and Dirac space by

$$\mathcal{T}^s_{\mu\nu}(\mathbf{k},\mathbf{q}) \equiv -\frac{\mathrm{Tr}\left[\gamma_\mu T_a^T\gamma_0\mathcal{M}_{\mathbf{q}}\gamma_0\mathcal{P}_s\Lambda^{(-)}_{\mathbf{q}}\gamma_\nu T_a\mathcal{M}^\dagger_{\mathbf{k}}\Lambda^{(+)}_{\mathbf{k}}\right]}{\mathrm{Tr}\left[\mathcal{M}_{\mathbf{k}}\mathcal{M}^\dagger_{\mathbf{k}}\Lambda^{(+)}_{\mathbf{k}}\right]}, \tag{35}$$

and $\mathcal{T}^s_t(\mathbf{k},\mathbf{q}) \equiv -(\delta^{ij} - \hat{p}^i\hat{p}^j)\,\mathcal{T}^s_{ij}(\mathbf{k},\mathbf{q})$. The two terms inside the square bracket in Eq. (34) correspond to the contributions from electric and magnetic gluons. The dominant contribution comes from almost static gluons with $p_0 \ll p$. The static electric and almost static magnetic gluon propagator give

$$D_\ell(p) \;\equiv\; \frac{2}{p^2+3m_g^2} \tag{36}$$

$$D_t(p,\epsilon,\epsilon') \;\equiv\; \frac{p^4}{p^6 + M_g^4(\epsilon+\epsilon')^2} + (\epsilon' \to -\epsilon'), \tag{37}$$

where $M_g^2 \equiv (3\pi/4)m_g^2$. With the gap equation now stated fully explicitly, all that remains is to solve it.

We can solve (34) for the zero temperature gap Δ on the Fermi surface. Or, we can solve for T in the $\Delta \to 0$ limit, thus obtaining the critical temperature T_c. Solving for Δ, we find that it has a weak coupling expansion of the form

$$\log\left(\frac{\Delta}{\mu}\right) = -\frac{b_{-1}}{g} - \bar{b}_0\log(g) - b_0 - \ldots. \tag{38}$$

In our treatment of the fermion propagator, the gluon propagator, and in our truncation of the self-energy in Fig. 4 to one loop (for example neglecting vertex renormalization) we have been careful to keep all effects that contribute to b_0, but we have neglected many that contribute at order $g\log g$ and g. The formalism that we have presented can be used to evaluate b_{-1}, $\bar{b}_0$ and b_0, and we shall describe the results in Sec. IV E.

Before turning to quantitative results, it is worth highlighting the origin and the importance of the leading $-1/g$ behavior in (38), namely the fact that $(\Delta/\mu) \sim \exp(-\text{constant}/g)$. If in the gap equation of Fig. 4 we were to replace the exchanged gluon by a contact interaction, we would obtain a gap equation of the form

$$\Delta \propto g^2\int d\xi\frac{\Delta}{\sqrt{\xi^2+\Delta^2}} \tag{39}$$

with $\xi \equiv k - \mu$. This always has the solution $\Delta = 0$; to seek nonzero solutions, we cancel Δ from both sides of the equation. Then, if Δ were 0, the remaining integral would diverge logarithmically at small ξ. Therefore, we find a nonzero Δ for any positive nonzero g no matter how small, with $\Delta \propto \exp(-\text{constant}/g^2)$. This is the original BCS argument for superconductivity as a consequence of an attractive interaction at a Fermi surface. However, once we restore the gluon propagator the argument is modified. The crucial point is that magnetic gluon exchange is an unscreened long-range interaction, meaning that the angular integral will diverge logarithmically at forward scattering in the absence of any mechanism that screens the magnetic interaction. The gap equation therefore takes the form

$$\Delta \propto g^2\int d\xi\frac{\Delta}{\sqrt{\xi^2+\Delta^2}}d\theta\frac{\mu^2}{\theta\mu^2+\delta^2} \tag{40}$$

where θ is the angle between the external momentum $\mathbf{k}$ and the loop momentum $\mathbf{q}$ and where δ is some quantity with the dimensions of mass that cuts off the logarithmic collinear divergence of the angular integral. In the superconducting phase this divergence will at the least be cut off by the Meissner effect, which screens gluon modes with $p < \Delta$ (since the Cooper pairs have size $1/\Delta$) giving $\delta \sim \Delta$. This yields $\Delta \sim g^2\Delta(\log\Delta)^2$ and hence a nonzero gap $\Delta \sim \exp(-\text{constant}/g)$. This consequence of the long-range nature of the magnetic gluon exchange was first discovered by Barrois [18]. However, pursuing the argument as just stated yields the wrong value of the constant b_{-1}; it was Son who realized that the collinear divergence is cut off by Landau damping at a larger value of the angle θ than that at which the Meissner effect does so. Loosely speaking, Landau damping leads to $\delta \sim (\Delta m_g^2)^{1/3} \gg \Delta$. Son was then able to calculate the coefficients of the $1/g$ term and of the logarithm in (38) [55]. The calculation of the constant b_0 was initiated in [209, 226–229] and completed in [230, 231]. Higher order terms are expected to be of order $g\log g$, order g, and at higher order still may contain fractional powers and logarithms of g, see Sec. V A 2.

The $(\Delta/\mu) \propto \exp(-\text{constant}/g)$ behavior means that the color superconducting gap is parametrically larger at $\mu \to \infty$ than it would be for any four-fermion interaction. Furthermore, asymptotic freedom ensures that $1/g(\mu)^2$ increases logarithmically with μ, which means that $\exp[-\text{constant}/g(\mu)]$ decreases more slowly than $1/\mu$ at large μ. We can therefore conclude that Δ increases with increasing μ at asymptotically large μ, although of course Δ/μ decreases.

We conclude this subsection with a derivation of the correct value of the coefficient b_{-1}, namely the constant in $(\Delta/\mu) \propto \exp(-\text{constant}/g)$. This coefficient turns out to be independent of the spin-color-flavor structure $\mathcal{M}$, and it is therefore simplest to present its derivation in the 2SC phase, in which there is only one gap parameter $\Delta_k \equiv \Delta_{k,r=1}$, $\epsilon_k \equiv \epsilon_{k,r=1}$. The leading behavior of the gap is completely determined by magnetic gluon exchanges. We can also approximate the trace term by its value in the forward direction $\mathcal{T}_t(\mathbf{k},\mathbf{q}) \simeq \mathcal{T}_t(\mathbf{k},\mathbf{k}) = 2/3$ and set the wave function renormalization $Z(q_0) = 1$ (in the forward limit we also find $\mathcal{T}_{00}(\mathbf{k},\mathbf{q}) \simeq \mathcal{T}_t(\mathbf{k},\mathbf{q})$). Carrying out the angular integrals in the gap equation gives

$$\Delta_k = \frac{g^2}{18\pi^2}\int dq\,\frac{\Delta_q}{\epsilon_q}\,\frac{1}{2}\log\left(\frac{\mu^2}{|\epsilon_q^2-\epsilon_k^2|}\right). \tag{41}$$

Son observed that at this order we can replace the logarithm by $\max\{\log(\mu/\epsilon_k),\log(\mu/\epsilon_q)\}$. Introducing logarithmic variables $x = \log[2\mu/(\xi_k+\epsilon_k)]$ with $\xi_k = |k-\mu|$, the integral equation (41) can be written as a differential equation

$$\Delta''(x) = -\frac{g^2}{18\pi^2}\Delta(x), \tag{42}$$

with the boundary conditions $\Delta(0) = 0$ and $\Delta'(x_0) = 0$. Here, $x_0 = \log(2\mu/\Delta)$ determines the gap on the Fermi surface. The solution is

$$\Delta(x) = \Delta\sin\left(\frac{gx}{3\sqrt{2}\pi}\right),\ \ \Delta = 2\mu\exp\left(-\frac{3\pi^2}{\sqrt{2}g}\right), \tag{43}$$

and thus $b_{-1} = 3\pi^2/\sqrt{2}$. We conclude that in the weak-coupling limit the gap function is peaked near the Fermi surface, with a width that is much smaller than μ but much larger than Δ. Had we not set $Z(q_0) = 1$, the x-dependence of $\Delta(x)$ would be more complicated than the simple sinusoid in (43), but the conclusion remains unchanged [231].

E. Gap and critical temperature at weak coupling

The gap on the Fermi surface of a color superconductor at zero temperature can be written as

$$\Delta = \mu g^{-\bar{b}_0} e^{-b_0}\exp\left(-\frac{3\pi^2}{\sqrt{2}g}\right), \tag{44}$$

to order g^0 in the weak-coupling expansion of $\log(\Delta/\mu)$. We have derived the coefficient b_{-1} in the exponent above, starting from a simplified version of the gap equation (34), with no wave function renormalization and a simplified gluon propagator. Upon restoring these effects, analysis of the gap equation (34) yields

$$g^{-\bar{b}_0} e^{-b_0} = g^{-5}512\pi^4\left(\frac{2}{N_f}\right)^{5/2} e^{-b_0'}\,e^{-d}\,e^{-\zeta}\ . \tag{45}$$

In the following we shall define and explain the origin of each of the terms in this equation; we shall not present a complete derivation.

- The factor g^{-5} and the numerical factor in Eq. (45) are due to large angle magnetic as well as electric gluon exchanges and are independent of the pattern of pairing in the color superconducting phase, i.e. independent of $\mathcal{M}$.

- The factor

$$e^{-b_0'} = \exp\left(-\frac{\pi^2+4}{8}\right) \simeq 0.177 \tag{46}$$

  arises from the wave function renormalization factor $Z(q_0)$ in (26) [230, 231] and is also independent of $\mathcal{M}$ and hence the same for all color superconducting phases.

- The factors that we have written as $e^{-d}e^{-\zeta}$ are different in different color superconducting phases. The factor e^{-d} is due to the angular structure of the gap. For the $J = 0$ condensates whose gap equation we have derived, $e^{-d} = 1$. Upon redoing the angular integrals for spin-1 condensates, we find that they are strongly suppressed [130, 133, 180]. For spin-1 pairing patterns in which quarks of the same chirality form Cooper pairs, $d = 6$. A smaller suppression occurs when quarks of opposite chirality pair, $d = 4.5$. Superpositions of these states yield values of d between these limits. Regardless, perturbative QCD predicts spin-1 gaps to be two to three orders of magnitude smaller than spin-0 gaps.

- The factor $e^{-\zeta}$ depends on $\mathcal{M}$, the color-flavor-spin matrix that describes the pattern of pairing in a particular color superconducting phase. In a phase in which $\mathcal{M}\mathcal{M}^\dagger$ has two different eigenvalues λ_1 and λ_2, describing $\mathrm{Tr}[\mathcal{P}_1]$ and $\mathrm{Tr}[\mathcal{P}_2]$ quasiparticles respectively, we find

$$\zeta = \frac{1}{2}\frac{\langle \mathrm{Tr}[\mathcal{P}_1]\lambda_1 \log\lambda_1 + \mathrm{Tr}[\mathcal{P}_2]\lambda_2 \log\lambda_2\rangle}{\langle \mathrm{Tr}[\mathcal{P}_1]\lambda_1 + \mathrm{Tr}[\mathcal{P}_2]\lambda_2\rangle}\,, \tag{47}$$

  where the angular brackets denote an angular average (trivial for $J = 0$ phases). In the CFL phase, $\lambda_1 = 1$ and $\mathrm{Tr}[\mathcal{P}_1] = 8$ while $\lambda_2 = 4$ and $\mathrm{Tr}[\mathcal{P}_2] = 1$, meaning that there are 8 quasiparticles with gap Δ and 1 with gap 2Δ. Evaluating Eq. (47), we find $e^{-\zeta} = 2^{-1/3}$ in the CFL phase [94]. In the 2SC phase, $e^{-\zeta} = 1$. Note that the ratio $\Delta_{\rm CFL}/\Delta_{\rm 2SC}$ is also $2^{-1/3}$ in an NJL model analysis [33]; this result depends on the structure of the condensates not on the nature of the interaction. From $\Delta_{\rm CFL}/\Delta_{\rm 2SC} = 2^{-1/3}$ we can conclude the discussion begun in Sec. IV C, noting now that the condensation energy in the CFL phase is larger than that in the 2SC phase by a factor $3 \cdot 2^{-2/3}$.

- We can also determine the admixture of a color symmetric condensate in the CFL phase. In this case we have to use a two-parameter ansatz for the gap and solve two coupled gap equations. The color-symmetric gap parameter Δ_6 is parametrically small compared to the color-antisymmetric gap $\Delta_{\bar{3}}$, and the two gap equations decouple. We find $\Delta_6/\Delta_{\bar{3}} = \sqrt{2}\log(2)g/(36\pi)$ which is suppressed by both the coupling constant g and a large numerical factor.

In evaluating (44) and (45), it suffices at present to evaluate g at the scale μ. The effect of choosing $g(a\mu)$ with a either some purely numerical constant or some constant proportional to g or $\log\Delta$ is order g, meaning that we cannot and need not determine a within our present calculation of $\log\Delta$ to order g^0. For a numerical estimate of the effects of a running g on Δ, see [232]. The effects are not as large as envisioned in [233].

We shall discuss a systematic approach to the calculation of corrections beyond $\mathcal{O}(g^0)$ in $\log(\Delta/\mu)$ in Sec. V A 2. There are a number of effects that have been considered, and were shown not to contribute at $\mathcal{O}(g^0)$, but for which the actual size of the $\mathcal{O}(g)$ (or higher) correction is not known. These include vertex corrections [64], the imaginary part of the gap function [234, 235], and the modification of the gluon propagator due to the Meissner effect [236].

It is instructive to extrapolate the perturbative results to lower baryon densities for which the running coupling constant is not small. Taking $\mu \simeq 400 - 500$ MeV, and a strong coupling constant $g \simeq 3.5$ (note that $g = 3.56$ at $\mu = 400$ MeV according to the two-loop QCD beta function, which of course should not be taken seriously at these low densities) one obtains $\Delta \simeq 20$ MeV. This is comparable to (but on the small side of) the range of typical gaps $\Delta \sim (20 - 100)$ MeV [33] obtained using models in which the interaction between quarks is described via a few model parameters whose values are chosen based upon consideration of zero-density physics, like the NJL models that we shall discuss in Sec. VI or numerical solutions of the Dyson-Schwinger equations [237, 238]. This qualitative agreement between two completely different approaches, one based on using a model to extrapolate from $\mu = 0$ to $\mu = 400 - 500$ MeV and the other based on applying a rigorous calculation that is valid for $\mu > 10^8$ MeV where the QCD coupling is weak at $\mu = 400 - 500$ MeV gives us confidence that we understand the magnitude of Δ, the fundamental energy scale that characterizes color superconductivity. Furthermore, the one nonperturbative interaction in QCD whose contribution to Δ has been evaluated reliably at high density, namely that due to the 't Hooft interaction induced

by instantons, serves to increase Δ, bringing the high density computation into even better agreement with the model-based approaches [24, 25, 134, 232, 239, 240].

Finally, we can use the gap equation (34) to extract the critical temperature T_c. The result is [133, 180, 209, 221, 228, 230, 231]

$$\frac{T_c}{\Delta} = \frac{e^\gamma}{\pi} e^\zeta \,, \tag{48}$$

where $\gamma \simeq 0.577$ is the Euler-Mascheroni constant. This should be compared to the BCS result $T_c/\Delta = e^\gamma/\pi \simeq 0.57$. We observe that deviations from the BCS ratio occur in the case of two-gap structures and/or anisotropic gaps. Nevertheless, since e^ζ is of order one, the critical temperature is always of the same order of magnitude as the zero-temperature gap. We see that for the 2SC phase T_c/Δ is as in BCS theory, whereas in the CFL phase this ratio is larger by a factor of $2^{1/3}$. It therefore turns out that T_c is the same in the CFL and 2SC phases.

These estimates of T_c neglect gauge field fluctuations, making them valid only at asymptotic densities. We shall see in Sec. V B that including the gauge field fluctuations turns the second order phase transition that we find by analyzing (34) into a first order phase transition, and increases T_c by a factor $1 + \mathcal{O}(g)$, see Eq. (74).

F. Color and electromagnetic Meissner effect

One of the characteristic properties of a superconductor is the Meissner effect, the fact that an external magnetic field does not penetrate into the superconductor. The external field is shielded by supercurrents near the interface between the normal phase and the superconducting phase. The inverse penetration length defines a mass scale which can be viewed as an effective magnetic gauge boson mass.

This effect can also be described as the Anderson-Higgs phenomenon [241, 242]. The difermion condensate acts as a composite Higgs field which breaks all or part of the gauge symmetry of the theory. The gauge fields acquire a mass from the Higgs vacuum expectation value, and the would-be Goldstone bosons become the longitudinal components of the gauge fields. A well known example in particle physics is provided by the electroweak sector of the standard model. The $SU(2)_L \times U(1)_Y$ gauge symmetry of the electroweak standard model is broken down to $U(1)_Q$ by the expectation value of an $SU(2)$ Higgs doublet which carries hypercharge. There are three massive gauge bosons, the $W^\pm$ and the Z boson. The Z is a linear combination of the original I_3 and Y gauge bosons. The orthogonal linear combination is the photon, which remains massless because the Higgs condensate is electrically neutral.

The gauge symmetry in QCD is $SU(3)_c \times U(1)_Q$. Different color superconducting order parameters realize different Higgs phases. The color gauge group may be partially or fully broken, and mixing between diagonal gluons and photons can occur. In the following we shall concentrate on the 2SC and CFL phases and briefly mention other phases at the end of the section. Our starting point is the one-loop gauge boson polarization tensor [113, 243–246],

$$\Pi^{\mu\nu}_{ab}(P) \equiv \frac{1}{2}\frac{T}{V}\sum_K \mathrm{Tr}[\hat\Gamma^\mu_a\, S(K)\, \hat\Gamma^\nu_b\, S(K-P)] \,, \tag{49}$$

where

$$\hat\Gamma^\mu_a \equiv \begin{cases} \mathrm{diag}(g\,\gamma^\mu T_a, -g\,\gamma^\mu T_a^T) & \text{for} \quad a = 1,\ldots,8 \,, \\ \\ \mathrm{diag}(e\,\gamma^\mu Q, -e\,\gamma^\mu Q) & \text{for} \quad a = 9 \,. \end{cases} \tag{50}$$

Here, Q is the electric charge matrix $Q = \mathrm{diag}(2/3, -1/3, -1/3)$, and e the electromagnetic coupling constant. The polarization function can be defined as the second derivative of the thermodynamic potential with respect to an external gauge field. This quantity is equal to the derivative of the induced charge/current with respect to the gauge field. Electric charge screening is governed by the zero momentum limit of the Π_{00} component of the polarization tensor. The Meissner effect is related to a non-vanishing zero momentum limit of the spatial components Π_{ij}. We can define electric (Debye) and magnetic screening masses as

$$m^2_{D,ab} \;\equiv\; -\lim_{p\to 0}\Pi^{00}_{ab}(0,\mathbf{p}) \,, \tag{51a}$$

$$m^2_{M,ab} \;\equiv\; \frac{1}{2}\lim_{p\to 0}(\delta^{ij} - \hat p^i \hat p^j)\Pi^{ij}_{ab}(0,\mathbf{p}) \,. \tag{51b}$$

A calculation of the full momentum dependence of $\Pi_{\mu\nu}$ in the 2SC and CFL phases can be found in [236] and [247], respectively. One result that we shall need in Sec. V C is the electric screening mass for gluons in the CFL phase,

which is given by

$$m_{D,aa}^2 = \frac{21-8\log 2}{36}\frac{g^2\mu^2}{\pi^2}\,. \tag{52}$$

The numerical factor $21-8\log 2$ can be written as $15+(6-8\log 2)$, where the first term comes from diagrams in which the gluon couples to two octet quasiparticles and the second from coupling to one octet and one singlet quasiparticle. The $\log 2$ factor is the log of the ratio of the singlet and octet gaps.

In the following, we shall discuss the Meissner masses. Results for the CFL phase [243, 246, 248, 249] and the 2SC phase [149, 244] are summarized in Table II, where we also list the screening masses for the single-flavor CSL phase [182, 250].

We observe that the chromomagnetic screening masses are of order $g\mu$. This means that the screening length is much shorter than the coherence length $\xi = 1/\Delta$, and color superconductivity is type I, see Sec. V B. The fact that the screening masses are independent of the gap does not contradict the fact that there is no magnetic screening in the normal phase. Magnetic screening disappears for energies and momenta larger than the gap. Therefore, if the $\Delta \to 0$ limit is taken before the limit $p \to 0$ then the magnetic screening vanishes, as expected. Of course, magnetic screening masses also vanish as the temperature approaches T_c.

We also note that $m_{M,ab}^2$ is a 9×9 matrix, and the physical masses are determined by the eigenvalues of this matrix. In the CFL phase, all magnetic gluons acquire the same nonzero mass, reflecting the residual $SU(3)_{c+L+R}$. In the 2SC phase, the Meissner masses of the gluons 1 through 3 vanish, reflecting the symmetry breaking pattern $SU(3)_c \to SU(2)_c$. The unscreened gluons correspond to the generators of the unbroken $SU(2)_c$, as they only see the first two colors, red and green. Cooper pairs are red-green singlets and so cannot screen these low momentum gluons.

In both 2SC and CFL phases, the off-diagonal masses vanish except for the eighth gluon and the photon, $m_{M,\gamma 8}^2 = m_{M,8\gamma}^2 \neq 0$. The two-by-two part of the gauge boson mass matrices that describe the eighth gluon and the photon has one vanishing eigenvalue and one nonzero eigenvalue. The eigenvectors are characterized by a mixing angle θ, given in the last column of Table II. This angle defines the new gauge fields,

$$\tilde{A}_\mu^8 = \cos\theta\, A_\mu^8 + \sin\theta\, A_\mu\,, \tag{53a}$$

$$\tilde{A}_\mu = -\sin\theta\, A_\mu^8 + \cos\theta\, A_\mu\,, \tag{53b}$$

where A_μ^8 and A_μ denote the fields for the eighth gluon and the photon, respectively. The $\tilde{A}_\mu^8$ gauge boson feels a Meissner effect; it is the analogue of the massive Z-boson in the electroweak standard model. The $\tilde{A}_\mu$ gauge boson, on the other hand, experiences no Meissner effect because the diquark condensate is $\tilde{Q}$-neutral. This is the photon of the unbroken Abelian $U(1)_{\tilde{Q}}$ gauge symmetry, consisting of simultaneous color and flavor (i.e. electromagnetic) rotations. The $\tilde{A}_\mu$ field satisfies Maxwell's equations. Because $g \gg e$, the mixing angle is very small and the $\tilde{A}_\mu$ photon contains only a small admixture of the original eighth gluon.

In contrast, $J = 1$ color superconductors show an electromagnetic Meissner effect [182, 250]. For example, in the CSL phase there is no mixing between the gluons and the photon, as can be seen in the last row of Table II. The photon acquires a mass since the electromagnetic group is spontaneously broken. Other candidate spin-1 phases, such as the polar, planar, or A phase involve mixing but also (except for a one-flavor system) exhibit an electromagnetic Meissner effect. This difference in phenomenology of spin-0 vs. spin-1 color superconductors may have consequences in compact stars [251].

	$m_{M,aa}^2$								$m_{M,a\gamma}^2 = m_{M,\gamma a}^2$		$m_{M,\gamma\gamma}^2$	$\tilde{m}_{M,88}^2$	$\tilde{m}_{M,\gamma\gamma}^2$	$\cos^2\theta$
a	1	2	3	4	5	6	7	8	1-7	8	9			
CFL	$\eta\, g^2$								0	$-\frac{2}{\sqrt{3}}\,\eta\, eg$	$\frac{4}{3}\,\eta\, e^2$	$\left(\frac{4}{3}e^2+g^2\right)\,\eta$	0	$3g^2/(3g^2+4e^2)$
2SC	0			$\frac{1}{2}g^2$				$\frac{1}{3}g^2$	0	$\frac{1}{3\sqrt{3}}eg$	$\frac{1}{9}e^2$	$\frac{1}{3}g^2+\frac{1}{9}e^2$	0	$3g^2/(3g^2+e^2)$
CSL	βg^2	αg^2	βg^2	βg^2	αg^2	βg^2	αg^2	βg^2	0	0	$6q^2e^2$	βg^2	$6q^2e^2$	1

TABLE II: Zero-temperature Meissner masses m_M, rotated Meissner masses $\tilde{m}_M$, and gluon/photon mixing angle θ. The number a labels the gluons ($a = 1,\ldots,8$) and the photon ($a = 9$). All masses are given in units of $N_f\mu^2/(6\pi^2)$, where $N_f = 3, 2, 1$ in the CFL, 2SC, CSL phases, respectively. We have abbreviated $\eta \equiv (21-8\log 2)/54$, $\alpha \equiv (3+4\log 2)/27$, $\beta \equiv (6-4\log 2)/9$. For the one-flavor CSL phase we denoted the quark electric charge by q. While the rotated photon in the CFL and 2SC phases is massless, the photon acquires a Meissner mass in the CSL phase.

G. Chromomagnetic instability

We have just seen in Sec. IV F that color superconductors have nonzero Meissner masses for some gluons and/or the photon, indicating a color or electromagnetic Meissner effect. However, as we discussed previously, in Sec. III B, if the CFL phase is stressed by a nonzero strange quark mass to the point that Cooper pairs break, the resulting gapless CFL (gCFL) phase found in analyses that presume a translationally invariant condensate exhibits *imaginary* Meissner masses [158, 159]. This phenomenon was first discovered in the simpler gapless 2SC (g2SC) phase [156, 252] and can be understood in either the gCFL or g2SC context via a simplified analysis involving two quark species only [93] that we introduced in Sec. I E and shall pursue here. The negative Meissner mass squared implies that these phases are unstable toward the spontaneous generation of currents, that break translation invariance. In this section we shall review the calculation of the Meissner mass in a gapless color superconductor.

We have seen in Sec. II that the introduction of a nonzero strange quark mass, combined with the requirement that matter be neutral and in beta equilibrium, serve to exert a stress on the CFL pairing that is controlled by the parameter $m_s^2/(2\mu)$. This stress seeks to separate the bu and rs Fermi surfaces (and the bd and gs Fermi surfaces) but in the CFL phase they remain locked together in order to gain pairing energy $\propto \Delta$ per Cooper pair. In the gCFL phase, on the other hand, there are unpaired bu and bd quarks in regions of momentum space in which the corresponding rs and gs states are empty — Cooper pairs have been broken yielding gapless excitations. We can describe the resulting chromomagnetic instability generically by picking one of these pairs, calling the quarks 1 and 2, and labelling their effective chemical potentials μ_1 and μ_2. The quasiparticle dispersion relations are

$$\epsilon_k \equiv \left| \sqrt{(k-\bar{\mu})^2 + \Delta^2} \pm \delta\mu \right| , \tag{54}$$

with the average chemical potential $\bar{\mu}$ and the mismatch in chemical potentials $\delta\mu$ as in Eq. (4). (Note that the leading effect of the strange mass, $\propto m_s^2/(2\mu)$, is included in the effective chemical potential, meaning that we may use the massless dispersion relation of Eq. (54).) For $\mu_1 = \mu_2$ this yields identical dispersion relations for both degrees of freedom (and the same with a minus sign for the corresponding hole degrees of freedom which are omitted here). This is the usual situation of BCS superconductivity. For $\mu_1 \neq \mu_2$, however, one obtains two different quasiparticle excitations. A qualitative change appears at $\delta\mu = \Delta$. For $\delta\mu > \Delta$ the dispersion relations become gapless at the two momenta

$$k_\pm = \bar{\mu} \pm \sqrt{\delta\mu^2 - \Delta^2} , \tag{55}$$

meaning that there are gapless quasiparticles on two spheres in momentum space. In the region of momentum space between these two spheres, the states of species 1 are filled while those of species 2 are empty: the 1-2 pairing has been "breached" [152]. (We have taken $\delta\mu > 0$.) This seems a natural way for the system to respond to the stress $\delta\mu$, by reducing the number of 2 particles relative to the number of 1 particles, albeit at the expense of lost pairing energy. In the larger gCFL context, such a response serves to alleviate the stress introduced by the requirements of neutrality and weak equilibrium.

Gapless superconductivity [253] refers to the circumstance in which two species of fermions are paired in some regions of momentum space but in a shell (breach) in momentum space, bounded by two spherical effective Fermi surfaces, one finds unpaired fermions of just one of the two species. The term does not refer to situations in which some fermion species pair throughout momentum space while others do not pair at all, as for example in the 2SC phase. Nor does it apply to anisotropic superconductors in which the gap parameter vanishes in certain directions on the Fermi surface, as for example in some single-flavor color superconductors or in the curCFL-K^0 and crystalline color superconducting phases. The g2SC and gCFL phases are gapless superconductors, in which the same quarks pair, yielding a nonzero order parameter Δ, while simultaneously featuring gapless excitations. Such phases turn out to suffer from the chromomagnetic instability as we now explain.

The calculation of the Meissner mass can be done starting from Eq. (49). At zero temperature, in this simple context with two fermion species one finds

$$m_M^2 = m_0^2 \left[1 - \frac{\delta\mu\, \Theta(\delta\mu - \Delta)}{\sqrt{\delta\mu^2 - \Delta^2}} \right] , \tag{56}$$

where m_0 is the Meissner mass obtained upon setting $\delta\mu = 0$, removing the stress. This expression shows that the Meissner mass becomes imaginary if and only if the spectrum is gapless.

In essence, this is also what happens in the CFL phase [158, 159]. In this case, of course, there are nine gauge bosons whose Meissner masses were discussed in Sec. IV F for the case of pairing in the absence of stress. The Meissner masses for pairing with mismatched Fermi surfaces are complicated and have to be computed numerically in general.

However, the reason for the negativity of m_M^2 is the same as in Eq. (56): a negative term $\propto \delta\mu/\sqrt{\delta\mu^2-\Delta^2}$ appears for $\delta\mu > \Delta$. At the onset of gapless modes, $\delta\mu = \Delta$, this term diverges and thus it dominates the Meissner masses at least for $\delta\mu$ close to, but larger than, Δ. This is the story for the gluons A_1, A_2, but it turns out that the Meissner masses for the gluons A_a, $a = 4, 5, 6, 7$, at first remain well-behaved for values of $\delta\mu$ larger than Δ before eventually also becoming imaginary for sufficiently large mismatches. The gluons A_3, A_8 and the photon mix with each other. Two of the resulting new gauge bosons acquire an imaginary mass, just as the first two gluons. The third combination, $A_{\tilde{Q}}$, remains massless, as expected from symmetry arguments. (The mixing between these gauge bosons is a function of the mismatch and cannot be described by the mixing angle given in Table II.) Although the details are clearly more complicated than in the simple two-species model, the conclusion remains that the chromomagnetic instability occurs if and only if there are gapless modes.

This statement is not always correct, as the analysis of the gapless 2SC phase demonstrates [156, 252, 254, 255]. In this phase, the gluons 1,2 and 3 are massless for arbitrary mismatches, reflecting the unbroken $SU(2)_c$. One combination of the eighth gluon with the photon behaves as in Eq. (56) while the other combination is massless. The Meissner masses for the gluons 4-7, however, are imaginary for $\delta\mu > \Delta$ as before but they are also imaginary in the parameter region $\Delta/\sqrt{2} < \delta\mu < \Delta$. Hence, the 2SC phase is unstable in a region where there are no gapless modes. Possible consequences of this interesting behavior are discussed in [184] and have been related to gluon condensation [183].

We also know of an example where gapless pairing need not be accompanied by an instability. This is a two-species system where the coupling is allowed to grow so large that the gap becomes of the order of $\bar{\mu}$ and even larger. In this case, a strong coupling regime has been identified where the gapless phase is free of the chromomagnetic instability [256]. See [257] for a similar analysis in a non-relativistic system. The scenario in these examples cannot arise in QCD, since before $\bar{\mu}$ drops so low that $\Delta \gtrsim \bar{\mu}$, quark matter is replaced by nuclear matter.

The chromomagnetic instability of the gCFL phase only demonstrates that this phase is unstable; it does not determine the nature of the stable phase. However, the nature of the instability suggests that the stable phase should feature currents, which must be counterpropagating since in the ground state there can be no net current. Among the possible resolutions to the instability that we have enumerated in Sec. III, two stand out by this argument. In the meson supercurrent phase of Sec. III D, that we shall discuss further in Sec. V F, the phase of the CFL kaon condensate varies in space, yielding a current [179]. Ungapped fermion modes carry a counter-propagating current such that the total current vanishes. In the crystalline color superconducting phases of Sec. III C, that we shall discuss further in Sec. VI, the diquark condensate varies in space in some crystalline pattern constructed as the sum of multiple plane waves. If the total current carried by the condensate is nonzero, it is cancelled by a counter-propagating current carried by the ungapped fermion modes that are also found in the crystalline phases. It is important to note that in both these phases, the ungapped modes have different Fermi surface topologies compared to that in the gCFL phase: they are anisotropic in momentum space, with unpaired fermions accommodated in one or many "caps" rather than in spherically symmetric shells. It turns out that in both these phases, the Meissner masses are real, meaning that these phases do not suffer from a chromomagnetic instability. This was shown in the meson supercurrent phase in [178] and in the crystalline color superconducting phase in [173]. We compare the free energies of these phases in Fig. 3. These two phases have to date been analyzed "in isolation". It remains to be seen whether when they are analyzed in a sufficiently general framework that currents of either or both types are possible they are distinct possibilities or different limits of the same more general inhomogeneous phase.

V. EFFECTIVE THEORIES OF THE CFL PHASE

At energies below the gap the response of superconducting quark matter is carried by collective excitations of the superfluid condensate. The lightest of these excitations are Goldstone bosons associated with broken global symmetries. Effective theories for the Goldstone modes have a number of applications. They can be used to compute low temperature thermodynamic and transport properties, and to study the response to perturbations like nonzero quark masses and lepton chemical potentials. Other light degrees of freedom appear near special points in the phase diagram. Fermion modes become light near the CFL-gCFL transition, and fluctuations of the magnitude of the gap become light near T_c.

Effective field theories can be constructed "top down", by integrating out high energy degrees of freedom, or "bottom up", by writing down the most general effective Lagrangian consistent with the symmetries of a given phase. In QCD at moderate or low density the microscopic theory is nonperturbative, and the top down approach is not feasible. In this case the parameters of the effective Lagrangian can be estimated using dimensional analysis or models of QCD. If the density is very large then effective theories can be derived using the top down method. However, even in this case it is often easier to follow the bottom up approach, and determine the coefficients of the effective Lagrangian using matching arguments. Matching expresses the condition that low energy Green functions in the effective and

fundamental theory have to agree.

Quark matter at very high density is characterized by several energy scales. In the limit of massless quarks the most important scales are the chemical potential μ, the screening scale m_g, and the pairing gap Δ. In the weak coupling limit we have $\mu \gg m_g \gg \Delta$. This hierarchy of scales can be exploited in order to simplify calculations of the properties of low energy degrees of freedom in the color superconducting phase. For this purpose we introduce an intermediate effective theory, the high density effective theory (HDET), which describes quark and gluon degrees of freedom at energies below m_g. This theory will be described in Secs. V A 1-V A 3. Secs. V B-V E are devoted to effective theories of the CFL phase that allow us to determine the physics of the its low energy excitations. As we shall see in Secs. VII and VIII, these theories govern the phenomenology of the CFL phase even at densities not high enough for the weak coupling calculation of the gap parameter described in Sec. IV to be reliable. In V G we briefly mention effective field theories for some other color superconducting phases.

A. High density effective theory

The formalism discussed in Sec. IV can be extended to include higher orders in the coupling constants and the effects of nonzero quark masses. It can also be used to compute more complicated observables, like the dispersion relations of collective excitations. In practice these calculations are quite difficult, because the number of possible gap structures quickly proliferate, and it is difficult to estimate the relative importance of corrections due to the truncation of the Dyson-Schwinger equations, kinematic approximations, etc., a priori.

There are two, related, strategies for addressing these issues: effective field theories and the renormalization group. Within the effective field theory approach we try to derive an effective Lagrangian for quasi-quarks and gluons near the Fermi surface, together with a power counting scheme that can be used to determine the magnitude of diagrams constructed from the propagators and interaction terms of the theory. This is the strategy that we will describe in Secs. V A 1-V A 3 below.

In the renormalization group approach we consider a general effective action for quarks and gluons at high baryon density, and study the evolution of the action as high energy degrees of freedom, energetic gluons and quarks far away from the Fermi surface, are integrated out [72, 258]. This approach was applied to QCD with short range interactions in [259–261]. In this case one can show that for typical initial conditions the color antisymmetric, flavor antisymmetric, $J = 0$, BCS interaction does indeed grow faster than all other terms, confirming in another way the arguments of Secs. I and II that these are the channels in which the dominant diquark condensation occurs. In order to use the renormalization group approach more quantitatively, one has to deal with the unscreened long range gluon exchanges, which is more difficult. Son studied the evolution of the BCS interaction using the hard dense loop gluon propagator as an input [55]. The coupled evolution of static and dynamic screening and the BCS interaction has not been solved yet. A general scheme constructing effective actions by integrating out hard modes was proposed in [262].

1. *Effective Lagrangian*

Consider the equation of motion of a free quark with a chemical potential μ

$$(\boldsymbol{\alpha} \cdot \mathbf{p} - \mu)\, \psi_\pm = E_\pm \psi_\pm \ , \tag{57}$$

where $\psi_\pm$ are eigenvectors of $(\boldsymbol{\alpha} \cdot \hat{\mathbf{p}})$ with eigenvalue ± 1 and $E_\pm = -\mu \pm p$. If the quark momentum is near the Fermi momentum, $p \sim p_F = \mu$, then the solution ψ_+ describes a low energy excitation $E_+ \sim 0$, whereas $E_- \sim -2\mu$ corresponds to a high energy excitation. In order to construct an effective field theory based on this observation we define low and high-energy components of the quark field [263, 264]

$$\psi_\pm = e^{i p_F v_\mu x^\mu} \left(\frac{1 \pm \boldsymbol{\alpha} \cdot \hat{\mathbf{v}}_F}{2} \right) \psi \ , \tag{58}$$

where $\mathbf{v}_F$ is the Fermi velocity and $v_\mu = (1, \mathbf{v}_F)$. The prefactor removes the rapid phase variation common to all fermions in some patch on the Fermi surface specified by $\hat{\mathbf{v}}_F$. We can insert the decomposition Eq. (58) into the QCD Lagrangian and integrate out the ψ_- field as well as hard gluon exchanges. This generates an expansion of the QCD Lagrangian in powers of $1/p_F$. At tree level, integrating out the ψ_- fields is equivalent to solving their equation of motion

$$\psi_{-,L} = \frac{1}{2p_F} \left(i \boldsymbol{\alpha}_\perp \cdot \mathbf{D}\, \psi_{+,L} + \gamma^0 M \psi_{+,R} \right) \ , \tag{59}$$

where $\boldsymbol{\gamma}_\parallel \equiv \hat{\mathbf{v}}_F(\hat{\mathbf{v}}_F\cdot\boldsymbol{\gamma})$, $\boldsymbol{\gamma}_\perp = \boldsymbol{\gamma}-\boldsymbol{\gamma}_\parallel$ and M is the quark mass matrix. At $\mathcal{O}(1/p_F)$ the effective Lagrangian for ψ_+ is

$$\mathcal{L} \;=\; \psi^\dagger_{+,L}(iv^\mu D_\mu)\psi_{+,L} - \frac{1}{2p_F}\psi^\dagger_{+,L}\left[(\not{D}_\perp)^2 + MM^\dagger\right]\psi_{+,L} + \left(L\leftrightarrow R, M\leftrightarrow M^\dagger\right) + \ldots. \tag{60}$$

The low energy expansion was studied in more detail in [265]. There are a number of physical effects that have to be included in order to obtain a well-defined expansion. First, four-fermion operators have to be included. These operators naturally appear at $\mathcal{O}(1/p_F^2)$ but their effects are enhanced by the large density of states $N\sim p_F^2$ on the Fermi surface. The most important of these operators is the BCS interaction $[\psi(\mathbf{v})\psi(-\mathbf{v})][\psi^\dagger(\mathbf{v}')\psi^\dagger(-\mathbf{v}')]$. The coefficient of the BCS operator was determined in [265].

Because of the large density of states it is also necessary to resum quark loop insertions in gluon n-point functions. There is a simple generating functional for these effects, known as the hard dense loop (HDL) effective action [223]

$$\mathcal{L}_{\rm HDL} = -\frac{m^2}{2}\sum_v G^a_{\mu\alpha}\frac{v^\alpha v^\beta}{(v^\lambda D_\lambda)^2}G^a_{\mu\beta}. \tag{61}$$

This is a gauge invariant, but non-local, effective Lagrangian. Expanding $\mathcal{L}_{\rm HDL}$ in powers of the gauge field produces $2,3,\ldots$ gluon vertices. The quadratic term describes dielectric screening of electric modes and Landau damping of magnetic modes. Higher order terms contain corrections to the gluon self interaction in a dense medium.

2. Non-Fermi liquid effects and the gap equation

In this section we shall analyze the low energy expansion in the regime $\Delta < k_0 < m_g$ [266]. This energy range gives the dominant contribution to the pairing gap and other low energy constants in the superconducting phase. Since electric fields are screened the interaction is dominated by the exchange of magnetic gluons. The transverse gauge boson propagator is

$$D_{ij}(K) = -\frac{i(\delta_{ij}-\hat{k}_i\hat{k}_j)}{k_0^2-k^2+iM_g^2\frac{k_0}{k}}, \tag{62}$$

where $M_g^2 = (3\pi/4)m_g^2$ and we have assumed that $|k_0|<k$. We observe that the propagator becomes large in the regime $|k_0|\sim k^3/m_g^2$. If the energy is small, $|k_0|\ll m_g$, then the typical energy is much smaller than the typical momentum,

$$k\sim (m_g^2|k_0|)^{1/3} \gg |k_0|. \tag{63}$$

This implies that the gluon is very far off its energy shell and not a propagating state. We can compute loop diagrams containing quarks and transverse gluons by picking up the pole in the quark propagator, and then integrate over the cut in the gluon propagator using the kinematics dictated by Eq. (63). In order for a quark to absorb the large momentum carried by a gluon and stay close to the Fermi surface the gluon momentum has to be transverse to the momentum of the quark. This means that the term $k_\perp^2/(2\mu)$ in the quark propagator is relevant and has to be kept at leading order. Eq. (63) shows that $k_\perp^2/(2\mu)\gg k_0$ as $k_0\to 0$. This means that the pole of the quark propagator is governed by the condition $k_{||}\sim k_\perp^2/(2\mu)$. We find

$$k_\perp \sim g^{2/3}\mu^{2/3}k_0^{1/3}, \qquad k_{||}\sim g^{4/3}\mu^{1/3}k_0^{2/3}. \tag{64}$$

In this regime propagators and vertices can be simplified even further. The quark and gluon propagators are

$$S_{\alpha\beta}(K) = \frac{i\delta_{\alpha\beta}}{k_0-k_{||}-\frac{k_\perp^2}{2\mu}+i\epsilon{\rm sgn}(k_0)}, \tag{65}$$

$$D_{ij}(K) = \frac{i\delta_{ij}}{k_\perp^2 - iM_g^2\frac{k_0}{k_\perp}}, \tag{66}$$

and the quark gluon vertex is $gv_i(\lambda^a/2)$. Higher order corrections can be found by expanding the quark and gluon propagators as well as the HDL vertices in powers of the small parameter $\epsilon\equiv(k_0/m)$.

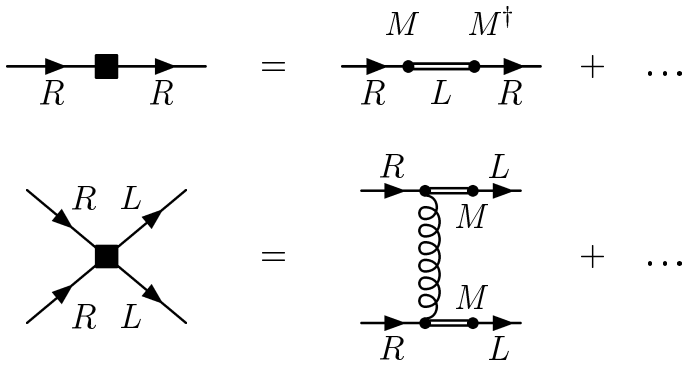

FIG. 5: Mass terms in the high density effective theory. The first diagram shows a $\mathcal{O}(MM^\dagger)$ term that arises from integrating out the ψ_- field in the QCD Lagrangian. The second diagram shows a $\mathcal{O}(M^2)$ four-fermion operator which arises from integrating out ψ_- and hard gluon exchanges.

The regime characterized by Eq. (64) is completely perturbative, i.e. graphs with extra loops are always suppressed by extra powers of $\epsilon^{1/3}$ [266]. The power of ϵ can be found by using the fact that loop integrals scale as $(k_0 k_{||} k_\perp^2) \sim k_0^{7/3}$, fermion propagators scale as $1/k_{||} \sim 1/k_0^{2/3}$, gluon propagators scale as $1/k_\perp^2 \sim 1/k_0^{2/3}$, and the quark-gluon vertex scales as a constant. Quark matter in the regime $\Delta < k_0 < m$ is a non-Fermi liquid. The excitations are quasi-particles with the quantum numbers of quarks, but Green functions scale with fractional powers and logarithms of the energy and the coupling constant [67, 222, 267].

The corrections to Fermi liquid theory do not upset the logic that underlies the argument that leads to the BCS instability. For quark pairs with back-to-back momenta the basic one gluon exchange interaction has to be summed to all orders, but all other interactions remain perturbative [266]. The gap equation that sums the leading order transverse gluon exchange in the color-anti-symmetric channel is

$$\Delta(p_0) \;=\; -i\frac{2g^2}{3}\int\frac{dk_0}{2\pi}\int\frac{dk_\perp^2}{(2\pi)^2}\;\frac{k_\perp}{k_\perp^3 + iM_g^2(k_0-p_0)}\int\frac{dk_{||}}{2\pi}\;\frac{\Delta(k_0)}{k_0^2+k_{||}^2+\Delta(k_0)^2}. \tag{67}$$

This equation is exactly equivalent to Eq. (41). In particular, all the kinematic approximations that were used to derive Eq. (41), like the low energy approximation to the HDL self energies and the forward approximation to the Dirac traces, are built into the effective field theory vertices and propagators. The effective theory can now be used to study corrections to the leading order result. Higher order corrections to the propagators and vertices of the effective theory modify the kernel of the integral equation Eq. (67). The resulting correction to the gap function can be computed perturbatively, without having to solve the integral equation again, using a method that is similar to Rayleigh-Schrödinger perturbation theory [64, 265].

The coefficients b_0 and $\bar{b}_0$ introduced in Sec. IV D can be determined by matching the four-fermion operators in the effective theory [265]. The b_0 term also receives contributions from the fermion wave function renormalization $Z \sim \log(k_0)$. All other terms give corrections beyond $\mathcal{O}(g^0)$ in $\log(\Delta_0/\mu)$. Vertex corrections scale as $\Gamma \sim p_0^{1/3}$ and are suppressed compared to the fermion wave function renormalization. The analogous statement in the case of phonon-induced electronic superconductors is known as Migdal's theorem. Gluon self energy insertions beyond the $k_0/k_\perp$ term included in the leading order propagator are also suppressed by fractional powers of the coupling and the gluon energy.

3. Mass terms

A systematic determination of mass corrections to the high density effective theory is needed for calculations of the Goldstone boson masses in the CFL phase, and in order to understand the response of the CFL ground state to nonzero quark masses. Mass terms affect both the quark propagator and the quark-quark interaction. From Eq. (59) and (60) we see that integrating out the ψ_- field gives a correction to the energy of the ψ_+ field of the form $MM^\dagger/(2p_F)$. This term can be viewed as an effective flavor dependent chemical potential. We also note that this term is just the first in a tower of operators that arise from expanding out the energy of a free massive quark, $E = (p^2+m^2)^{1/2}$, for momenta near the Fermi surface. Higher order terms correspond to additional corrections to the chemical potential, the Fermi velocity, and to non-linear terms in the dispersion relation.

There are no mass corrections to the quark-gluon vertex at $\mathcal{O}(1/p_F^2)$. There are, however, mass corrections to the quark-quark interaction. In connection with color superconductivity we are mainly interested in the BCS interaction. The diagram shown in Fig. 5 gives [268]

$$\mathcal{L} \;=\; \frac{g^2}{32p_F^4}\left(\psi^{a\,\dagger}_{i,L}C\psi^{b\,\dagger}_{j,L}\right)\left(\psi^{c}_{k,R}C\psi^{d}_{l,R}\right)\left[(\boldsymbol{\lambda})^{ac}(\boldsymbol{\lambda})^{bd}(M)_{ik}(M)_{jl}\right] \;+\; \left(L\leftrightarrow R, M\leftrightarrow M^\dagger\right)\,. \tag{68}$$

This is the leading interaction that couples the gap equations for left and right handed fermions. We shall also see that the mass correction to the BCS interaction gives the leading contribution to the mass shift in the condensation energy, and the masses of the Goldstone bosons.

B. Ginzburg-Landau theory

At zero temperature fluctuations of the superconducting state are dominated by fluctuations of the phase of the order parameter. Near the critical temperature the gap becomes small and fluctuations of the magnitude of the gap are important, too. This regime can be described using the Ginzburg-Landau theory. Ginzburg and Landau argued that in the vicinity of a second order phase transition the thermodynamic potential of the system can be expanded in powers of the order parameter and its derivatives. This method was used very successfully in the study of superfluid phases of ^{3}He.

The Ginzburg-Landau approach was first applied to color superconductivity in [20]. The problem was revisited by [84], who included the effects of unscreened gluon exchanges and charge neutrality. Consider the s-wave color anti-triplet condensate in QCD with three massless flavors. The order parameter can be written as

$$\langle\psi^\alpha_i C\gamma_5\psi^\beta_j\rangle = \epsilon^{\alpha\beta A}\epsilon_{ijB}\phi^B_A \tag{69}$$

where ϕ^B_A is a matrix in color-flavor space. Note that here we have included the energy gap into ϕ^B_A, in contrast to Eq. (24), where ϕ^B_A is dimensionless. We have fixed the orientations of left and right-handed condensates. Fluctuations in the relative color-flavor orientation of the left- and right-handed fermions correspond to the Goldstone modes related to chiral symmetry breaking, and will be considered in Sec. V C. Therefore, the ansatz (69) implies the assumption that chiral fluctuations near T_c are small compared to non-chiral gap fluctuations and fluctuations of the gauge field. The thermodynamic potential can be expanded as

$$\Omega \;=\; \Omega_0 + \alpha\,\mathrm{Tr}\left(\phi^\dagger\phi\right) + \beta_1\left[\mathrm{Tr}\left(\phi^\dagger\phi\right)\right]^2 + \beta_2\,\mathrm{Tr}\left(\left[\phi^\dagger\phi\right]^2\right) + \kappa\,\mathrm{Tr}\left(\nabla\phi\nabla\phi^\dagger\right) + \ldots \tag{70}$$

The coefficients α, β_i, κ can be treated as unknown parameters, or determined in QCD at weak coupling. The weak coupling QCD result is [84]

$$\alpha \;=\; 4N\frac{T-T_c}{T}, \quad \beta_1 = \beta_2 = \frac{7\zeta(3)}{8(\pi T_c)^2}\,N, \tag{71}$$

$$\kappa \;=\; \frac{7\zeta(3)}{8\pi^2 T_c^2}\,N \tag{72}$$

where $N = \mu^2/(2\pi^2)$ is the density of states on the Fermi surface. This result agrees with the BCS result. Using Eq. (71) we can verify that the ground state is in the CFL phase $\phi^B_A \sim \delta^B_A$. We can also study many other issues, like the gluon screening lengths, the structure of vortices, the effects of electric and color neutrality, and the effects of nonzero quark masses [110, 269, 270].

From the study of electronic superconductors, it is known that the nature of the finite temperature phase transition depends on the ratio $\kappa = \lambda/\xi$ of the screening length λ and the correlation length ξ. If $\kappa > 1/\sqrt{2}$ the superconductor is type II, fluctuations of the order parameter are more important than fluctuations of the gauge field, and the transition is second order. In a type I superconductor the situation is reversed, and fluctuations of the gauge field drive the transition first order [271].

In the weak coupling limit, $\xi \sim 1/\Delta \gg \lambda \sim 1/(g\mu)$ and color superconductivity is strongly type I. The role of gauge field fluctuations was studied in [21, 272–275]. The contribution to the thermodynamic potential is

$$\Omega_{fl} = 8T\int\frac{d^3k}{(2\pi)^3}\left\{\log\left(1+\frac{m_A^2(k)}{k^2}\right) - \frac{m_A^2(k)}{k^2}\right\}, \tag{73}$$

where $m_A(k)$ is the gauge field screening mass. In QCD the momentum dependence of m_A cannot be neglected. The contribution of the fluctuations Ω_{fl} induces a cubic term $\propto \phi^3$ in the thermodynamic potential which drives the transition first order. The first order transition occurs at a critical temperature T_c^* [275]

$$\frac{T_c^* - T_c}{T_c} = \frac{\pi^2}{12\sqrt{2}}\, g, \tag{74}$$

where T_c is the critical temperature of the second order transition obtained upon neglecting the cubic term. Although the result (74) cannot be trusted quantitatively at accessible densities, say $\mu \sim 400$ MeV where $g \sim 3.6$, it does make it clear that the phase transition between the CFL (or 2SC) phase and the quark-gluon plasma will be strongly first order. Noronha et al. [274] argue that Eq. (74) gives the complete $O(g)$ correction to the critical temperature (see, however, [273]). This implies that the transition to the color superconducting phase will occur at a critical temperature that is significantly elevated relative to the BCS estimate $T_c = 0.57\Delta$ that we obtained in Sec. IV E. The effects of gluon fluctuations are much more important here than those of photon fluctuations in a conventional type I superconductor.

C. Goldstone bosons in the CFL phase

1. *Effective Lagrangian*

In the CFL phase the pattern of chiral symmetry breaking is identical to the one at $T = \mu = 0$. This implies that the effective Lagrangian has the same structure as chiral perturbation theory. The main difference is that Lorentz-invariance is broken and only rotational invariance is a good symmetry. The effective Lagrangian for the Goldstone modes is given by [276]

$$\begin{aligned}\mathcal{L}_{\rm eff} &= \frac{f_\pi^2}{4}{\rm Tr}\left[\partial_0\Sigma\partial_0\Sigma^\dagger - v_\pi^2\partial_i\Sigma\partial_i\Sigma^\dagger\right] + \left[B{\rm Tr}(M\Sigma^\dagger) + h.c.\right] \\ &\quad + \left[A_1{\rm Tr}(M\Sigma^\dagger){\rm Tr}(M\Sigma^\dagger) + A_2{\rm Tr}(M\Sigma^\dagger M\Sigma^\dagger) + A_3{\rm Tr}(M\Sigma^\dagger){\rm Tr}(M^\dagger\Sigma) + h.c.\right] + \ldots .\end{aligned} \tag{75}$$

Here $\Sigma = \exp(i\phi^a\lambda^a/f_\pi)$ is the chiral field, f_π is the pion decay constant and M is a complex mass matrix. The fields ϕ^a describe the octet of Goldstone bosons $(\pi^\pm, \pi^0, K^\pm, K^0, \bar{K}^0, \eta)$. These Goldstone bosons are an octet under the unbroken $SU(3)_{c+L+R}$ symmetry of the CFL phase and their $\tilde{Q}$-charges under the unbroken gauge symmetry of the CFL phase are ± 1 and 0 as indicated by the superscripts, meaning that they have the same $\tilde{Q}$-charges as the Q-charges of the vacuum pseudoscalar mesons. The chiral field and the mass matrix transform as $\Sigma \to L\Sigma R^\dagger$ and $M \to LMR^\dagger$ under chiral transformations $(L, R) \in SU(3)_L \times SU(3)_R$. For the present, we have suppressed the singlet fields associated with the breaking of the exact $U(1)_B$ and approximate $U(1)_A$ symmetries. We will give the effective Lagrangian for the massless Goldstone boson associated with superfluidity (i.e. from $U(1)_B$ breaking) below.

The form of the effective Lagrangian follows from the symmetries of the CFL phase. It is nevertheless useful to understand how this Lagrangian arises upon integrating out high energy degrees of freedom. We start from the high density effective Lagrangian in the presence of a CFL gap term

$$\mathcal{L} = {\rm Tr}\left[\psi_L^\dagger(iv^\mu D_\mu)\psi_L\right] + \frac{\Delta}{2}\left\{{\rm Tr}\left(X^\dagger\psi_L X^\dagger\psi_L\right) - \left[{\rm Tr}\left(X^\dagger\psi_L\right)\right]^2 + h.c.\right\} + (L \leftrightarrow R, X \leftrightarrow Y)\,. \tag{76}$$

Here, $\psi_{L,R}$ are left and right-handed quark fields which transform as $\psi_L \to L\psi_L U^T$ and $\psi_R \to R\psi_R U^T$ under chiral transformations $(L, R) \in SU(3)_L \times SU(3)_R$ and color transformations $U \in SU(3)_c$. We have suppressed the spinor indices and defined $\psi\psi = \psi^\alpha C^{\alpha\beta}\psi^\beta$, where C is the charge conjugation matrix. The traces run over color or flavor indices and X, Y are fields that transform as $X \to LXU^T$ and $Y \to RYU^T$. We will assume that the vacuum expectation value is $\langle X\rangle = \langle Y\rangle = 1$. This corresponds to the CFL gap term $\Delta\psi_i^\alpha\psi_j^\beta\,\epsilon_{\alpha\beta A}\epsilon^{ijA}$. X, Y parametrize fluctuations around the CFL ground state. Note that fluctuations of the type $X = Y$ correspond to the field ϕ introduced in the previous section.

For simplicity we have assumed that the gap term is completely anti-symmetric in flavor. We will derive the effective Lagrangian in the chiral limit $M = M^\dagger = 0$ and study mass terms later. We can redefine the fermion fields according to

$$\chi_L \equiv \psi_L X^\dagger, \qquad \chi_R \equiv \psi_R Y^\dagger. \tag{77}$$

In terms of the new fields the Lagrangian takes the form

$$\begin{aligned}\mathcal{L} &= \mathrm{Tr}\left[\chi_L^\dagger (iv^\mu\partial_\mu)\chi_L\right] - i\,\mathrm{Tr}\left[\chi_L^\dagger \chi_L X v^\mu \left(\partial_\mu - iA_\mu^T\right) X^\dagger\right] \\ &\quad + \frac{\Delta}{2}\left\{\mathrm{Tr}\left(\chi_L\chi_L\right) - \left[\mathrm{Tr}\left(\chi_L\right)\right]^2\right\} + (L\leftrightarrow R, X\leftrightarrow Y)\,. \end{aligned} \tag{78}$$

At energies below the gap we can integrate out the fermions. The fermion determinant generates a kinetic term for the chiral fields X and Y [276]

$$\mathcal{L} = -\frac{f_\pi^2}{2}\mathrm{Tr}\left[(X^\dagger D_0 X)^2 - v_\pi^2 (X^\dagger D_i X)^2\right] + (X\leftrightarrow Y) \tag{79}$$

For simplicity we have ignored the flavor singlet components of X and Y.

The low energy constants f_π and v_π were calculated by matching the effective theory to weak coupling QCD calculations in [246, 277], see also [142, 249, 278, 279]. The results are

$$f_\pi^2 = \frac{21-8\log 2}{18}\frac{\mu^2}{2\pi^2}, \qquad v_\pi^2 = \frac{1}{3}. \tag{80}$$

The simplest way to derive these results, given the results that we have already reviewed in Sec. IV F, is to recall that the gluon field acquires a magnetic mass due to the Higgs mechanism and an electric mass due to Debye screening, and then to notice that Eq. (79) shows that the electric mass is $m_D^2 = g^2 f_\pi^2$, while the magnetic mass is $m_M^2 = v_\pi^2 m_D^2$. This means that f_π and v_π are determined by the Debye and Meissner masses for the gluons in the CFL phase that we have presented in Sec. IV F, see Eq. (52) and Table II.

Since the gluon is heavy, it can also be integrated out. Using Eq. (79) we get

$$A_\mu^T = \frac{i}{2}\left(X^\dagger\partial_\mu X + Y^\dagger\partial_\mu Y\right) + \ldots \tag{81}$$

This result can be substituted back into the effective Lagrangian. The result is

$$\mathcal{L}_{\rm eff} = \frac{f_\pi^2}{4}\mathrm{Tr}\left[\partial_0\Sigma\partial_0\Sigma^\dagger - v_\pi^2\partial_i\Sigma\partial_i\Sigma^\dagger\right]\ , \tag{82}$$

where the Goldstone boson field is given by $\Sigma = XY^\dagger$. This shows that the light degrees of freedom correspond to fluctuations of the color-flavor orientation of the left-handed CFL condensate relative to the right-handed one, as expected since these are the fluctuations associated with the spontaneously broken global symmetry.

2. $U(1)_B$ modes and superfluid hydrodynamics

Finally, we quickly summarize the effective theory for the $U(1)_B$ Goldstone mode. At order $\mathcal{O}((\partial\varphi)^2)$ we get [246, 277]

$$\mathcal{L} = \frac{f^2}{2}\left[(\partial_0\varphi)^2 - v^2(\nabla\varphi)^2\right] + \ldots, \tag{83}$$

where the low energy constants f and v are given by

$$f^2 = \frac{6\mu^2}{\pi^2}, \qquad v^2 = \frac{1}{3}. \tag{84}$$

The field φ transforms as $\varphi\to\varphi+\alpha$ under $U(1)_B$ transformation of the quark fields $\psi\to\exp(i\alpha)\psi$. Because $U(1)_B$ is an Abelian symmetry, the two-derivative terms do not contain any Goldstone boson self interactions. These terms are needed in order to compute transport properties of the CFL phase. Son noticed that self-interactions are constrained by Lorentz invariance (of the microscopic theory) and $U(1)_B$ invariance [280]. The analogous argument for non-relativistic superfluids is described in [281]. To leading order in g the effective theory of the $U(1)_B$ Goldstone boson can be written as

$$\mathcal{L} = \frac{3}{4\pi^2}\left[(\partial_0\varphi-\mu)^2 - (\nabla\varphi)^2\right]^2 + \ldots, \tag{85}$$

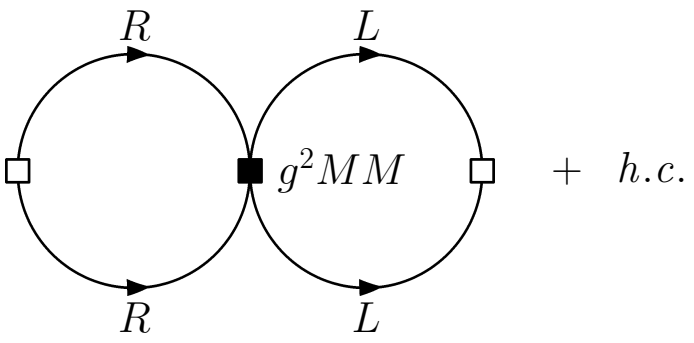

FIG. 6: Contribution of the $\mathcal{O}(M^2)$ BCS four-fermion operator to the condensation energy in the CFL phase. The open squares correspond to insertions of the anomalous self energy Δ.

where the omitted terms are of the form $\partial^i\varphi^k$ with $i > k$. Expanding Eq. (85) to second order in derivatives reproduces Eq. (83). In addition to that, Eq. (85) contains the leading three and four boson interactions. Using microscopic models one can obtain more detailed information on the properties of collective modes. A calculation of the spectral properties of the φ mode in an NJL model at $T = 0$ and $T \neq 0$ can be found in [99].

The spontaneous breaking of $U(1)_B$ is related to superfluidity, and the $U(1)_B$ effective theory can be interpreted as superfluid hydrodynamics [280]. We can define the fluid velocity as

$$u_\alpha = -\frac{1}{\mu_0} D_\alpha\varphi, \tag{86}$$

where $D_\alpha\varphi \equiv \partial_\alpha\varphi + (\mu, \mathbf{0})$ and $\mu_0 \equiv (D_\alpha\varphi D^\alpha\varphi)^{1/2}$. Note that this definition ensures that the flow is irrotational, $\nabla \times \mathbf{u} = 0$. The identification (86) is motivated by the fact that the equation of motion for the $U(1)$ field φ can be written as a continuity equation

$$\partial^\alpha(n_0 u_\alpha) = 0, \tag{87}$$

where $n_0 = 3\mu_0^3/\pi^2$ is the superfluid number density. At $T = 0$ the superfluid density is equal to the total density of the system, $n = dP/d\mu|_{\mu=\mu_0}$. The energy-momentum tensor has the ideal fluid form

$$T_{\alpha\beta} = (\epsilon + P)u_\alpha u_\beta - P g_{\alpha\beta}, \tag{88}$$

and the conservation law $\partial^\alpha T_{\alpha\beta} = 0$ corresponds to the relativistic Euler equation of ideal fluid dynamics. We conclude that the effective theory for the $U(1)_B$ Goldstone mode accounts for the defining characteristics of a superfluid: irrotational, non-dissipative hydrodynamic flow.

3. Mass terms

The structure of the mass terms in Eq. (75) is completely determined by chiral symmetry. The coefficients B, A_i can be determined by repeating the steps discussed in the previous section, but keeping the mass terms in the high density effective theory. In practice it is somewhat easier to compute the coefficients of the chiral Lagrangian using matching arguments. For example, we noticed that the easiest way to determine f_π is to compute the gluon screening mass in the microscopic theory.

In Sec. V A 3 we showed that $X_L \equiv MM^\dagger/(2p_F)$ and $X_R \equiv M^\dagger M/(2p_F)$ act as effective chemical potentials for left and right-handed fermions, respectively. Formally, the effective Lagrangian has an $SU(3)_L \times SU(3)_R$ gauge symmetry under which $X_{L,R}$ transform as the temporal components of non-Abelian gauge fields. We can implement this approximate gauge symmetry in the CFL chiral theory by promoting time derivatives to covariant derivatives [142],

$$\partial_0\Sigma \to \nabla_0\Sigma \equiv \partial_0\Sigma + i\left(\frac{MM^\dagger}{2p_F}\right)\Sigma - i\Sigma\left(\frac{M^\dagger M}{2p_F}\right). \tag{89}$$

The mass dependent terms in the quark-quark interaction contribute to the gap and to the condensation energy. In the chiral theory the shift in the condensation energy due to the quark masses is

$$\mathcal{E} \;=\; -B\mathrm{Tr}(M) - A_1\left[\mathrm{Tr}(M)\right]^2 - A_2\mathrm{Tr}\left(M^2\right) - A_3\mathrm{Tr}(M)\mathrm{Tr}(M^\dagger) + h.c. + \ldots. \tag{90}$$

The contribution to the condensation energy from the mass correction to the BCS interaction is shown in Fig. 6. The diagram is proportional to the square of the condensate

$$\langle \psi^\alpha_{i,L} C \psi^\beta_{j,L} \rangle = \epsilon^{\alpha\beta A}\epsilon_{ijA}\Delta \frac{3\sqrt{2}\pi}{g}\left(\frac{\mu^2}{2\pi^2}\right), \tag{91}$$

with the dependence on the mass matrix M arising from the contraction of the BCS interaction with the CFL condensate. We get

$$\epsilon^{\alpha\beta A}\epsilon_{ijA}\,(T^a)^{\alpha\gamma}\,(T^a)^{\beta\delta}\,(M)_{ik}(M)_{jl}\epsilon^{\gamma\delta B}\epsilon_{klB} = -\frac{4}{3}\left\{\Big(\mathrm{Tr}[M]\Big)^2 - \mathrm{Tr}\Big[M^2\Big]\right\}, \tag{92}$$

where $T^a = \lambda^a/2$. We note that the four-fermion operator is proportional to g^2 and the explicit dependence of the diagram on g cancels. We find [246, 268, 277]

$$\mathcal{E} = -\frac{3\Delta^2}{4\pi^2}\left\{\Big(\mathrm{Tr}[M]\Big)^2 - \mathrm{Tr}\Big[M^2\Big]\right\} + \Big(M \leftrightarrow M^\dagger\Big). \tag{93}$$

This result can be matched against Eq. (90). We find $B = 0$ and

$$A_1 = -A_2 = \frac{3\Delta^2}{4\pi^2} \equiv A, \qquad A_3 = 0. \tag{94}$$

The result $A_1 = -A_2$ reflects the fact that the CFL order parameter is anti-symmetric in flavor (pure $\bar{\mathbf{3}}$) to leading order in g. Using Eqs. (89) and (94) we can compute the energies of the flavored Goldstone bosons

$$\begin{aligned}
E_{\pi^\pm} &= \mu_{\pi^\pm} + \left[v_\pi^2 p^2 + \frac{4A}{f_\pi^2}(m_u + m_d)m_s\right]^{1/2}, \\
E_{K^\pm} &= \mu_{K^\pm} + \left[v_\pi^2 p^2 + \frac{4A}{f_\pi^2} m_d(m_u + m_s)\right]^{1/2}, \\
E_{K^0,\bar{K}^0} &= \mu_{K^0,\bar{K}^0} + \left[v_\pi^2 p^2 + \frac{4A}{f_\pi^2} m_u(m_d + m_s)\right]^{1/2},
\end{aligned} \tag{95}$$

where

$$\begin{aligned}
\mu_{\pi^\pm} &= \mp\frac{m_d^2 - m_u^2}{2\mu}, \qquad \mu_{K^\pm} = \mp\frac{m_s^2 - m_u^2}{2\mu}, \\
\mu_{K^0,\bar{K}^0} &= \mp\frac{m_s^2 - m_d^2}{2\mu}.
\end{aligned} \tag{96}$$

The mass matrix for the remaining neutral Goldstone bosons, which mix, can be found in [246, 277, 278]. We observe that the $\mathcal{O}(m)$ terms lead to an inverted mass spectrum with the kaons being lighter than the pions. This can be understood from the microscopic derivation of the chiral Lagrangian. The Goldstone boson field is $\Sigma = XY^\dagger$, and a mode with the quantum number of the pion is given by $\pi^+ \sim \epsilon^{abc}\epsilon^{ade}(\bar{d}^b_R \bar{s}^c_R)(u^d_L s^e_L)$. The structure of the field operators suggests that the mass is controlled by $(m_u + m_d)m_s$. By the same argument the mass of the K^+ is governed by $(m_u + m_s)m_d$, and $m_K < m_\pi$. We also note that the $\mathcal{O}(m^2)$ terms split the energies of different charge states. This can be understood from the fact that these terms act as an effective chemical potential for flavor. Explicit calculations in an NJL model reproduce f_π in (80) and the results (95), albeit with a different value of A [282, 283]. This serves as a reminder that in the CFL phase at moderate densities, the effective theory is valid but the values of coefficients in it may not take on the values obtained by matching to high density calculations.

In perturbation theory the coefficient B of the $\mathrm{Tr}(M\Sigma)$ term is zero. B receives non-perturbative contributions from instantons. Instantons are semi-classical gauge configurations in the Euclidean time functional integral that induce a fermion vertex of the form [284]

$$\mathcal{L} \sim G \det_f(\bar{\psi}_L \psi_R) + h.c., \tag{97}$$

where $\det_f$ denotes a determinant in flavor space. The 't Hooft vertex (97) can be written as the product of the CFL condensate and its conjugate times $\langle\bar{\psi}\psi\rangle$, meaning that in the CFL phase Eq. (97) induces a nonzero quark

condensate $\langle\bar{\psi}\psi\rangle$, as well as Goldstone boson masses $m_{GB}^2 \sim m\langle\bar{\psi}\psi\rangle/f_\pi^2$. The instanton has gauge field $A_\mu \sim 1/g$, so its action is $S = 8\pi^2/g^2$. The effective coupling G is proportional to $\exp(-S) \sim \exp(-8\pi^2/g^2)$, where g is the running coupling constant at a scale set by the instanton size ρ.

In dense quark matter perturbative gauge field screening suppresses instantons of size $\rho > 1/\mu$, and the effective coupling G can be computed reliably [143]. Combined with the weak coupling result for $\langle\psi\psi\rangle$, see Eq. (91), we get

$$B = c\left[\frac{3\sqrt{2}\pi}{g}\Delta\left(\frac{\mu^2}{2\pi^2}\right)\right]^2\left(\frac{8\pi^2}{g^2}\right)^6\frac{\Lambda_{QCD}^9}{\mu^{12}}, \tag{98}$$

where $c = 0.155$ and Λ_{QCD} is the QCD scale factor. In terms of B, $\langle\bar{\psi}\psi\rangle = -2B$ and the instanton contribution to the K^0 mass is $\delta m_{K^0}^2 = B(m_d + m_s)/(2f_\pi^2)$ [285]. In the weak coupling limit, $\mu \gg \Lambda_{QCD}$, the instanton contribution is very small. However, because of the strong dependence on Λ_{QCD} the numerical value of B is quite uncertain. Using phenomenological constraints on the instanton size distribution [143] concluded that the instanton contribution to the kaon mass at $\mu = 500$ MeV is of order 10 MeV.

Finally, we summarize the structure of the chiral expansion in the CFL phase. Ignoring non-perturbative effects the effective Lagrangian has the form

$$\mathcal{L} \sim f_\pi^2\Delta^2\left(\frac{\partial_0\Sigma}{\Delta}\right)^k\left(\frac{\vec{\partial}\Sigma}{\Delta}\right)^l\left(\frac{MM^\dagger}{\mu\Delta}\right)^m\left(\frac{MM}{\mu^2}\right)^n. \tag{99}$$

Higher order vertices are suppressed by $\partial\Sigma/\Delta$ whereas Goldstone boson loops are suppressed by powers of $\partial\Sigma/(4\pi f_\pi)$. Since the pion decay constant scales as $f_\pi \sim \mu$ the effects of Goldstone boson loops can be neglected relative to higher order contact interactions. This is different from chiral perturbation theory at zero baryon density. We also note that the quark mass expansion contains two parameters, m^2/μ^2 and $m^2/(\mu\Delta)$. Since $\Delta \ll \mu$ the chiral expansion breaks down if $m^2 \sim \mu\Delta$. This is the same scale at which BCS calculations find a transition from the CFL phase to a less symmetric state. We also note that the result for the Goldstone boson energies given in Eq. (95) contains terms of $\mathcal{O}(m^2/\mu^2)$ and $\mathcal{O}([m^2/(\mu\Delta)]^2)$, but neglects corrections of $\mathcal{O}([m^2/\mu^2]^2)$.

The effective Lagrangians (75) and (83) describe the physics of the low momentum pseudo-Goldstone and Goldstone bosons of the CFL phase at any density. We have described the weak coupling computation of the coefficients f_π, v_π, A_1, A_2, A_3, B, f and v as well as the $\mu_{\rm eff}$'s in (96). With the exception of B, all these results are expressed simply in terms of Δ, μ and the quark masses, with g not appearing anywhere. This suggests that the range of validity of these results, when viewed as a function of Δ, is bigger than the range of validity of the weak coupling calculations on which they are based. As we decrease the density down from the very large densities at which the weak coupling calculation of Δ is under control, there is no indication that the relations between the effective theory coefficients and Δ and μ that we have derived in this section break down. The only sense in which we lose control of our understanding of the CFL phase is that we must treat Δ as a parameter, in terms of which all the other effective theory coefficients are known. Since B introduces $U(1)_A$-breaking physics that is not present at weak coupling and that does not enter the effective theory through any other coupling, it is not well constrained.

D. Kaon condensation

If the effective chemical potential in Eq. (96) becomes larger than the corresponding mass term in Eq. (95), then the energy of a Goldstone boson can become negative. In the physically relevant case $m_s \gg m_u \sim m_d$ this applies in particular to the K^0 and the K^+. When the Goldstone boson energy becomes negative the CFL ground state is reorganized and a Goldstone boson condensate is formed. The physical reason is that a nonzero m_s disfavors strange quarks relative to non-strange quarks. In normal quark matter the system responds to this stress by turning s quarks into (mostly) d quarks. In CFL matter this is difficult, since all quarks are gapped. Instead, the system can respond by populating mesons that contain d quarks and s holes.

The ground state can be determined from the effective potential

$$V_{\rm eff} \;=\; \frac{f_\pi^2}{4}{\rm Tr}\left[2X_L\Sigma X_R\Sigma^\dagger - X_L^2 - X_R^2\right] - A_1\left\{\left[{\rm Tr}(M\Sigma^\dagger)\right]^2 - {\rm Tr}\left[(M\Sigma^\dagger)^2\right]\right\}, \tag{100}$$

where $X_L = MM^\dagger/(2p_F)$, $X_R = M^\dagger M/(2p_F)$ and $M = {\rm diag}(m_u, m_d, m_s) = {\rm diag}(m, m, m_s)$. Here we only discuss the $T = 0$ case. For nonzero temperature effects, in particular the calculation of the critical temperature of kaon condensation, see [287]. The first term on the right-hand side of Eq. (100) contains the effective chemical potential

$$\mu_s \equiv -\mu_{K^0} \simeq \frac{m_s^2}{2p_F} \tag{101}$$

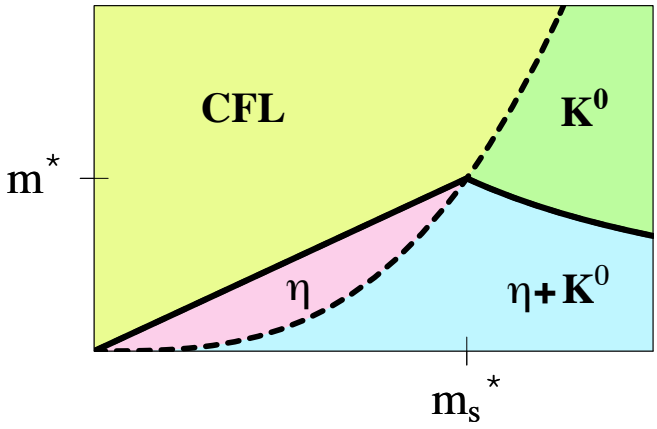

FIG. 7: (Color online) Phase structure of CFL matter as a function of the light quark mass m and the strange quark mass m_s, from [286]. CFL denotes pure CFL matter, while K^0 and η denote CFL phases with K^0 and/or η condensation. Solid lines are first order transitions, dashed lines are second order. Instanton effects have been neglected.

and favors states with a deficit of strange quarks. The second term favors the neutral ground state $\Sigma = 1$. The lightest excitation with positive strangeness is the K^0 meson. We consider the ansatz $\Sigma = \exp(i\alpha\lambda_4)$ which allows the order parameter to rotate in the K^0 direction. The vacuum energy is

$$V(\alpha) \;=\; f_\pi^2\left[-\frac{1}{2}\Big(\frac{m_s^2-m^2}{2p_F}\Big)^2\sin^2\alpha + m_{K^0}^2(1-\cos\alpha)\right], \tag{102}$$

where $m_{K^0}^2 = (4A_1/f_\pi^2)m_u(m_d+m_s) + B(m_d+m_s)/(2f_\pi^2)$. Minimizing the vacuum energy we obtain

$$\cos(\alpha) = \begin{cases} 1 & \mu_s < m_{K^0} \\ \frac{m_{K^0}^2}{\mu_s^2} & \mu_s > m_{K^0} \end{cases} \tag{103}$$

We conclude that there is a second order phase transition to a kaon condensed state at $\mu_s = m_{K^0}$. The strange quark mass breaks the $SU(3)$ flavor symmetry to $SU(2)_I \times U(1)_Y$. In the kaon condensed phase this symmetry is spontaneously broken to $U(1)_{\tilde{Q}}$. If $m_u = m_d$, isospin is an exact symmetry and there are two exact Goldstone modes [288, 289] with zero energy gap, the K^0 and the K^+. Isospin breaking leads to a small energy gap for the K^+.

Using the perturbative result for A_1, and neglecting instanton effects by setting $B = 0$, we can get an estimate of the critical strange quark mass. The critical strange quark mass scales as $m_u^{1/3}\Delta^{2/3}$. Taking $\mu = 500$ MeV, $\Delta = 50$ MeV, $m_u = 4$ MeV and $m_d = 7$ MeV, we find $m_s^{\rm crit} \simeq 68$ MeV, a result that corresponds to $m_{K^0}^{\rm crit} = 5$ MeV. If instanton contributions increase m_{K^0} by 10 MeV, this would increase $m_s^{\rm crit}$ to 103 MeV, corresponding to the onset of kaon condensation depicted in Fig. 3.

The difference in condensation energy between the CFL phase and the kaon condensed state is not necessarily small. In the limit $\mu_s \to \Delta$ we have $\sin\alpha \sim 1$ and $V(\alpha) \sim f_\pi^2\Delta^2/2$. Since f_π^2 is of order $\mu^2/(2\pi^2)$ this is an $\mathcal{O}(1)$ correction to the pairing energy in the CFL phase. Microscopic NJL model calculations of the condensation energy in the kaon condensed phase can be found in [144, 145, 282, 283, 290], see also [291, 292].

The CFL phase also contains a very light flavor neutral mode which can potentially become unstable. This mode is a linear combination of the η and η' and its mass is proportional to $m_u m_d$. Because this mode has zero strangeness it is not affected by the μ_s term in the effective potential. However, since $m_u, m_d \ll m_s$ this state is sensitive to perturbative $\alpha_s m_s^2$ corrections [286]. The resulting phase diagram is shown in Fig. 7. The precise value of the tetra-critical point (m^*, m_s^*) depends sensitively on the value of the coupling constant. At very high density m^* is extremely small, but at moderate density m^* can become as large as 5 MeV, comparable to the physical values of the up and down quark mass.

E. Fermions in the CFL phase

A single quark excitation with energy close to Δ is long-lived and interacts only weakly with the Goldstone modes in the CFL phase. This means that it is possible to include quarks in the chiral Lagrangian. This Lagrangian not

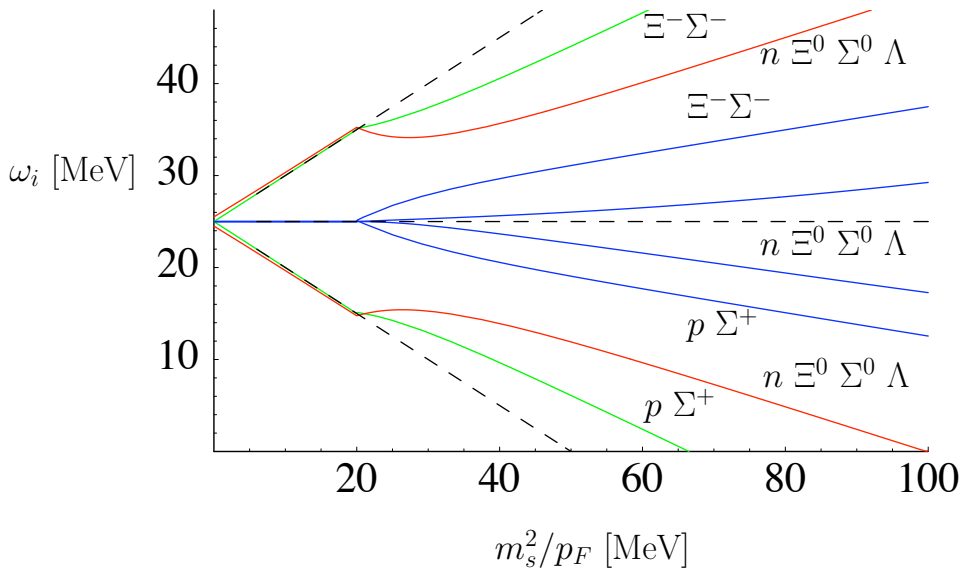

FIG. 8: (Color online) This figure shows the fermion spectrum in the CFL phase. For $m_s = 0$ there are eight fermions with gap Δ (set to 25 MeV as in Fig. 3) and one fermion with gap 2Δ (not shown). As discussed in Sec. III, the octet quasiparticles have the $SU(3)$ and $U(1)_{\tilde{\mathrm{Q}}}$ quantum numbers of the octet baryons. Without kaon condensation gapless fermion modes appear at $\mu_s = \Delta$ (dashed lines). With kaon condensation gapless modes appear at $\mu_s = 4\Delta/3$. (Note that the scale on the horizontal axis is $2\mu_s$.)

only controls the interaction of quarks with pions and kaons, but it also constrains the dependence of the gap in the fermionic quasiparticle spectrum on the quark masses. This is of interest in connection with the existence and stability of the gapless CFL phase [91], as we have discussed in Secs. I E, II B, and III B.

The effective Lagrangian for fermions in the CFL phase is [174, 175]

$$\begin{aligned}\mathcal{L} &= \mathrm{Tr}\left(N^\dagger i v^\mu D_\mu N\right) - D\mathrm{Tr}\left(N^\dagger v^\mu \gamma_5 \{\mathcal{A}_\mu, N\}\right) - F\mathrm{Tr}\left(N^\dagger v^\mu \gamma_5 [\mathcal{A}_\mu, N]\right) \\ &\quad + \frac{\Delta}{2}\Big[\Big(\mathrm{Tr}\left(N_L N_L\right) - \left[\mathrm{Tr}\left(N_L\right)\right]^2\Big) - (L \leftrightarrow R) + h.c.\Big]. \end{aligned} \tag{104}$$

$N_{L,R}$ are left and right handed baryon fields in the adjoint representation of flavor $SU(3)$. The baryon fields originate from quark-hadron complementarity [124, 293]. We can think of N as describing a quark which is surrounded by a diquark cloud, $N_L \sim q_L \langle q_L q_L \rangle$. The covariant derivative of the nucleon field is given by $D_\mu N = \partial_\mu N + i[\mathcal{V}_\mu, N]$. The vector and axial-vector currents are

$$\mathcal{V}_\mu = -\frac{i}{2}\left(\xi\partial_\mu\xi^\dagger + \xi^\dagger\partial_\mu\xi\right), \quad \mathcal{A}_\mu = -\frac{i}{2}\xi\left(\nabla_\mu\Sigma^\dagger\right)\xi, \tag{105}$$

where ξ is defined by $\xi^2 = \Sigma$. It follows that ξ transforms as $\xi \to L\xi U^\dagger = U\xi R^\dagger$ with $U \in SU(3)_V$. The fermion field transforms as $N \to UNU^\dagger$. For pure $SU(3)$ flavor transformations $L = R = V$ we have $U = V$. F and D are low energy constants that determine the baryon axial coupling. In QCD at weak coupling, we find $D = F = 1/2$ [174].

The effective theory given in Eq. (104) can be derived from QCD in the weak coupling limit. However, the structure of the theory is completely determined by chiral symmetry, even if the coupling is not weak. In particular, there are no free parameters in the baryon coupling to the vector current. Mass terms are also strongly constrained by chiral symmetry. The effective chemical potentials (X_L, X_R) appear as left and right-handed gauge potentials in the covariant derivative of the nucleon field. We have

$$\begin{aligned} D_0 N &= \partial_0 N + i[\Gamma_0, N], \\ \Gamma_0 &= -\frac{i}{2}\left[\xi\left(\partial_0 + iX_R\right)\xi^\dagger + \xi^\dagger\left(\partial_0 + iX_L\right)\xi\right], \end{aligned} \tag{106}$$

where $X_L = MM^\dagger/(2p_F)$ and $X_R = M^\dagger M/(2p_F)$ as before. (X_L, X_R) covariant derivatives also appears in the axial vector current given in Eq. (105).

We can now study how the fermion spectrum depends on the quark mass. In the CFL state we have $\xi = 1$. For $\mu_s = 0$ the baryon octet has an energy gap Δ and the singlet has gap 2Δ. The leading correction to this result comes from the commutator term in Eq. (106). We find that the gap of the proton and neutron is lowered, $\Delta_{p,n} = \Delta - \mu_s$, while the gap of the cascade particles Ξ^-, Ξ^0 is increased, $\Delta_\Xi = \Delta + \mu_s$. As a consequence we find gapless (p, n) excitations at $\mu_s = \Delta$. This result agrees with the spectrum discussed in Sec. III B if the identification $p \equiv (bu)$ and $n \equiv (bd)$ is made.

The situation is more complicated when kaon condensation is taken into account. In the kaon condensed phase there is mixing in the $(p, \Sigma^+, \Sigma^-, \Xi^-)$ and $(n, \Sigma^0, \Xi^0, \Lambda^8, \Lambda^0)$ sector. For $m_{K^0} \ll \mu_s \ll \Delta$ the spectrum is given by

$$\omega_{p\Sigma^\pm\Xi^-} = \begin{cases} \Delta \pm \frac{3}{4}\mu_s, \\ \Delta \pm \frac{1}{4}\mu_s, \end{cases} \qquad \omega_{n\Sigma^0\Xi^0\Lambda} = \begin{cases} \Delta \pm \frac{1}{2}\mu_s, \\ \Delta, \\ 2\Delta. \end{cases} \tag{107}$$

Numerical results for the eigenvalues are shown in Fig. 8. We observe that mixing within the charged and neutral baryon sectors leads to level repulsion. There are two modes that become light in the CFL window $\mu_s \leq 2\Delta$. One mode is a charged mode which is a linear combination of the proton and the Σ^+, while the other mode is a linear combination of the neutral baryons $(n, \Sigma^0, \Xi^0, \Lambda^8, \Lambda^0)$. The charged mode becomes gapless first, at $\mu_s = 4\Delta/3$. Corrections to this result were studied in the NJL model calculation of [145], which includes various subleading condensates and obtains $\mu_s = 1.22\Delta$ at $\mu = 500$ MeV. The neutral mode becomes gapless only at $\mu_s = 2\Delta$. The most important difference as compared to the spectrum in the gapless CFL phase without kaon condensation is that for $\mu_s < 2\Delta$ only the charged mode is gapless.

F. Goldstone boson currents

In Sec. IV G we showed that gapless fermion modes lead to instabilities of the superfluid phase. Here we will discuss how these instabilities arise, and how they can be resolved, in the context of low energy theories of the CFL state, by the formation of the meson supercurrent state introduced in Sec. III D. The chromomagnetic instability is an instability towards the spontaneous generation of currents, that is to say the spontaneous generation of spatial variation in the phase of the diquark condensate. Consider a spatially varying $U(1)_Y$ rotation of the neutral kaon condensate

$$\xi(\mathbf{x}) = U(\mathbf{x})\xi_K U^\dagger(\mathbf{x}), \tag{108}$$

where $\xi_K = \exp(i\pi\lambda_4)$ and $U(\mathbf{x}) = \exp(i\phi_K(\mathbf{x})\lambda_8)$. This state is characterized by nonzero vector and axial-vector currents, see Eq. (105). We shall study the dependence of the vacuum energy on the kaon current $\boldsymbol{\jmath}_K = \nabla\phi_K$. The gradient term in the meson part of the effective Lagrangian gives a positive contribution

$$\mathcal{E}_m = \frac{1}{2}v_\pi^2 f_\pi^2 \jmath_K^2. \tag{109}$$

A negative contribution can arise from gapless fermions. In order to determine this contribution we have to calculate the fermion spectrum in the presence of a nonzero current. The relevant couplings are obtained from the covariant derivative of the fermion field in Eq. (106) and the D and F-terms in Eq. (104). The fermion spectrum is quite complicated. The dispersion relation of the lowest mode is approximately given by

$$\omega_l = \Delta + \frac{(l - l_0)^2}{2\Delta} - \frac{3}{4}\mu_s - \frac{1}{4}\mathbf{v}\cdot\boldsymbol{\jmath}_K, \tag{110}$$

where $l = \mathbf{v}\cdot\mathbf{p} - p_F$ and we have expanded ω_l near its minimum $l_0 = (\mu_s + \mathbf{v}\cdot\boldsymbol{\jmath}_K)/4$. Eq. (110) shows that there is a gapless mode if $\mu_s > 4\Delta/3 - \jmath_K/3$. The contribution of the gapless mode to the vacuum energy is

$$\mathcal{E}_q = \frac{\mu^2}{\pi^2}\int dl \int \frac{d\Omega}{4\pi}\,\omega_l\theta(-\omega_l), \tag{111}$$

where $d\Omega$ is an integral over the Fermi surface. The energy functional $\mathcal{E}_m + \mathcal{E}_q$ was analyzed in [176, 177]. There is an instability near the point $\mu_s = 4\Delta/3$. The instability is resolved by the formation of a Goldstone boson current. If electric charge neutrality is enforced the magnitude of the current is very small, and there is no tendency towards the generation of multiple currents. It was also shown that all gluonic screening masses are real [178]. The situation is more complicated if the neutral fermion mode becomes gapless, too. In this case the magnitude of the current is not small, and multiple currents may appear. This regime corresponds to the portion of the curCFL-K^0 curve in Fig. 3 that is only slightly (invisibly) below the gCFL curve.

G. Other effective theories

Effective Lagrangians have also been been constructed for color superconducting phases other than the CFL phase. The effective theory for the light singlet axial mode in the 2SC phase can be found in [278]. The phonon effective theory in the crystalline color superconducting phase is discussed in Sec. VI C.

It is also interesting to study effective theories in QCD-like theories at large density. Some of these theories do not have a sign problem and can be studied on the lattice with algorithms that are available today. Of particular interest are QCD with $N_c = 2$ colors [41–49] and QCD at finite isospin density [50–52].

VI. NJL MODEL COMPARISONS AMONG CANDIDATE PHASES BELOW CFL DENSITIES

As we have explained in Sec. II, at sufficiently high densities, where the up, down and strange quarks can be treated on an equal footing and the disruptive effects of the strange quark mass can be neglected, quark matter is in the CFL phase. At asymptotic densities, the CFL gap parameter $\Delta_{\rm CFL}$ and indeed any property of CFL quark matter can be calculated in full QCD, as described in Sec. IV. At any density at which the CFL phase arises, its low energy excitations, and hence its properties and phenomenology, can be described by the effective field theory of Sec. V, whose form is known and whose parameters can be systematically related to the CFL gap $\Delta_{\rm CFL}$. If we knew that the only form of color superconducting quark matter that arises in the QCD phase diagram were CFL, there would therefore be no need to resort to model analyses. However, as we have discussed in Sec. III, $M_s^2/(\mu\Delta_{\rm CFL})$ may not be small enough (at $\mu = \mu_{\rm nuc}$ where the nuclear $\rightarrow$ quark matter transition occurs) for the QCD phase diagram to be this simple.

Even at the very center of a neutron star, μ cannot be larger than about 500 MeV, meaning that the (density dependent) strange quark mass M_s cannot be neglected. In concert with the requirement that bulk matter must be neutral and must be in weak equilibrium, a nonzero M_s favors separation of the Fermi momenta of the three different flavors of quarks, and thus disfavors the cross-species BCS pairing that characterizes the CFL phase. If CFL pairing is disrupted by the heaviness of the strange quark at a higher μ than that at which color superconducting quark matter is superseded by baryonic matter, the CFL phase must be replaced by some phase of quark matter in which there is less, and less symmetric, pairing.

Within a spatially homogeneous ansatz, the next phase down in density is the gapless CFL (gCFL) phase described in Sec. III B. However, as we have described in Sec. IV G, such gapless paired states suffer from a chromomagnetic instability: they can lower their energy by the formation of counter-propagating currents. It seems likely, therefore, that a ground state with counter-propagating currents is required. This could take the form of a crystalline color superconductor, that we have introduced in Sec. III C. Or, given that the CFL phase itself is likely augmented by kaon condensation as described in Secs. II C and V D, it could take the form of the phase we have described in Sec. V F in which a CFL kaon condensate carries a current in one direction balanced by a counter-propagating current in the opposite direction carried by gapless quark quasiparticles.

Determining which phase or phases of quark matter occupy the regime of density between hadronic matter and CFL quark matter in the QCD phase diagram, if there is such a regime, remains an outstanding challenge. Barring a major breakthrough that would allow lattice QCD calculations to be brought to bear despite the fermion sign problem, a from-first-principles determination seems out of reach. This leaves two possible paths forward. First, as we describe in this section, we can analyze and compare many of the possible phases within a simplified few parameter model, in so doing seeking qualitative insight into what phase(s) are favorable. Second, as we shall describe in Sec. VIII, we can determine the observable consequences of the presence of various possible color superconducting phases in neutron stars, and then seek to use observational data to rule possibilities out or in.

A. Model, pairing ansatz, and homogeneous phases

We shall employ a Nambu–Jona-Lasinio (NJL) model in which the QCD interaction between quarks is replaced by a point-like four-quark interaction, with the quantum numbers of single-gluon exchange, analyzed in mean field theory. This is not a controlled approximation. However, it suffices for our purposes: because this model has attraction in the same channels as in QCD, its high density phase is the CFL phase; and, the Fermi surface splitting effects whose qualitative consequences we wish to study can be built into the model. Note that we shall assume throughout that $\Delta_{\rm CFL} \ll \mu$. This weak coupling assumption means that the pairing is dominated by modes near the Fermi surfaces. Quantitatively, this means that results for the gaps and condensation energies of candidate phases are independent of the cutoff in the NJL model when expressed in terms of the CFL gap $\Delta_{\rm CFL}$: if the cutoff is changed with the NJL coupling constant adjusted so that $\Delta_{\rm CFL}$ stays fixed, the gaps and condensation energies for the candidate crystalline

phases also stay fixed. This makes the NJL model valuable for making the comparisons that are our goal. The NJL model has two parameters: the CFL gap $\Delta_{\rm CFL}$ which parametrizes the strength of the interaction and $M_s^2/(4\mu)$, the splitting between Fermi surfaces in neutral quark matter in the absence of pairing. The free energy of candidate patterns of pairing can be evaluated and compared as a function of these two parameters.

As a rather general pairing ansatz, we shall consider

$$\begin{aligned}\langle ud\rangle &\sim \Delta_3 \sum_a \exp\left(2i\mathbf{q}_3^a\cdot\mathbf{r}\right)\\ \langle us\rangle &\sim \Delta_2 \sum_a \exp\left(2i\mathbf{q}_2^a\cdot\mathbf{r}\right)\\ \langle ds\rangle &\sim \Delta_1 \sum_a \exp\left(2i\mathbf{q}_1^a\cdot\mathbf{r}\right)\ .\end{aligned} \tag{112}$$

If we set all the wave vectors $\mathbf{q}_I^a$ to zero, we can use this ansatz to compare spatially homogeneous phases including the CFL phase ($\Delta_1=\Delta_2=\Delta_3\equiv\Delta_{\rm CFL}$), the gCFL phase ($\Delta_3>\Delta_2>\Delta_1>0$) and the 2SC phase ($\Delta_3\equiv\Delta_{\rm 2SC}$; $\Delta_1=\Delta_2=0$). Choosing different sets of wave vectors will allow us to analyze and compare different crystalline color superconducting phases of quark matter.

NJL models of varying degrees of complexity have been used for a variety of purposes beyond the scope of this review. For example, whereas we treat $\Delta_{\rm CFL}$ and quark masses as parameters and use the NJL model to compare different patterns of pairing at fixed values of these parameters and μ, it is possible instead to fix the NJL coupling or couplings and then self-consistently solve for the gap parameters and the $\langle\bar{s}s\rangle$ condensate as functions of μ [139–141, 146, 147, 290, 294–297]. Doing so reintroduces sensitivity to the cutoff in the NJL model and so does not actually reduce the number of parameters. Also, these models tend to find rather larger values of M_s than in analyses that go beyond NJL models, for example the analysis using Dyson-Schwinger equations in [298]. There have also been many investigations of the phase diagram in the μ-T plane in NJL models (either with $\Delta_{\rm CFL}$ and M_s as parameters or solved for self-consistently) [138, 141, 147, 154, 239, 270, 299–305]. Although many of their features are sensitive to the cutoff as well as the chosen couplings, these NJL phase diagrams indicate how rich the QCD phase diagram may turn out to be, as different condensates vanish at different temperatures. One result that has been obtained using the Ginzburg-Landau approximation as well as in NJL models and so is of more general validity is that upon heating the CFL phase at nonzero but small M_s^2/μ, as T increases Δ_2 vanishes first, then Δ_1, and then Δ_3 [138, 154, 269]. However, it remains to be seen how this conclusion is modified by the effects of gauge-field fluctuations, which for $M_s=0$ turn the mean-field Ginzburg-Landau second order transition into a strong first order phase transition at a significantly elevated temperature, see Sec. V B and Eq. (74).

We shall analyze quark matter containing massless u and d quarks and s quarks with an effective mass M_s. The Lagrangian density describing this system in the absence of interactions is given by

$$\mathcal{L}_0 = \bar{\psi}_{i\alpha}\left(i\,\partial\!\!\!/\,\delta^{\alpha\beta}\delta_{ij} - M_{ij}^{\alpha\beta} + \mu_{ij}^{\alpha\beta}\,\gamma_0\right)\psi_{\beta j}\ , \tag{113}$$

where $i,j=1,2,3$ are flavor indices and $\alpha,\beta=1,2,3$ are color indices and we have suppressed the Dirac indices, where $M_{ij}^{\alpha\beta}=\delta^{\alpha\beta}\,{\rm diag}(0,0,M_s)_{ij}$ is the mass matrix, and where the quark chemical potential matrix is given by

$$\mu_{ij}^{\alpha\beta} = (\mu\delta_{ij} - \mu_e Q_{ij})\delta^{\alpha\beta} + \delta_{ij}\left(\mu_3 T_3^{\alpha\beta} + \frac{2}{\sqrt{3}}\mu_8 T_8^{\alpha\beta}\right)\ , \tag{114}$$

with $Q_{ij}={\rm diag}(2/3,-1/3,-1/3)_{ij}$ the quark electric-charge matrix and T_3 and T_8 the diagonal color generators. In QCD, μ_e, μ_3 and μ_8 are the zeroth components of electromagnetic and color gauge fields, and the gauge field dynamics ensure that they take on values such that the matter is neutral [85–88], satisfying the neutrality conditions (3). In the NJL model, quarks interact via four-fermion interactions and there are no gauge fields, so we introduce μ_e, μ_3 and μ_8 by hand, and choose them to satisfy the neutrality constraints (3). The assumption of weak equilibrium is built into the calculation via the fact that the only flavor-dependent chemical potential is μ_e, ensuring for example that the chemical potentials of d and s quarks with the same color must be equal. Because the strange quarks have greater mass, the equality of their chemical potentials implies that the s quarks have smaller Fermi momenta than the d quarks in the absence of BCS pairing. In the absence of pairing, then, because weak equilibrium drives the massive strange quarks to be less numerous than the down quarks, electrical neutrality requires a $\mu_e>0$, which makes the up quarks less numerous than the down quarks and introduces some electrons into the system. In the absence of pairing, color neutrality is obtained with $\mu_3=\mu_8=0$.

The Fermi momenta of the quarks and electrons in quark matter that is electrically and color neutral and in weak

equilibrium are given in the absence of pairing by

$$\begin{aligned} p_F^d &= \mu + \frac{\mu_e}{3} \\ p_F^u &= \mu - \frac{2\mu_e}{3} \\ p_F^s &= \sqrt{\left(\mu + \frac{\mu_e}{3}\right)^2 - M_s^2} \approx \mu + \frac{\mu_e}{3} - \frac{M_s^2}{2\mu} \\ p_F^e &= \mu_e \ , \end{aligned} \tag{115}$$

where we have simplified p_F^s by working to linear order in μ_e and M_s^2. To this order, electric neutrality requires $\mu_e = M_s^2/(4\mu)$, yielding

$$\begin{aligned} p_F^d &= \mu + \frac{M_s^2}{12\mu} = p_F^u + \frac{M_s^2}{4\mu} \\ p_F^u &= \mu - \frac{M_s^2}{6\mu} \\ p_F^s &= \mu - \frac{5M_s^2}{12\mu} = p_F^u - \frac{M_s^2}{4\mu} \\ p_F^e &= \frac{M_s^2}{4\mu} \ , \end{aligned} \tag{116}$$

as illustrated in Fig. 2. We see from (115) that to leading order in M_s^2 and μ_e, the effect of the strange quark mass on unpaired quark matter is as if instead one reduced the strange quark chemical potential by $M_s^2/(2\mu)$. We shall make this approximation throughout. Upon making this assumption, we need no longer be careful about the distinction between p_F's and μ's, as we can simply think of the three flavors of quarks as if they have chemical potentials

$$\begin{aligned} \mu_d &= \mu_u + 2\delta\mu_3 \\ \mu_u &= p_F^u \\ \mu_s &= \mu_u - 2\delta\mu_2 \end{aligned} \tag{117}$$

with

$$\delta\mu_3 = \delta\mu_2 = \frac{M_s^2}{8\mu} \equiv \delta\mu \ , \tag{118}$$

where the choice of subscripts indicates that $2\delta\mu_2$ is the splitting between the Fermi surfaces for quarks 1 and 3 and $2\delta\mu_3$ is that between the Fermi surfaces for quarks 1 and 2, identifying u, d, s with $1, 2, 3$.

As described in [85, 91, 92, 146], BCS pairing introduces qualitative changes into the analysis of neutrality. For example, in the CFL phase $\mu_e = 0$ and μ_8 is nonzero and of order M_s^2/μ. This arises because wherever BCS pairing occurs between fermions whose Fermi surface would be split in the absence of pairing, the Fermi momenta of these fermions are locked together. This maximizes the pairing energy gain while at the same time exacting a kinetic energy price and changing the relation between the chemical potentials and the particle numbers. This means that the μ's required for neutrality can change qualitatively as happens in the CFL example.

The NJL interaction term with the quantum numbers of single-gluon exchange that we add to the Lagrangian (113) is

$$\mathcal{L}_{\rm interaction} = -\frac{3}{8}\lambda(\bar\psi\Gamma^{A\nu}\psi)(\bar\psi\Gamma_{A\nu}\psi) \ , \tag{119}$$

where we have suppressed the color and flavor indices that we showed explicitly in (113), and have continued to suppress the Dirac indices. The full expression for $\Gamma^{A\nu}$ is $(\Gamma^{A\nu})_{\alpha i,\beta j} = \gamma^\nu (T^A)_{\alpha\beta}\delta_{ij}$. The NJL coupling constant λ has dimension -2, meaning that an ultraviolet cutoff Λ must be introduced as a second parameter in order to fully specify the interaction. We shall define Λ as restricting the momentum integrals to a shell around the Fermi surface, $\mu - \Lambda < |\mathbf{p}| < \mu + \Lambda$.

In the mean-field approximation, the interaction Lagrangian (119) takes on the form

$$\mathcal{L}_{\rm interaction} = \frac{1}{2}\bar\psi\Delta(x)\bar\psi^T + \frac{1}{2}\psi^T\bar\Delta(x)\psi, \tag{120}$$

where $\Delta(x)$ is related to the diquark condensate by the relations

$$\begin{aligned}\Delta(x) &= \frac{3}{4}\lambda\Gamma^{A\nu}\langle\psi\psi^T\rangle(\Gamma_{A\nu})^T \\ \bar{\Delta}(x) &= \frac{3}{4}\lambda(\Gamma^{A\nu})^T\langle\bar{\psi}^T\bar{\psi}\rangle\Gamma_{A\nu} = \gamma^0\Delta^\dagger(x)\gamma^0 \ .\end{aligned} \tag{121}$$

The ansatz (112) can now be made precise: we take

$$\Delta(x) = \Delta_{CF}(x)\otimes C\gamma^5 \ , \tag{122}$$

with the color-flavor part

$$\Delta_{CF}(x)_{\alpha i,\beta j} = \sum_{I=1}^{3}\sum_{\mathbf{q}_I^a}\Delta(\mathbf{q}_I^a)e^{2i\mathbf{q}_I^a\cdot\mathbf{r}}\epsilon_{I\alpha\beta}\epsilon_{Iij} \ . \tag{123}$$

We have introduced notation that allows for the possibility of gap parameters $\Delta(\mathbf{q}_I^a)$ with different magnitudes for different I *and for different* a. In fact, we shall only consider circumstances in which $\Delta(\mathbf{q}_I^a) = \Delta_I$, as in (112).

The full Lagrangian, given by the sum of (113) and (120), is then quadratic and can be written very simply upon introducing the two component Nambu-Gorkov spinors (12) in terms of which

$$\mathcal{L} = \frac{1}{2}\bar{\Psi}\begin{pmatrix} i\partial\!\!\!/ + \mu\!\!\!/ & \Delta(x) \\ \bar{\Delta}(x) & (i\partial\!\!\!/ - \mu\!\!\!/)^T \end{pmatrix}\Psi \ . \tag{124}$$

Here, $\mu\!\!\!/ \equiv \mu\gamma_0$ and μ is the matrix (114).

The propagator corresponding to the Lagrangian (124) is given by

$$\langle\Psi(x)\bar{\Psi}(x')\rangle = \begin{pmatrix} \langle\psi(x)\bar{\psi}(x')\rangle & \langle\psi(x)\psi^T(x')\rangle \\ \langle\bar{\psi}^T(x)\bar{\psi}(x')\rangle & \langle\bar{\psi}^T(x)\psi^T(x')\rangle \end{pmatrix} = \begin{pmatrix} iG(x,x') & iF(x,x') \\ i\bar{F}(x,x') & i\bar{G}(x,x') \end{pmatrix} , \tag{125}$$

where G and $\bar{G}$ are the "normal" components of the propagator and F and $\bar{F}$ are the "anomalous" components. They satisfy the coupled differential equations

$$\begin{pmatrix} i\partial\!\!\!/ + \mu\!\!\!/ & \Delta(x) \\ \bar{\Delta}(x) & (i\partial\!\!\!/ - \mu\!\!\!/)^T \end{pmatrix}\begin{pmatrix} G(x,x') & F(x,x') \\ \bar{F}(x,x') & \bar{G}(x,x') \end{pmatrix} = \begin{pmatrix} 1 & 0 \\ 0 & 1 \end{pmatrix}\delta^{(4)}(x-x') \ . \tag{126}$$

We can now rewrite (121) as

$$\begin{aligned}\Delta(x) &= \frac{3i}{4}\lambda\Gamma^{A\nu}F(x,x)(\Gamma_{A\nu})^T \\ \bar{\Delta}(x) &= \frac{3i}{4}\lambda(\Gamma^{A\nu})^T\bar{F}(x,x)\Gamma_{A\nu} \ ,\end{aligned} \tag{127}$$

either one of which is the self-consistency equation, or gap equation, that we must solve.

Without further approximation, (127) is not tractable. It yields an infinite set of coupled gap equations, one for each $\Delta(\mathbf{q}_I^a)$, because without further approximation it is not consistent to choose finite sets $\{\mathbf{q}_I\}$. When several plane waves are present in the condensate, they induce an infinite tower of higher momentum condensates [168]. In the next subsection, we shall make a Ginzburg-Landau (i.e. small-Δ) approximation which eliminates these higher harmonics.

Of course, an even more dramatic simplification is obtained if we set all the wave vectors $\mathbf{q}_I^a$ to zero. Still, even in this case obtaining the general solution with $M_s \neq 0$ and $\Delta_1 \neq \Delta_2 \neq \Delta_3$ is somewhat involved [91, 137, 138]. We shall not present the resulting analysis of the CFL→gCFL transition and the gCFL phase here. The free energies of these phases are depicted in Fig. 3, and their gap parameters are depicted below in Fig. 10.

If we simplify even further, by setting $M_s = 0$ and $\Delta_1 = \Delta_2 = \Delta_3 \equiv \Delta_{\rm CFL}$, the gap equation determining the CFL gap parameter $\Delta_{\rm CFL}$ can then be evaluated analytically, yielding [168]

$$\Delta_{\rm CFL} = 2^{\frac{2}{3}}\Lambda\exp\left[-\frac{\pi^2}{2\mu^2\lambda}\right] \ . \tag{128}$$

We shall see below that in the limit in which $\Delta \ll \Delta_{\rm CFL}, \delta\mu \ll \mu$, all results for the myriad possible crystalline phases can be expressed in terms of $\Delta_{\rm CFL}$; neither λ nor Λ shall appear. This reflects the fact that in this limit

the physics of interest is dominated by quarks near the Fermi surfaces, not near Λ, and so once $\Delta_{\rm CFL}$ is used as the parameter describing the strength of the attraction between quarks, Λ is no longer visible; the cutoff Λ only appears in the relation between $\Delta_{\rm CFL}$ and λ, not in any comparison among different possible paired phases. We are using the NJL model in a specific, limited, fashion in which it serves as a two parameter model allowing the comparison among different possible paired phases at a given $\Delta_{\rm CFL}$ and M_s. NJL models have also been employed to estimate the value of $\Delta_{\rm CFL}$ at a given μ [24–26, 33, 239, 240]; doing so requires normalizing the four-fermion interaction by calculating some zero density quantity like the vacuum chiral condensate, and in so doing introduces a dependence on the cutoff Λ. Such mean-field NJL analyses are important complements to extrapolation down from an analysis that is rigorous at high density and hence weak coupling, described in Sec. IV, and give us confidence that we understand the magnitude of $\Delta_{\rm CFL} \sim 10 - 100$ MeV. This estimate receives further support from the lattice-NJL calculation of [53] which finds diquark condensation and a ~ 60 MeV gap in an NJL model whose parameters are normalized via calculation of f_π, m_π and a constituent quark mass in vacuum. With these as inputs, Δ is then calculated on the lattice, i.e. without making a mean-field approximation. With an understanding of its magnitude in hand, we shall treat $\Delta_{\rm CFL}$ as a parameter, thus making our results insensitive to Λ.

We shall focus below on the use of the NJL model that we have introduced to analyze and compare different possible crystalline phases, comparing their free energies to that of the CFL phase as a benchmark. The free energy of the 2SC phase is easily calculable in the same model, and the free energies of the unstable gapless CFL and gapless 2SC phases can also be obtained [137]. These free energies are all shown in Fig. 3. The free energies of phases with various patterns of single-flavor pairing have also been calculated in the same model [132]. The NJL model is not a natural starting point for an analysis of the kaon condensate in the CFL-K^0 phase, but with considerable effort this has been accomplished in [144, 145, 283, 290]. The curCFL-K^0 phase of Secs. III D and V F, in which the K^0-condensate carries a current, has not been analyzed in an NJL model. But, because both the CFL-K^0 and curCFL-K^0 phases are continuously connected to the CFL phase, they can both be analyzed in a model-independent fashion using the effective field theory described in Sec. V. The CFL-K^0 and curCFL-K^0 curves in Fig. 3 were obtained as described in Sec. V. It remains a challenge for future work to do a calculation in which both curCFL-K^0 and crystalline phases are possible, allowing a direct comparison of their free energies within a single calculation and a study of whether they are distinct as current results seem to suggest or are instead different limits of some more general inhomogeneous color superconducting phase.

B. Crystalline phases

Crystalline color superconductivity [167–171, 173, 220, 306–314] naturally permits pairing between quarks living at split Fermi surfaces by allowing Cooper pairs with nonzero net momentum. In three-flavor quark matter, this allows pairing to occur even with the Fermi surfaces split in the free-energetically optimal way as in the absence of pairing, meaning that neutral crystalline phases are obtained in three-flavor quark matter with the chemical potential matrix (114) simplified to $\mu = \delta^{\alpha\beta} \otimes \mathrm{diag}\,(\mu_u, \mu_d, \mu_s)$ with the flavor chemical potentials given simply by (117) [170–172], up to higher order corrections that have been investigated in [313]. This is the origin of the advantage that crystalline color superconducting phases have over the CFL and gCFL phases at large values of the splitting $\delta\mu$. For example, by allowing u quarks with momentum $\mathbf{p} + \mathbf{q}_3$ to pair with d quarks with momentum $-\mathbf{p} + \mathbf{q}_3$, for any $\mathbf{p}$, we can pair u and d quarks along rings on their respective Fermi surfaces. In coordinate space, this corresponds to a condensate of the form $\langle ud \rangle \sim \Delta_3 \exp\bigl(2i\mathbf{q_3} \cdot \mathbf{r}\bigr)$. The net free energy gained due to pairing is then a balance between increasing $|\mathbf{q}_3|$ yielding pairing on larger rings while exacting a greater kinetic energy cost. The optimum choice turns out to be $|\mathbf{q}_3| = \eta\delta\mu_3$ with $\eta = 1.1997$, corresponding to pairing rings on the Fermi surfaces with opening angle 67.1° [167]. Pairing with only a single $\mathbf{q}_3$ is disadvantaged because the only quarks on each Fermi surface that can then pair are those lying on a single ring. This disadvantage can be overcome in two ways. First, increasing Δ widens the pairing rings on the Fermi surfaces into pairing bands which fill in, forming pairing caps, at large enough Δ [171]. Second, it is possible to cover larger areas of the Fermi surfaces by allowing Cooper pairs with the same $|\mathbf{q}_3|$ but various $\hat{\mathbf{q}}_3$, yielding $\langle ud \rangle \sim \Delta_3 \sum_{\mathbf{q}_3^a} \exp\bigl(2\,i\,\mathbf{q}_3^a \cdot \mathbf{r}\bigr)$ with the $\mathbf{q}_3^a$ chosen from some specified set $\{\mathbf{q}_3^1, \mathbf{q}_3^2, \mathbf{q}_3^3, \ldots\} \equiv \{\mathbf{q}_3\}$. This is a condensate modulated in position space in some crystalline pattern, with the crystal structure defined by $\{\mathbf{q}_3\}$. In this two-flavor context, a Ginzburg-Landau analysis reveals that the best $\{\mathbf{q}_3\}$ contains eight vectors pointing at the corners of a cube, say in the $(\pm 1, \pm 1, \pm 1)$ directions in momentum space, yielding a face-centered cubic structure in position space [168].

This subsection describes the analysis of three-flavor crystalline phases in [315]. We use the ansatz given by (122) and (123) for the three-flavor crystalline color superconducting condensate. This is antisymmetric in color (α, β), spin, and flavor (i, j) indices and is a generalization of the CFL condensate to crystalline color superconductivity. We set $\Delta_1 = 0$, neglecting $\langle ds \rangle$ pairing because the d and s Fermi surfaces are twice as far apart from each other as each is from the intervening u Fermi surface. Hence, I can be taken to run over 2 and 3 only. $\{\mathbf{q}_2\}$ and $\{\mathbf{q}_3\}$ define

the crystal structures of the $\langle us\rangle$ and $\langle ud\rangle$ condensates respectively. We only consider crystal structures in which all the vectors in $\{\mathbf{q}_2\}$ are equivalent to each other in the sense that any one can be transformed into any other by a symmetry operation of $\{\mathbf{q}_2\}$ and same for $\{\mathbf{q}_3\}$. This justifies our simplifying assumption that the $\langle us\rangle$ and $\langle ud\rangle$ condensates are each specified by a single gap parameter (Δ_2 and Δ_3 respectively), avoiding having to introduce one gap parameter per $\mathbf{q}$. We furthermore only consider crystal structures which are exchange symmetric, meaning that $\{\mathbf{q}_2\}$ and $\{\mathbf{q}_3\}$ can be exchanged by some combination of rigid rotations and reflections applied simultaneously to all the vectors in both sets. This simplification, together with $\delta\mu_2 = \delta\mu_3$ (an approximation corrected only at order M_s^4/μ^3), guarantees that we find solutions with $\Delta_2 = \Delta_3$.

We analyze and compare candidate crystal structures by evaluating the free energy $\Omega(\Delta_2, \Delta_3)$ for each crystal structure in a Ginzburg-Landau expansion in powers of the Δ's. This approximation is controlled if $\Delta_2, \Delta_3 \ll \Delta_{\rm CFL}, \delta\mu$, with $\Delta_{\rm CFL}$ the gap parameter in the CFL phase at $M_s^2/\mu = 0$. The terms in the Ginzburg-Landau expansion must respect the global $U(1)$ symmetry for each flavor, meaning that each Δ_I can only appear in the combination $|\Delta_I|^2$. (The $U(1)$ symmetries are spontaneously broken by the condensate, but not explicitly broken.) Therefore, $\Omega(\Delta_2, \Delta_3)$ is given to sextic order by

$$\begin{aligned}\Omega(\Delta_2,\Delta_3) \;&=\; \frac{2\mu^2}{\pi^2}\Bigg[P_2\alpha_2|\Delta_2|^2 + P_3\alpha_3|\Delta_3|^2 + \frac{1}{2}\Big(\beta_2|\Delta_2|^4 + \beta_3|\Delta_3|^4 + \beta_{32}|\Delta_2|^2|\Delta_3|^2\Big) \\ &+\; \frac{1}{3}\Big(\gamma_2|\Delta_2|^6 + \gamma_3|\Delta_3|^6 + \gamma_{322}|\Delta_3|^2|\Delta_2|^4 + \gamma_{233}|\Delta_3|^4|\Delta_2|^2\Big)\Bigg]\,, \end{aligned} \tag{129}$$

where we have chosen notation consistent with that used in the two flavor study of [168], which arises as a special case of (129) if we take Δ_2 or Δ_3 to be zero. P_I is the number of vectors in the set $\{\mathbf{q}_I\}$. The form of the Ginzburg-Landau expansion (129) is model-independent, whereas the expressions for the coefficients α_I, β_I, β_{IJ}, γ_I, and γ_{IJJ} for a specific crystal structure are model-dependent. We calculate them in the NJL model described in Sec. VI A. For exchange symmetric crystal structures, $\alpha_2 = \alpha_3 \equiv \alpha$, $\beta_2 = \beta_3 \equiv \beta$, $\gamma_2 = \gamma_3 \equiv \gamma$ and $\gamma_{233} = \gamma_{322}$.

Because setting one of the Δ_I to zero reduces the problem to one with two-flavor pairing only, we can obtain α, β and γ via applying the two-flavor analysis described in [168] to either $\{\mathbf{q}_2\}$ or $\{\mathbf{q}_3\}$ separately. Using α as an example, we learn that

$$\alpha_I = \alpha(q_I, \delta\mu_I) \;=\; -1 + \frac{\delta\mu_I}{2q_I}\log\left(\frac{q_I+\delta\mu_I}{q_I-\delta\mu_I}\right) - \frac{1}{2}\log\left(\frac{\Delta_{\rm 2SC}^2}{4(q_I^2-\delta\mu_I^2)}\right). \tag{130}$$

Here, $q_I \equiv |\mathbf{q}_I|$ and $\Delta_{\rm 2SC}$ is the gap parameter for the 2SC (2-flavor, 2-color) BCS pairing obtained with $\delta\mu_I = 0$ and Δ_I nonzero with the other two gap parameters set to zero. Assuming that $\Delta_{\rm CFL} \ll \mu$, the 2SC gap parameter is given by $\Delta_{\rm 2SC} = 2^{\frac{1}{3}}\Delta_{\rm CFL}$ [94], see Sec. IV. In the Ginzburg-Landau approximation, in which the Δ_I are assumed small, we must first minimize the quadratic contribution to the free energy, and only then investigate the quartic and sextic contributions. Minimizing α_I fixes the length of all the vectors in the set $\{\mathbf{q}_I\}$, and eliminates the possibility of waves at higher harmonics, yielding $q_I = \eta\,\delta\mu_I$ with $\eta = 1.1997$ the solution to $\frac{1}{2\eta}\log\left[(\eta+1)/(\eta-1)\right] = 1$ [167]. Upon setting $q_I = \eta\,\delta\mu_I$, (130) becomes

$$\alpha_I(\delta\mu_I) = -\frac{1}{2}\log\left(\frac{\Delta_{\rm 2SC}^2}{4\delta\mu_I^2(\eta^2-1)}\right)\,. \tag{131}$$

Once the q_I have been fixed, the only dimensionful quantities on which the quartic and sextic coefficients can depend are the $\delta\mu_I$ [168, 172], meaning that for exchange symmetric crystal structures and with $\delta\mu_2 = \delta\mu_3 = \delta\mu$ we have $\beta = \bar\beta/\delta\mu^2$, $\beta_{32} = \bar\beta_{32}/\delta\mu^2$, $\gamma = \bar\gamma/\delta\mu^4$ and $\gamma_{322} = \bar\gamma_{322}/\delta\mu^4$ where the barred quantities are dimensionless numbers which depend only on $\{\hat{\mathbf{q}}_2\}$ and $\{\hat{\mathbf{q}}_3\}$ that must be evaluated for each crystal structure. Doing so requires evaluating one-loop Feynman diagrams with 4 or 6 insertions of Δ_I's. Each insertion of Δ_I (Δ_I^*) adds (subtracts) momentum $2\mathbf{q}_I^a$ for some a. The vector sum of all these external momenta inserted into a given one-loop diagram must vanish, meaning that the calculation consists of a bookkeeping task (determining which combinations of 4 or 6 $\mathbf{q}_I^a$'s selected from the sets $\{\mathbf{q}_I\}$ satisfy this momentum-conservation constraint) that grows rapidly in complexity with the complexity of the crystal structure, and a loop integration that is nontrivial because the momentum in the propagator changes after each insertion. In [172], this calculation is carried out explicitly for 11 crystal structures in the mean-field NJL model of Sec. VI A upon making the weak coupling ($\Delta_{\rm CFL}$ and $\delta\mu$ both much less than μ) approximation. Note that in this approximation neither the NJL cutoff nor the NJL coupling constant appear in any quartic or higher Ginzburg-Landau coefficient, and as we have seen above they appear in α only within $\Delta_{\rm CFL}$. Hence, the details of the model do not matter as long as one thinks of $\Delta_{\rm CFL}$ as a parameter, kept $\ll \mu$.

It is easy to show that for exchange symmetric crystal structures any extrema of $\Omega(\Delta_2, \Delta_3)$ in (Δ_2, Δ_3)-space must either have $\Delta_2 = \Delta_3 = \Delta$, or have one of Δ_2 and Δ_3 vanishing [172]. It is also possible to show that the three-flavor crystalline phases with $\Delta_2 = \Delta_3 = \Delta$ are electrically neutral whereas two-flavor solutions in which only one of the Δ's is nonzero are not [172]. We therefore analyze only solutions with $\Delta_2 = \Delta_3 = \Delta$. We find that $\Omega(\Delta, \Delta)$ is positive for large Δ for all the crystal structures that have been investigated to date [172].[4] This allows us to minimize $\Omega(\Delta, \Delta)$ with respect to Δ, thus evaluating Δ and Ω.

We begin with the simplest three-flavor "crystal" structure in which $\{\mathbf{q}_2\}$ and $\{\mathbf{q}_3\}$ each contain only a single vector, making the $\langle us \rangle$ and $\langle ud \rangle$ condensates each a single plane wave [170]. We call this the 2PW phase. Unlike in the more realistic crystalline phases we describe below, in this "crystal" the magnitude of the $\langle ud \rangle$ and $\langle us \rangle$ condensates are unmodulated. This simple condensate nevertheless yields a qualitative lesson which proves helpful in winnowing the space of multiple plane wave crystal structures [172]. For this simple "crystal" structure, all the coefficients in the Ginzburg-Landau free energy can be evaluated analytically [170–172]. The terms that occur in the three-flavor case but not in the two-flavor case, namely $\bar{\beta}_{32}$ and $\bar{\gamma}_{322}$, describe the interaction between the two condensates, and depend on the angle ϕ between $\mathbf{q}_2$ and $\mathbf{q}_3$. For any angle ϕ, both $\bar{\beta}_{32}$ and $\bar{\gamma}_{322}$ are positive. And, both increase monotonically with ϕ and diverge as $\phi \to \pi$ This divergence tells us that choosing $\mathbf{q}_2$ and $\mathbf{q}_3$ precisely antiparallel exacts an infinite free energy price in the combined Ginzburg-Landau and weak-coupling limit in which $\Delta \ll \delta\mu, \Delta_{\rm CFL} \ll \mu$, meaning that in this limit if we chose $\phi = \pi$ we find $\Delta = 0$. Away from the Ginzburg-Landau limit, when the pairing rings on the Fermi surfaces widen into bands, choosing $\phi = \pi$ exacts a finite price meaning that Δ is nonzero but smaller than that for any other choice of ϕ. The high cost of choosing $\mathbf{q}_2$ and $\mathbf{q}_3$ precisely antiparallel can be understood qualitatively as arising from the fact that in this case the ring of states on the u-quark Fermi surface that "want to" pair with d-quarks coincides precisely with the ring that "wants to" pair with s-quarks [171]. This simple two plane wave ansatz has been analyzed upon making the weak-coupling approximation but without making the Ginzburg-Landau approximation [171]. All the qualitative lessons learned from the Ginzburg-Landau approximation remain valid and we learn further that the Ginzburg-Landau approximation always underestimates Δ [171].

The analysis of the simple two plane wave "crystal" structure, together with the observation that in more complicated crystal structures with more than one vector in $\{\mathbf{q}_2\}$ and $\{\mathbf{q}_3\}$ the Ginzburg-Landau coefficient β_{32} (γ_{322}) is given in whole (in part) by a sum of many two plane wave contributions, yields one of two rules for constructing favorable crystal structures for three-flavor crystalline color superconductivity [172]: $\{\mathbf{q}_2\}$ and $\{\mathbf{q}_3\}$ should be rotated with respect to each other in a way that best keeps vectors in one set away from the antipodes of vectors in the other set. The second rule is that the sets $\{\mathbf{q}_2\}$ and $\{\mathbf{q}_3\}$ should each be chosen to yield crystal structures which, seen as separate two-flavor crystalline phases, are as favorable as possible. The 11 crystal structures analyzed in [172] allow one to make several pairwise comparisons that test these two rules. There are instances of two structures which differ only in the relative orientation of $\{\mathbf{q}_2\}$ and $\{\mathbf{q}_3\}$ and in these cases the structure in which vectors in $\{\mathbf{q}_2\}$ get closer to the antipodes of vectors in $\{\mathbf{q}_3\}$ are disfavored. And, there are instances where the smallest angle between a vector in $\{\mathbf{q}_2\}$ and the antipodes of a vector in $\{\mathbf{q}_3\}$ are the same for two different crystal structures, and in these cases the one with the more favorable two-flavor structure is more favorable. These considerations, together with explicit calculations, indicate that two structures, which we denote "2Cube45z" and "CubeX", are particularly favorable.

In the 2Cube45z crystal, $\{\mathbf{q}_2\}$ and $\{\mathbf{q}_3\}$ each contain eight vectors pointing at the corners of a cube. If we orient $\{\mathbf{q}_2\}$ so that its vectors point in the $(\pm 1, \pm 1, \pm 1)$ directions in momentum space, then $\{\mathbf{q}_3\}$ is rotated relative to $\{\mathbf{q}_2\}$ by 45° about the z-axis. In this crystal structure, the $\langle ud \rangle$ and $\langle us \rangle$ condensates are each given by the most favored two-flavor crystal structure [168]. The relative rotation maximizes the separation between any vector in $\{\mathbf{q}_2\}$ and the nearest antipodes of a vector in $\{\mathbf{q}_3\}$.

We arrive at the CubeX structure by reducing the number of vectors in $\{\mathbf{q}_2\}$ and $\{\mathbf{q}_3\}$. This worsens the two-flavor free energy of each condensate separately, but allows vectors in $\{\mathbf{q}_2\}$ to be kept farther away from the antipodes of vectors in $\{\mathbf{q}_3\}$. We have not analyzed all structures obtainable in this way, but we have found one and only one which has a condensation energy comparable to that of the 2Cube45z structure. In the CubeX structure, $\{\mathbf{q}_2\}$ and $\{\mathbf{q}_3\}$ each contain four vectors forming a rectangle. The eight vectors together point toward the corners of a cube. The 2 rectangles intersect to look like an "X" if viewed end-on. The color, flavor and position space dependence of the CubeX condensate is given by

$$\epsilon_{2\alpha\beta}\epsilon_{2ij}\left[\cos\frac{2\pi}{a}\left(x+y+z\right)+\cos\frac{2\pi}{a}\left(-x-y+z\right)\right]+\epsilon_{3\alpha\beta}\epsilon_{3ij}\left[\cos\frac{2\pi}{a}\left(-x+y+z\right)+\cos\frac{2\pi}{a}\left(x-y+z\right)\right], \quad (132)$$

[4] This is in marked contrast with what happens with only two flavors (and upon ignoring the requirement of neutrality.) in that context, many crystal structures have negative γ and hence sextic order free energies that are unbounded from below [168].

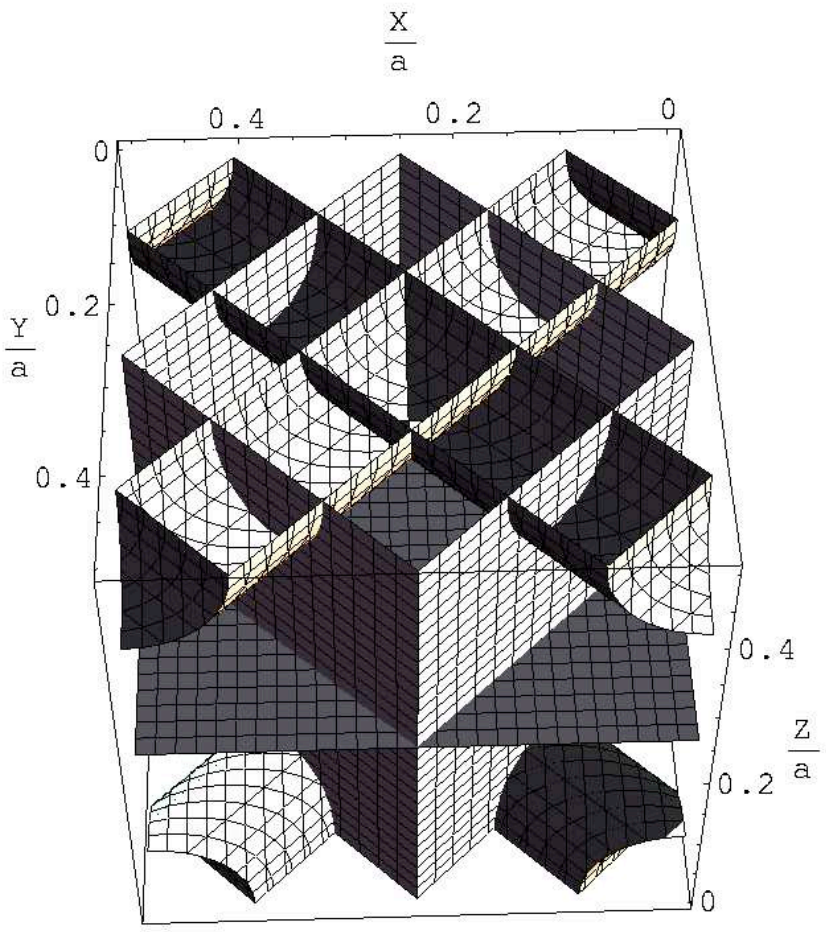

FIG. 9: The CubeX crystal structure of Eq. (132). The figure extends from 0 to $a/2$ in the x, y and z directions. Both $\Delta_2(\mathbf{r})$ and $\Delta_3(\mathbf{r})$ vanish at the horizontal plane. $\Delta_2(\mathbf{r})$ vanishes on the darker vertical planes, and $\Delta_3(\mathbf{r})$ vanishes on the lighter vertical planes. On the upper (lower) dark cylinders and the lower (upper) two small corners of dark cylinders, $\Delta_2(\mathbf{r}) = +3.3\Delta$ ($\Delta_2(\mathbf{r}) = -3.3\Delta$). On the upper (lower) lighter cylinders and the lower (upper) two small corners of lighter cylinders, $\Delta_3(\mathbf{r}) = -3.3\Delta$ ($\Delta_3(\mathbf{r}) = +3.3\Delta$). The largest value of $|\Delta_I(\mathbf{r})|$ is 4Δ, occurring along lines at the centers of the cylinders. The lattice spacing is a when one takes into account the signs of the condensates; if one looks only at $|\Delta_I(\mathbf{r})|$, the lattice spacing is $a/2$.

where $a = \sqrt{3}\pi/q = 4.536/\delta\mu = 36.29\mu/M_s^2$ is the lattice spacing. For example, with $M_s^2/\mu = 100, 150, 200$ MeV the lattice spacing is $a = 72, 48, 36$ fm. We depict this condensate in Fig. 9.

In Figs. 10 and 3, we plot Δ and Ω versus M_s^2/μ for the most favorable crystal structures that we have found, namely the CubeX and 2Cube45z structures described above. We have taken the CFL gap parameter $\Delta_{\rm CFL} = 25$ MeV in these figures, but they can easily be rescaled to any value of $\Delta_{\rm CFL} \ll \mu$ [172]: if the Δ and M_s^2/μ axes are rescaled by $\Delta_{\rm CFL}$ and the energy axis is rescaled by $\Delta_{\rm CFL}^2$. Fig. 10 shows that the gap parameters are large enough that the Ginzburg-Landau approximation is at the edge of its domain of reliability. However, results obtained for the simpler 2PW crystal structures suggest that the Ginzburg-Landau calculation underestimates Δ and the condensation energy and that, even when it breaks down, it is a good qualitative guide to the favorable structure [171]. We therefore trust the result, evident in Fig. 3, that these crystalline phases are both impressively robust, with one or other of them favored over a wide swath of M_s^2/μ and hence density. We do not trust the Ginzburg-Landau calculation to discriminate between these two structures, particularly given that although we have a qualitative understanding of why these two are favorable we have no qualitative argument for why one should be favored over the other. We are confident that 2Cube45z is the most favorable structure obtained by rotating one cube relative to another. We are not as confident that CubeX is the best possible structure with fewer than 8+8 vectors. Regardless, the 2Cube45z and CubeX crystalline phases together make the case that three-flavor crystalline color superconducting phases are the ground state of cold quark matter over a wide range of densities. If even better crystal structures can be found, this will only further strengthen this case.

Fig. 3 shows that over most of the range of M_s^2/μ where it was once considered a possibility, the gCFL phase can

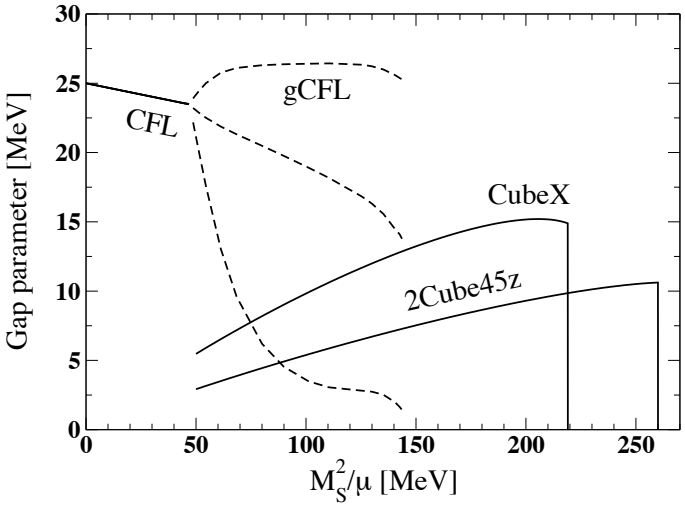

FIG. 10: Gap parameter Δ versus M_s^2/μ for: the CFL gap parameter (set to 25 MeV at $M_s^2/\mu = 0$), the three gap parameters $\Delta_1 < \Delta_2 < \Delta_3$ describing $\langle ds \rangle$, $\langle us \rangle$ and $\langle ud \rangle$ pairing in the gCFL phase, and the gap parameters in the crystalline color superconducting phases with CubeX and 2Cube45z crystal structures. Increasing M_s^2/μ corresponds to decreasing density.

be replaced by a *much* more favorable three-flavor crystalline color superconducting phase. We find that the two most favorable crystal structures have large condensation energies, easily 1/3 to 1/2 of that in the CFL phase with $M_s = 0$, which is $3\Delta_{\rm CFL}^2\mu^2/\pi^2$. This is at first surprising, given that the only quarks that pair are those lying on rings on the Fermi surfaces, whereas in the CFL phase with $M_s = 0$ pairing occurs over the entire u, d and s Fermi surfaces. It can to a degree be understood qualitatively once we recall that there are in fact many rings, and note that as Δ increases, the pairing rings spread into bands on the Fermi surfaces, and for Δ as large as that we find to be favored these bands have expanded and filled in, becoming many "polar caps" on the Fermi surfaces [171]. In addition to being free-energetically favorable, these crystalline phases are, as far as we know, stable: they do not suffer from the chromomagnetic instability [173, 316–318] and they are also stable with respect to kaon condensation [319]. In simplified analogue contexts, it has even been possible to trace the path in configuration space from the unstable gapless phase (analogue of gCFL) downward in free energy to the stable crystalline phase [44, 164].

Fig. 3 also shows that it is hard to find a crystalline phase with lower free energy than the gCFL phase at the lower values of M_s^2/μ (highest densities) within the "gCFL window". At these densities, however, the calculations described in Sec. V demonstrate that the gCFL phase is superseded by the stable CFL-K^0 and curCFL-K^0 phases, as shown in Fig. 3.

The three-flavor crystalline color superconducting phases with CubeX and 2Cube45z crystal structures are the lowest free energy phases that we know of, and hence candidates for the ground state of QCD, over a wide range of densities. Within the Ginzburg-Landau approximation to the NJL model that we have employed, one or other is favored over the CFL, gCFL and unpaired phases for $2.9\Delta_{\rm CFL} < M_s^2/\mu < 10.4\Delta_{\rm CFL}$, as shown in Fig. 3. For $\Delta_{\rm CFL} = 25$ MeV and $M_s = 250$ MeV, this translates to 240MeV $< \mu <$ 847MeV. With these choices of parameters, the lower part of this range of μ (higher part of the range of M_s^2/μ) is certainly superseded by nuclear matter. And, the high end of this range extends beyond the $\mu \sim 500$ MeV characteristic of the quark matter at the densities expected at the center of neutron stars. This qualitative feature persists in the analysis of [294] in which M_s is solved for rather than taken as a parameter. If neutron stars do have quark matter cores, then, it is reasonable to include the possibility that the *entire* quark matter core could be in a crystalline color superconducting phase on the menu of options that must ultimately be winnowed by confrontation with astrophysical observations. (Recall, that if $\Delta_{\rm CFL}$ is larger, say ~ 100 MeV, the entire quark matter core could be in the CFL phase.) As we shall see in the next subsection, crystalline color superconducting quark matter is rigid, with a very large shear modulus, while at the same time being superfluid. This provides a possible origin for pulsar glitches, as we shall discuss in Sec. VIII F

C. Rigidity of crystalline color superconducting quark matter

The crystalline phases of color superconducting quark matter that we have described in the previous subsection are unique among all forms of dense matter that may arise within neutron star cores in one respect: they are rigid [320]. They are not solids in the usual sense: the quarks are not fixed in place at the vertices of some crystal structure.

Instead, in fact, these phases are superfluid since the condensates all spontaneously break the $U(1)_B$ symmetry corresponding to quark number. We shall always write the condensates as real. This choice of overall phase breaks $U(1)_B$, and spatial gradients in this phase correspond to supercurrents. And yet, we shall see that crystalline color superconductors are rigid solids with large shear moduli. The diquark condensate, although spatially inhomogeneous, can carry supercurrents [167, 320]. It is the spatial modulation of the gap parameter that breaks translation invariance, as depicted for the CubeX phase in Fig. 9, and it is this pattern of modulation that is rigid.[5] This novel form of rigidity may sound tenuous upon first hearing, but we shall present the effective Lagrangian that describes the phonons in the CubeX and 2Cube45z crystalline phases, whose lowest order coefficients have been calculated in the NJL model that we are employing [320]. We shall then extract the shear moduli from the phonon effective action, quantifying the rigidity and indicating the presence of transverse phonons. The fact that the crystalline phases are simultaneously rigid and superfluid means that their presence within neutron star cores has potentially observable consequences, as we shall describe in Sec. VIII F.

The shear moduli of a crystal may be extracted from the effective Lagrangian that describes phonons in the crystal, namely space- and time-varying displacements of the crystalline pattern. Phonons in two-flavor crystalline phases were first investigated in [311, 312]. In the present context, we introduce displacement fields for the $\langle ud\rangle$, $\langle us\rangle$ and $\langle ds\rangle$ condensates by making the replacement

$$\Delta_I \sum_{\mathbf{q}_I^a} e^{2i\mathbf{q}_I^a\cdot\mathbf{r}} \to \Delta_I \sum_{\mathbf{q}_I^a} e^{2i\mathbf{q}_I^a\cdot(\mathbf{r}-\mathbf{u}_I(\mathbf{r}))} \tag{133}$$

in (123). One way to obtain the effective action describing the dynamics of the displacement fields $\mathbf{u}_I(\mathbf{r})$, including both its form and the values of its coefficients within the NJL model that we are employing, is to begin with the NJL model of Sec. VI A but with (133) and integrate out the fermion fields. After a lengthy calculation [320], this yields

$$S[\mathbf{u}] = \frac{1}{2}\int d^4x \sum_I \kappa_I \left[\left(\sum_{\mathbf{q}_I^a} (\hat{q}_I^a)^m (\hat{q}_I^a)^n \right) (\partial_0 u_I^m)(\partial_0 u_I^n) - \left(\sum_{\mathbf{q}_I^a} (\hat{q}_I^a)^m (\hat{q}_I^a)^v (\hat{q}_I^a)^n (\hat{q}_I^a)^w \right) (\partial_v u_I^m)(\partial_w u_I^n) \right] \tag{134}$$

where m, n, v and w are spatial indices running over x, y and z and where we have defined

$$\kappa_I \equiv \frac{2\mu^2|\Delta_I|^2\eta^2}{\pi^2(\eta^2-1)} \ . \tag{135}$$

Upon setting $\Delta_1 = 0$ and $\Delta_2 = \Delta_3 = \Delta$,

$$\kappa_2 = \kappa_3 \equiv \kappa = \frac{2\mu^2|\Delta|^2\eta^2}{\pi^2(\eta^2-1)} \simeq 0.664\,\mu^2|\Delta^2| \ . \tag{136}$$

$S[\mathbf{u}]$ is the low energy effective action for phonons in any crystalline color superconducting phase, valid to second order in derivatives, to second order in the gap parameters Δ_I and to second order in the phonon fields $\mathbf{u}_I$. Because we are interested in long wavelength, small amplitude, phonon excitations, expanding to second order in derivatives and in the phonon fields is satisfactory. More complicated terms will arise at higher order, for example terms that couple the different $\mathbf{u}_I$'s, but it is legitimate to neglect these complications [320]. Extending this calculation to higher order in the Ginzburg-Landau approximation would be worthwhile, however, since as we saw in Sec. VI B this approximation is at the edge of its domain of reliability.

In order to extract the shear moduli, we need to compare the phonon effective action to the general theory of elastic media [327], which requires introducing the strain tensor

$$s_I^{mv} \equiv \frac{1}{2}\Big(\frac{\partial u_I^m}{\partial x^v} + \frac{\partial u_I^v}{\partial x^m}\Big). \tag{137}$$

We then wish to compare the action (134) to

$$\mathcal{S}[\mathbf{u}] \ = \ \frac{1}{2}\int d^4x \left(\sum_I \sum_m \rho_I^m (\partial_0 u_I^m)(\partial_0 u_I^m) - \sum_I \sum_{\substack{mn\\vw}} \lambda_I^{mvnw} s_I^{mv} s_I^{nw} \right), \tag{138}$$

[5] Supersolids [321–326] are another example of rigid superfluids, but they differ from crystalline color superconductors in that they are rigid by virtue of the presence of an underlying lattice of atoms.

which is the general form of the action in the case in which the effective action is quadratic in displacements and which defines the elastic modulus tensor λ_I^{mvnw} for this case. In this case, the stress tensor (in general the derivative of the potential energy with respect to s_I^{mv}) is given by

$$\sigma_I^{mv} = \lambda_I^{mvnw} s_I^{nw} \ . \tag{139}$$

The diagonal components of σ are proportional to the compression exerted on the system and are therefore related to the bulk modulus of the crystalline color superconducting quark matter. Since unpaired quark matter has a pressure $\sim \mu^4$, it gives a contribution to the bulk modulus that completely overwhelms the contribution from the condensation into a crystalline phase, which is of order $\mu^2\Delta^2$. We shall therefore not calculate the bulk modulus. On the other hand, the response to shear stress arises only because of the presence of the crystalline condensate. The shear modulus is defined as follows. Imagine exerting a static external stress σ_I having only an off-diagonal component, meaning $\sigma_I^{mv} \neq 0$ for a pair of space directions $m \neq v$, and all the other components of σ are zero. The system will respond with a strain s_I^{nw}. The shear modulus in the mv plane is then

$$\nu_I^{mv} \equiv \frac{\sigma_I^{mv}}{2 s_I^{mv}} = \frac{1}{2}\lambda_I^{mvmv} \ , \tag{140}$$

where the indices m and v are not summed. For a general quadratic potential with σ_I^{mv} given by (139), ν_I^{mv} simplifies partially but the full simplification given by the last equality in (140) only arises for special cases in which the only nonzero entries in λ^{mvnw} with $m \neq v$ are the λ^{mvmv} entries, as is the case for all the crystal structures that we consider.

For a given crystal structure, upon evaluating the sums in (134) and then using the definition (137) to compare (134) to (138), we can extract expressions for the λ tensor and thence for the shear moduli. This analysis, described in detail in [320], shows that in the CubeX phase

$$\nu_2 = \frac{16}{9}\kappa \begin{pmatrix} 0 & 0 & 1 \\ 0 & 0 & 0 \\ 1 & 0 & 0 \end{pmatrix} \ , \quad \nu_3 = \frac{16}{9}\kappa \begin{pmatrix} 0 & 0 & 0 \\ 0 & 0 & 1 \\ 0 & 1 & 0 \end{pmatrix} \ , \tag{141}$$

while in the 2Cube45z phase

$$\nu_2 = \frac{16}{9}\kappa \begin{pmatrix} 0 & 1 & 1 \\ 1 & 0 & 1 \\ 1 & 1 & 0 \end{pmatrix} \ , \quad \nu_3 = \frac{16}{9}\kappa \begin{pmatrix} 0 & 0 & 1 \\ 0 & 0 & 1 \\ 1 & 1 & 0 \end{pmatrix} \ . \tag{142}$$

We shall see in Sec. VIII F that it is relevant to check that both these crystals have enough nonzero entries in their shear moduli ν_I that if there are rotational vortices are pinned within them, a force seeking to move such a vortex is opposed by the rigidity of the crystal structure described by one or more of the nonzero entries in the ν_I. This is demonstrated in [320].

We see that all the nonzero shear moduli of both the CubeX and 2Cube45z crystalline color superconducting phases turn out to take on the same value,

$$\nu_{\rm CQM} = \frac{16}{9}\kappa \tag{143}$$

with κ defined by (136). Evaluating κ yields

$$\begin{aligned} \nu_{\rm CQM} &= 1.18\,\mu^2\Delta^2 \\ &= 2.47\,\frac{\rm MeV}{\rm fm^3}\left(\frac{\Delta}{10\ {\rm MeV}}\right)^2\left(\frac{\mu}{400\ {\rm MeV}}\right)^2 . \end{aligned} \tag{144}$$

From (144) we first of all see that the shear modulus is in no way suppressed relative to the scale $\mu^2\Delta^2$ that could have been guessed on dimensional grounds. And, second, we discover that a quark matter core in a crystalline color superconducting phase is 20 to 1000 times more rigid than the crust of a conventional neutron star [320, 328]. Finally, see [320] for the extraction of the phonon dispersion relations from the effective action (134). The transverse phonons, whose restoring force is provided by the shear modulus and which correspond to propagating ripples in a condensation pattern like that in Fig. 9, turn out to have direction-dependent velocities that are typically a substantial fraction of the speed of light, in the specific instances evaluated in [320] being given by $\sqrt{1/3}$ and $\sqrt{2/3}$. This is yet a third way of seeing that this superfluid phase of matter is rigid indeed.

VII. TRANSPORT PROPERTIES AND NEUTRINO PROCESSES

In Sec. VIII we shall discuss how the observation of neutron star properties constrains the phase structure of dense quark matter. A crucial ingredient in these analyses are the transport properties as well as neutrino emissivities and opacities of different phases of quark matter.

Using the methods introduced in Sec. V it is possible to perform rigorous calculations of transport properties of the CFL phase. The results are parameter free predictions of QCD at asymptotically large density, and rigorous consequences of QCD expressed in terms of a few phenomenological parameters (f_π, m_π, ...) at lower density.

In the case of other color superconducting phases we perform calculations using perturbative QCD or models of QCD. For many quantities the results depend mainly on the spectrum of quark modes, and not on details of the quark-quark interaction.

A. Viscosity and thermal conductivity

Viscosity and thermal conductivity determine the dissipated energy $\dot{E}$ in a fluid with nonzero gradients of the velocity $\mathbf{v}$ and the temperature T,

$$\dot{E} \;=\; -\frac{\eta}{2}\int d^3x\,\left(\partial_i v_j+\partial_j v_i-\frac{2}{3}\delta_{ij}\partial_k v_k\right)^2-\zeta\int d^3x\,\left(\partial_i v_i\right)^2-\frac{\kappa}{T}\int d^3x\,\left(\partial_i T\right)^2\,. \tag{145}$$

The transport coefficients η, ζ and κ are the shear and bulk viscosity and the thermal conductivity, respectively. Eq. (145) is strictly valid only for non-relativistic fluids. In the case of relativistic fluids there is an extra contribution to the dissipated energy which is proportional to κ and the gradient of μ [329]. In terms of its hydrodynamic properties a superfluid can be viewed as a mixture of a normal and a superfluid component characterized by separate flow velocities. The shear viscosity is entirely due to the normal component, but there are contributions to the bulk viscosity which are related to stresses in the superfluid flow relative to the normal one [330–332]. In the following we shall neglect these effects and interpret v_i in Eq. (145) as the normal fluid velocity.

In neutron stars an important contribution to the bulk viscosity arises from electroweak effects. In a bulk compression mode the density changes periodically and electroweak interactions may not be sufficiently fast to reestablish weak equilibrium. Weak effects occur on the same time scale as the oscillation period of the neutron star and the frequency dependence of the bulk viscosity is important. We define

$$\zeta(\omega)=2\left\langle\dot{E}\right\rangle\left(\frac{V_0}{\delta V_0}\right)^2\frac{1}{\omega^2}\,, \tag{146}$$

where ω is the oscillation frequency, $\langle\ldots\rangle$ is a time average, and $\delta V_0/V_0$ is the fractional change in the volume. The coefficient ζ in Eq. (145) is the $\omega\to 0$ limit of $\zeta(\omega)$. If a single weak process is responsible for reestablishing chemical equilibrium, the frequency dependent bulk viscosity can be written in the form

$$\zeta(\omega)=C\frac{\gamma}{\gamma^2+\omega^2}\,. \tag{147}$$

The prefactor C accounts for the dependence of the equilibrium densities (e.g., the net difference between the density of strange and non-strange quarks if the weak process changes strangeness) on the respective chemical potentials, and γ is the characteristic inverse time scale of the flavor changing process. Eq. (147) shows that, for a given ω, ζ has a maximum at $\gamma=\omega$. At this point the time scale of the microscopic process matches the one of the external oscillation. If more than one weak process contributes to reequilibration, Eq. (147) becomes more complicated [333–335]

1. CFL phase

The normal fluid is composed of quasi-particle excitations. In the CFL phase all quark modes are gapped and the relevant excitations are Goldstone bosons. At very low temperature, transport properties are dominated by the massless Goldstone boson φ associated with the breaking of the $U(1)_B$ symmetry. Using the results in Sec. V C 2, we can compute the mean free path l_φ of the φ due to $\varphi\leftrightarrow\varphi+\varphi$ and $\varphi+\varphi\leftrightarrow\varphi+\varphi$ scattering. Small angle scattering contributions give rise to $l_\varphi\propto\mu^4/T^5$ [336] and $l_\varphi\simeq 1$ km at $T=0.1$ MeV, while large angle scattering contributions yield an even longer $l_\varphi\propto\mu^8/T^9$ [337]. The thermal conductivity κ due to the φ is given by [337]

$$\kappa=\frac{2\pi^2T^3}{45v^2}\,l_\varphi\,, \tag{148}$$

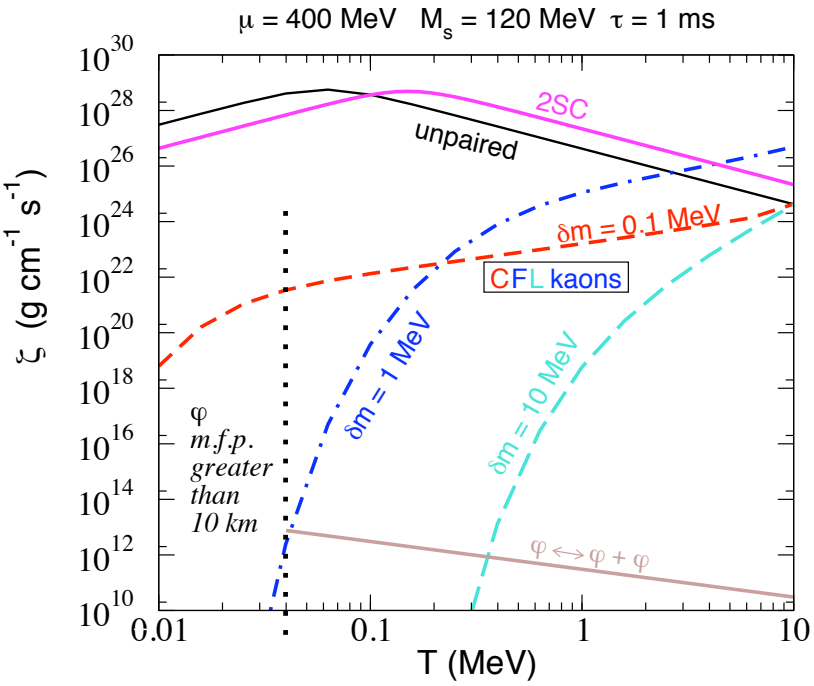

FIG. 11: (Color online) Bulk viscosities as functions of temperature for an oscillation period $\tau = 2\pi/\omega = 1$ ms. CFL phase: contribution from the process $K^0 \leftrightarrow \varphi + \varphi$ for different values of $\delta m \equiv m_{K^0} - \mu_{K^0}$ and contribution from $\varphi \leftrightarrow \varphi + \varphi$, see Eq. (150). 2SC phase and unpaired quark matter: contribution from the process $u + d \leftrightarrow u + s$.

where ℓ_φ is the φ mean-free path between large angle scatterings and v is the φ velocity from Eqs. (83) and (84). For temperatures below ~ 1 MeV the thermal conductivity is very large and macroscopic amounts of CFL matter are expected to be isothermal. The electric conductivity in CFL matter is dominated by thermal electrons and positrons and was estimated in [112].

At low temperatures, the shear viscosity of the CFL phase is dominated by the φ contribution, which was computed in [336] and is given by

$$\eta = 1.3 \times 10^{-4} \, \frac{\mu^8}{T^5} \, . \tag{149}$$

The bulk viscosity ζ vanishes in an exactly scale invariant system. For realistic quark masses the dominant source of scale breaking is the strange quark mass. The contribution from the process $\varphi \leftrightarrow \varphi + \varphi$ is [338]

$$\zeta = 0.011 \frac{M_s^4}{T} \, . \tag{150}$$

We show this contribution in Fig. 11. The other contribution to the CFL bulk viscosity presented in the figure comes from the process $K^0 \leftrightarrow \varphi + \varphi$ and was studied for arbitrary ω in [339]. We observe that at $T \simeq (1 - 10)$ MeV the bulk viscosity of CFL matter is comparable to that of unpaired quark matter. For $T < 1$ MeV, ζ is strongly suppressed. Depending on the poorly known value for $\delta m \equiv m_{K^0} - \mu_{K^0}$ (here assumed to be positive, a negative value corresponds to kaon condensation), the pure φ contribution given in Eq. (150) may dominate over the $K^0 \leftrightarrow \varphi + \varphi$ reaction at low enough temperatures. However, for $T < 0.1$ MeV the φ mean free path is on the order of the size of the star, i.e., the system is in the collisionless rather than in the hydrodynamic regime, and the result ceases to be meaningful.

Thermal conductivity and viscosities for the CFL-K^0 phase have not yet been computed. The existence of a gapless K^0 Goldstone mode in this phase will introduce new contributions. However, since the CFL results for κ and η are already dominated by a gapless mode, namely the φ, the modifications to these quantities are not expected to be significant. The modification to ζ will be more significant, since the kaon contribution to this quantity is already important in the CFL phase.

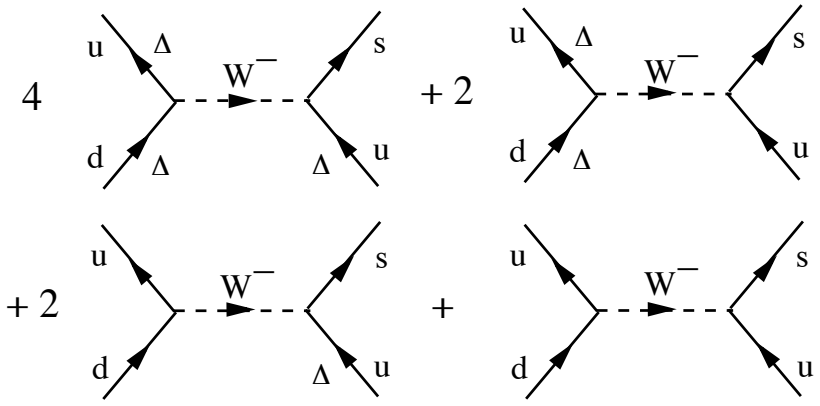

FIG. 12: Contributions to the process $u + d \to u + s$ in the 2SC phase. A gapped fermion is marked with the gap Δ at the respective line. (We have omitted (small) contributions from anomalous propagators.)

2. Other phases

For unpaired, ultrarelativistic three-flavor quark matter, thermal and electric conductivity as well as shear viscosity have been computed in [340]. In the low-temperature limit (in particular $T \ll m_D$ with the electric screening mass $m_D^2 = N_f g^2 \mu^2/(2\pi^2)$) they are

$$\kappa \;\simeq\; 0.5 \frac{m_D^2}{\alpha_s^2}\,, \qquad \sigma_{\rm el} \simeq 0.01 \frac{e^2 \mu^2 m_D^{2/3}}{\alpha_s^2 T^{5/3}}\,, \tag{151}$$

and

$$\eta \;\simeq\; 4.4 \times 10^{-3}\, \frac{\mu^4 m_D^{2/3}}{\alpha_s^2 T^{5/3}}\,. \tag{152}$$

These quantities have not yet been computed for partially gapped color superconductors such as the 2SC phase. The presence of ungapped modes, however, suggests that the results only differ by a numerical factor from the unpaired phase results.

The dominant flavor changing process that contributes to the bulk viscosity in unpaired quark matter is the reaction [341, 342]

$$u + d \leftrightarrow u + s\,. \tag{153}$$

Other relevant processes are the semi-leptonic processes $u + e \leftrightarrow d + \nu_e$ and $u + e \leftrightarrow s + \nu_e$ [335, 343].

In a partially gapped phase the bulk viscosity is also dominated by the process (153). In the 2SC phase of three flavor quark matter, the number of d-quarks produced per unit time and volume, Γ, due to (153) can be computed from the diagrams shown in Fig. 12. The combinatorical factors in front of the diagrams are obtained upon counting color degrees of freedom: one can attach one of three colors to each of the two weak vertices, giving rise to 9 possibilities. In the 2SC phase all blue quarks and all strange quarks are unpaired while all other modes are paired, see Table I. Consequently, 4 of the 9 possibilities contain three gapped modes (red or green for both vertices), 2 contain two gapped modes (red or green for one, blue for the other vertex), 2 contain one gapped mode (blue for one, red or green for the other vertex), and one contains only unpaired modes (blue for both vertices). Therefore, at very low temperature, $T \ll \Delta$, where the contributions of gapped quarks are exponentially suppressed, Γ is to a very good approximation given by [344]

$$\Gamma^{\rm 2SC} = \frac{1}{9}\Gamma^{\rm unp} \qquad \text{for } T \ll \Delta\,, \tag{154}$$

since only the one reaction containing only unpaired modes contributes. The rate $\Gamma^{\rm unp}$ was computed in [345].

For larger temperatures, the contribution from gapped modes cannot be neglected. Each diagram yields a contribution which (for one direction of the process) schematically reads

$$\Gamma \;\propto\; \sum_{\{e_i\}} \int_{\{p_i\}} \mathcal{F}\, \delta(e_1\varepsilon_1 + e_2\varepsilon_2 - e_3\varepsilon_3 - e_4\varepsilon_4 + \delta\mu) f(e_1\varepsilon_1) f(e_2\varepsilon_2) f(-e_3\varepsilon_3) f(-e_4\varepsilon_4)\,. \tag{155}$$

Here, ε_i are the quasiparticle energies, $\delta\mu = \mu_s - \mu_d$, and f is the Fermi distribution function. $\mathcal{F}$ is a function of the momenta p_i and the signs $e_i = \pm 1$. The sum over the signs e_i is very important in a paired system: the process $u + d \to u + s$ not only receives contributions from $2 \to 2$ processes, but also from $3 \to 1$ and $1 \to 3$ reactions involving pairs created or absorbed by the condensate.

From the net production rate of d quarks Γ one obtains the characteristic inverse time scale γ needed for the bulk viscosity in Eq. (147). For small external volume oscillations $\delta V_0/V_0$, Γ is linear in the resulting oscillation in chemical potentials, $\Gamma = \lambda\,\delta\mu$. Then, $\gamma \equiv B\lambda$, where B depends only on the equilibrium flavor densities. The resulting bulk viscosity as a function of temperature for a typical oscillation frequency $\omega/(2\pi) = 1\mathrm{ms}^{-1}$ is shown in Fig. 11. A critical temperature of $T_c = 30$ MeV is assumed. For low temperatures, the time scale of the nonleptonic process is much smaller than the oscillation frequency $\gamma \ll \omega$, implying $\zeta \propto \gamma$. Consequently, from Eq. (154) we conclude $\zeta_{\mathrm{2SC}} = \zeta_{\mathrm{unp}}/9$. For large temperatures, however, we have $\gamma \gg \omega$ and thus $\zeta \propto 1/\gamma$. Consequently, the superconducting phase, which has the slower rate, has the larger bulk viscosity.

The bulk viscosity has also been computed for two-flavor quark matter with single-flavor pairing [346]. In this case there are also ungapped modes and thus the result is similar to the one of the 2SC phase. The main difference is the lower critical temperature for single-flavor pairing. As a consequence, these phases are unlikely to exist for temperatures larger than that at which the bulk viscosity of the unpaired phase is maximal. Therefore, the bulk viscosity cannot be larger than that of the unpaired phase.

B. Neutrino emissivity and specific heat

Neutrino emissivity determines the rate at which quark matter can loose heat via neutrino emission. For the purpose of studying how neutron stars with ages ranging from tens of seconds to millions of years cool, as we shall discuss in Sec. VIII C, it is appropriate to treat the matter as completely transparent to the neutrinos that it emits.

1. CFL phase

In CFL quark matter, all quasifermion modes are gapped and neutrino emissivity is dominated by reactions involving (pseudo)-Goldstone modes such as

$$\pi^\pm, K^\pm \;\to\; e^\pm + \bar{\nu}_e\,, \tag{156a}$$

$$\pi^0 \;\to\; \nu_e + \bar{\nu}_e\,, \tag{156b}$$

$$\varphi + \varphi \;\to\; \varphi + \nu_e + \bar{\nu}_e\,. \tag{156c}$$

These processes were studied in [347, 348]. The decay rates of the massive mesons $\pi^\pm$, $K^\pm$, and π^0 are proportional to their number densities and are suppressed by Boltzmann factors $\exp(-E/T)$, where E is the energy gap of the meson. Since the pseudo-Goldstone boson energy gaps are on the order of a few MeV, the emissivities are strongly suppressed as compared to unpaired quark matter for temperatures below this scale. Neutrino emission from processes involving the φ is not exponentially suppressed, but it involves a very large power of T,

$$\epsilon_\nu \sim \frac{G_F^2 T^{15}}{f^2\mu^4}\,, \tag{157}$$

and is numerically very small. Reddy et al. also studied the neutrino mean free path l_ν. For $T \sim 30$ MeV the mean free path is on the order of 1 m, but for $T < 1$ MeV, $l_\nu > 10$ km [348]. In the CFL-K^0 phase, l_ν is almost the same as in the CFL phase, while the neutrino emissivity is larger [349].

The specific heat of CFL matter is also dominated by the φ, yielding

$$c_V = \frac{2\pi^2}{15v^3}\,T^3\,. \tag{158}$$

This is much smaller than the specific heat of any phase containing unpaired quarks, as we shall see below.

2. Other phases

The density of thermally excited ungapped fermions is proportional to $\mu^2 T$ while that of ungapped bosons is T^3. This means that in any degenerate system ($T \ll \mu$) ungapped fermion modes, if they exist, will dominate the neutrino

phase	gap structure	$\mathcal{G}(\phi) \propto$	$\mathcal{K}(\phi) \propto$
CSL	isotropic (no nodes)	$\phi \exp(-\sqrt{2}\phi)$	$\phi^{5/2} \exp(-\sqrt{2}\phi)$
planar	anisotropic (no nodes)	$\phi^{1/2} \exp(-\phi)$	$\phi^2 \exp(-\phi)$
polar	point nodes (linear)	ϕ^{-2}	ϕ^{-2}
A	point nodes (quadratic)	ϕ^{-1}	ϕ^{-1}

TABLE III: Suppression function $\mathcal{G}(\phi)$ for neutrino emissivity in direct Urca processes and suppression function $\mathcal{K}(\phi)$ for specific heat for four spin-one color-superconducting phases (abbreviating $\phi \equiv \Delta/T$, and everything in the limit $\phi \to \infty$). While fully gapped modes yield exponential suppression, nodes in the gap yield power law suppressions. The gap functions in the polar and A phases differ in the angular direction in the vicinity of the point nodes. A linear behavior leads to a stronger suppression than a quadratic behavior.

rates. In unpaired quark matter neutrino emissivity is dominated by the direct Urca processes

$$u + e \;\to\; d + \nu_e \qquad (\text{electron capture})\,, \tag{159a}$$

$$d \;\to\; u + e + \bar{\nu}_e \qquad (\beta\text{-decay})\,. \tag{159b}$$

The radiated energy per unit of time and volume is [350]

$$\epsilon_\nu \simeq \frac{457}{630} \alpha_s G_F^2 T^6 \mu_e \mu_u \mu_d\,. \tag{160}$$

Note that this result is proportional to the strong coupling constant α_s. The tree-level processes for massless quarks are approximately collinear and the weak matrix element vanishes in the forward direction. A nonzero emissivity arises from strong interaction corrections, which depress quark Fermi momenta relative to their chemical potentials. Because they do not at the same time depress the electron Fermi momentum, this opens up phase space for the reactions (159). A nonzero emissivity can also arise from quark mass effects, or higher order corrections in T/μ. Since strange quark decays are Cabbibo suppressed and T/μ is small the dominant contribution is likely to be that proportional to α_s, namely (160). Note that we have not included non-Fermi liquid corrections of $O(\alpha_s \log(T))$ [351].

In order to determine the rate at which neutron stars cool we also need to know the specific heat. In unpaired quark matter

$$c_V = \frac{N_c N_f}{3} \mu^2 T\,, \tag{161}$$

where we have again neglected terms of $O(\alpha_s \log(T))$ [67] and assumed the flavor chemical potentials to be equal. We see that the specific heat (158) in the CFL phase, whose excitations are bosonic, is much smaller than that in unpaired quark matter.

In the case of 2SC matter, the neutrino emissivity at low temperature is 1/3 of that of unpaired quark matter. The 2SC emissivity for arbitrary temperatures can be found in [352]. In addition to the direct Urca process neutrino pair production

$$q + q \to q + q + \nu_\ell + \bar{\nu}_\ell \tag{162}$$

(q is any quark flavor and ℓ denotes neutrino flavor) has also been studied [353]. The rate of this process is parametrically smaller than the direct Urca process for very small temperatures ($\exp(-2\Delta/T)$ vs. $\exp(-\Delta/T)$), but it may play a significant role for temperatures close to the superconducting phase transition temperature T_c.

For the LOFF phase similar arguments apply. The presence of ungapped modes renders its specific heat [309] and its neutrino emissivity due to direct Urca processes virtually indistinguishable from the unpaired phase [354]. However, interesting effects of crystalline structures may be expected for other cooling mechanisms. This is not unlike effects in the crust of a conventional neutron star, where for instance electron-phonon scattering as well as Bragg diffraction of electrons lead to neutrino emission via bremsstrahlung processes, see [355] and references therein.

The direct Urca processes have also been considered for the gapless CFL phase. A distinctive feature of this phase is the fact that the energy of one of the quark modes is approximately quadratic in momentum. This implies a strong enhancement in the specific heat, which leads to very slow cooling at very small temperatures when photon emission from the surface dominates the energy loss [155]. However, the instability of this phase at small temperatures suggests that this result is most probably of no relevance for astrophysics.

Finally, it is interesting to consider neutrino emission from single flavor paired matter. Single flavor spin-one pairing involves small gaps, as well as nodes in the gap parameter, and the emissivity is expected to be larger than that of

matter with spin zero pairing. The emissivity of two-flavor quark matter with $\langle uu\rangle$ and $\langle dd\rangle$ pairing was studied for different spin-one order parameters in [356, 357]. The result can be written as

$$\epsilon_\nu = \frac{457}{630}\alpha_s G_F^2 T^6 \mu_e \mu_u \mu_d \left[\frac{1}{3} + \frac{2}{3}\,\mathcal{G}(\Delta/T)\right] , \tag{163}$$

where the u-quark and d-quark gaps are assumed to be identical. All spin-one phases analyzed in [356, 357] and described by Eq. (163) contain ungapped modes similar to the 2SC phase. Therefore, the emissivity at low temperatures is simply one third of that of unpaired quark matter. (In the case of color-spin locking, all excitations become gapped if one takes into account nonzero quark masses [356, 358] and/or more complicated structures of the order parameter [238].) The contribution to (163) that arises from the paired quarks, is described by the nontrivial function $\mathcal{G}(\Delta/T)$; see [356] for the explicit form and numerical evaluation of this function for arbitrary temperatures. In Table III, we present the behavior of this function for temperatures much smaller than the gap, $T \ll \Delta$, for various single-flavor spin-one color superconducting phases. Although this contribution is small compared to the contribution of the ungapped modes, we can use it to show the effect of different (anisotropic) gap structures on the parametric behavior of the neutrino emissivity. We see that, while fully gapped modes lead to an exponential suppression of the emissivity, nodes in the gap weaken this suppression to a power law. The power law depends on the behavior of the gap in the vicinity of the nodes.

The specific heat can be written as

$$c_V = T(\mu_u^2 + \mu_d^2)\,\left[\frac{1}{3} + \frac{2}{3}\mathcal{K}(\Delta/T)\right] . \tag{164}$$

We show the suppression function $\mathcal{K}(\Delta/T)$ for the specific heat in Table III. We see that an exponential suppression of the emissivity goes along with an exponential suppression of the specific heat.

VIII. COLOR SUPERCONDUCTIVITY IN NEUTRON STARS

Neutron stars are the densest material objects in the universe, with masses of order that of the sun ($M_\odot$) and radii of order ten km. Depending on their mass and on the stiffness of the equation of state of the material of which they are composed, their central density lies between ~ 3 and ~ 12 times nuclear saturation density ($n_0 = 0.16$ nucleons/fm^3) [359, 360]. Neutron stars consist of an outer crust made of a rigid lattice of positive ions embedded within a fluid of electrons and (in the inner layer of the crust) superfluid neutrons [361]. Inside this crust, one finds a fluid "mantle" consisting of neutrons and protons, both likely superfluid, and electrons. Determining the composition of neutron star cores, namely of the densest matter in the universe, remains an outstanding challenge.[6] If the nuclear equation of state is stiff enough, neutron stars are made of neutrons, protons and electrons all the way down to their centers. If higher densities are reached, other phases of baryonic matter (including either a pion condensate [368–372], a kaon condensate [373, 374], or a nonzero density of one or several hyperons [375]) may result. Or, neutron star cores may be made of color superconducting quark matter.

The density at which the transition from baryonic matter to quark matter occurs is not known; this depends on a comparison between the equations of state for both, which is not well-determined for either. Very roughly, we expect this transition to occur when the density exceeds one nucleon per nucleon volume, a criterion which suggests a transition to quark matter at densities $\gtrsim 3n_0$. The question we shall pose in this section is how astrophysical observation of neutron stars could determine whether they do or do not contain quark matter within their cores. We have seen throughout the earlier sections of this review that quark matter at potentially accessible densities may be in the CFL phase, with all quarks paired, or may be in one of a number of possible phases in which there are some unpaired quarks, some of which are spatially inhomogeneous. If quark matter does exist within neutron stars, with their temperatures far below the critical temperatures for these paired phases, it will be in some color superconducting phase. We shall see in this section that these different phases have different observational consequences, making it possible for a combination of different types of observational data to cast light upon the question of which phase of color superconducting quark matter is favored in the QCD phase diagram, if in fact neutron stars do feature quark matter cores.

Before turning to the signatures of quark matter in neutron star cores, we mention here the more radical possibility that nuclear matter in bulk is metastable at zero pressure, with the true ground state of strongly interacting matter

[6] For review articles on neutron stars as laboratories for understanding dense matter, see for instance [360, 362–367].

in the infinite volume limit being color superconducting three-flavor quark matter. According to this "strange quark matter hypothesis" [376–378], ordinary nuclei are either stabilized by virtue of their small size or are metastable with lifetimes vastly exceeding the age of the universe. If this hypothesis is correct, some of the stars that we think are neutron stars may be strange stars, made entirely of quark matter [378–381]. Strange stars may have a thin crust (of order 100 meters thick) of positive ions suspended above the quark matter surface by an electric field [379], or they may have a comparably thin crust of positive ions embedded within the (negatively charged) outer layer of the quark matter itself [194, 195]. They cannot, however, have a conventional, km thick, crust. And, there are many indications that neutron stars in fact do have conventional crusts. For example, the rich phenomenology of X-ray bursts is well-understood only within this setting. More recent evidence comes from the analysis of the quasi-periodic oscillations with frequencies in the tens of Hz detected in the aftermath of magnetar superbursts [382–386], which can be understood as seismic oscillations of a conventional neutron star crust [383, 385, 386] whereas the thin crusts of a strange star would oscillate at much higher frequencies [387]. Even if most compact stars are neutron stars not strange stars, it remains a logical possibility that some strange stars exist, meaning that all ordinary neutron stars are metastable. Although possible this scenario is unlikely, given that merger events in which strange stars in an inspiralling binary are tidally disrupted would litter the universe with small chunks of quark matter ("strangelets") and one must then understand why these have not catalyzed the conversion of all neutron stars to strange stars [388]. We shall devote the remainder of this section to the more challenging task of using observational data to constrain the more conservative scenario that quark matter exists only above some nonzero transition pressure, namely within the cores of conventional neutron stars.

A. Mass-radius relation

It has long been a central goal of neutron star astrophysics to measure the masses M and radii R of many neutron stars to a reasonable accuracy. Mapping out the curve in the mass-radius plane along which neutron stars are found would yield a strong constraint on the equation of state of dense matter. As this program represents such a large fraction of the effort to use observations of neutron stars to constrain dense matter physics, we begin by considering its implications for the presence of quark matter within neutron star cores.

The larger the maximum mass that can be attained by a neutron star, the stiffer the equation of state of dense matter, and if stars with masses close to 2 $M_\odot$ are found then the existence of phases with a soft equation of state, such as baryonic matter with kaon or pion condensation, can be ruled out. However, although the quark matter equation of state is not known from first principles, it may easily be as stiff as the stiffer equations of state posited for ordinary nuclear matter, and neutron stars with quark matter cores can in fact reach masses of order 2 $M_\odot$ [214, 389–392].

The equation of state for CFL quark matter can be parametrized to a good approximation as [391]

$$\Omega = -P = -\frac{3}{4\pi^2}(1-c)\mu^4 + \frac{3}{4\pi^2}(M_s^2 - 4\Delta^2)\mu^2 + B_{\rm eff} \ . \tag{165}$$

If c were zero, the μ^4 term would be that for noninteracting quarks; c parametrizes the leading effect of interactions, modifying the relation between p_F and μ. At high densities, $c = 2\alpha_s/\pi$ to leading order in the strong coupling constant [12, 14]. Analysis of higher order corrections suggests that $c \gtrsim 0.3$ at accessible densities [390]. $B_{\rm eff}$ can be thought of as parametrizing our ignorance of the μ at which the nuclear matter to quark matter transition occurs. The $M_s^2\mu^2$ term is the leading effect of the strange quark mass, and is common to all quark matter phases. The pressure of a color superconducting phase with less pairing than in the CFL phase would have a smaller coefficient of the $\Delta^2\mu^2$ term, and would also differ at order M_s^4, here lumped into a change in $B_{\rm eff}$. Because pairing is a Fermi surface phenomenon, it only modifies the μ^2 term, leaving the larger μ^4 term untouched. However, it can nevertheless be important because at accessible densities the μ^4 term is largely cancelled by $B_{\rm eff}$, enhancing the importance of the μ^2 term [393, 394]. Remarkably, and perhaps coincidentally, if we make the (reasonable) parameter choices $c = 0.3$, $M_s = 275$ MeV and $\Delta = 100$ MeV and choose $B_{\rm eff}$ such that nuclear matter gives way to CFL quark matter at the relatively low density 1.5 n_0, then over the entire range of higher densities relevant to neutron stars the quark matter equation of state (165) is almost indistinguishable from the nuclear equation of state due to Akmal, Pandharipande and Ravenhall (APR) [395] that is one of the stiffest nuclear equations of state in the compendium found in [360, 366]. Neutron stars made entirely of nuclear matter with the APR equation of state and neutron stars with a quark matter core with the equation of state (165) with the parameters just described fall along almost indistinguishable curves on a mass vs. radius plot, with the most significant difference being that the APR equation of state admits neutron stars with maximum mass $2.3M_\odot$, whereas the introduction of a quark matter core reduces the maximum mass slightly, to $2.0M_\odot$ [391].

The similarity between a representative quark matter equation of state and a representative nuclear equation of state makes clear that it will be very hard to use a future determination of the equation of state to discern the

presence of quark matter. However, although the numbers in the above paragraph should be taken as indicative rather than definitive, they do suggest that the existence of a neutron star whose mass was reliably determined to be $> 2M_\odot$ would make it hard to envision such a star (and hence any lighter stars) having a quark matter core of any appreciable size. Now that the mass of PSR J0751+1807 has been revised downward from $(2.1 \pm 0.2)M_\odot$ [396] to $(1.26^{+.14}_{-.12})M_\odot$ [397], the heaviest known neutron star orbited by a white dwarf is PSR J0621+1002, whose mass is $(1.69^{+0.11}_{-0.16})M_\odot$ [397, 398]. Also, one of the two pulsars Ter5I and Ter5J (in a globular cluster) must have a mass that is $> 1.68M_\odot$ at the 95% confidence level [399], and the mass of the X-ray pulsar Vela X-1 is above 1.6 $M_\odot$ [400].

Given our lack of knowledge of the equations of state for nuclear and quark matter, measuring neutron star masses and radii alone do not allow us to reach our goals.

B. Signatures of the compactness of neutron stars

If we could detect gravity waves from neutron stars spiraling into black holes in binary systems, the gravitational wave form during the last few orbits, when the neutron star is being tidally disrupted, will encode information about the density profile of the neutron star. For example, upon assuming a conventional density profile, the gravity wave form encodes information about the ratio M/R [401], essentially via encoding the value of the orbital frequency at which tidal deformation becomes significant. This suggests a scenario in which the presence of an interface separating a denser quark core from a less-dense nuclear mantle could manifest itself via the existence of two orbital frequency scales in the wave form, the first being that at which the outer layers are deformed while the denser quark core remains spherical and the second being the time at which even the quark core is disrupted [193]. This idea must be tested in numerical relativity calculations, and it may turn out to be better formulated in some other way. For example, perhaps the gravity wave form can be used to constrain the first few moments of the density profile, and this information can then be used to contrast neutron stars with standard density profiles characterized by a single length scale R with those which are anomalously compact because they have a "step" in their density profile. Whatever the best formulation turns out to be, it seems clear that if LIGO sees events in which the tidal disruption of a neutron star occurs within the LIGO band-width, the gravity wave data will constrain the "compactness" of the neutron star, providing information about the density profile that is complementary to that obtained from a mass-radius relation.

If there is a "step" in the density profile at an interface, LIGO gravity waves may provide evidence for its presence. But, should a density step be expected if color superconducting quark matter is found in the core of a neutron star? There are two qualitatively distinct possibilities for the density profile, depending on the surface tension of the quark matter/nuclear matter interface σ. If σ is large enough, there will be a stable, sharp, interface between two phases having different densities (but the same chemical potential). If σ is small enough, it becomes favorable instead to form a macroscopic volume filled with a net-neutral mixture of droplets of negatively charged quark matter and positively charged nuclear matter, see Sec. III H, which allows a continuous density profile. The distinction between these two scenarios has been analyzed quantitatively for the case of a first order phase transition from nuclear matter to CFL quark matter [193]. This is the simplest possible phase diagram of QCD, with a single transition between the phases known to exist at nuclear density and at asymptotically high density. We have seen earlier in this review that this simple QCD phase diagram is obtained if $\Delta_{\rm CFL}$ is large enough, allowing CFL pairing to fend off stresses that seek to split Fermi surfaces, all the way down in density until the nuclear matter takes over from quark matter. A sharp interface between the (electrically insulating) CFL phase and (electrically conducting) nuclear matter features charged boundary layers on either side of the interface, which play an important role in determining the σ above which this step in the density profile is stable [193]. The critical σ is about 40 MeV/fm^3, lower than dimensional analysis would indicate should be expected, meaning that the sharp interface with a density step is more likely than a mixture of charged components. The increase in the density at the interface can easily be by a factor of two. The critical σ above which a sharp interface is favored has not been evaluated for the case of a first order phase transition between nuclear matter and color superconducting phases other than the CFL phase.

It is also possible that the long term analysis of the binary double pulsar PSR J0737-3039A [402, 403] may yield a measurement of the moment of inertia of this 1.34 solar mass neutron star [404–407]. This could be another route to constraining the compactness of a neutron star, and perhaps gaining evidence for or against a step in the density profile of this star.

C. Cooling

The avenues of investigation that we have described so far may constrain the possible existence of quark matter within neutron star cores, but they are not sensitive to the differences among different color superconducting phases

of quark matter. We turn now to the first of three observational signatures that have the potential to differentiate between CFL quark matter and other color superconducting phases.

Within less than a minute of its birth in a supernova, a neutron star cools below about 1 MeV and becomes transparent to neutrinos. For the next million years or so it cools mainly via neutrino emission from its interior. Photon emission from the surface becomes dominant only later than that. This means that information about properties of the interior, in particular its neutrino emissivity and heat capacity, can be inferred from measurements of the temperature and age of neutron stars. Because all forms of dense matter are good heat conductors [337], neutron star interiors are isothermal and the rate at which they cool is determined by the volume integrals over the entire interior of the local emissivity and the local specific heat. This means that the cooling tends to be dominated by the properties of whichever phase has the highest neutrino emissivity and whichever phase has the highest specific heat.

Different forms of dense matter fall into three categories, ordered by decreasing neutrino emissivity. The first category includes any phase of matter that can emit neutrinos via direct Urca processes, yielding an emissivity $\epsilon_\nu \propto T^6$. Examples include unpaired quark matter, phases of quark matter with some unpaired quarks including the crystalline phases and the phases with single flavor pairing in Table III, baryonic matter containing hyperons, nucleonic matter augmented by either a pion or a kaon condensate, and even ordinary nuclear matter at sufficiently high densities that the proton fraction exceeds about 0.1. For the specific case of unpaired quark matter, the emissivity is given by (160) [350, 408], which can be written as

$$\epsilon_\nu \simeq (4\times 10^{25}\text{erg cm}^{-3}\text{ s}^{-1})\,\frac{\alpha_s}{0.5}\left(\frac{M_s^2/\mu}{100\text{ MeV}}\right)\left(\frac{\mu}{500\text{ MeV}}\right)^2\left(\frac{T}{10^9\text{ K}}\right)^6, \tag{166}$$

where we have taken $\mu_e = M_s^2/(4\mu)$, appropriate for neutral unpaired quark matter. (Note that $\alpha_s \sim 0.5$ is comparable to the value $c \sim 0.3$ that we used in Sec. VIII A, according to the lowest order relation $c = 2\alpha_s/\pi$. The $\alpha_s/0.5$ factor in (166) could be replaced by $c/0.3$.) The emissivity of other phases of quark matter in which only some quarks are unpaired, including the crystalline phases, is reduced relative to (166), but only by factors of order unity.

Ordinary nuclear matter at densities not too far above n_0, where the proton fraction is less than 0.1, falls into a second category in which there is no phase space for direct Urca processes and neutrino emission occurs only via modified Urca processes like $n + X \to p + X + e + \bar{\nu}$ with X some spectator nucleon, giving the much lower emissivity

$$\epsilon_\nu^{nm} = (1.2\times 10^{20}\text{erg cm}^{-3}\text{ s}^{-1})\left(\frac{n}{n_0}\right)^{2/3}\left(\frac{T}{10^9\text{ K}}\right)^8. \tag{167}$$

Neutron stars whose interiors emit neutrinos at this rate, perhaps modified by effects of nucleon superfluidity, cool following a family of standard cooling curves (see [355, 409, 410] and references therein), taking 10^5 to 10^6 years to cool below 10^8 K.

CFL quark matter constitutes a third category. As we have seen in Sec. VII, it is unique among all phases of dense matter in having an emissivity $\propto T^{15}$ that is many orders of magnitude smaller than (167). Furthermore, whereas all other phases of dense matter have a specific heat $\propto T$, in the CFL phase the specific heat is controlled by bosonic excitations making it $\propto T^3$. This means that if a neutron star has a CFL core, the total neutrino emissivity and the total heat capacity of the star are both utterly dominated by the contributions of the outer layers, whether these are made of nuclear matter or of some phase that admits direct Urca reactions. The CFL core holds little heat, and emits few neutrinos, but is a good conductor and so stays at the same temperature as the rest of the star. The rest of the star controls how the star cools.

Finally, the single-flavor color superconducting phases are interesting because they represent a potential transition from the first to the third categories [358, 411]: their critical temperatures are so low that if some quarks can only pair in spin-one channels, they will not pair until after the star has cooled through an initial epoch of direct Urca emission; and, in certain cases [238, 356, 358] all quarks can be gapped below the critical temperature for color-spin locked pairing, meaning that these phases ultimately become like CFL quark matter, playing no role in the cooling of the star which at late times will be controlled by the modified Urca processes in the nuclear matter mantle.

We can now describe a possible future path to the discovery of CFL quark matter cores within neutron stars. Suppose that LIGO detects the gravitational waves from the tidal disruption of a neutron star with some known mass spiralling into a black hole and, as we discussed in Sec. VIII B, suppose that evidence is found that the density profile of the neutron star has a denser core within a less dense mantle, consistent with the existence of a step in the density profile. Suppose furthermore that it was understood by then that neutron stars with that mass cool following one of the family of standard cooling curves, meaning that there can be no component of their interior within which direct Urca processes are allowed at any time. This combination of observations would rule out the possibility that the dense core, inside the density step, contained any of the color superconducting phases that we have discussed except CFL.

The scenario above may be unlikely, because there are a growing number of lines of evidence that although the cooling of many neutron stars is broadly consistent with the standard cooling curves, some fraction of neutron stars cool much more quickly. Examples of neutron stars that are too cold for their age include those in the supernova remnants 3C58 and CTA1 [363, 409]. A second, less direct, piece of evidence is provided by an unsuccessful search for the X-ray emission from a cooling neutron star in 15 other supernova remnants [412–414]. Although some of these supernovae may have been Type IA supernovae which do not produce neutron stars, and although some may have produced black holes, it is likely that many of these supernovae remnants do contain neutron stars. Their nonobservation results in an upper limit on their temperatures, and in all cases this upper limit falls below the standard cooling curves. A third line of evidence comes from neutron stars that undergo transient bouts of accretion [415]. X-ray observations of one of these, SAX J1808.4-3658, during its quiescent phase yield an upper limit on the thermal luminosity of the neutron star [416]. The mean accretion rate averaged over many transient accretion episodes is known, meaning that the average accretion heating of the star is known. The fact that the thermal luminosity is as low as it is means that the accretion heating of the star must be balanced by cooling by neutrino emission at a rate that far exceeds (167). The emissivity for unpaired quark matter (160) is consistent with the data, as are the direct Urca rates for sufficiently dense nuclear matter and for hyperon matter. Pion condensation or kaon condensation yield emissivities that are proportional to T^6 but with prefactors that are about two orders of magnitude smaller than that in (160), and are ruled out as explanations for the ability of SAX J1808.4-3658 to keep cool [416]. Similar conclusions can also be inferred from the (even lower) limit on the quiescent luminosity of the soft X-ray transient 1H 1905+000 [417–419], although in this instance the time-averaged accretion rate is not as well known.

By now it certainly seems clear that some neutron stars cool much faster than others. It is then reasonable to speculate that lighter neutron stars cool following the standard cooling curve and are composed of nuclear matter throughout whereas, based on the three lines of evidence above, heavier neutron stars cool faster because they contain some form of dense matter that can radiate neutrinos via the direct Urca process. This could be quark matter in one of the non-CFL color superconducting phases, but there are other, baryonic, possibilities. If this speculation is correct, then if neutron stars contain CFL cores they must be "inner cores", within an outer core made of whatever is responsible for the rapid neutrino emission.

D. r-modes limiting pulsar spins

A rapidly spinning neutron star will quickly slow down if it is unstable with respect to bulk flows known as Rossby modes, or r-modes, whose restoring force is due to the Coriolis effect and which transfer the star's angular momentum into gravitational radiation [420–424]. For any given interior composition and temperature, above some critical spin frequency there is an instability which leads to an exponentially growing r-mode. This means that as a neutron star is spun up by accretion, its spin will be limited by a value very slightly above this critical frequency, at which the accretion torque is balanced by gravitational radiation from the r-mode flows [422, 423, 425–427]. From a microphysical point of view, the r-mode instability is limited by viscous damping: the greater the damping, the higher the critical spin above which r-modes become unstable. The critical frequency is controlled by the shear viscosity in some regimes of temperature (typically lower) and by the bulk viscosity in others (typically higher). This means that the existence of pulsars with a given spin, as well as any observational evidence for an upper limit on pulsar spins, can yield constraints on the viscosities of neutron star interiors.

There is observational evidence for a physical limit on pulsar spins. The fastest known pulsar is a recently discovered radio pulsar spinning at 716 Hz [428]. However, it is not easy to draw inferences from the distribution of spins of the many known radio pulsars as to whether 716 Hz is close to some physical limit on the spin frequency because there are significant observational biases that make it harder to find faster radio pulsars. The most rapid pulsars are "recycled", meaning that they were spun-up during an episode of accretion from a binary companion. During such accretion, a neutron star may be visible as an X-ray pulsar. The spin frequencies of the 13 known millisecond X-ray pulsars lie between 270 and 619 Hz. What makes this significant is first of all that the episodes of accretion have long enough durations that they could easily spin a neutron star up beyond 1000 Hz, and second of all that there are no selection biases that preclude the discovery of X-ray pulsars with frequencies as large as 2000 Hz [429, 430]. Analysis of the observed distribution of X-ray pulsar spin frequencies leads to two conclusions: first, the distribution is consistent with being uniform;[7] and, second, there is some physical effect that sets a limit on the allowed spin of a pulsar which

[7] These data thus rule out a proposal for how small quark matter cores could have been detected [431]. If slowly-rotating neutron stars just barely reach quark-matter densities in their center, then rapidly spinning oblate neutron stars, which have slightly lower central density, will not contain quark matter. This "spinning out" of a quark matter core could be detected either by anomalies in braking

(with 95% confidence) is at 730 Hz or lower [429, 430]. It is unlikely that a spin-limit in this vicinity can be attributed to centrifugal break-up of the spinning neutron star: unless neutron star radii are larger than anticipated, this "mass shedding limit" is significantly higher, above 1 kHz. On the other hand, if the observed limit on pulsar spin frequencies is attributed to the onset of the r-mode instability, the resulting constraint on the viscosities of neutron star interiors is broadly consistent with the viscosities of nuclear matter, although this consistency is somewhat loose given the uncertainties in neutron star densities and in their temperatures while being spun up [422, 433].

The physics of the r-mode instability definitively rules out the possibility that accreting X-ray binary pulsars are strange stars that are composed of CFL quark matter throughout [344]. From the results of Sec. VII, we can conclude that CFL quark matter has negligible shear damping, and significantly smaller bulk viscosity than nuclear matter. (See [333, 434, 435], for calculations of bulk viscosity in nuclear matter, [436, 437] for baryonic matter containing hyperons, and [438] for baryonic matter containing a kaon condensate.) A CFL strange star would therefore have a critical frequency at which the r-mode instability sets in measured in Hz or fractions of Hz, in gross disagreement with the data on spin frequencies of both X-ray and radio pulsars.[8]

It is a very interesting question, at present unresolved, whether the presence of a CFL quark matter core within an ordinary neutron star introduces unstable r-modes at low spin frequencies. If there is a density step at the nuclear/CFL interface, there may be oscillation modes localized near that interface. The question is whether there are r-modes that are sufficiently well localized on the CFL side of the interface that they are undamped, or whether the tails of the mode wave functions that extend into the nuclear matter side of the interface result in enough damping to prevent the modes from becoming unstable. Nobody has solved for the r-mode wave functions for a rotating star whose density profile has a step at an interface, with viscous dissipation occurring on one side of the interface only.[9] If it were to turn out that a star with a CFL core is even close to as unstable with respect to r-modes as a star that is made entirely of CFL matter, the existence of pulsars spinning with hundreds of Hz frequencies would immediately rule out the possibility that these neutron stars have CFL cores.

E. Supernova neutrinos

The only time when a neutron star emits enough neutrinos to be detectable on earth as a neutrino source is during the first few seconds after the supernova explosion. The time-of-arrival distribution of supernova neutrinos could teach us about possible phase transitions to CFL quark matter [347–349, 440, 441]. All phases of quark matter and nuclear matter except CFL have short enough mean free paths that the neutrinos detected from a supernova are emitted from a surface of last scattering called the neutrinosphere, inside of which they were diffusing. This surface of last scattering moves inward to higher densities during the first seconds after the supernova, as the protoneutron star cools. Suppose that a volume in the core of the protoneutron star has made a transition into the CFL phase, in which neutrinos scatter only off Goldstone bosons which are less numerous (number density $\propto T^3$ rather than $\propto \mu^2 T$ for ungapped quark excitations). As this core cools, the neutrino mean free path within a CFL core becomes longer than in any phase of matter in which there are unpaired quarks (or nucleons) off which the neutrinos can scatter. The last supernova neutrinos to arrive could carry information about conditions when the neutrinosphere reaches the CFL core. Perhaps there may even be enhanced neutrino luminosity at the end of an otherwise dropping time-of-arrival distribution, as all those neutrinos that were previously trapped within the transparent core fly out unimpeded [440]. Determining whether this proposed signature can arise requires implementing the transition to a CFL core, with its long neutrino mean free paths, within a full-fledged simulation of neutrino transport during a supernova.

F. Rigid quark matter and pulsar glitches

The existence of a rigid crystalline color superconducting core within neutron stars may have a variety of observable consequences. For example, if some agency (like magnetic fields not aligned with the rotation axis) could maintain

---

indices of radio pulsars that are slowing down [432] or by anomalous population statistics of X-ray pulsars that are being spun up by accretion [431]. The data on X-ray pulsars show no sign of such an effect [429, 430] indicating that, if quark matter is present, spinning the star and making it oblate does not get rid of it. If neutron stars do have quark matter cores, therefore, the quark matter must occupy a reasonable fraction of the star.

[8] Strange stars made of unpaired quark matter or of 2SC quark matter can be consistent with the data [344].

[9] Certain other oscillation modes ("f-modes" and "g-modes") of a nonrotating neutron star whose density profile includes a density step have been computed [439].

the rigid core in a shape that has a nonzero quadrupole moment, gravity waves would be emitted. The LIGO non-detection of such gravity waves from nearby neutron stars [442] already limits the possibility that they have rigid cores that are deformed to the maximum extent allowed by the shear modulus (168), upon assuming a range of possible breaking strains, and this constraint will tighten as LIGO continues to run [443, 444]. (The analogous constraint on strange stars that are rigid throughout was obtained in [445].) Perhaps the most exciting implication of a rigid core, however, is the possibility that (some) pulsar "glitches" could originate deep within a neutron star, in its quark matter core.

A spinning neutron star observed as a pulsar gradually spins down as it loses rotational energy to electromagnetic radiation. But, every once in a while the angular velocity at the crust of the star is observed to increase suddenly in a dramatic event called a glitch. The standard explanation [446–455] requires the presence of a superfluid in some region of the star which also features a rigid array of spatial inhomogeneities which can pin the vortices in the rotating superfluid. In the standard explanation of pulsar glitches, these conditions are met in the inner crust of a neutron star which features a neutron superfluid coexisting with a rigid array of positively charged nuclei that may serve as vortex pinning sites. We shall see below that a rigid core made of crystalline color superconducting quark matter also meets the basic requirements.

The viability of the standard scenario for the origin of pulsar glitches in neutron star crusts has recently been questioned [456]. Explaining the issue requires understanding how the basic requirements come into play in the generation of a glitch. As a spinning pulsar slowly loses angular momentum over years, since the angular momentum of any superfluid component of the star is proportional to the density of vortices the vortices "want" to move apart. However, if within the inner crust the vortices are pinned to a rigid structure, these vortices do not move and after a time this superfluid component of the star is spinning faster than the rest of the star. When the "tension" built up in the array of pinned vortices reaches a critical value, there is a sudden "avalanche" in which vortices unpin, move outwards reducing the angular momentum of the superfluid, *and then re-pin*. As this superfluid suddenly loses angular momentum, the rest of the star, including in particular the surface whose angular velocity is observed, speeds up — a glitch. We see that this scenario requires superfluidity coexisting with a rigid structure to which vortices can pin that does not easily deform when vortices pinned to it are under tension. In very recent work, Link has questioned whether this scenario is viable because once neutron vortices are moving through the inner crust, as must happen during a glitch, they are so resistant to bending that they may never re-pin [456]. Link concludes that we do not have an understanding of any dynamics that could lead to the re-pinning of moving vortices, and hence that we do not currently understand glitches as a crustal phenomenon.

We have seen in Sec. VI B that if neutron star cores are made of quark matter but $\Delta_{\rm CFL}$ is not large enough for this quark matter to be in the CFL phase, then all of the quark matter core — and hence a significant fraction of the moment of inertia of the star — may be in one of the crystalline phases described in Sec. VI B. By virtue of being simultaneously superfluids and rigid solids, the crystalline phases of quark matter provide all the necessary conditions to be the locus in which (some) pulsar glitches originate. Their shear moduli (144), namely

$$\nu = 3.96 \times 10^{33} {\rm erg/cm}^3 \left(\frac{\Delta}{10\ {\rm MeV}}\right)^2 \left(\frac{\mu}{400\ {\rm MeV}}\right)^2 \tag{168}$$

with Δ the gap parameter in the crystalline phase as in Fig. 10, make this form of quark matter 20 to 1000 times more rigid than the crust of a neutron star [320, 328], and hence more than rigid enough for glitches to originate within them. The crystalline phases are at the same time superfluid, and it is reasonable to expect that the superfluid vortices that will result when a neutron star with such a core rotates will have lower free energy if they are centered along the intersections of the nodal planes of the underlying crystal structure, i.e. along lines along which the condensate already vanishes even in the absence of a rotational vortex. A crude estimate of the pinning force on vortices within crystalline color superconducting quark matter indicates that it is sufficient [320]. So, the basic requirements for superfluid vortices pinning to a rigid structure are all present. The central questions that remain to be addressed are the explicit construction of vortices in the crystalline phase and the calculation of their pinning force, as well as the calculation of the timescale over which sudden changes in the angular momentum of the core are communicated to the (observed) surface, presumably either via the common electron fluid or via magnetic stresses.

Much theoretical work remains before the hypothesis that pulsar glitches originate within a crystalline color superconducting neutron star core is developed fully enough to allow it to confront data on the magnitudes, relaxation timescales, and repeat rates that characterize glitches. Nevertheless, this hypothesis offers one immediate advantage over the conventional scenario that relied on vortex pinning in the neutron star crust. It is impossible for a neutron star anywhere within which rotational vortices are pinned to precess on $\sim$ year time scales [457–459], and yet there is now evidence that several pulsars are precessing [460–462]. Since *all* neutron stars have crusts, the precession of any pulsar is inconsistent with the pinning of vortices within the crust, a requirement in the standard explanation of glitches. On the other hand, perhaps not all neutron stars have crystalline quark matter cores — for example, perhaps the lightest neutron stars have nuclear matter cores. Then, if vortices are never pinned in the crust but are

pinned within a crystalline quark matter core, those neutron stars that do have a crystalline quark matter core can glitch but cannot precess while those that don't can precess but cannot glitch.

Acknowledgments

We acknowledge helpful conversations with N. Andersson, M. Braby, D. Chakrabarty, T. Hatsuda, S. Hughes, D.L. Kaplan, B. Link, M. Mannarelli, C. Manuel, D. Nice, D. Page, A. Rebhan, S. Reddy, R. Sharma, I. Stairs, Q. Wang, and F. Wilczek. This research was supported in part by the Offices of Nuclear Physics and High Energy Physics of the Office of Science of the U.S. Department of Energy under contracts #DE-FG02-91ER40628, #DE-FG02-05ER41375 (OJI), #DE-FG02-94ER40818, #DE-FG02-03ER41260.

[1] P. Carruthers, Coll. Phen. **1**, 147 (1973).
[2] D. D. Ivanenko and D. F. Kurdgelaidze, Astrophysics **1**, 479 (1965).
[3] F. Pacini, Nature **209**, 389 (1966).
[4] D. Boccaletti, V. de Sabbata, and C. Gualdi, Nuovo Cim. **45**, 513 (1966).
[5] N. Itoh, Prog. Theor. Phys. **44**, 291 (1970).
[6] D. D. Ivanenko and D. F. Kurdgelaidze, Lett. Nuovo Cim. **IIS1**, 13 (1969).
[7] D. D. Ivanenko and D. F. Kurdgelaidze, Sov. Phys. J. **13**, 1015 (1970).
[8] D. J. Gross and F. Wilczek, Phys. Rev. Lett. **30**, 1343 (1973).
[9] H. D. Politzer, Phys. Rev. Lett. **30**, 1346 (1973).
[10] J. C. Collins and M. J. Perry, Phys. Rev. Lett. **34**, 1353 (1975).
[11] M. B. Kislinger and P. D. Morley, Phys. Rev. D **13**, 2765 (1976).
[12] B. A. Freedman and L. D. McLerran, Phys. Rev. **D16**, 1169 (1977).
[13] B. Freedman and L. D. McLerran, Phys. Rev. **D17**, 1109 (1978).
[14] G. Baym and S. A. Chin, Phys. Lett. **B62**, 241 (1976).
[15] G. Chapline and M. Nauenberg, Nature **264**, 235 (1976).
[16] G. Chapline and M. Nauenberg, Phys. Rev. **D16**, 450 (1977).
[17] B. C. Barrois, Nucl. Phys. **B129**, 390 (1977).
[18] B. C. Barrois, Ph.D. thesis, California Institute of Technology, Pasadena, California (1979), UMI 79-04847.
[19] S. C. Frautschi (1978), presented at Workshop on Hadronic Matter at Extreme Energy Density, Erice, Italy, Oct 13-21, 1978.
[20] D. Bailin and A. Love, J. Phys. **A12**, L283 (1979).
[21] D. Bailin and A. Love, Phys. Rept. **107**, 325 (1984).
[22] M. Iwasaki and T. Iwado, Phys. Lett. **B350**, 163 (1995).
[23] M. Iwasaki, Prog. Theor. Phys. Suppl. **120**, 187 (1995).
[24] M. G. Alford, K. Rajagopal, and F. Wilczek, Phys. Lett. **B422**, 247 (1998), hep-ph/9711395.
[25] R. Rapp, T. Schäfer, E. V. Shuryak, and M. Velkovsky, Phys. Rev. Lett. **81**, 53 (1998), hep-ph/9711396.
[26] M. G. Alford, K. Rajagopal, and F. Wilczek, Nucl. Phys. **B537**, 443 (1999), hep-ph/9804403.
[27] I. A. Shovkovy, Found. Phys. **35**, 1309 (2005), nucl-th/0410091.
[28] G. Nardulli, Riv. Nuovo Cim. **25N3**, 1 (2002), hep-ph/0202037.
[29] M. Huang, Int. J. Mod. Phys. **E14**, 675 (2005), hep-ph/0409167.
[30] M. Buballa, Phys. Rept. **407**, 205 (2005), hep-ph/0402234.
[31] H.-c. Ren (2004), hep-ph/0404074.
[32] S. D. H. Hsu (2000), hep-ph/0003140.
[33] K. Rajagopal and F. Wilczek (2000), hep-ph/0011333.
[34] M. G. Alford, Ann. Rev. Nucl. Part. Sci. **51**, 131 (2001), hep-ph/0102047.
[35] D. K. Hong, Acta Phys. Polon. **B32**, 1253 (2001), hep-ph/0101025.
[36] D. H. Rischke, Prog. Part. Nucl. Phys. **52**, 197 (2004), nucl-th/0305030.
[37] T. Schäfer (2003), hep-ph/0304281.
[38] S. Reddy, Acta Phys. Polon. **B33**, 4101 (2002), nucl-th/0211045.
[39] M. G. Alford and K. Rajagopal, in *Pairing in Fermionic Systems: Basic Concepts and Modern Applications* (World Scientific, 2006), pp. 1–36, hep-ph/0606157.
[40] C. Schmidt, PoS **LAT2006**, 021 (2006), hep-lat/0610116.
[41] Y. Nishida, K. Fukushima, and T. Hatsuda, Phys. Rept. **398**, 281 (2004), hep-ph/0306066.
[42] J. B. Kogut, M. A. Stephanov, and D. Toublan, Phys. Lett. **B464**, 183 (1999), hep-ph/9906346.
[43] J. B. Kogut, M. A. Stephanov, D. Toublan, J. J. M. Verbaarschot, and A. Zhitnitsky, Nucl. Phys. **B582**, 477 (2000), hep-ph/0001171.
[44] K. Fukushima and K. Iida, Phys. Rev. **D76**, 054004 (2007), 0705.0792.

[45] S. Hands, J. B. Kogut, M.-P. Lombardo, and S. E. Morrison, Nucl. Phys. **B558**, 327 (1999), hep-lat/9902034.
[46] J. B. Kogut, D. K. Sinclair, S. J. Hands, and S. E. Morrison, Phys. Rev. **D64**, 094505 (2001), hep-lat/0105026.
[47] S. Hands, S. Kim, and J.-I. Skullerud, Eur. Phys. J. **C48**, 193 (2006), hep-lat/0604004.
[48] J. B. Kogut, D. Toublan, and D. K. Sinclair, Nucl. Phys. **B642**, 181 (2002), hep-lat/0205019.
[49] B. Alles, M. D'Elia, and M. P. Lombardo, Nucl. Phys. **B752**, 124 (2006), hep-lat/0602022.
[50] J. B. Kogut and D. K. Sinclair, Phys. Rev. **D66**, 034505 (2002), hep-lat/0202028.
[51] K. Splittorff, D. T. Son, and M. A. Stephanov, Phys. Rev. **D64**, 016003 (2001), hep-ph/0012274.
[52] D. T. Son and M. A. Stephanov, Phys. Rev. Lett. **86**, 592 (2001), hep-ph/0005225.
[53] S. Hands and D. N. Walters, Phys. Rev. **D69**, 076011 (2004), hep-lat/0401018.
[54] R. D. Pisarski and D. H. Rischke, Phys. Rev. Lett. **83**, 37 (1999), nucl-th/9811104.
[55] D. T. Son, Phys. Rev. **D59**, 094019 (1999), hep-ph/9812287.
[56] J. Bardeen, L. Cooper, and J. Schrieffer, Phys. Rev. **106**, 162 (1957).
[57] T. Holstein, A. E. Norton, and P. Pincus, Phys. Rev. **B8**, 2649 (1973).
[58] A. Ipp, K. Kajantie, A. Rebhan, and A. Vuorinen, Phys. Rev. **D74**, 045016 (2006), hep-ph/0604060.
[59] S. Chakravarty, R. E. Norton, and O. F. Syljuasen, Phys. Rev. Lett **75**, 1423 (1995).
[60] G. Baym, H. Monien, C. J. Pethick, and D. G. Ravenhall, Phys. Rev. Lett. **64**, 1867 (1990).
[61] B. Vanderheyden and J.-Y. Ollitrault, Phys. Rev. **D56**, 5108 (1997), hep-ph/9611415.
[62] C. Manuel, Phys. Rev. **D62**, 076009 (2000), hep-ph/0005040.
[63] C. Manuel, Phys. Rev. **D62**, 114008 (2000), hep-ph/0006106.
[64] W. E. Brown, J. T. Liu, and H.-c. Ren, Phys. Rev. **D62**, 054013 (2000), hep-ph/0003199.
[65] D. Boyanovsky and H. J. de Vega, Phys. Rev. **D63**, 034016 (2001), hep-ph/0009172.
[66] D. Boyanovsky and H. J. de Vega, Phys. Rev. **D63**, 114028 (2001), hep-ph/0011354.
[67] A. Ipp, A. Gerhold, and A. Rebhan, Phys. Rev. **D69**, 011901 (2004), hep-ph/0309019.
[68] A. Gerhold, A. Ipp, and A. Rebhan, Phys. Rev. **D70**, 105015 (2004), hep-ph/0406087.
[69] J. Polchinski, Nucl. Phys. **B422**, 617 (1994).
[70] C. Nayak and F. Wilczek, Nucl. Phys. **B430**, 534 (1994).
[71] D. V. Deryagin, D. Y. Grigoriev, and V. A. Rubakov, Int. J. Mod. Phys. **A7**, 659 (1992).
[72] R. Shankar, Rev. Mod. Phys. **66**, 129 (1994).
[73] E. Shuster and D. T. Son, Nucl. Phys. **B573**, 434 (2000), hep-ph/9905448.
[74] L. McLerran and R. D. Pisarski, Nucl. Phys. **A796**, 83 (2007), 0706.2191.
[75] S. B. Ruester, V. Werth, M. Buballa, I. A. Shovkovy, and D. H. Rischke, Phys. Rev. **D73**, 034025 (2006), hep-ph/0509073.
[76] D. B. Kaplan and S. Reddy, Phys. Rev. **D65**, 054042 (2002), hep-ph/0107265.
[77] V. Laporta and M. Ruggieri, Phys. Lett. **B633**, 734 (2006), hep-ph/0511155.
[78] J. Berdermann, D. Blaschke, and H. Grigorian (2004), astro-ph/0404079.
[79] P. Amore, M. C. Birse, J. A. McGovern, and N. R. Walet, Phys. Rev. **D65**, 074005 (2002), hep-ph/0110267.
[80] H. T. Elze, W. Greiner, and J. Rafelski, Phys. Lett. **B124**, 515 (1983).
[81] H.-T. Elze, W. Greiner, and J. Rafelski, Z. Phys. **C24**, 361 (1984).
[82] M. Buballa and I. A. Shovkovy, Phys. Rev. **D72**, 097501 (2005), hep-ph/0508197.
[83] K. Rajagopal and A. Schmitt, Phys. Rev. **D73**, 045003 (2006), hep-ph/0512043.
[84] K. Iida and G. Baym, Phys. Rev. **D63**, 074018 (2001), hep-ph/0011229.
[85] M. G. Alford and K. Rajagopal, JHEP **06**, 031 (2002), hep-ph/0204001.
[86] A. Gerhold and A. Rebhan, Phys. Rev. **D68**, 011502 (2003), hep-ph/0305108.
[87] A. Kryjevski, Phys. Rev. **D68**, 074008 (2003), hep-ph/0305173.
[88] D. D. Dietrich and D. H. Rischke, Prog. Part. Nucl. Phys. **53**, 305 (2004), nucl-th/0312044.
[89] A. M. Clogston, Phys. Rev. Lett. **9**, 266 (1962).
[90] B. S. Chandrasekhar, Appl. Phys. Lett. **1**, 7 (1962).
[91] M. G. Alford, C. Kouvaris, and K. Rajagopal, Phys. Rev. Lett. **92**, 222001 (2004), hep-ph/0311286.
[92] K. Rajagopal and F. Wilczek, Phys. Rev. Lett. **86**, 3492 (2001), hep-ph/0012039.
[93] M. G. Alford and Q.-h. Wang, J. Phys. **G31**, 719 (2005), hep-ph/0501078.
[94] T. Schäfer, Nucl. Phys. **B575**, 269 (2000), hep-ph/9909574.
[95] M. Kitazawa, D. H. Rischke, and I. A. Shovkovy, Phys. Lett. **B663**, 228 (2008), 0709.2235.
[96] M. Kitazawa, T. Koide, T. Kunihiro, and Y. Nemoto, Prog. Theor. Phys. **114**, 117 (2005), hep-ph/0502035.
[97] M. Kitazawa, T. Koide, T. Kunihiro, and Y. Nemoto, Phys. Rev. **D65**, 091504 (2002), nucl-th/0111022.
[98] M. Kitazawa, T. Kunihiro, and Y. Nemoto, Phys. Lett. **B631**, 157 (2005), hep-ph/0505070.
[99] K. Fukushima and K. Iida, Phys. Rev. **D71**, 074011 (2005), hep-ph/0501276.
[100] H. Abuki, T. Hatsuda, and K. Itakura, Phys. Rev. **D65**, 074014 (2002), hep-ph/0109013.
[101] M. Kitazawa, T. Koide, T. Kunihiro, and Y. Nemoto, Phys. Rev. **D70**, 056003 (2004), hep-ph/0309026.
[102] D. N. Voskresensky, Phys. Rev. **C69**, 065209 (2004).
[103] N. Yamamoto, M. Tachibana, T. Hatsuda, and G. Baym, Phys. Rev. **D76**, 074001 (2007), 0704.2654.
[104] T. Hatsuda, M. Tachibana, N. Yamamoto, and G. Baym, Phys. Rev. Lett. **97**, 122001 (2006), hep-ph/0605018.
[105] M. Srednicki and L. Susskind, Nucl. Phys. **B187**, 93 (1981).
[106] I. A. Shovkovy and L. C. R. Wijewardhana, Phys. Lett. **B470**, 189 (1999), hep-ph/9910225.
[107] R. D. Pisarski and D. H. Rischke (1999), nucl-th/9907094.
[108] A. P. Balachandran, S. Digal, and T. Matsuura, Phys. Rev. **D73**, 074009 (2006), hep-ph/0509276.

[109] E. Nakano, M. Nitta, and T. Matsuura (2007), arXiv:0708.4096 [hep-ph].
[110] K. Iida and G. Baym, Phys. Rev. **D66**, 014015 (2002), hep-ph/0204124.
[111] M. M. Forbes and A. R. Zhitnitsky, Phys. Rev. **D65**, 085009 (2002), hep-ph/0109173.
[112] I. A. Shovkovy and P. J. Ellis, Phys. Rev. **C67**, 048801 (2003), hep-ph/0211049.
[113] D. F. Litim and C. Manuel, Phys. Rev. **D64**, 094013 (2001), hep-ph/0105165.
[114] C. Manuel and K. Rajagopal, Phys. Rev. Lett. **88**, 042003 (2002), hep-ph/0107211.
[115] M. G. Alford and G. Good, Phys. Rev. **D70**, 036008 (2004), hep-ph/0404214.
[116] M. G. Alford, J. Berges, and K. Rajagopal, Nucl. Phys. **B571**, 269 (2000), hep-ph/9910254.
[117] E. J. Ferrer, V. de la Incera, and C. Manuel, Phys. Rev. Lett. **95**, 152002 (2005), hep-ph/0503162.
[118] E. J. Ferrer, V. de la Incera, and C. Manuel, Nucl. Phys. **B747**, 88 (2006), hep-ph/0603233.
[119] E. J. Ferrer and V. de la Incera, Phys. Rev. **D76**, 045011 (2007), nucl-th/0703034.
[120] J. L. Noronha and I. A. Shovkovy, Phys. Rev. **D76**, 105030 (2007), 0708.0307.
[121] K. Fukushima and H. J. Warringa, Phys. Rev. Lett. **100**, 032007 (2008), 0707.3785.
[122] D. T. Son, M. A. Stephanov, and A. R. Zhitnitsky, Phys. Rev. Lett. **86**, 3955 (2001), hep-ph/0012041.
[123] T. Schäfer and F. Wilczek, Phys. Rev. **D60**, 074014 (1999), hep-ph/9903503.
[124] M. G. Alford, J. Berges, and K. Rajagopal, Nucl. Phys. **B558**, 219 (1999), hep-ph/9903502.
[125] R. L. Jaffe and F. Wilczek, Phys. Rev. Lett. **91**, 232003 (2003), hep-ph/0307341.
[126] A. Selem and F. Wilczek (2006), hep-ph/0602128.
[127] F. E. Close and N. A. Tornqvist, J. Phys. **G28**, R249 (2002), hep-ph/0204205.
[128] R. L. Jaffe, Phys. Rev. **D15**, 267 (1977).
[129] M. Anselmino, E. Predazzi, S. Ekelin, S. Fredriksson, and D. B. Lichtenberg, Rev. Mod. Phys. **65**, 1199 (1993).
[130] T. Schäfer, Phys. Rev. **D62**, 094007 (2000), hep-ph/0006034.
[131] M. Buballa, J. Hosek, and M. Oertel, Phys. Rev. Lett. **90**, 182002 (2003), hep-ph/0204275.
[132] M. G. Alford, J. A. Bowers, J. M. Cheyne, and G. A. Cowan, Phys. Rev. **D67**, 054018 (2003), hep-ph/0210106.
[133] A. Schmitt, Q. Wang, and D. H. Rischke, Phys. Rev. **D66**, 114010 (2002), nucl-th/0209050.
[134] R. Rapp, T. Schäfer, E. V. Shuryak, and M. Velkovsky, Annals Phys. **280**, 35 (2000), hep-ph/9904353.
[135] N. J. Evans, J. Hormuzdiar, S. D. H. Hsu, and M. Schwetz, Nucl. Phys. **B581**, 391 (2000), hep-ph/9910313.
[136] H. Malekzadeh, Phys. Rev. **D74**, 065011 (2006), hep-ph/0604260.
[137] M. G. Alford, C. Kouvaris, and K. Rajagopal, Phys. Rev. **D71**, 054009 (2005), hep-ph/0406137.
[138] K. Fukushima, C. Kouvaris, and K. Rajagopal, Phys. Rev. **D71**, 034002 (2005), hep-ph/0408322.
[139] H. Abuki, M. Kitazawa, and T. Kunihiro, Phys. Lett. **B615**, 102 (2005), hep-ph/0412382.
[140] D. Blaschke, S. Fredriksson, H. Grigorian, A. M. Oztas, and F. Sandin, Phys. Rev. **D72**, 065020 (2005), hep-ph/0503194.
[141] S. B. Rüster, V. Werth, M. Buballa, I. A. Shovkovy, and D. H. Rischke, Phys. Rev. **D72**, 034004 (2005), hep-ph/0503184.
[142] P. F. Bedaque and T. Schäfer, Nucl. Phys. **A697**, 802 (2002), hep-ph/0105150.
[143] T. Schäfer, Phys. Rev. **D65**, 094033 (2002), hep-ph/0201189.
[144] M. Buballa, Phys. Lett. **B609**, 57 (2005), hep-ph/0410397.
[145] M. M. Forbes, Phys. Rev. **D72**, 094032 (2005), hep-ph/0411001.
[146] A. W. Steiner, S. Reddy, and M. Prakash, Phys. Rev. **D66**, 094007 (2002), hep-ph/0205201.
[147] H. Abuki and T. Kunihiro, Nucl. Phys. **A768**, 118 (2006), hep-ph/0509172.
[148] D. H. Rischke, D. T. Son, and M. A. Stephanov, Phys. Rev. Lett. **87**, 062001 (2001), hep-ph/0011379.
[149] R. Casalbuoni, R. Gatto, M. Mannarelli, and G. Nardulli, Phys. Lett. **B524**, 144 (2002), hep-ph/0107024.
[150] R. Ouyed and F. Sannino, Phys. Lett. **B511**, 66 (2001), hep-ph/0103168.
[151] I. Shovkovy and M. Huang, Phys. Lett. **B564**, 205 (2003), hep-ph/0302142.
[152] E. Gubankova, W. V. Liu, and F. Wilczek, Phys. Rev. Lett. **91**, 032001 (2003), hep-ph/0304016.
[153] M. G. Alford, C. Kouvaris, and K. Rajagopal (2004), hep-ph/0407257.
[154] S. B. Rüster, I. A. Shovkovy, and D. H. Rischke, Nucl. Phys. **A743**, 127 (2004), hep-ph/0405170.
[155] M. G. Alford, P. Jotwani, C. Kouvaris, J. Kundu, and K. Rajagopal, Phys. Rev. **D71**, 114011 (2005), astro-ph/0411560.
[156] M. Huang and I. A. Shovkovy, Phys. Rev. **D70**, 094030 (2004), hep-ph/0408268.
[157] I. Giannakis and H.-C. Ren, Phys. Lett. **B611**, 137 (2005), hep-ph/0412015.
[158] R. Casalbuoni, R. Gatto, M. Mannarelli, G. Nardulli, and M. Ruggieri, Phys. Lett. **B605**, 362 (2005), hep-ph/0410401.
[159] K. Fukushima, Phys. Rev. **D72**, 074002 (2005), hep-ph/0506080.
[160] S. Reddy and G. Rupak, Phys. Rev. **C71**, 025201 (2005), nucl-th/0405054.
[161] M. Huang, Phys. Rev. **D73**, 045007 (2006), hep-ph/0504235.
[162] K. Iida and K. Fukushima, Phys. Rev. **D74**, 074020 (2006), hep-ph/0603179.
[163] M. Hashimoto, Phys. Lett. **B642**, 93 (2006), hep-ph/0605323.
[164] K. Fukushima, Phys. Rev. **D73**, 094016 (2006), hep-ph/0603216.
[165] A. I. Larkin and Y. N. Ovchinnikov, Sov. Phys. JETP **20**, 762 (1965).
[166] P. Fulde and R. A. Ferrell, Phys. Rev. **135**, A550 (1964).
[167] M. G. Alford, J. A. Bowers, and K. Rajagopal, Phys. Rev. **D63**, 074016 (2001), hep-ph/0008208.
[168] J. A. Bowers and K. Rajagopal, Phys. Rev. **D66**, 065002 (2002), hep-ph/0204079.
[169] R. Casalbuoni and G. Nardulli, Rev. Mod. Phys. **76**, 263 (2004), hep-ph/0305069.
[170] R. Casalbuoni, R. Gatto, N. Ippolito, G. Nardulli, and M. Ruggieri, Phys. Lett. **B627**, 89 (2005), hep-ph/0507247.
[171] M. Mannarelli, K. Rajagopal, and R. Sharma, Phys. Rev. **D73**, 114012 (2006), hep-ph/0603076.
[172] K. Rajagopal and R. Sharma, Phys. Rev. **D74**, 094019 (2006), hep-ph/0605316.

[173] M. Ciminale, G. Nardulli, M. Ruggieri, and R. Gatto, Phys. Lett. **B636**, 317 (2006), hep-ph/0602180.
[174] A. Kryjevski and T. Schäfer, Phys. Lett. **B606**, 52 (2005), hep-ph/0407329.
[175] A. Kryjevski and D. Yamada, Phys. Rev. **D71**, 014011 (2005), hep-ph/0407350.
[176] T. Schäfer, Phys. Rev. Lett. **96**, 012305 (2006), hep-ph/0508190.
[177] A. Kryjevski, Phys. Rev. **D77**, 014018 (2008), hep-ph/0508180.
[178] A. Gerhold, T. Schäfer, and A. Kryjevski, Phys. Rev. **D75**, 054012 (2007), hep-ph/0612181.
[179] A. Gerhold and T. Schäfer, Phys. Rev. **D73**, 125022 (2006), hep-ph/0603257.
[180] A. Schmitt, Phys. Rev. **D71**, 054016 (2005), nucl-th/0412033.
[181] M. G. Alford and G. A. Cowan, J. Phys. **G32**, 511 (2006), hep-ph/0512104.
[182] A. Schmitt, Q. Wang, and D. H. Rischke, Phys. Rev. Lett. **91**, 242301 (2003), nucl-th/0301090.
[183] E. V. Gorbar, M. Hashimoto, and V. A. Miransky, Phys. Lett. **B632**, 305 (2006), hep-ph/0507303.
[184] E. V. Gorbar, M. Hashimoto, V. A. Miransky, and I. A. Shovkovy, Phys. Rev. **D73**, 111502 (2006), hep-ph/0602251.
[185] M. Hashimoto and V. A. Miransky, Prog. Theor. Phys. **118**, 303 (2007), 0705.2399.
[186] E. V. Gorbar, M. Hashimoto, and V. A. Miransky, Phys. Rev. **D75**, 085012 (2007), hep-ph/0701211.
[187] E. J. Ferrer and V. de la Incera, Phys. Rev. **D76**, 114012 (2007), 0705.2403.
[188] D. K. Hong (2005), hep-ph/0506097.
[189] M. Huang and I. Shovkovy, Nucl. Phys. **A729**, 835 (2003), hep-ph/0307273.
[190] M. G. Alford and Q.-h. Wang, J. Phys. **G32**, 63 (2006), hep-ph/0507269.
[191] D. G. Ravenhall, C. J. Pethick, and J. R. Wilson, Phys. Rev. Lett. **50**, 2066 (1983).
[192] N. K. Glendenning, Phys. Rev. **D46**, 1274 (1992).
[193] M. G. Alford, K. Rajagopal, S. Reddy, and F. Wilczek, Phys. Rev. **D64**, 074017 (2001), hep-ph/0105009.
[194] P. Jaikumar, S. Reddy, and A. W. Steiner, Phys. Rev. Lett. **96**, 041101 (2006), nucl-th/0507055.
[195] M. G. Alford, K. Rajagopal, S. Reddy, and A. W. Steiner, Phys. Rev. **D73**, 114016 (2006), hep-ph/0604134.
[196] F. Neumann, M. Buballa, and M. Oertel, Nucl. Phys. **A714**, 481 (2003), hep-ph/0210078.
[197] S. Giorgini, L. P. Pitaevskii, and S. Stringari (2007), arXiv:0706.3360.
[198] Y. Chin, M. W. Zwierlein, C. H. Schunck, A. Schirotzek, and W. Ketterle, Phys. Rev. Lett. **97**, 030401 (2006), cond-mat/0606432.
[199] M. W. Zwierlein, A. Schirotzek, C. H. Schunck, and W. Ketterle, Science **311**, 492 (2006), cond-mat/0511197.
[200] G. B. Partridge, W. Li, R. I. Kamar, Y. Liao, and R. G. Hulet, Science **311**, 503 (2006), cond-mat/0511752.
[201] D. E. Sheehy and L. Radzihovsky, Ann. Phys **322**, 1790 (2007).
[202] D. E. Sheehy and L. Radzihovsky, Phys. Rev. Lett. **96**, 060401 (2006), cond-mat/0508430.
[203] M. Mannarelli, G. Nardulli, and M. Ruggieri, Phys. Rev. **A74**, 033606 (2006), cond-mat/0604579.
[204] P. F. Bedaque, H. Caldas, and G. Rupak, Phys. Rev. Lett. **91**, 247002 (2003), cond-mat/0306694.
[205] J. Carlson and S. Reddy, Phys. Rev. Lett. **95**, 060401 (2005), cond-mat/0503256.
[206] D. T. Son and M. A. Stephanov, Phys. Rev. A **74**, 013614 (2006), cond-mat/0507586.
[207] K. Rajagopal and E. Shuster, Phys. Rev. **D62**, 085007 (2000), hep-ph/0004074.
[208] R. D. Pisarski and D. H. Rischke, Phys. Rev. **D60**, 094013 (1999), nucl-th/9903023.
[209] R. D. Pisarski and D. H. Rischke, Phys. Rev. **D61**, 074017 (2000), nucl-th/9910056.
[210] A. Schmitt, Ph.D. thesis, Johann-Wolfgang-Goethe-Universität, Frankfurt/Main, Germany (2004), nucl-th/0405076.
[211] A. Abrikosov, L. Gorkov, and I. Dzyaloshinski, *Methods of Quantum field theory in statistical physics* (Prentice-Hall, Inc., Englewood Cliffs, N.J., 1963).
[212] A. Fetter and J. Walecka, *Quantum theory of many-particle systems* (McGraw-Hill, New York, 1971).
[213] H. Abuki, Prog. Theor. Phys. **110**, 937 (2003), hep-ph/0306074.
[214] S. B. Rüster and D. H. Rischke, Phys. Rev. **D69**, 045011 (2004), nucl-th/0309022.
[215] V. A. Miransky, I. A. Shovkovy, and L. C. R. Wijewardhana, Phys. Rev. **D64**, 096002 (2001), hep-ph/0104194.
[216] S. Takagi, Prog. Theor. Phys. **109**, 233 (2003), hep-ph/0210227.
[217] J. M. Luttinger and J. C. Ward, Phys. Rev. **118**, 1417 (1960).
[218] G. Baym, Phys. Rev. **127**, 1391 (1962).
[219] J. M. Cornwall, R. Jackiw, and E. Tomboulis, Phys. Rev. **D10**, 2428 (1974).
[220] A. K. Leibovich, K. Rajagopal, and E. Shuster, Phys. Rev. **D64**, 094005 (2001), hep-ph/0104073.
[221] W. E. Brown, J. T. Liu, and H.-c. Ren, Phys. Rev. **D62**, 054016 (2000), hep-ph/9912409.
[222] A. Gerhold and A. Rebhan, Phys. Rev. **D71**, 085010 (2005), hep-ph/0501089.
[223] E. Braaten and R. D. Pisarski, Phys. Rev. **D45**, 1827 (1992).
[224] R. D. Pisarski and D. H. Rischke, Nucl. Phys. **A702**, 177 (2002), nucl-th/0111070.
[225] D.-f. Hou, Q. Wang, and D. H. Rischke, Phys. Rev. **D69**, 071501 (2004), hep-ph/0401152.
[226] T. Schäfer and F. Wilczek, Phys. Rev. **D60**, 114033 (1999), hep-ph/9906512.
[227] D. K. Hong, V. A. Miransky, I. A. Shovkovy, and L. C. R. Wijewardhana, Phys. Rev. **D61**, 056001 (2000), hep-ph/9906478.
[228] R. D. Pisarski and D. H. Rischke, Phys. Rev. **D61**, 051501 (2000), nucl-th/9907041.
[229] S. D. H. Hsu and M. Schwetz, Nucl. Phys. **B572**, 211 (2000), hep-ph/9908310.
[230] W. E. Brown, J. T. Liu, and H.-c. Ren, Phys. Rev. **D61**, 114012 (2000), hep-ph/9908248.
[231] Q. Wang and D. H. Rischke, Phys. Rev. **D65**, 054005 (2002), nucl-th/0110016.
[232] T. Schäfer (2004), hep-ph/0402032.
[233] S. R. Beane, P. F. Bedaque, and M. J. Savage, Nucl. Phys. **A688**, 931 (2001), nucl-th/0004013.
[234] B. Feng, D.-f. Hou, J.-r. Li, and H.-c. Ren, Nucl. Phys. **B754**, 351 (2006), nucl-th/0606015.

[235] P. T. Reuter, Phys. Rev. **D74**, 105008 (2006), nucl-th/0608020.
[236] D. H. Rischke, Phys. Rev. **D64**, 094003 (2001), nucl-th/0103050.
[237] D. Nickel, J. Wambach, and R. Alkofer, Phys. Rev. **D73**, 114028 (2006), hep-ph/0603163.
[238] F. Marhauser, D. Nickel, M. Buballa, and J. Wambach, Phys. Rev. **D75**, 054022 (2007), hep-ph/0612027.
[239] J. Berges and K. Rajagopal, Nucl. Phys. **B538**, 215 (1999), hep-ph/9804233.
[240] G. W. Carter and D. Diakonov, Phys. Rev. **D60**, 016004 (1999), hep-ph/9812445.
[241] P. W. Anderson, Phys. Rev. **130**, 439 (1963).
[242] P. W. Higgs, Phys. Lett. **12**, 132 (1964).
[243] D. H. Rischke, Phys. Rev. **D62**, 054017 (2000), nucl-th/0003063.
[244] D. H. Rischke, Phys. Rev. **D62**, 034007 (2000), nucl-th/0001040.
[245] D. H. Rischke and I. A. Shovkovy, Phys. Rev. **D66**, 054019 (2002), nucl-th/0205080.
[246] D. T. Son and M. A. Stephanov, Phys. Rev. **D61**, 074012 (2000), hep-ph/9910491.
[247] H. Malekzadeh and D. H. Rischke, Phys. Rev. **D73**, 114006 (2006), hep-ph/0602082.
[248] R. Casalbuoni, R. Gatto, and G. Nardulli, Phys. Lett. **B498**, 179 (2001), hep-ph/0010321.
[249] K. Zarembo, Phys. Rev. **D62**, 054003 (2000), hep-ph/0002123.
[250] A. Schmitt, Q. Wang, and D. H. Rischke, Phys. Rev. **D69**, 094017 (2004), nucl-th/0311006.
[251] D. N. Aguilera, Astrophys. Space Sci. **308**, 443 (2007), hep-ph/0608041.
[252] M. Huang and I. A. Shovkovy, Phys. Rev. **D70**, 051501 (2004), hep-ph/0407049.
[253] M. G. Alford, J. Berges, and K. Rajagopal, Phys. Rev. Lett. **84**, 598 (2000), hep-ph/9908235.
[254] O. Kiriyama, Phys. Rev. **D74**, 114011 (2006), hep-ph/0609185.
[255] O. Kiriyama, Phys. Rev. **D74**, 074019 (2006), hep-ph/0608109.
[256] M. Kitazawa, D. H. Rischke, and I. A. Shovkovy, Phys. Lett. **B637**, 367 (2006), hep-ph/0602065.
[257] E. Gubankova, A. Schmitt, and F. Wilczek, Phys. Rev. **B74**, 064505 (2006), cond-mat/0603603.
[258] J. Polchinski (1992), hep-th/9210046.
[259] N. J. Evans, S. D. H. Hsu, and M. Schwetz, Phys. Lett. **B449**, 281 (1999), hep-ph/9810514.
[260] N. J. Evans, S. D. H. Hsu, and M. Schwetz, Nucl. Phys. **B551**, 275 (1999), hep-ph/9808444.
[261] T. Schäfer and F. Wilczek, Phys. Lett. **B450**, 325 (1999), hep-ph/9810509.
[262] P. T. Reuter, Q. Wang, and D. H. Rischke, Phys. Rev. **D70**, 114029 (2004), nucl-th/0405079.
[263] D. K. Hong, Phys. Lett. **B473**, 118 (2000), hep-ph/9812510.
[264] D. K. Hong, Nucl. Phys. **B582**, 451 (2000), hep-ph/9905523.
[265] T. Schäfer, Nucl. Phys. **A728**, 251 (2003), hep-ph/0307074.
[266] T. Schäfer and K. Schwenzer, Phys. Rev. Lett. **97**, 092301 (2006), hep-ph/0512309.
[267] T. Schäfer and K. Schwenzer, Phys. Rev. **D70**, 054007 (2004), hep-ph/0405053.
[268] T. Schäfer, Phys. Rev. **D65**, 074006 (2002), hep-ph/0109052.
[269] K. Iida, T. Matsuura, M. Tachibana, and T. Hatsuda, Phys. Rev. Lett. **93**, 132001 (2004), hep-ph/0312363.
[270] K. Iida, T. Matsuura, M. Tachibana, and T. Hatsuda, Phys. Rev. **D71**, 054003 (2005), hep-ph/0411356.
[271] B. i. Halperin, T. C. Lubensky, and S.-k. Ma, Phys. Rev. Lett. **32**, 292 (1974).
[272] I. Giannakis and H.-c. Ren, Nucl. Phys. **B669**, 462 (2003), hep-ph/0305235.
[273] T. Matsuura, K. Iida, T. Hatsuda, and G. Baym, Phys. Rev. **D69**, 074012 (2004), hep-ph/0312042.
[274] J. L. Noronha, H.-c. Ren, I. Giannakis, D. Hou, and D. H. Rischke, Phys. Rev. **D73**, 094009 (2006), hep-ph/0602218.
[275] I. Giannakis, D.-f. Hou, H.-c. Ren, and D. H. Rischke, Phys. Rev. Lett. **93**, 232301 (2004), hep-ph/0406031.
[276] R. Casalbuoni and R. Gatto, Phys. Lett. **B464**, 111 (1999), hep-ph/9908227.
[277] D. T. Son and M. A. Stephanov, Phys. Rev. **D62**, 059902 (2000), hep-ph/0004095.
[278] S. R. Beane, P. F. Bedaque, and M. J. Savage, Phys. Lett. **B483**, 131 (2000), hep-ph/0002209.
[279] M. Rho, A. Wirzba, and I. Zahed, Phys. Lett. **B473**, 126 (2000), hep-ph/9910550.
[280] D. T. Son (2002), hep-ph/0204199.
[281] M. Greiter, F. Wilczek, and E. Witten, Mod. Phys. Lett. **B3**, 903 (1989).
[282] M. Ruggieri, JHEP **07**, 031 (2007), arXiv:0705.2974 [hep-ph].
[283] V. Kleinhaus, M. Buballa, D. Nickel, and M. Oertel, Phys. Rev. **D76**, 074024 (2007), 0707.0632.
[284] G. 't Hooft, Phys. Rev. Lett. **37**, 8 (1976).
[285] C. Manuel and M. H. G. Tytgat, Phys. Lett. **B479**, 190 (2000), hep-ph/0001095.
[286] A. Kryjevski, D. B. Kaplan, and T. Schäfer, Phys. Rev. **D71**, 034004 (2005), hep-ph/0404290.
[287] M. G. Alford, M. Braby, and A. Schmitt, J. Phys. **G35**, 025002 (2008), 0707.2389.
[288] T. Schäfer, D. T. Son, M. A. Stephanov, D. Toublan, and J. J. M. Verbaarschot, Phys. Lett. **B522**, 67 (2001), hep-ph/0108210.
[289] V. A. Miransky and I. A. Shovkovy, Phys. Rev. Lett. **88**, 111601 (2002), hep-ph/0108178.
[290] H. J. Warringa (2006), hep-ph/0606063.
[291] D. Ebert, K. G. Klimenko, and V. L. Yudichev, Eur. Phys. J. **C53**, 65 (2008), 0705.2666.
[292] D. Ebert and K. G. Klimenko, Phys. Rev. **D75**, 045005 (2007), hep-ph/0611385.
[293] T. Schäfer and F. Wilczek, Phys. Rev. Lett. **82**, 3956 (1999), hep-ph/9811473.
[294] N. D. Ippolito, G. Nardulli, and M. Ruggieri, JHEP **04**, 036 (2007), hep-ph/0701113.
[295] M. Buballa and M. Oertel, Nucl. Phys. **A703**, 770 (2002), hep-ph/0109095.
[296] A. Mishra and H. Mishra, Phys. Rev. **D74**, 054024 (2006), hep-ph/0605223.
[297] A. Mishra and H. Mishra, Phys. Rev. **D69**, 014014 (2004), hep-ph/0306105.

[298] D. Nickel, R. Alkofer, and J. Wambach, Phys. Rev. **D74**, 114015 (2006), hep-ph/0609198.
[299] T. M. Schwarz, S. P. Klevansky, and G. Papp, Phys. Rev. **C60**, 055205 (1999), nucl-th/9903048.
[300] K. Kashiwa, M. Matsuzaki, H. Kouno, and M. Yahiro, Phys. Lett. **B657**, 143 (2007), 0705.1196.
[301] S. B. Rüster, V. Werth, M. Buballa, I. A. Shovkovy, and D. H. Rischke (2006), nucl-th/0602018.
[302] H. J. Warringa, D. Boer, and J. O. Andersen, Phys. Rev. **D72**, 014015 (2005), hep-ph/0504177.
[303] A. Barducci, R. Casalbuoni, G. Pettini, and L. Ravagli, Phys. Rev. **D69**, 096004 (2004), hep-ph/0402104.
[304] A. Mishra and H. Mishra, Phys. Rev. **D71**, 074023 (2005), hep-ph/0412213.
[305] L. He, M. Jin, and P. Zhuang, Phys. Rev. **D75**, 036003 (2007), hep-ph/0610121.
[306] J. A. Bowers, J. Kundu, K. Rajagopal, and E. Shuster, Phys. Rev. **D64**, 014024 (2001), hep-ph/0101067.
[307] R. Casalbuoni, R. Gatto, M. Mannarelli, and G. Nardulli, Phys. Lett. **B511**, 218 (2001), hep-ph/0101326.
[308] J. Kundu and K. Rajagopal, Phys. Rev. **D65**, 094022 (2002), hep-ph/0112206.
[309] R. Casalbuoni et al., Phys. Lett. **B575**, 181 (2003), hep-ph/0307335.
[310] R. Casalbuoni et al., Phys. Rev. **D70**, 054004 (2004), hep-ph/0404090.
[311] R. Casalbuoni, R. Gatto, and G. Nardulli, Phys. Lett. **B543**, 139 (2002), hep-ph/0205219.
[312] R. Casalbuoni, E. Fabiano, R. Gatto, M. Mannarelli, and G. Nardulli, Phys. Rev. **D66**, 094006 (2002), hep-ph/0208121.
[313] R. Casalbuoni, M. Ciminale, R. Gatto, G. Nardulli, and M. Ruggieri, Phys. Lett. **B642**, 350 (2006), hep-ph/0606242.
[314] I. Giannakis, J. T. Liu, and H.-c. Ren, Phys. Rev. **D66**, 031501 (2002), hep-ph/0202138.
[315] K. Rajagopal and R. Sharma, J. Phys. **G32**, S483 (2006), hep-ph/0606066.
[316] I. Giannakis and H.-C. Ren, Nucl. Phys. **B723**, 255 (2005), hep-th/0504053.
[317] I. Giannakis, D.-f. Hou, and H.-C. Ren, Phys. Lett. **B631**, 16 (2005), hep-ph/0507306.
[318] R. Gatto and M. Ruggieri, Phys. Rev. **D75**, 114004 (2007), hep-ph/0703276.
[319] R. Anglani, R. Gatto, N. D. Ippolito, G. Nardulli, and M. Ruggieri, Phys. Rev. **D76**, 054007 (2007), 0706.1781.
[320] M. Mannarelli, K. Rajagopal, and R. Sharma, Phys. Rev. **D76**, 074026 (2007), hep-ph/0702021.
[321] A. F. Andreev and I. M. Lifshitz, Sov. Phys. JETP **29**, 2057 (1969).
[322] G. V. Chester, Phys. Rev. **A2**, 256 (1970).
[323] A. J. Leggett, Phys. Rev. Lett. **25**, 1543 (1970).
[324] E. Kim and M. H. W. Chan, Nature **427**, 225 (2004).
[325] E. Kim and M. H. W. Chan, Science **305**, 1941 (2004).
[326] D. T. Son, Phys. Rev. Lett. **94**, 175301 (2005), cond-mat/0501658.
[327] L. D. Landau and E. M. Lifshitz, *Theory of Elasticity* (Pergamon, Oxford, 1981), 3rd ed.
[328] T. Strohmayer, H. M. van Horn, S. Ogata, H. Iyetomi, and S. Ichimaru, Astrophys. J. **375**, 679 (1991).
[329] L. D. Landau and E. M. Lifshitz, *Fluid Mechanics* (Pergamon, Oxford, 1987), 2nd ed.
[330] M. E. Gusakov, Phys. Rev. **D76**, 083001 (2007), 0704.1071.
[331] N. Andersson and G. L. Comer (2006), gr-qc/0605010.
[332] I. Khalatnikov, *An Introduction to the Theory of Superfluidity* (Addison-Wesley, New York, 1989).
[333] P. Haensel, K. P. Levenfish, and D. G. Yakovlev, Astron. Astrophys. **357**, 1157 (2000), astro-ph/0004183.
[334] M. G. Alford and A. Schmitt, J. Phys. **G34**, 67 (2007), nucl-th/0608019.
[335] B. A. Sa'd, I. A. Shovkovy, and D. H. Rischke, Phys. Rev. **D75**, 125004 (2007), astro-ph/0703016.
[336] C. Manuel, A. Dobado, and F. J. Llanes-Estrada, JHEP **09**, 076 (2005), hep-ph/0406058.
[337] I. A. Shovkovy and P. J. Ellis, Phys. Rev. **C66**, 015802 (2002), hep-ph/0204132.
[338] C. Manuel and F. J. Llanes-Estrada, JCAP **0708**, 001 (2007), 0705.3909.
[339] M. G. Alford, M. Braby, S. Reddy, and T. Schäfer, Phys. Rev. **C75**, 055209 (2007), nucl-th/0701067.
[340] H. Heiselberg and C. J. Pethick, Phys. Rev. **D48**, 2916 (1993).
[341] J. D. Anand, N. Chandrika Devi, V. K. Gupta, and S. Singh, Pramana **54**, 737 (2000).
[342] J. Madsen, Phys. Rev. **D46**, 3290 (1992).
[343] H. Dong, N. Su, and Q. Wang, Phys. Rev. **D75**, 074016 (2007), astro-ph/0702104.
[344] J. Madsen, Phys. Rev. Lett. **85**, 10 (2000), astro-ph/9912418.
[345] J. Madsen, Phys. Rev. **D47**, 325 (1993).
[346] B. A. Sa'd, I. A. Shovkovy, and D. H. Rischke, Phys. Rev. **D75**, 065016 (2007), astro-ph/0607643.
[347] P. Jaikumar, M. Prakash, and T. Schäfer, Phys. Rev. **D66**, 063003 (2002), astro-ph/0203088.
[348] S. Reddy, M. Sadzikowski, and M. Tachibana, Nucl. Phys. **A714**, 337 (2003), nucl-th/0203011.
[349] S. Reddy, M. Sadzikowski, and M. Tachibana, Phys. Rev. **D68**, 053010 (2003), nucl-th/0306015.
[350] N. Iwamoto, Phys. Rev. Lett. **44**, 1637 (1980).
[351] T. Schäfer and K. Schwenzer, Phys. Rev. **D70**, 114037 (2004), astro-ph/0410395.
[352] P. Jaikumar, C. D. Roberts, and A. Sedrakian, Phys. Rev. **C73**, 042801 (2006), nucl-th/0509093.
[353] P. Jaikumar and M. Prakash, Phys. Lett. **B516**, 345 (2001), astro-ph/0105225.
[354] R. Anglani, G. Nardulli, M. Ruggieri, and M. Mannarelli, Phys. Rev. **D74**, 074005 (2006), hep-ph/0607341.
[355] D. G. Yakovlev, A. D. Kaminker, O. Y. Gnedin, and P. Haensel, Phys. Rept. **354**, 1 (2001), astro-ph/0012122.
[356] A. Schmitt, I. A. Shovkovy, and Q. Wang, Phys. Rev. **D73**, 034012 (2006), hep-ph/0510347.
[357] Q. Wang, Z.-g. Wang, and J. Wu, Phys. Rev. **D74**, 014021 (2006), hep-ph/0605092.
[358] D. N. Aguilera, D. Blaschke, M. Buballa, and V. L. Yudichev, Phys. Rev. **D72**, 034008 (2005), hep-ph/0503288.
[359] J. M. Lattimer and M. Prakash, Astrophys. J. **550**, 426 (2001), astro-ph/0002232.
[360] J. M. Lattimer and M. Prakash, Phys. Rept. **442**, 109 (2007), astro-ph/0612440.
[361] J. W. Negele and D. Vautherin, Nucl. Phys. **A207**, 298 (1973).

[362] F. Weber, A. Torres i Cuadrat, A. Ho, and P. Rosenfield, PoS **JHW2005**, 018 (2006), astro-ph/0602047.
[363] D. Page and S. Reddy, Ann. Rev. Nucl. Part. Sci. **56**, 327 (2006), astro-ph/0608360.
[364] F. Weber, *Pulsars as Astrophysical Laboratories for Nuclear and Particle Physics* (IOP Publishing Ltd., Bristol, 1999).
[365] M. Prakash, J. M. Lattimer, J. A. Pons, A. W. Steiner, and S. Reddy, Lect. Notes Phys. **578**, 364 (2001), astro-ph/0012136.
[366] J. M. Lattimer and M. Prakash, Science **304**, 536 (2004), astro-ph/0405262.
[367] D. G. Yakovlev and C. J. Pethick, Ann. Rev. Astron. Astrophys. **42**, 169 (2004), astro-ph/0402143.
[368] J. N. Bahcall and R. A. Wolf, Phys. Rev. **B140**, 1452 (1965).
[369] A. B. Migdal, Zh. Eksp. Teor. Fiz. **61**, 2209 (1971).
[370] R. F. Sawyer, Phys. Rev. Lett. **29**, 382 (1972).
[371] D. J. Scalapino, Phys. Rev. Lett. **29**, 386 (1972).
[372] G. Baym and D. K. Campbell (1978), in *Mesons in Nuclei*, ed. M. Rho, D. Wilkinson, Vol III, 1031. Amsterdam: North Holland.
[373] D. B. Kaplan and A. E. Nelson, Phys. Lett. **B175**, 57 (1986).
[374] G. E. Brown (1995), in *Bose-Einstein Condensation*, ed. A. Griffin, et al. 438. Cambridge: Cambridge University Press.
[375] N. K. Glendenning, Astrophys. J. **293**, 470 (1985).
[376] A. R. Bodmer, Phys. Rev. **D4**, 1601 (1971).
[377] E. Witten, Phys. Rev. **D30**, 272 (1984).
[378] E. Farhi and R. L. Jaffe, Phys. Rev. **D30**, 2379 (1984).
[379] C. Alcock, E. Farhi, and A. Olinto, Astrophys. J. **310**, 261 (1986).
[380] P. Haensel, J. L. Zdunik, and R. Schaeffer, Astron. Astrophys. **160**, 121 (1986).
[381] C. Alcock and A. Olinto, Ann. Rev. Nucl. Part. Sci. **38**, 161 (1988).
[382] G. Israel et al., Astrophys. J. **628**, L53 (2005), astro-ph/0505255.
[383] T. E. Strohmayer and A. L. Watts, Astrophys. J. **632**, L111 (2005), astro-ph/0508206.
[384] A. L. Watts and T. E. Strohmayer, Astrophys. J. **637**, L117 (2006), astro-ph/0512630.
[385] T. E. Strohmayer and A. L. Watts, Astrophys. J. **653**, 593 (2006), astro-ph/0608463.
[386] A. L. Watts and T. E. Strohmayer, Astrophys. Space Sci. **308**, 625 (2007), astro-ph/0608476.
[387] A. L. Watts and S. Reddy, Mon. Not. Roy. Astron. Soc. **379**, L63 (2007), astro-ph/0609364.
[388] J. L. Friedman and R. R. Caldwell, Phys. Lett. **B264**, 143 (1991).
[389] M. Baldo et al., Phys. Lett. **B562**, 153 (2003), nucl-th/0212096.
[390] E. S. Fraga, R. D. Pisarski, and J. Schaffner-Bielich, Phys. Rev. **D63**, 121702 (2001), hep-ph/0101143.
[391] M. G. Alford, M. Braby, M. W. Paris, and S. Reddy, Astrophys. J. **629**, 969 (2005), nucl-th/0411016.
[392] D. B. Blaschke, D. Gomez Dumm, A. G. Grunfeld, T. Klahn, and N. N. Scoccola, Phys. Rev. **C75**, 065804 (2007), nucl-th/0703088.
[393] M. G. Alford and S. Reddy, Phys. Rev. **D67**, 074024 (2003), nucl-th/0211046.
[394] G. Lugones and J. E. Horvath, Phys. Rev. **D66**, 074017 (2002), hep-ph/0211070.
[395] A. Akmal, V. R. Pandharipande, and D. G. Ravenhall, Phys. Rev. **C58**, 1804 (1998), nucl-th/9804027.
[396] D. J. Nice et al., Astrophys. J. **634**, 1242 (2005), astro-ph/0508050.
[397] D. Nice and I. Stairs, private communication (2007).
[398] E. M. Splaver et al., Astrophys. J. **581**, 509 (2002), astro-ph/0208281.
[399] S. M. Ransom et al., Science **307**, 892 (2005), astro-ph/0501230.
[400] O. Barziv, L. Kaper, M. H. van Kerkwijk, J. H. Telting, and J. van Paradijs, Astron. Astrophys. **377**, 925 (2001), astro-ph/0108237.
[401] J. A. Faber, P. Grandclement, F. A. Rasio, and K. Taniguchi, Phys. Rev. Lett. **89**, 231102 (2002), astro-ph/0204397.
[402] M. Burgay et al., Nature. **426**, 531 (2003), astro-ph/0312071.
[403] A. G. Lyne et al., Science **303**, 1153 (2004), astro-ph/0401086.
[404] M. Kramer et al. (2004), astro-ph/0405179.
[405] I. A. Morrison, T. W. Baumgarte, S. L. Shapiro, and V. R. Pandharipande, Astrophys. J. **617**, L135 (2004), astro-ph/0411353.
[406] J. M. Lattimer and B. F. Schutz, Astrophys. J. **629**, 979 (2005), astro-ph/0411470.
[407] M. Kramer et al., Science **314**, 97 (2006), astro-ph/0609417.
[408] N. Iwamoto, Ann. Phys. (N.Y.) **141**, 1 (1982).
[409] D. Page, J. M. Lattimer, M. Prakash, and A. W. Steiner, Astrophys. J. Suppl. **155**, 623 (2004), astro-ph/0403657.
[410] D. G. Yakovlev et al., Nucl. Phys. **A752**, 590 (2005), astro-ph/0409751.
[411] H. Grigorian, D. Blaschke, and D. Voskresensky, Phys. Rev. **C71**, 045801 (2005), astro-ph/0411619.
[412] D. L. Kaplan et al., Astrophys. J. Suppl. **153**, 269 (2004), astro-ph/0403313.
[413] D. L. Kaplan, B. M. Gaensler, S. R. Kulkarni, and P. O. Slane, Astrophys. J. Suppl. **163**, 344 (2006), astro-ph/0602312.
[414] D. L. Kaplan, private communication (2007).
[415] E. F. Brown, L. Bildsten, and R. E. Rutledge, Astrophys. J. Lett. **504**, L95 (1998), astro-ph/9807179.
[416] C. O. Heinke, P. G. Jonker, R. Wijnands, and R. E. Taam, Astrophys. J. **660**, 1424 (2007), astro-ph/0612232.
[417] P. G. Jonker et al., Mon. Not. Roy. Astron. Soc. **368**, 1803 (2006), astro-ph/0602625.
[418] P. G. Jonker, D. Steeghs, D. Chakrabarty, and A. M. Juett, Astrophys. J. **665**, L147 (2007), arXiv:0706.3421 [astro-ph].
[419] D. Chakrabarty, private communication (2007).
[420] N. Andersson, Astrophys. J. **502**, 708 (1998), gr-qc/9706075.
[421] J. L. Friedman and S. M. Morsink, Astrophys. J. **502**, 714 (1998), gr-qc/9706073.

[422] N. Andersson, K. D. Kokkotas, and N. Stergioulas, Astrophys. J. **516**, 307 (1999), astro-ph/9806089.
[423] N. Andersson, K. D. Kokkotas, and B. F. Schutz, Astrophys. J. **510**, 846 (1999), astro-ph/9805225.
[424] N. Andersson and G. L. Comer, Mon. Not. Roy. Astron. Soc. **328**, 1129 (2001), astro-ph/0101193.
[425] L. Lindblom, B. J. Owen, and S. M. Morsink, Phys. Rev. Lett. **80**, 4843 (1998), gr-qc/9803053.
[426] B. J. Owen et al., Phys. Rev. **D58**, 084020 (1998), gr-qc/9804044.
[427] L. Bildsten, Astrophys. J. **501**, L89 (1998), astro-ph/9804325.
[428] J. W. T. Hessels et al., Science **311**, 1901 (2006), astro-ph/0601337.
[429] D. Chakrabarty et al., Nature **424**, 42 (2003), astro-ph/0307029.
[430] D. Chakrabarty, p. 279 (2004), in *Binary Radio Pulsars*, ed. F. A. Rasio and I. H. Stairs, (San Francisco: Astron. Soc. Pacific Conf. 328), astro-ph/0408004.
[431] N. K. Glendenning and F. Weber, Astrophys. J. **559**, L119 (2001), astro-ph/0003426.
[432] N. K. Glendenning, S. Pei, and F. Weber, Phys. Rev. Lett. **79**, 1603 (1997), astro-ph/9705235.
[433] Y. Levin and G. Ushomirsky, Mon. Not. Roy. Astron. Soc. **324**, 917 (2001), astro-ph/0006028.
[434] P. Haensel, K. P. Levenfish, and D. G. Yakovlev (2001), astro-ph/0103290.
[435] R. F. Sawyer, Phys. Rev. **D39**, 3804 (1989).
[436] P. Haensel, K. P. Levenfish, and D. G. Yakovlev (2001), astro-ph/0110575.
[437] L. Lindblom and B. J. Owen, Phys. Rev. **D65**, 063006 (2002), astro-ph/0110558.
[438] D. Chatterjee and D. Bandyopadhyay, Phys. Rev. **D75**, 123006 (2007), astro-ph/0702259.
[439] H. Sotani, K. Tominaga, and K.-i. Maeda, Phys. Rev. **D65**, 024010 (2002), gr-qc/0108060.
[440] G. W. Carter and S. Reddy, Phys. Rev. **D62**, 103002 (2000), hep-ph/0005228.
[441] J. Kundu and S. Reddy, Phys. Rev. **C70**, 055803 (2004), nucl-th/0405055.
[442] B. Abbott et al. (LIGO Scientific), Phys. Rev. **D76**, 042001 (2007), gr-qc/0702039.
[443] B. Haskell, N. Andersson, D. I. Jones, and L. Samuelsson (2007), arXiv:0708.2984 [gr-qc].
[444] L.-M. Lin, Phys. Rev. **D76**, 081502 (2007), 0708.2965.
[445] B. J. Owen, Phys. Rev. Lett. **95**, 211101 (2005), astro-ph/0503399.
[446] P. W. Anderson and N. Itoh, Nature **256**, 25 (1975).
[447] M. A. Alpar, Astrophys. J. **213**, 527 (1977).
[448] M. A. Alpar, P. W. Anderson, D. Pines, and J. Shaham, Astrophys. J. **278**, 791 (1984).
[449] M. A. Alpar, S. A. Langer, and J. A. Sauls, Astrophys. J. **282**, 533 (1984).
[450] R. I. Epstein and G. Baym, Astrophys. J. **387**, 276 (1992).
[451] B. Link, R. I. Epstein, and G. Baym, Astrophys. J. **403**, 285 (1993).
[452] P. B. Jones, Phys. Rev. Lett. **79**, 792 (1997).
[453] M. A. Alpar, H. F. Chau, K. S. Cheng, and D. Pines, Astrophys. J. **459**, 706 (1996).
[454] D. Pines and M. A. Alpar, Nature **316**, 27 (1985).
[455] B. Link and R. I. Epstein, Astrophys. J. **457**, 854 (1996), astro-ph/9508021.
[456] B. Link, talk given at INT workshop on The Neutron Star Crust and Surface, Seattle, and private communication (2007).
[457] B. Link, Astron. Astrophys. **458**, 881 (2006), astro-ph/0608319.
[458] A. Sedrakian, I. Wasserman, and J. M. Cordes, Astrophys. J. **524**, 341S (1999), astro-ph/9801188.
[459] B. Link, Astrophys. and Space Sci. **308**, 435 (2007).
[460] I. H. Stairs, A. G. Lyne, and S. L. Shemar, Nature **406**, 484 (2000).
[461] T. V. Shabanova, A. G. Lyne, and J. O. Urama, Astrophys. J. **552**, 321 (2001), astro-ph/0101282.
[462] A. E. Chukwude, A. A. Ubachukwu, and P. N. Okeke, Astron. Astrophys. **399**, 231 (2003).